NASA TECHNICAL REPORT

NASA TR R-252

NASA TR R-252

SYNCOM ENGINEERING REPORT

VOLUME II

by Syncom Projects Office

Goddard Space Flight Center
Greenbelt, Md.

NATIONAL AERONAUTICS AND SPACE ADMINISTRATION • WASHINGTON, D. C. • APRIL 1967

NASA TR R-252

SYNCOM ENGINEERING REPORT

VOLUME II

By Syncom Projects Office

Goddard Space Flight Center
Greenbelt, Md.

NATIONAL AERONAUTICS AND SPACE ADMINISTRATION

For sale by the Clearinghouse for Federal Scientific and Technical Information
Springfield, Virginia 22151 – CFSTI price $3.00

ABSTRACT

This report, the second of two volumes on the Syncom Satellite System, will cover the launch of the Syncom III satellite, its performance during the first 100 days in orbit, the televising of the 1964 Summer Olympic Games by means of the satellite and various communications tests conducted with it. Syncom III was launched on 19 August 1964. All three stages of the Thrust-Augmented Delta vehicle performed satisfactorily and subsequent orbital maneuvers placed the satellite into a nominally synchronous equatorial (stationary) orbit over the International Date Line. Live television of the Olympic Games from Japan via Syncom III was a technical success. The satellite also enabled the establishment of the first 24-hour-per-day, 7 day-per-week reliable communications network across the Pacific Ocean. The attainment of a stationary orbit, which permits the use of fixed ground antennas without the expense of costly tracking systems, and Syncom III's excellent performance indicate the operational and economic advantages of the synchronous communication satellite.

CONTENTS

SYNCOM ENGINEERING REPORT
VOLUME II

by
Syncom Projects Office
Goddard Space Flight Center

CHAPTER I

INTRODUCTION

This second volume of the Syncom Engineering Report, based on material furnished by the Hughes Aircraft Company and the U. S. Army Satellite Communications Agency, will cover the launch of the Syncom III satellite, its performance during the first 100 days in orbit, televising of the 1964 Summer Olympic Games by means of the satellite, and various communication tests conducted with it. Syncom III is one of three communications satellites designed and built by Hughes for the Goddard Space Flight Center which have been launched into synchronous orbit. Syncom I was successfully launched in February 1963, but radio contact with the spacecraft was lost shortly after the apogee motor was fired, probably because of an explosion of a nitrogen control system tank. Syncom II was successfully launched in July 1963, becoming the world's first operational synchronous satellite. This satellite was eventually placed at an area of low perturbation forces over the Indian Ocean after all control system propellant had been expended. From this position it has provided communication links between the Far East, Africa and Europe. The launch and performance of Syncom II, is described in Volume I.*

After the launch of Syncom II, the following modifications were made in the Syncom spacecraft:

1. The nitrogen control unit was replaced with a second hydrogen peroxide control unit.
2. The apogee motor timer was deleted and redundant provisions were made for a firing by ground command.
3. Four temperature sensors were provided instead of the previous two sensors.
4. The standby battery was eliminated.
5. The P-N type solar cells were replaced by N-P cells and the 0.006-inch cover glass was replaced by 0.012-inch fused quartz covering.

*NASA Technical Report TR R-233, March 1966.

6. The 500-kc bandpass communications channel was eliminated and replaced by a 10-Mc bandwidth channel for television tests with a 50-kc option for small station testing.

Prior to the Syncom III launch, booster thrust limitations precluded any attempt to reduce the inclination of the Syncom orbit with maneuvers during the boost phase of launch. As a result, Syncom II, although in a synchronous orbit, moves 32° north and south of the Equator daily. The ultimate objective of synchronous communications advocates has been to place a satellite into synchronous orbit in the equatorial plane. The satellite would then appear to remain stationary and would permit the use of fixed ground antennas without the expense of costly tracking systems. The achievement of this objective by Syncom III became possible with the development in early 1964 of the higher powered Thrust Augmented Delta launch vehicle that could provide enough thrust to permit inflight maneuvers to decrease the orbit inclination.

With the Summer Olympic Games of 1964 scheduled to be held in Japan in early October, the use of Syncom III to present live television coverage of the Olympic Games for the American public became a second launch object.

Syncom III was launched on 19 August 1964 from Pad 17A at Cape Kennedy, Florida. The launch was near-perfect. The maneuver to reorient the third stage for firing at the Equator crossing was also near-perfect. Third stage burn was good, but coning was experienced after burnout. Syncom III separated with a 14-degree attitude error. Seventeen hours and fifteen minutes later, as the spacecraft approached its second apogee over South America, this error was corrected and the spacecraft was oriented to the proper attitude in preparation for apogee motor firing. At third apogee, 29 hours and 2 minutes after liftoff, at a point above the Equator in Borneo, the apogee motor was fired. Syncom III went into synchronous equatorial orbit and later was maneuvered to a position above the intersection of the Equator and the International Date Line.

Since the launch of Syncom III, the following achievements have been recorded, demonstrating the operational and economic advantages of the synchronous communication satellite:

1. The satellite was put into synchronous equatorial (stationary) orbit over the International Date Line. Ground stations are able to acquire the satellite and lock their antennas in place.
2. The first 24 hour-per-day, 7 day-per-week reliable communications network has been established across the Pacific Ocean (Figure I-1).
3. Live television of the Olympic Games from Japan was a technical success.
4. The first communications through an orbiting satellite to a commercial airliner in flight was demonstrated.
5. The narrow bandpass transponder (50 kc) has provided small-station communications capabilities.

The performance of Syncom III has been excellent and no malfunctions have occurred. The satellite has been in almost constant operation since liftoff. The only times the transponders have been off was during apogee motor firing and for a few hours each day when the satellite was in the eclipse season.

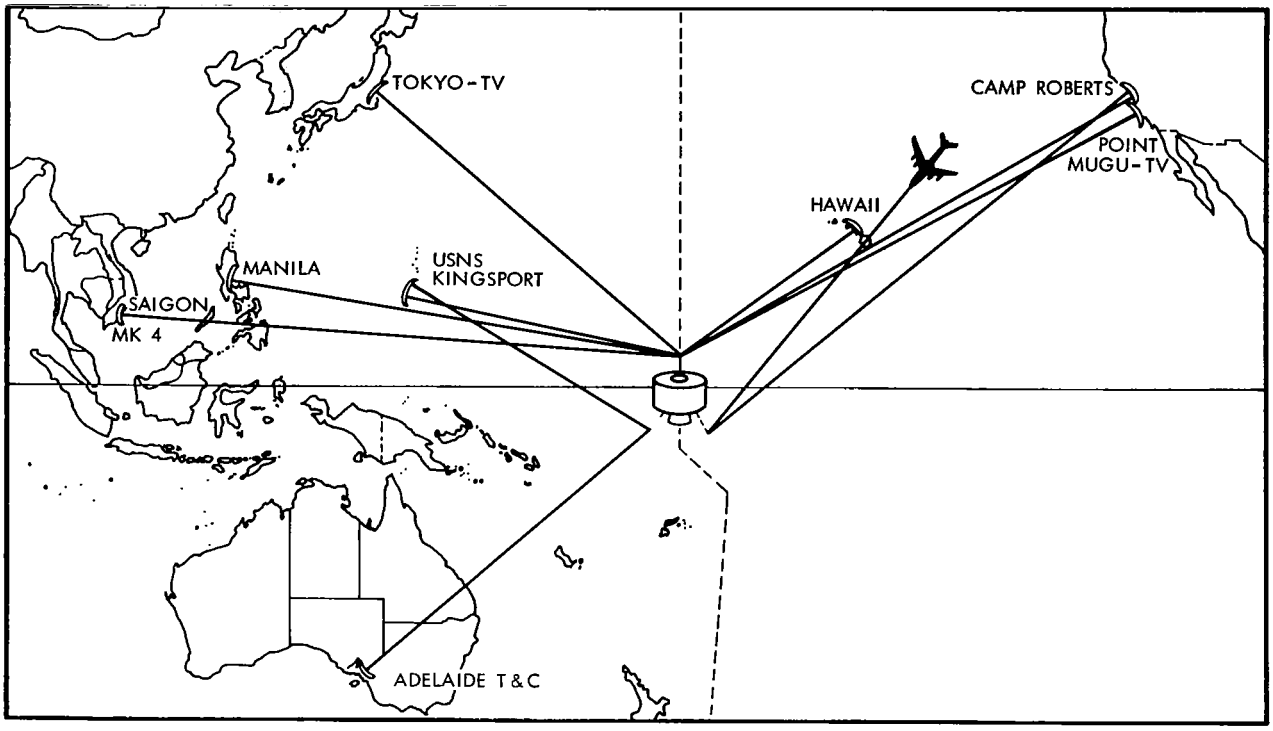

Figure 1-1—Syncom III communications network.

CHAPTER II

SPACECRAFT DESCRIPTION

SUMMARY

The Syncom spacecraft shown in Figures II-1 through II-5 is a spin-stabilized vehicle incorporating electronic, propulsion, and control elements, plus an electrical power supply and a structure. These are described briefly in the following paragraphs and shown in block diagram form in Figure II-6.

Electronic Elements

The spacecraft electronic system includes the communication, command, and telemetry subsystems.

Communication Subsystem

The communication subsystem is a redundant, frequency-translation, active-repeater system. Incoming signals from either one or two ground stations at a frequency of approximately 7400 Mc are received by an antenna with a pattern which is symmetrical about the satellite spin axis.

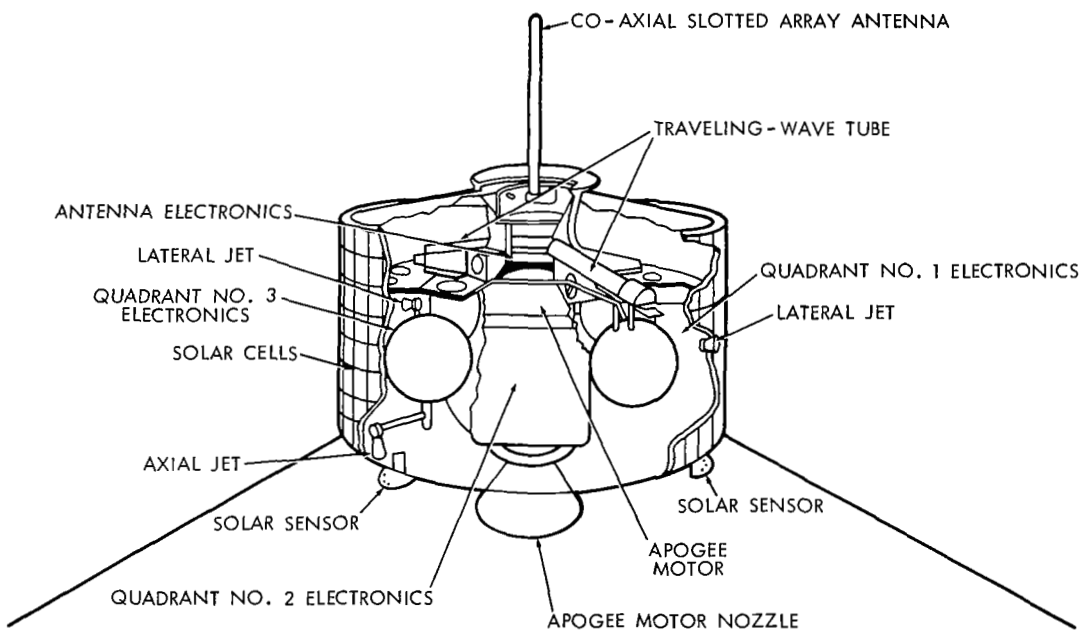

Figure II-1—Syncom spacecraft.

Figure II-2—Syncom C, side view with solar panels.

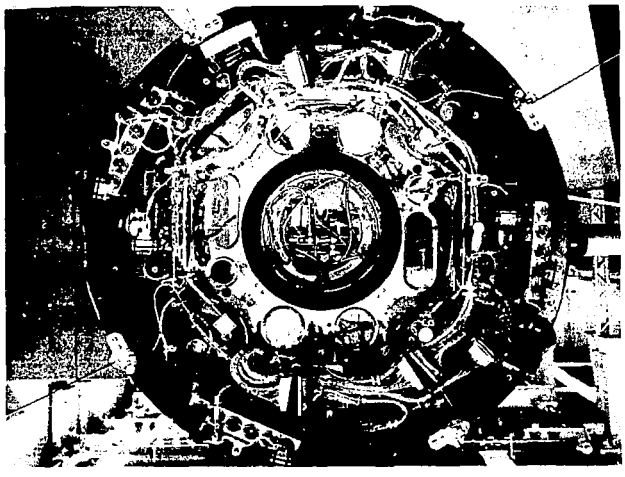

Figure II-3—Syncom C, top view, apogee motor not installed.

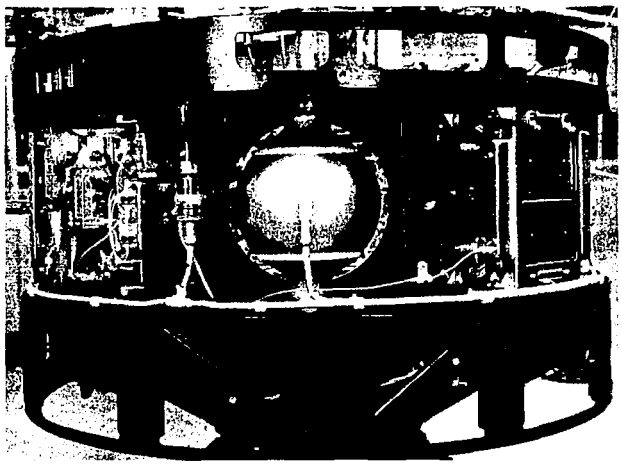

Figure II-4—Syncom C with solar panels removed, showing (l to r): quadrant 1 (10-Mc transponder), hydrogen peroxide system 2 and quadrant 2 (telemetry and command system 1).

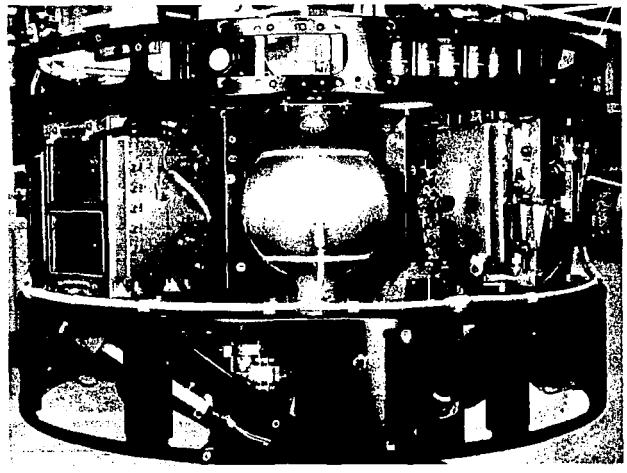

Figure II-5—Syncom C, side view showing (l to r): quadrant 2 (above), traveling-wave tube 2 (below), hydrogen peroxide system 1, and quadrant 3 (5-Mc transponder).

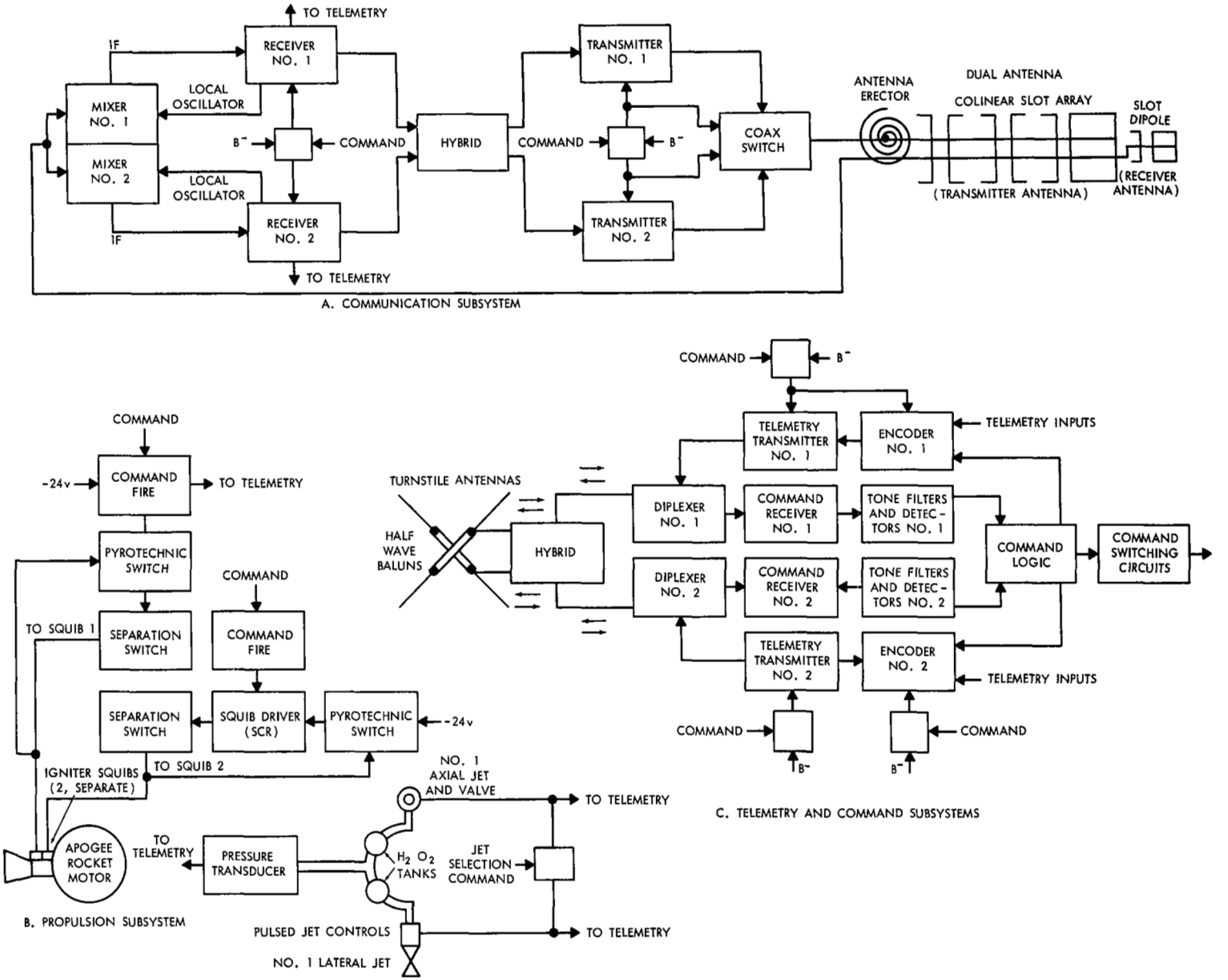

Figure II-6—Syncom spacecraft subsystems.

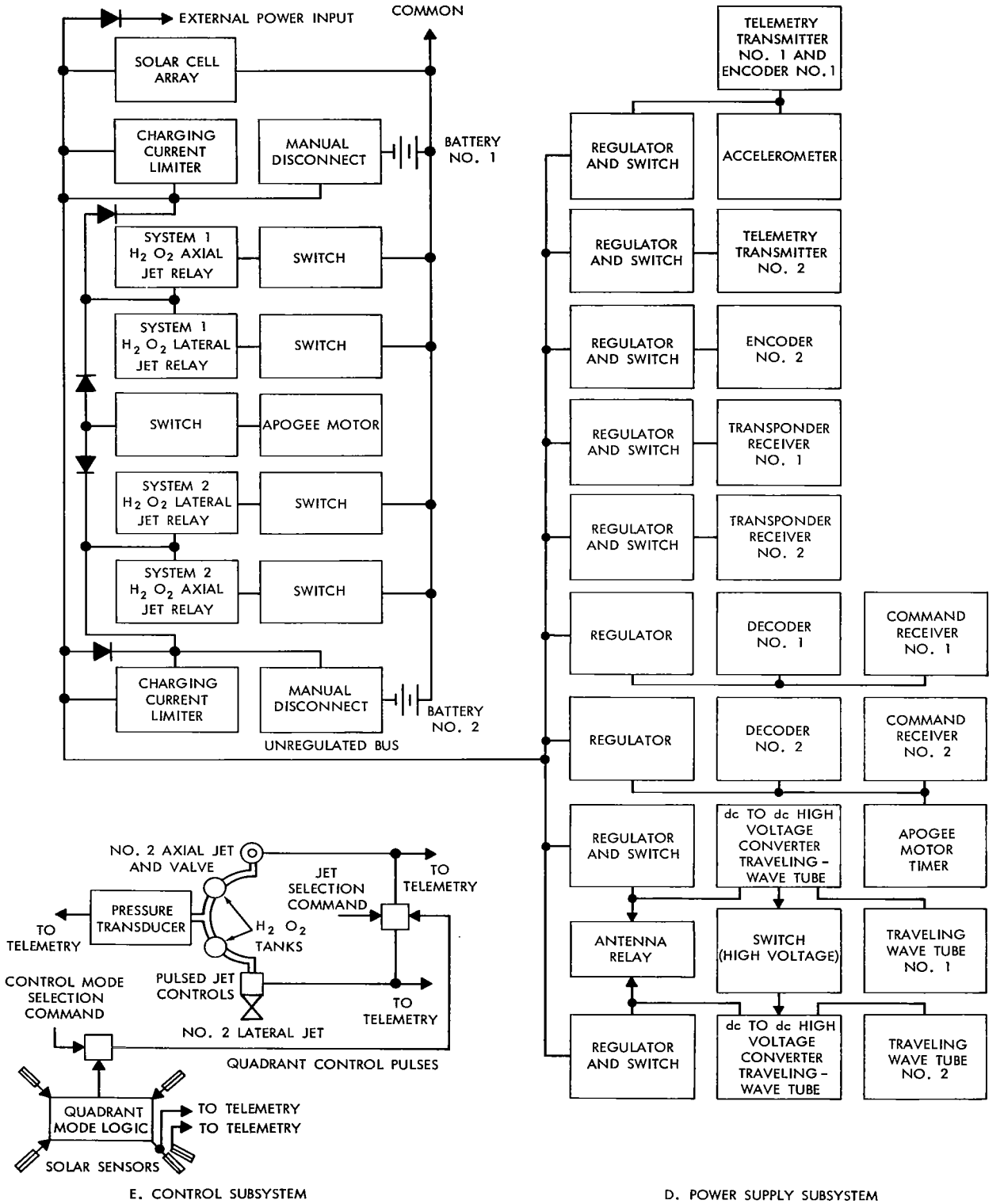

Figure II-6 (Continued)—Syncom spacecraft subsystems.

These signals are supplied to two receivers, only one of which is operating at any one time, the desired receiver being selected by command.

Both receivers are wide band, one with a bandwidth of 4.5 Mc between half-power points and the other with a bandwidth of 13.5 Mc between half-power points. In addition, the bandwidth of the 13-Mc receiver can be switched to 50 kc. Each receiver consists of a mixer, a local oscillator, an IF amplifier, and a limiter amplifier.

When simultaneous two-way, narrow-band communication takes place (duplex operation), the two signal channels are passed through the wide-band amplifier and its limiter. They then modulate the transmitter and are transmitted with power levels approximately proportional to their received signal level.

The number of carriers which can be handled on each wide-band system is dependent on the bandwidth apportionment between signals.

Following the receiver limiters, the outputs are mixed with a reference signal to provide a frequency-translated low-level output with carrier frequency at approximately 1800 Mc. These 1800-Mc outputs of the receivers are connected to a single hybrid network, the outputs of which are, in turn, connected to the two traveling-wave tube transmitters. Either traveling-wave tube may be selected by command for use with either receiver, but the receivers and transmitters are interlocked so that only one receiver and one transmitter may be activated at any instant, a turn-on command to either receiver or transmitter automatically turning off the other receiver or transmitter.

A portion of the receiver master oscillator is also transmitted and used on the ground as a reference to the equipment for range and range-rate determination. It may be used as a beacon for tracking the spacecraft with the ground communication system equipment.

The output of the transmitter is 2 watts. The power subsystem is designed to permit operation of the transponder at 100 percent duty cycle (except in eclipse), whether or not the batteries are operative.

The transmitting antenna consists of a coaxial slot array on the spin axis. The gain of this antenna is approximately 6db and the pattern is independent of angle about the spin axis. The antenna beam is a "pancake" with its plane perpendicular to the spin axis and is about 20 degrees wide. In operation, the spin axis of the satellite is perpendicular to the plane of the orbit, and the "pancake" beam therefore encompasses the earth at all times.

Command Subsystem

The command subsystem consists of receivers, decoders, and an antenna unit shared with the telemetry subsystem. The antennas consist of two pairs of whips connected through baluns to the two inputs of a hybrid. The two outputs of the hybrid correspond to the two polarization modes of the whips acting as a turnstile system. Each output is connected to a diplexer. Each diplexer

provides 148-Mc command signals to a receiver and accepts 136-Mc telemetry transmission from a telemetry transmitter.

The two command receivers are identical, parallel units each with mixer, IF amplifier, and AM detector. The detector outputs of the two receivers provide audio output tones recovered from the modulation on the command transmission from the ground. Each command receiver is associated with one of the two redundant command decoders. Either receiver/decoder can exercise complete command control of the spacecraft.

The audio signals are applied to two redundant groups of three tone-operated channels. Power is applied continuously to one channel in each group and on receipt of the correct audio tone, this channel turns power on to the other two channels in that group. Then the desired command can be inserted by sending a predetermined number of pulses from the ground at a second audio frequency. The command is verified through the telemetry system and then execution is accomplished by sending a tone on the third channel.

Functions accomplished by the command system include turning the communication transponder, telemetry carrier, and telemetry modulation on and off; selection of communication transmitter, communication receiver, telemetry transmitter, and encoder to be used; and all necessary control system functions. The logic of the command subsystem has been designed to achieve complete flexibility and reasonable security with a minimum number of channels.

Telemetry Subsystem

The telemetry subsystem consists of the antenna (shared with the command subsystem), two transmitters, each with its associated encoder, and the signal conversion elements. The 1.25-watt, 136-Mc transmitter is phase-modulated by a subcarrier which, in turn, is frequency-modulated by a time-division-multiplexed modulator that samples the amplitude of the various sensor signals. Certain critical control signals bypass the time-division-multiplexed modulator and are permitted to phase-modulate the telemetry transmitter directly.

Each transmitter and its associated encoder is one of a redundant pair, each pair operating at a unique frequency. Only one of the transmitter-encoder subsystems is permitted to function at one time, the power to the other subsystem being automatically turned off when the one is turned on. On command, encoder 2 may be disconnected, thereby removing the telemetry modulation and leaving the telemetry carrier to serve as a tracking beacon for the Minitrack network.

Sixteen channels of time-multiplexed data are telemetered. Included in these data are temperatures of selected points in the spacecraft, hydrogen peroxide tank pressures, stored but unexecuted commands, battery voltage, power bus voltage, and reference voltages.

Unmultiplexed data transmitted include responses to all "execute" signals, solar sensor "pips," and all gas jet actuations, whether sent from the ground control equipment or from the on-board control subsystem.

Orbit Injection Propulsion

The Syncom orbit injection propulsion subsystem supplies the boost necessary to inject the spacecraft into a nominally synchronous, circular orbit after the vehicle has reached the apogee of a transfer orbit at the required altitude. The spacecraft is launched into the transfer orbit by the Thrust-Augmented Delta vehicle.

The propulsion subsystem consists of a single solid-propellant rocket motor. This motor is required to impart a velocity increment of 4696 fps to the spacecraft, which initially weighs 144.77 pounds. The following parameters apply to this motor:

Specific impulse	274.2 seconds
Propellant weight	60.5 pounds
Case and nozzle weight (including provision for attachment)	10.5 pounds
Motor weight	71.0 pounds
Diameter	12.0 inches
Payload	75.8 pounds

The required performance and objectives given above are met by the JPL rocket engine designated the Starfinder.

Control Subsystem

The control subsystem consists of the components necessary to establish the desired longitude, to maintain a synchronous orbital velocity, and to orient the satellite spin axis from boost attitude to operating attitude. The subsystem consists of two pulsed-jet hydrogen peroxide propulsion units for velocity and orientation control, solar sensors, and control circuits. An accelerometer for indicating firing is part of the control subsystem.

Electrical Power Subsystem

The electrical power subsystem consists of silicon solar cells, a nickel-cadmium battery, combined voltage regulators and switches. The subsystem is capable of supplying approximately 31 watts without drain on the battery when the satellite is not shadowed by the earth. The solar cells are arrayed on the external cylindrical surface. In the operating configuration, the sunline will be within 25 degrees of normal to the axis of the cylinder, a condition met by suitable choice of launch time.

Structure

The spacecraft structure includes a central, circular member with the separation flange for the Delta third stage at one end and attachment fittings for the apogee motor at the other end. A circularly symmetric bulkhead with reinforcing ribs on the separation side is attached to the member. The electronic units, gas tanks, and four solar cell panels are mounted to the bulkhead.

The separation end of the central circular member carries the folding communication antenna. The whip antennas are attached at the apogee motor end of the solar cell panels. Both ends are closed by thermal shields; the shield at the antenna end also serves as an antenna ground plane.

COMMUNICATION SUBSYSTEM

The communication subsystem is composed of two wide-band transponders, with bandwidths of 4.5 Mc and 13 Mc at the half-power points. In addition the bandwidth of the 13-Mc channel can be switched by command to 50 kc. The ground station characteristics are shown in Table II-1.

In addition to relaying angle-modulated signals, the communication transponders transmit to the ground a reference signal derived from the master oscillator, which is used on the ground in a range and range-rate measurement system. The frequency of this reference signal must fall in the passband of the ground receiver low-noise preamplifier.

The communication subsystem employs a frequency translation type of transponder having a 2-watt (nominal saturated power output) traveling-wave tube for its power amplifier. The main beam of the transmitting antenna will be broad enough to encompass the earth at all times.

Table II-1

Ground Station Characteristics.

Transmitter power	20 kw
Transmitter antenna	30-foot-diameter parabola, 50 percent efficient, plane-polarized
Transmitter frequency	7360 ±5 Mc
Transmitter modulation	Angle modulation only (FM or PM)
Receiver frequency	1815 ±5 Mc
Receiver antenna	30-foot-diameter parabola, 50 percent efficient, plane-polarized
Receiver preamplifier bandwidth	10 Mc

The spacecraft power supply and thermal design allows for continuous operation of the communication system except during and shortly after periods of eclipse.

Transponder Design

The block diagram of a transponder designed to satisfy the above requirements is shown in Figure II-7. Some of the more important characteristics of the transponder are listed in Table II-2.

The transponders are interconnected in a manner which will allow either receiver to drive either transmitter. Only one receiver and one transmitter may be used at a time, the selection being made by ground commands. The interconnections among antennas, receivers, and transmitters are accomplished by stripline hybrid networks and a coaxial switch. These units, along with the receiver input mixers and preamplifiers, are packaged in the central member of the structure. All other units are mounted along the outer cylinder.

The signals received by the slot dipole antenna are introduced with less than 1db loss into the mixer of the "on" receiver. This is accomplished by the use of half-wave lengths of cable between

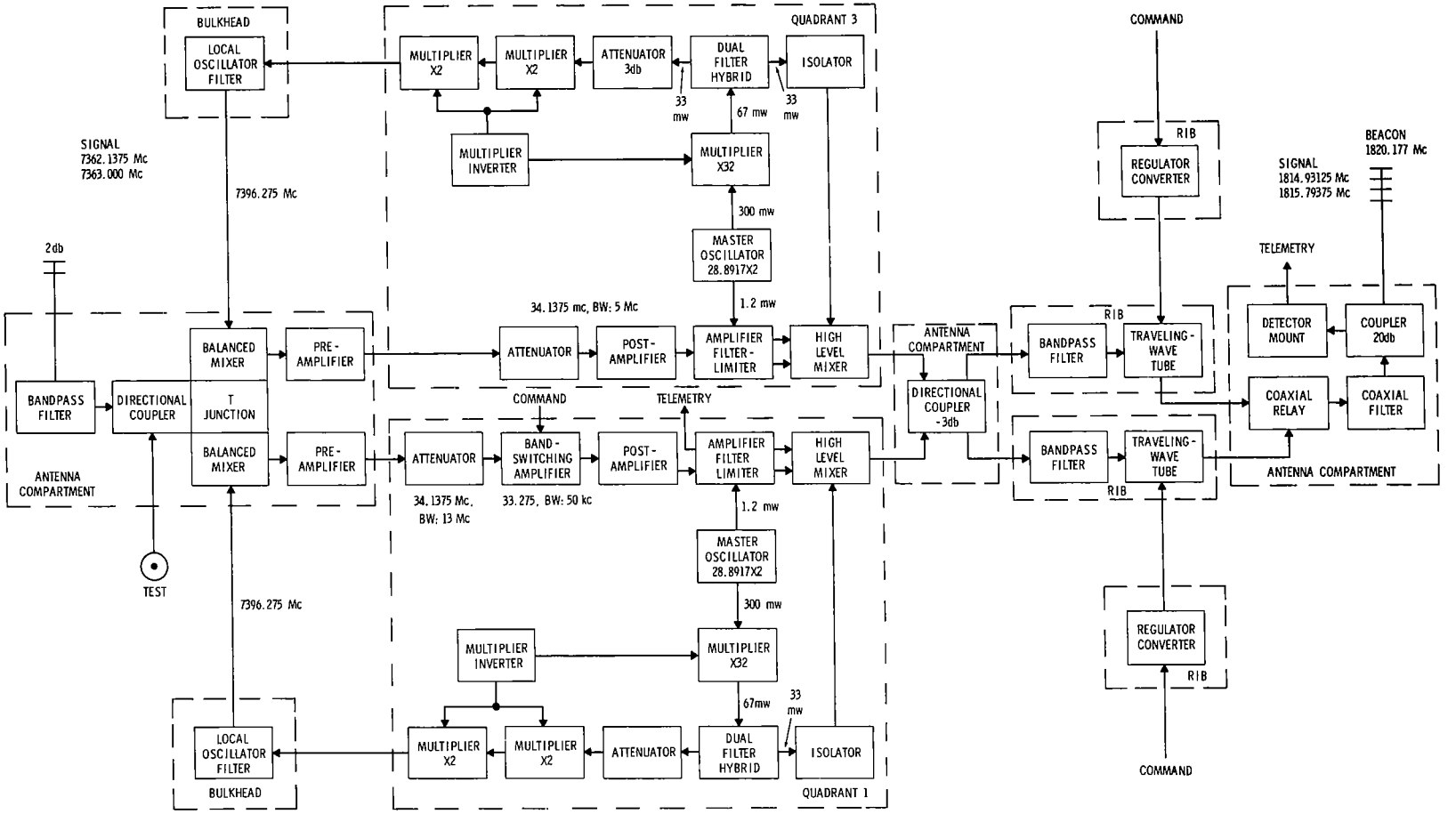

Figure II-7—Syncom C communications transponder.

the input junction and the mixers, and by back-biasing the crystal detectors of the "off" receiver, causing a high impedance to appear at its input junction. The received signals are converted to intermediate frequencies in the mixer with a reference frequency, 7396 Mc, that is the 256th harmonic of the master crystal oscillator which operates at 28.8917 Mc.

The frequency multiplication is accomplished in eight doublers, of which all but the first involve the use of varactor diodes connected push-push in efficient duo-mode networks. The first doubler uses a conventional transistor circuit. The IF signals are amplified in a linear amplifier consisting of a preamplifier having a 3 to 5db noise figure, and a postamplifier, with a combined gain of 90db. At this level, representing a power level of approximately 1 milliwatt, the signal is further amplified and limited.

Table II-2

Transponder Characteristics.

Transmitter type	Traveling-wave tube
Transmitter power output	2 watts (nominal)
Transmitter carrier frequencies	1814.931 Mc, 1815.794 Mc
Transmitter reference frequency	1820.177 Mc
Beacon power	100 milliwatts
Receiver type	Frequency translation
Receiver carrier frequencies	7362.1375 Mc, 7363.000 Mc
Receiver noise figure	10db
Receiver channel bandwidth	4.5 Mc, 13 Mc, 50 kc
Antenna type	Skirted collinear slot dipoles
Receiving antenna gain	2db (excluding losses)
Transmitting antenna gain	6db (excluding losses)
Total transponder weight	103 ounces (each)
Total transponder power consumption	14.6 watts

A portion of the master oscillator power is added to the received signal after it has been limited, and the combined signals are passed through a common limiter and introduced into the second mixer. The reference frequency of the second mixer is 1849 Mc, the 64th harmonic of the master oscillator. The output signal is filtered and introduced into the interconnecting hybrid which drives both transmitters at a power level of 1 milliwatt each.

The 13-Mc transponder is the same as the 5.0 Mc except for the difference in IF bandwidth. Also present in the 13-Mc transponder is a band-switching amplifier, which, on command, switches the transponder bandwidth from 13 Mc to 50 kc.

The transmitters are traveling-wave tubes having a signal gain of 33db, and nominally 2 watts of power output. The dc power for all tube elements is supplied through dc-to-dc converters, the inputs of which are regulated -24 volts. The power out of the "on" transmitter is directed to a collinear slot array antenna by a latching coaxial switch.

The 16 transistors of the "on" receiver draw approximately 1.4 watts from the regulated -24 volt bus. The "on" transmitter draws approximately 13.2 watts from this bus, for a total transponder power consumption of 14.6 watts.

Communication Subsystem Performance

The performance of the spacecraft communication transponder when operating in the full duplex mode is summarized in Table II-3. The ground station parameters are similar to those of the USNS Kingsport. A nominal transmitter power of 2 kw is assumed, although up to 20 kw is available if desired.

It is assumed that a FMFB receiver is used and that the peak carrier deviation is 40 kc when a 4-kc test tone is transmitted, resulting in a modulation index of 10. An IF bandwidth of 100 kc is adequate for this modulation index and therefore the reference noise bandwidth at the spacecraft transponder is assumed to be 100 kc. The actual transponder noise bandwidth may be greater than 10 Mc, depending on the transponder used.

The duplexing loss of 4.6db is a measured value for two equal carriers out of the traveling-wave tube (TWT). The saturated TWT power at the spacecraft antenna terminals is 2.0 watts for a single carrier. The ground antenna gain of 40.0db is a measured value for a 30-foot parabolic antenna and additional ground system losses of 2.0db are assumed. A feedback compression factor of 4 is assumed for the ground receiver resulting in a carrier-to-noise ratio in the IF of 12.3db. The receiver is thus operating close to its threshold when the noise contribution of the spacecraft is considered. It is assumed that preemphasis is used so that the noise spectrum out of the discrimination is approximately flat.

The resulting audio signal-to-noise ratio is about 36.9db. Higher values have been obtained from stations using 60-foot parabolic antennas.

During simplex operation (only one carrier at a time in the spacecraft), the final signal-to-noise ratio is increased by the duplex loss of 4.6db.

TELEMETRY SUBSYSTEM

The telemetry subsystem consists of two phase-modulated 136-Mc transmitters, two frequency-modulated, time-division-multiplexed encoders with analog telemetry inputs, and an antenna unit shared with the command subsystem by frequency diplexing. Block diagrams are shown in Figures II-8 and II-9.

Telemetry and Command Antennas

A turnstile antenna oriented at 25 degrees to the spin axis of the spacecraft is used for command and telemetry. Gain is essentially isotropic, the variations with spacecraft attitudes ranging from a maximum of +0.5db within 11 degrees of the perpendicular to the spin axis to a minimum of -3.2db at the worst axis orientation.

The antenna is constructed of four quarterwave whips at 90-degree intervals around the satellite circumference. The whips fold parallel to the satellite axis during ground handling and launch.

Table II-3

Signal and Noise Levels of Communication System.

Ground-to-Spacecraft Link		
Quantity	Value	Remarks
Transmitter power	33dbw	2-kw transmitter
Ground antenna gain	54.2db	30-foot parabola
Space attenuation, $\left(\frac{\lambda}{4\pi R}\right)^2$	-202.2db	λ = 0.132 foot
Spacecraft antenna gain	2.0db	Slot dipole
Received carrier power	-113.0dbw	
Noise power density	-228.6dbw/°K/cps	Boltzmann's constant
Effective receiver temperature, T	34.4db	10db noise figure
Receiver reference bandwidth, B	50.0db	100-kc bandwidth
Receiver noise, N	-144.2dbw	
Miscellaneous losses, L	5db	(Including atmospheric attenuation)
Receiver carrier-to-noise ratio, C/N	26.0db	

Spacecraft-to-Ground Link		
Quantity	Value	Remarks
Radiated power	1.6dbw	2 watts at antenna, -4.6db for duplexing
Spacecraft antenna gain	5.5db	Collinear slot array
Space attenuation, $\left(\frac{\lambda}{4\pi R}\right)^2$	-190.2db	λ = 0.52 foot
Ground antenna gain	40.0db	30-foot parabola, plane-polarized
Miscellaneous losses	2.0db	
Received carrier power	-148.3dbw	
Noise power density	-228.6dbw/°K/cps	Boltzmann's constant
Effective receiving system temperature	24.0db	250°K overall system temperature
IF bandwidth (FMFB receiver), B	44.0db	25-kc IF bandwidth for compression factor of 4
Receiver noise, N	-160.6dbw	
Carrier-to-noise ratio in IF (FMFB), $(C/N)_G$	12.3db	
Carrier-to-noise ratio including noise loading on ground-to-spacecraft link, $(C/N)_T$	11.9db	$\left(\frac{C}{N}\right)_T = \frac{1}{\left(\frac{N}{C}\right)_G + \left(\frac{N}{C}\right)_S \left(\frac{B_G}{B_S}\right)}$
Channel modulation index, M	10	
Audio signal-to-noise ratio, S/N	36.9db	$\frac{1}{2} M^2 \frac{C}{N} \frac{B}{B_a}$

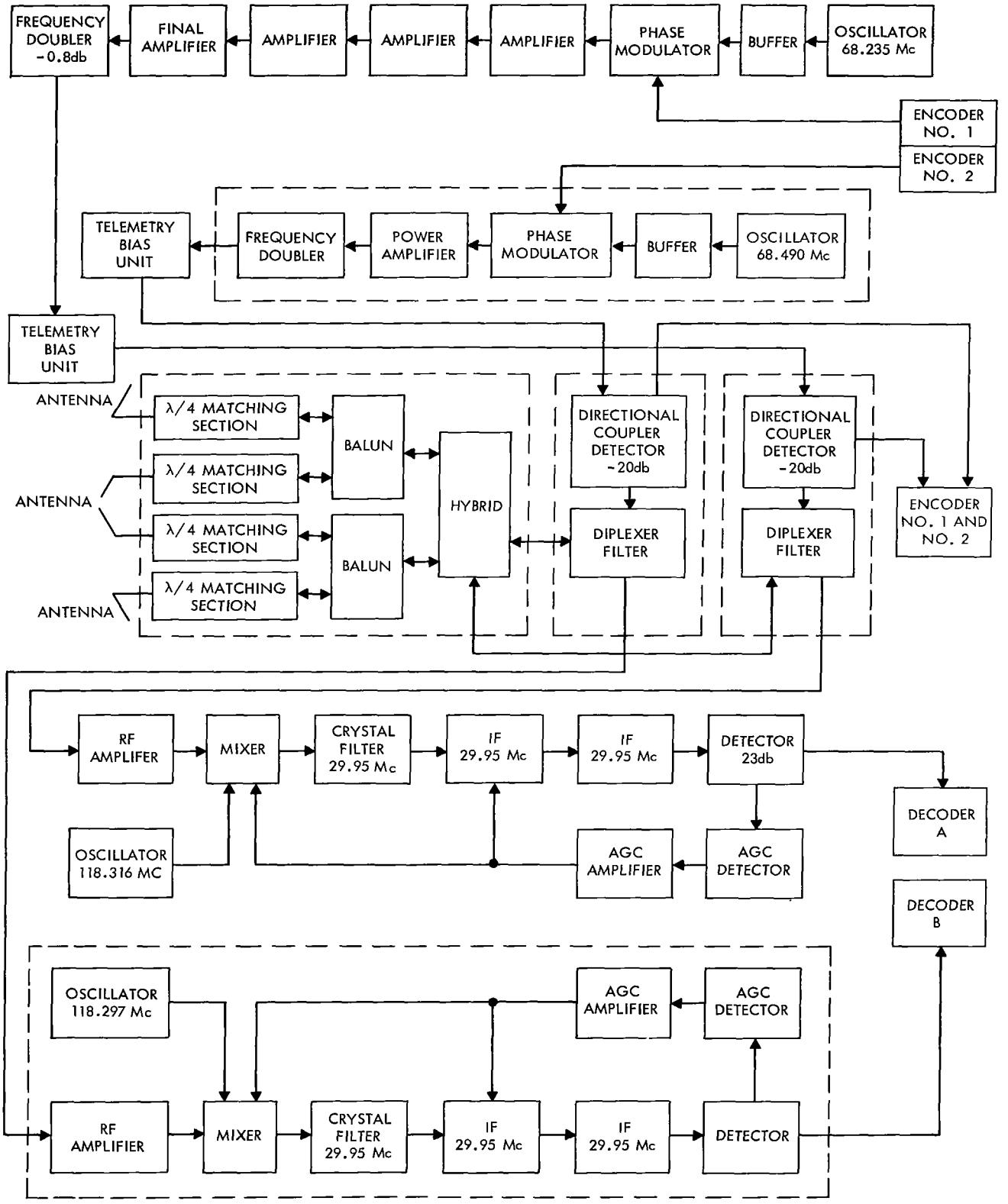

Figure II-8—Telemetry transmitter 1 and 2 and command receivers 1 and 2.

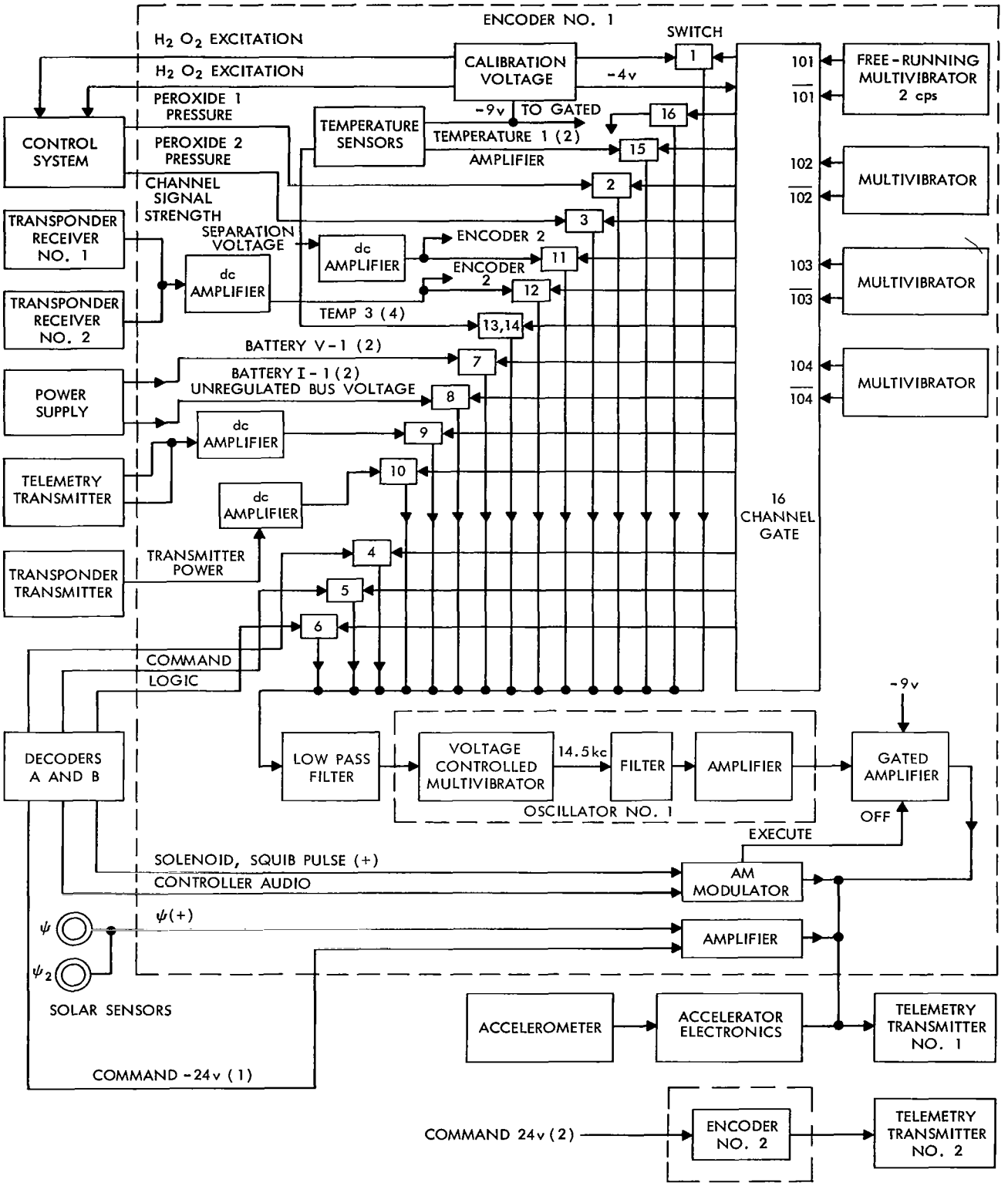

Figure II-9—Telemetry encoders.

Although this arrangement results in antenna detuning and mismatch, signal strengths during prelaunch checkout and liftoff tracking are sufficient because of proximity.

Since the spacecraft is between a quarter and a half wavelength in diameter at the command and telemetry frequencies, the dipole arms are fed from a balanced line. Thus each of the four whips tends to act independently as a monopole. The monopole separation is not large enough to introduce serious interference nulls in the radiation pattern.

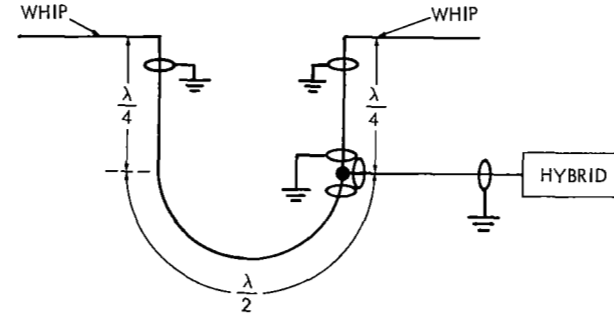

Figure II-10—Antenna balun.

Telemetry and Command Balun

The antenna balun (Figure II-10) consists of a half-wave coaxial section. The balun exhibits a four-to-one impedance stepup from the unbalanced end to the balanced ends, or a two-to-one impedance stepup to each of the two antenna ends.

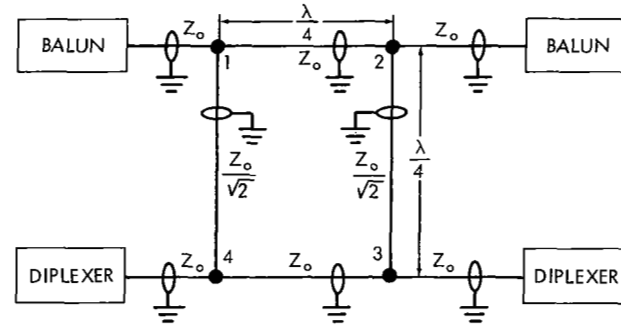

Figure II-11—Antenna hybrid.

Telemetry and Command Hybrid

The schematic diagram of the antenna hybrid is shown in Figure II-11. Input RF power at junction 1 produces half-power outputs at junctions 3 and 4, with zero output at junction 2. Thus the two antenna inputs are isolated from each other, as are the two diplexer inputs. This isolates the two command receiver inputs and the two telemetry transmitter outputs. Equal coaxial lengths are used between junctions 1 and 2 and the baluns. The inherent 90-degree phase difference between junctions 1 and 2 will provide the correct phase to the dipoles of the turnstile antenna.

Telemetry and Command Diplexer

A frequency diplexer is required to connect the telemetry transmitter and command receiver to the antenna without introducing excessive transmitter power into the receiver input. The rejection filter diplexer has the following characteristics:

Transmitter to RF output insertion loss	0.2db
Receiver to RF input insertion loss	1db
Transmitter to receiver isolation	> 60db
Receiver to transmitter isolation	> 20db

The isolation is shown graphically in Figure II-12.

Telemetry Transmitters

The telemetry transmitters consist of two 136-Mc, 1.6-watt transmitters. Both use a high-efficiency, varactor doubler in the output stage. Linear phase modulation by the tone encoder is provided.

The telemetry channel signal and noise levels are shown in Table II-4. Transmitter specifications are shown in Table II-5.

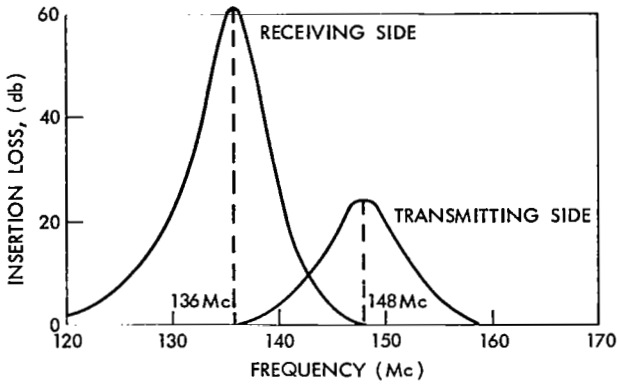

Figure II-12—Approximate diplexer characteristics.

Telemetry Encoders

The telemetry encoders consist of two identical circuits, each consisting of an electronic commutator, a voltage-controlled oscillator, and a gate-controlled output amplifier. A block diagram of the encoder system is shown in Figure II-9.

There are a total of 19 analog and pulse signals which are telemetered to the ground station. Most of these signals are redundant to both encoders. Table II-6 lists all the signals and the

Table II-4

Signal and Noise Levels for Satellite-to-Ground Telemetry Link (136 Mc).

Quantity	Value	Remarks
Effective radiated power	-2.5dbw	
Space attenuation	-167.4db	1.35×10^8-foot range
Ground antenna gain	23.0db	Nominal for TACO antenna
Miscellaneous ground losses	1.0db	
Receiver noise figure	2.0db	
Received carrier power	-147.9dbw	
System noise temperature	30.1db	1028°K including 1000°K galactic temperature referred to receiver input
Noise power density	-198.5dbw/cps	
Carrier modulation index	1.2	
Carrier tracking loop bandwidth	20.2db	106 cps
Carrier-to-noise in carrier tracking loop	26.9db	Modulated carrier
Fraction of power in first sideband pair	0.497	$2\left[J_1(1.2)\right]^2$
Subcarrier demodulation output filter bandwidth	20 cps	Low pass filter
Carrier-to-noise at output of subcarrier demodulator	31.6db	

encoder through which they are sent. All the analog inputs are sequentially multiplexed at a rate of four channels per second and they frequency-modulate a voltage-controlled oscillator which has a 14.5-kc center frequency. The solenoid-operated pulses amplitude-modulate the controller audio pulse which is a 9.745-kc note. The sun sensor outputs, which are dc pulses, directly modulate the telemetry transmitter through an amplifier. The accelerometer output is a 1.5-kc signal that directly modulates the telemetry transmitter through an amplifier.

Table II-5

Telemetry Transmitter Characteristics.

Frequency	136.470 Mc (TM 1) 136.980 Mc (TM 2)
Output impedance	50 ohms
RF power output	1.1 watts
Modulation index	1.2 radians
Spurious output	< -30dbw
Oscillator stability	±0.003 percent
Voltage	-24 volts
DC input power	5.5 watts
Weight	8 ounces each
Operating temperature	20 to 100°F

COMMAND SUBSYSTEM

The command subsystem consists of two amplitude-modulation 148-Mc command receivers and a redundant pulse-tone-operated decoder with associated switching circuitry. The antenna unit is shared with the telemetry subsystem, and a description of the antennas, baluns, hybrid, and diplexers is given in the preceding section. A block diagram of the command receivers appear in Figure II-8 rather than separately in this section, to illustrate more clearly the interconnections between the telemetry and command subsystems. The command decoder and switching circuits are shown in Figure II-13.

Command Receiver

The command receiver consists of two identical single-conversion AM receivers each having about 125db gain. Both receivers operate continuously and independently. The output of receiver 1 is fed into decoder A and the output of receiver 2 is fed into decoder B. The maximum audio modulation frequency is about 11 kc. Local oscillator stability is ±3.003 percent or ±3.5 kc. Assuming a ground command transmitter stability of ±0.001 percent or ±1.5 kc and doppler shift of -0.0034 percent or -5 kc, the required IF bandwidth is 37 kc. A 60-kc bandwidth half-lattice crystal filter preceding the IF amplifier provides a stable IF center frequency and noise bandwidth for AGC noise threshold.

The command receiver signal and noise levels are shown in Table II-7. Table II-8 shows the receiver specifications.

Command Decoder

The command decoder consists of the circuitry required to process the ground commands. The command functions along with the number of pulses required to actuate it are shown in Table II-9. A block diagram of the decoder unit is shown in Figure II-13.

Table II-6

Telemetry Inputs.

Multiplex Inputs				
Time Position	Encoder	Function	Form	Remarks
1	1, 2	Sync, calibrate	dc	5 volts from zener diode
2	1, 2	Peroxide pressure 1	dc	Strain gage pressure transducer
3	1, 2	Peroxide pressure 2	dc	Strain gage pressure transducer
4, 5, 6	1, 2	Decoder counter logic	dc	Readback of decoder setting
7	1	Battery voltage	dc	Scaled voltage from battery 1
7	2	Battery Voltage	dc	Scaled voltage from battery 2
8	1	Unregulated bus voltage	dc	Scaled voltage derived from current regulator
8	2	Unregulated bus voltage	dc	Scaled voltage derived from current regulator
9	1, 2	Telemetry transmitter power	dc	Directional coupler output
10	1, 2	Transponder transmitter power	dc	Directional coupler output
11	1, 2	Separation indication and transponder channel received power	dc	Bias on channel before separation and scaled detected signal derived from IF signal strength of operating receiver
12	1, 2	Transponder channel received power	dc	Scaled detected signal derived from IF signal strength of operating receiver
13, 14	1	Temperature 3	dc	Sensor located on apogee motor
13, 14	2	Temperature 4	dc	Sensor located on solar panel 1
15	1	Temperature 1	dc	Sensor located near TWT 2
15	2	Temperature 2	dc	Sensor located on hydrogen peroxide tank mount
16	1, 2	0 volt	0	Calibration

Other Inputs			
Encoder	Function	Form	Remarks
1, 2	Gas solenoid switch operate	Pulse	Modulates controller tone
1, 2	ψ signal	Pulse	Modulates telemetry transmitter
1, 2	ψ_2 signal	Pulse	Modulates telemetry transmitter
1, 2	Execute pulse	Pulse	Indicates generation of execute signal
1, 2	Controller audio	AC signal	Indicates arrival of execute command
1	Accelerometer	AC signal	Measurement of acceleration forces on spacecraft

The decoder utilizes two redundant groups of three tone-operated channels. Power is applied continuously to one channel (enable) in each group from the regulated bus which also supplies the command receivers.

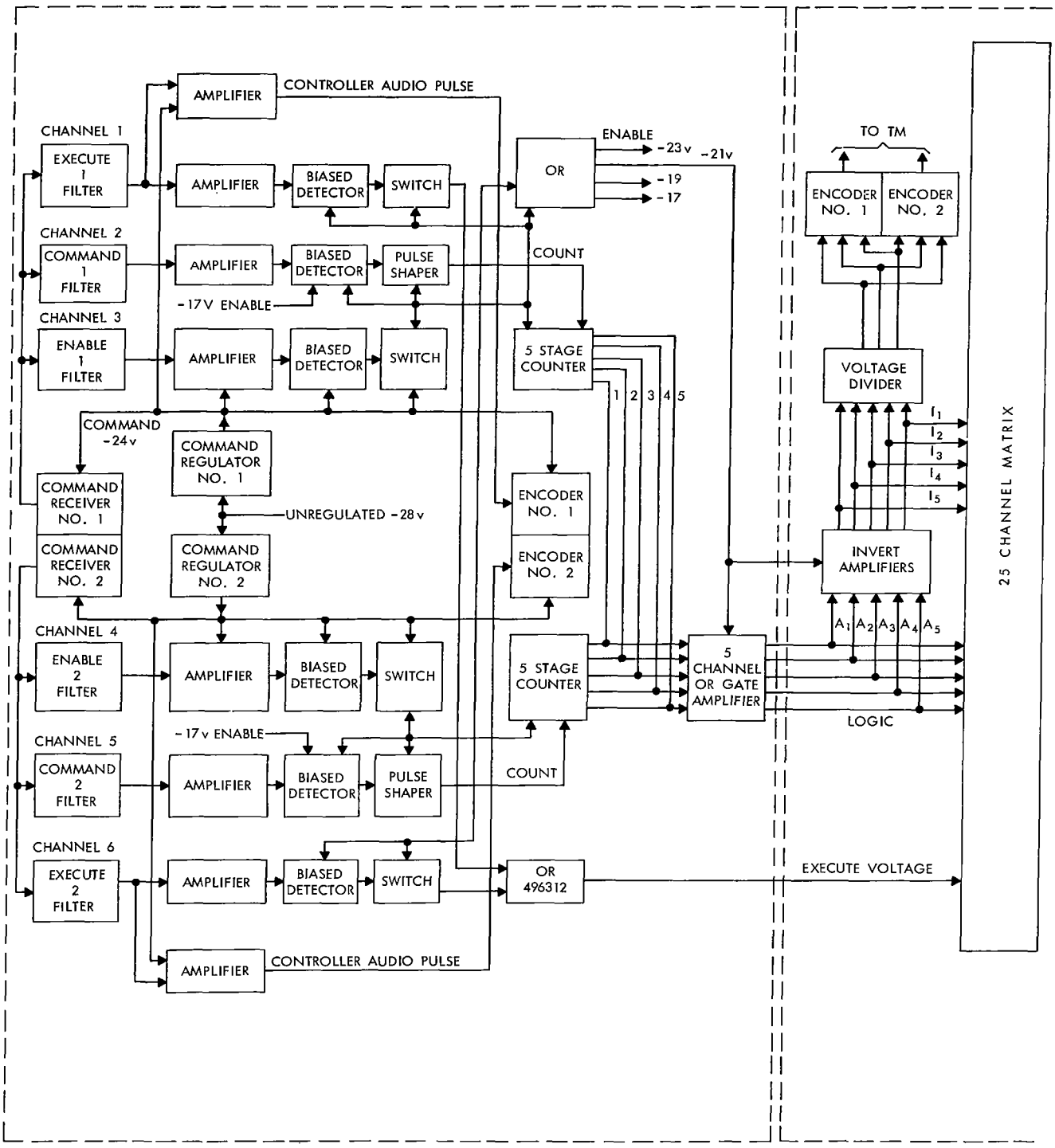

Figure II-13—Command decoders and switching.

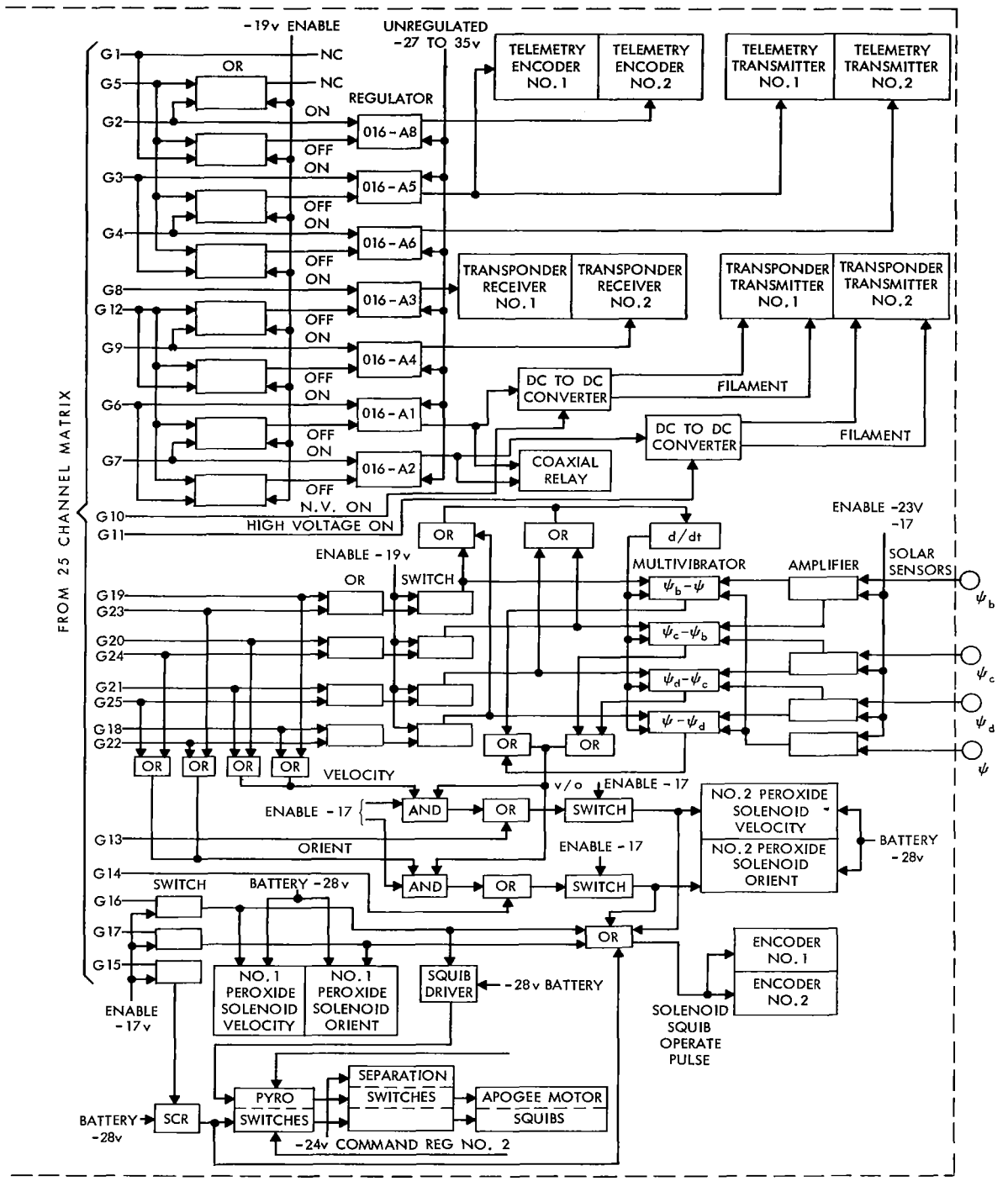

Figure II-13 (Continued)—Command decoders and switching.

Table II-7

Signal and Noise Levels for Ground-to-Satellite Command Link (148 Mc).

Quantity	Level	Remarks
Transmitter power	34.8dbw	3-kw transmitter
Ground antenna gain	14db	YAGI
Space attenuation, $(\lambda/4\pi A)^2$	-168db	1.35×10^8 foot range
Satellite antenna gain	-4.5db	
Diplexer loss	-2.5db	
Received carrier power	-126dbw	
Noise power density	-228.6dbw	Boltzmann's constant
Effective receiver temperature	29.4db	6db noise figure
Receiver IF bandwidth, B	47.8db	60 kc
Receiver noise, N	-151.4db	
Receiver carrier-to-noise ratio, C/N	+25.4db	
Channel modulation index factor, $(1/2\ M^2)$	-9db	M = 50 percent/tone
Tone channel bandwidth ratio B/B_a	23db	300-cps bandwidth tone channel
Tone signal-to-noise ratio, S/N	+39.4db	$1/2\ M^2\ C/N\ B/B_a$

While a tone is being detected by either enable, an electronic switch is closed, connecting the regulated bus to the other two channels and command decoder controlled by that enable.

The other two channels in a group are the command channel and the execute channel. When a tone is detected on the command channel, a change of dc state is produced at the audio detector output. When the tone is removed, the detector output assumes its original state. Thus, by alternately presenting and removing a tone on the logic channel, a series of pulses is generated at the detector output. The pulses are fed through a pulse shaper to the first stage of a five-stage binary counter. Each pulse received from the shaper advances the counter one position. The audio modulation frequencies for the enable command and execute channels are shown in Table II-10.

Table II-8

Command Receiver Characteristics.

Carrier frequency	148.260 Mc
RF input impedance	50 ohms
Noise figure	6db
RF input overload	-70dbw
IF bandwidth	60 kc
Image rejection	60db
Oscillator stability	±0.003 percent
DC voltage	-24 volts
DC power	500 mw
Weight	10 ounces
Operating temperature	20 to 100°F

The counter is composed of five two-transistor bistable multivibrators with pedestal gating. A special circuit in the counter ensures that when the enable channel connects it to the regulated supply voltage, all of the flip-flops are reset. The desired command is then selected by sending the correct number of pulses on the command channel. The command selected can then be checked on the ground as the counter position is telemetered.

The outputs from each counter are then connected together in five OR amplifiers so that either counter can drive the decoder outputs independent of the other. The five outputs from the OR

Table II-9

Command Functions.

Count	Function		Channels 4	5	6	Count	Function	Channels 4	5	6
0	- (enable positive)		4.2	4.2	4.0	15	-	3.1	4.2	0.
1	-		0.6	0.6	0.	16	-	3.1	4.2	4.0
2	Telemetry encoder	2 off	0.6	0.6	4.0	17	Lateral peroxide jet 2	1.9	0.6	0.
3	Telemetry encoder	2 on	0.6	3.1	0.	18	Axial peroxide jet 2	1.9	0.6	4.0
4	Telemetry transmitter and encoder	1 on, transmitter 2 off	0.6	3.1	4.0	19	Apogee engine squib	1.9	3.1	0.
5	Telemetry transmitter	2 on, 1 off	0.6	1.9	0.	20	Lateral peroxide jet 1, apogee engine squib	1.9	3.1	4.0
6	-		0.6	1.9	4.0	21	Axial peroxide jet 1	1.9	1.9	0.
7	Telemetry off		0.6	4.2	0.	22	-	1.9	1.9	4.0
8	Transponder transmitter filament	1 on, 2 off	0.6	4.2	4.0	23	Velocity jet $(\psi - \psi_b)1$	1.9	4.2	0.
9	Transponder transmitter filament	2 on, 1 off	3.1	0.6	0.	24	Velocity jet $(\psi_b - \psi_c)4$	1.9	4.2	4.0
						25	Velocity jet $(\psi_c - \psi_d)3$	4.2	0.6	0.
10	Transponder receiver	1 on, 2 off	3.1	0.6	4.0	26	Velocity jet $(\psi_d - \psi)2$	4.2	0.6	4.0
11	Transponder receiver	2 on, 1 off	3.1	3.1	0.	27	Orientation jet $(\psi - \psi_b)1$	4.2	3.1	0.
12	Transponder transmitter high voltage	1 on	3.1	3.1	4.0	28	Orientation jet $(\psi_b - \psi_c)4$	4.2	3.1	4.0
						29	Orientation jet $(\psi_c - \psi_d)3$	4.2	1.9	0.
13	Transponder transmitter high voltage	2 on	3.1	1.9	0.	30	Orientation jet $(\psi_d - \psi)2$	4.2	1.9	4.0
14	Transponder off		3.1	1.9	4.0	31	-	4.2	4.2	0.0

Table II-10

Audio Modulation Frequencies.

ENABLE 1	8.673 kc
ENABLE 2	7.700 kc
COMMAND	11.024 kc
EXECUTE	9.745 kc

amplifiers are then inverted so that the amplifier outputs along with the inverted outputs are available to provide the 10 binary inputs required to produce 32 commands. A logically equivalent scheme is to provide five or more OR amplifiers for the complementary outputs of the bistable multivibrators. However, the AND gating and output switch amplifiers are contained in a different electronic package from the counters and OR amplifiers so that no circuitry is added and five interpackage leads are eliminated by the indicated technique.

The command gates are standard diode AND gates driven by the OR amplifier and inverter outputs. These gates drive the amplifier/switches which provide the command decoding outputs.

Even with a command selected by the counter, the gates suppress command execution until the execute signal is received on the third decoder channel. A special provision of this third channel allows the undetected audio tone to go straight to the telemetry transmitter while the execute signal squelches the operating encoder.

CONTROL SUBSYSTEM

This control subsystem incorporates the following equipment, described in the subsequent paragraphs of this section:

1. Two hydrogen peroxide control units,
2. Solar sensors for spin rate and attitude determination, and
3. Ground-based synchronous controller to control the pulsing of the cold gas jet unit.

In addition, the telemetry subsystem and the command subsystem are employed in control of the spacecraft.

Operation of Control Subsystem

The hydrogen peroxide units are intended for adjustment of the spacecraft attitude and orbital velocity. The control of orbital velocity provided permits control of orbital period and hence of the longitudinal position as well as control of orbital eccentricity and inclination within the limits of the capacity of the system. Attitude control is needed after apogee motor boost to align the spin axis normal to the orbital plane. In the Syncom A-27 mission, this control will also be used prior to apogee boost to obtain the correct direction for the latter.

The sequence of orbit and attitude control operations planned for the A-27 launch may be described generally as follows: The elements of the transfer orbit are determined from range, range-rate, azimuth, and elevation data (obtained using the spacecraft transponder in conjunction with the USNS Kingsport and Clark AFB tracking stations) plus Minitrack direction cosine data derived

from the spacecraft 136-Mc telemetry signal. From the orbital elements the correct attitude and ignition time for the fourth stage are computed, taking into account the capability of the hydrogen peroxide control unit for subsequent corrections as well as possible errors in the apogee boost.* The spin axis attitude is determined from solar sensor and polarization angle data and from the direction of the third-stage boost. The latter is derived from nominal conditions, conditions computed from Bell Telephone Laboratories guidance data for the trajectory before third-stage burning, and the elements of the transfer orbit.

From the known initial and desired final attitude for apogee boost, the data required for reorientation are derived and the spacecraft is precessed to the required attitude by ground command from the Lakehurst station as the spacecraft approaches its second apogee. Nominal reorientation angle is 8.9 degrees. The proper attitude is verified by solar sensor and polarization data from Lakehurst, and subsequently from Clark AFB and the Kingsport. Ignition of the apogee motor will occur at the third northward Equator crossing, which nearly coincides with the third apogee.

For nominal performance, the orbit resulting from apogee motor boost will have an eastward drift rate of 7.5 degrees per orbit, and a period of approximately 8 days will be required to reach the desired longitude of 176 °E. If the transfer orbit energy is sufficiently above normal, the orbit resulting from apogee motor boost may have a westward drift. In this case, one of the axial hydrogen peroxide jets will be used either 0.5 or 1.5 orbital revolutions after apogee boost to provide an eastward drift.

The apogee of the nominal orbit after fourth-stage boost nearly coincides with the position at boost and is 630 n. mi. above the radius of a circular synchronous orbit. The perigee after apogee motor boost is 1240 n. mi. below the latter circular synchronous orbit radius. If the orbit were made synchronous by application of control at the apogee position the orbit would have an eccentricity of 0.02769. This eccentricity can be removed by two velocity increments of approximately 75 fps each, with the first applied at the apogee and the second at the perigee, giving a truly stationary orbit.†

Procedure subsequent to initiation of the desired eastward drift will depend on the amount of hydrogen peroxide which is still available and on the drift rate and eccentricity. It is preferred to leave the spin axis in the same attitude as at fourth stage ignition until the orbit is nearly at the correct longitude, synchronous, and circular. For the nominal condition, the most efficient procedure is to permit the satellite to overshoot the desired longitude (to the east), raise the perigee to the circular synchronous radius with a velocity increment from an axial jet of approximately 147 fps, which results in a westward drift rate, and subsequently, bring the orbit to synchronism at the desired longitude by application of axial jet control at the perigee. This procedure combines corrections for orbital period, inclination, and eccentricity. Alternatively, the orbit may be

*This computation includes the selection of one of five possible modes of operation; the selection depends primarily on the error in transfer orbit energy with respect to the nominal.

†Tradeoff studies show that for nominal performance, the total control requirement for a stationary final orbit is nearly independent of the initial apogee altitude, as long as the apogee motor boost occurs above the radius of the circular synchronous orbit.

approximately synchronized and the spin axis reoriented prior to correction of eccentricity with a pulsed lateral jet, with some fuel penalty.

After reorientation, the lateral hydrogen peroxide jets will be pulsed for fine corrections to longitude, drift rate, and eccentricity. The axial jets may be used in the pulsed mode for minor attitude corrections, and in the continuous mode for limited corrections to the inclination.

Operation of Pulsed Mode

Since the spacecraft is a spin-stabilized vehicle, the pulsing of the gas jets must be synchronized with the spin rate. Further, the impulses must take place at the time the spacecraft is in the proper roll attitude for the orientation and velocity change to take place in the desired direction. Solar sensors are incorporated in the design to determine the attitude of the spacecraft relative to the sunline. Their location on the spacecraft is shown in Figure II-14, which also indicates the location of the orientation and velocity jets. Figure II-15 shows the discrimination capability of the sun sensors. In the synchronous controller mode of operation, the outputs of the redundant ψ and ψ_2 sensors are telemetered to the ground.

The ψ sensors are oriented so that the plane of the beam is parallel to the spin axis. The time interval between pulses from these sensors is a direct measurement of spin period. The ψ_2 sensors are mounted so that their beam plane intersects the ψ beam plane at an angle of 35 degrees and the intersection of the two beam planes is perpendicular to the spin axis. The angle between the sunline and the spacecraft spin axis is determined by the time interval between the ψ and ψ_2 pulses and knowledge of the spin rate. The time interval between the ψ and ψ_2 pulses is measured and the angle computed by the synchronous controller described later in this section.

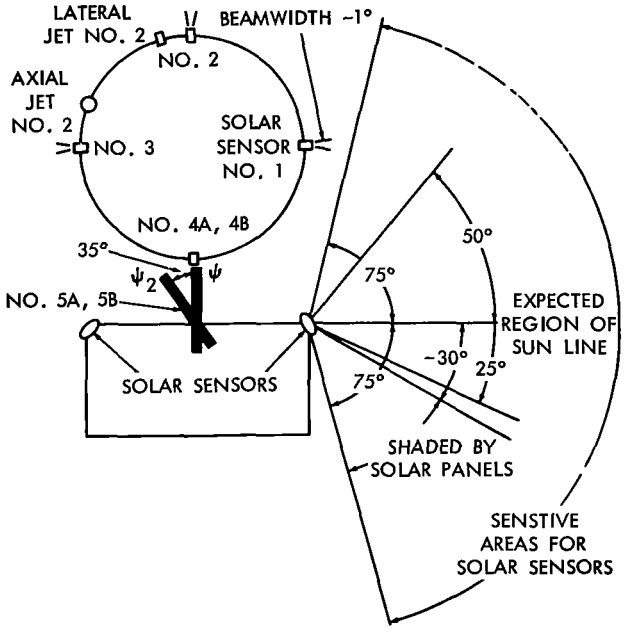

Figure II-14—Pulsed mode system geometry.

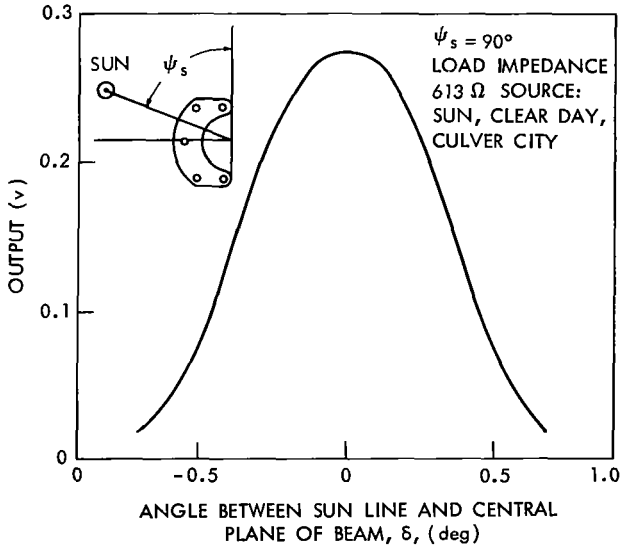

Figure II-15—Discrimination capability.

Since the synchronous controller mode of operation depends on the telemetering of the solar sensor pips, an additional, but less efficient, back-up mode of operation has been included which can be employed in the absence of telemetering. This mode of operation, the quadrant mode, employs the ψ sensor as well as three other solar sensors mounted at 90-degree intervals around the spin axis with their beams parallel to the spin axis. These four beams define quadrants of the spin angle relative to the sunline. If the lateral or axial jet is pulsed during one of these quadrants, the spacecraft will accelerate or precess with a known relation to the sunline since these quadrants bear a known geometric relation to the velocity and attitude jets. The quadrant to be employed is selected from the ground. The jet to be actuated (axial or lateral) is also selected from the ground. Bistable multivibrators connected to the various sensors and actuated by the sensor pulses turn the jets on and off during transit through the appropriate quadrant. The quadrant mode operate with hydrogen peroxide unit 2.

Probability of Obtaining Synchronism

The probability of obtaining synchronism is the most important performance criterion of the Syncom orbit control and orientation system. The 1σ value of the expected error in orbital velocity at burnout of the apogee motor is approximately 225 fps. The velocity increment available from the control subsystem is 560 to 600 fps, depending on method of usage. Thus, the capability of the control subsystem indicates a probability of between 95 and 97 percent of being able to achieve synchronous velocity without consideration of limitations of time to reach final nodal longitude and without reserves for stationkeeping.

Synchronous Control

As mentioned previously, pulsing of the axial or lateral jets must be synchronized with the spin rate of the spacecraft and also must take place at the proper roll angle to precess or change velocity in the desired direction. In the synchronous controller mode, proper pulsing is obtained on command from the ground using a synchronous controller.

The synchronous controller is a rotating drum contactor driven from a variable frequency oscillator and power amplifier. The frequency of this oscillator is controlled by the time interval between the ψ solar sensor output pulses which are telemetered from the spacecraft. Thus the frequency of rotation of the synchronous controller drum is essentially the same as the frequency of rotation of the spacecraft.

The correlation of the frequencies would be exact were it not for time delays in the system. Since the spin frequency of the spacecraft will change slowly during precession or velocity correction (the exact value depending on the accuracy of alignment of the attitude and velocity jets), monitoring of the output of the driving oscillator, with recalibration if its frequency shifts significantly, is sufficient to minimize this effect. The driving oscillator is designed to operate over a frequency range of approximately 65 to 108 cps which, through the 36:1 reduction in motor gearing, results in drum speeds of roughly 110 to 180 rpm. This range appears adequate to handle the 144 to 176 rpm spin speed expected from the TAD vehicle.

If the spin speed should be out of range of the present design (if, for example, one of the spin motors failed to fire), correct operation could still be attained after observing such variation by changing only the equipment on the ground. The output frequency of the driving oscillator will be continuously displayed.

In operation, the jet operating pulse, 60 degrees of spin rotation in width, generated by the synchronous controller will be transmitted through the command subsystem to the spacecraft (prior to issuance of the jet activation command). This pulse will in turn be transmitted, with essentially zero delay in the spacecraft through the telemetry subsystem from the spacecraft to the ground control station. During this same period, the ψ solar sensor pulse is telemetered to the ground. If the leading edge of the transponded jet operating pulse is adjusted through rotation of the movable contacts of the controller so that it coincides in time (as observed on an oscilloscope) with the ψ solar sensor pulse, the jet operating pulse will arrive at the spacecraft at the same time that the sunline falls within the ψ solar sensor beam. This condition represents a zero reference in which the effects of propagation delays are eliminated. Since the spin angle desired between the sunline and the start of the jet pulse can be determined from geometric considerations, rotation of the moving contacts of the controller through a calibrated dial to the desired angle ensures that the jet will be pulsed at the appropriate roll angle. Delays in value opening and closing which will be calibrated during system test will also be compensated in this adjustment.

Provision is also made in the synchronous controller to accurately measure the spin angle between the ψ and ψ_2 solar sensor pulses. A pulse generated by a movable contact is synchronized with the ψ solar sensor signal. A second pulse generated by another movable contact is synchronized with the ψ solar sensor signal. Neither pulse is transmitted to the spacecraft, and any differences in time delay of the synchronizing circuits is calibrated out. The difference between the dial readings associated with the generation of the two pulses then represents the spin angle between the ψ and ψ_2 pulses, which is translated into the angle between the sunline and the spacecraft spin axis.

A psi tracker is used in the input circuitry of the synchronous controller servo. This functions as a memory circuit to ensure controller lock-on if for some reason psi pulses from the spacecraft are lost. It also discriminates against noise and spurious signals from the telemetry receiver that might otherwise break controller lock-on.

The synchronous controller with its driving and power supply circuitry and the oscilloscope and synchronizing circuitry operate from 115 volts 60 cps ac power. A functional block diagram of the controller and auxiliary equipment is shown in Figure II-16. This system imposes no stringent requirements on the telemetry receiver but does require a high-quality receiver with phase-locked local oscillator and discriminator stages.

Hydrogen Peroxide Control Unit

Each hydrogen peroxide reaction control unit (when operating in a noncyclic control mode) is capable of providing a minimum effective velocity increment of 297 fps to a spacecraft having an

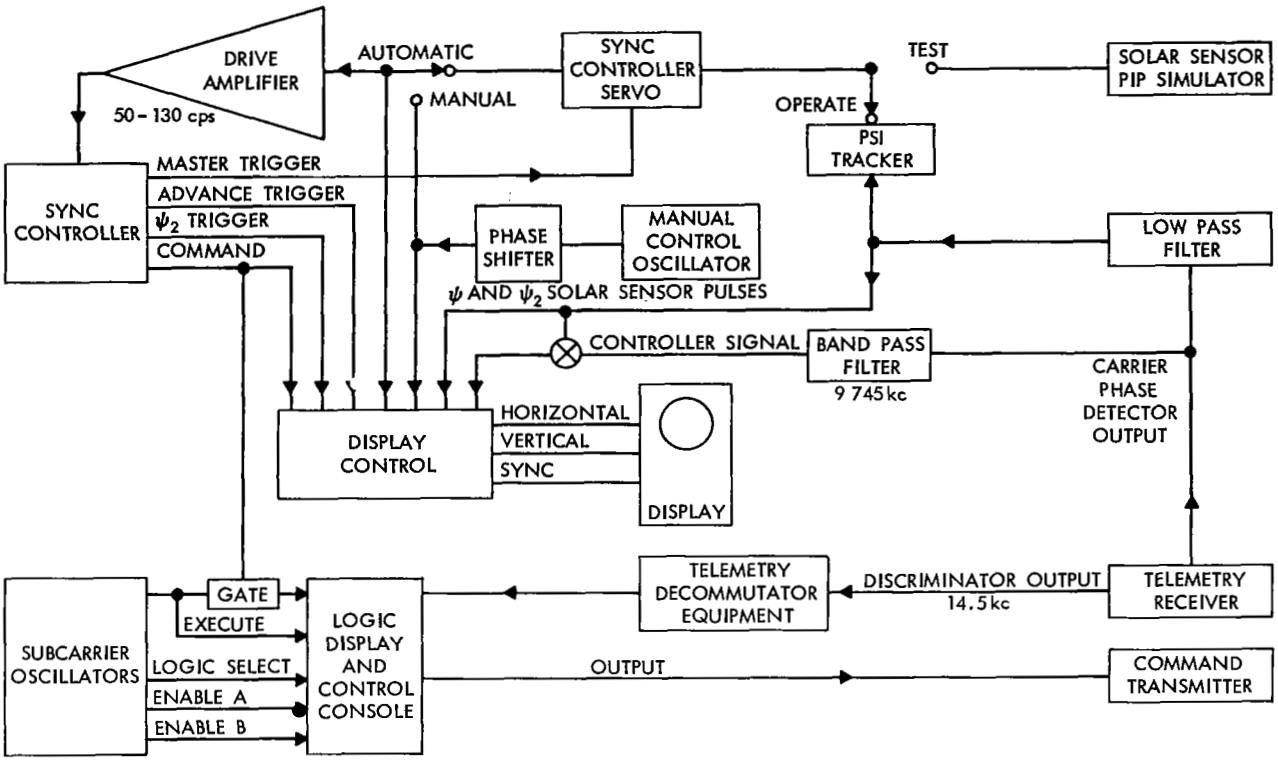

Figure II-16—Ground control equipment.

initial gross weight of 85.7 pounds (the gross weight includes the burnout weight of the apogee motor and the fully loaded weight of the hydrogen peroxide control unit). This capability is estimated to provide for orbital velocity corrections to achieve a nearly synchronous orbit while also providing for backup control capability, after spacecraft reorientation. The control, using 1, 2- to 3.1-pound force reaction jets, must therefore be capable of reliable operation in the space environment for up to one year following injection of the spacecraft into orbit.

Description of Unit

Each hydrogen peroxide reaction control unit consists of the following components:

1. Two spherical pressurized-propellant tanks mounted 180 degrees apart.
2. One combination fill, vent, and pressure relief valve for both the propellant and the pressurizing gas.
3. One low-thrust hydrogen peroxide thrust chamber (with integral heat barrier tube and propellant control valve) parallel to the spacecraft spin axis.
4. One low-thrust hydrogen peroxide thrust chamber (with integral heat barrier tube and propellant control valve) normal to the spin axis and thrusting through the spacecraft center of gravity.

5. One pressure transducer.

6. Associated manifolding and mounting clamps as required.

The unit components, except for the thrust chambers, are welded together as an integral system to minimize leakage. The thrust chambers are downstream from the propellant control valves and, therefore, have no effect on system leakage. Besides, if replacement of any thrust chamber is necessary, it can be accomplished without removing the unit from the spacecraft and incurring unit contamination.

For simplicity, light weight, and reliability, the propellant feed is designed to operate at an unregulated pressure as a "blowdown" system. The tanks are bladderless, since expulsion of the propellants and gas separation are aided by centrifugal forces created by the spacecraft spin.

During operation, the propellants move out toward the periphery of the spinning spacecraft. Therefore, the propellant manifolding is located at the outer periphery of the spacecraft adjacent to the solar panels. Equal propellant distribution in each tank (thus balance of the spinning spacecraft) is maintained by an interconnecting pressure equalization line located at the inner periphery of the spacecraft structure. This line is connected to each tank in a manner precluding the entrance of propellant during normal handling and operation.

The spacecraft structure is designed for installing each of the hydrogen peroxide control units as an integral unit. Each tank is attached to the main structure of the spacecraft with four fasteners at each end. Each thrust chamber is attached to the structure by three fasteners through an integral bracket. All propellant valves and manifold lines are attached to the structure by separate mounting clamps. Alignment of the thrust chamber nozzles is adjusted by shimming at the appropriate mounting points.

All components which are continually in contact with 90 percent hydrogen peroxide (with the exception of the valve poppet which is KEL-F) are fabricated from high-purity 1060 aluminum to minimize decomposition of the hydrogen peroxide during the one year of storage. The total unit weight, including mounting clamps, is approximately 9 pounds.

Before operation, each unit is loaded with a minimum of 4.9 pounds of 90 percent hydrogen peroxide. The tanks, approximately 60 percent full, are pressurized with nitrogen to approximately 200 psia at 70°F. The estimated steady-state performance of the unit as determined by analysis and past test results is shown in Table II-11. When operating under steady-state conditions, the control unit is capable of providing a minimum effective velocity increment of 297 fps to the spacecraft having an initial gross weight of 85.7 pounds.

Table II-11
Estimated System Performance of Each Hydrogen Peroxide Unit.

Thrust (vacuum)	
Initial at 70°F	3.1 lb_f
Final at 70°F	1.2 lb_f
Specific impulse	157 lb_f-sec/lb_m
Total impulse	754 lb_f/sec
Thrust coefficient	1.63

The mission operating sequence is as follows:

1. The unit will be "armed" as soon as the tanks are pressurized with nitrogen.
2. Actuation of the desired thrust chamber will be accomplished by a command signal from the Syncom ground control equipment.
3. Continuous or cyclic pulsed operation of either thrust chamber will be accomplished by either a continuous or a pulsed command signal for the desired period of time.
4. Cessation of electrical power to the propellant on-off valves will result in closure of the valves, and shutdown of the thrust chambers.

At the completion of the above sequence, the control system remains in a pressurized and "ready" state. It is capable of many starts and operation at any time during the desired one year period.

POWER SUBSYSTEM

Electrical power for the spacecraft is provided by solar cells and a rechargeable nickel-cadmium battery. Conservative design has been employed throughout the power subsystem with adequate allowance for power degradation to ensure reliable operation of the satellite for one year in orbit. The power subsystem, shown in Figure II-17, consists of the following:

1. The photovoltaic solar array is composed of 768 silicon solar cell (five-cell) modules mounted on an aluminum honeycomb substrate which forms the outer shell of the spacecraft. The cells are connected in 64 parallel electrical strings of 12 series-connected modules each. Isolating diodes connect each string to the unregulated voltage bus. The solar array provides the source of power for sunlight operation and for nickel-cadmium battery charging. The space efficiency of the solar cell modules at 77°F is 9.92 percent prior to degradation allowances.
2. Energy storage is provided by two nickel-cadmium batteries, each consisting of 22 hermetically sealed cells connected in series. These batteries supply power when the satellite is not illuminated during the boost period and during eclipses. They also supply energy for pulse loads such as for firing the apogee motor and the gas solenoids.
3. A manual disconnect removes the power sources from the voltage bus. When in the OFF position, the manual disconnect prevents the command receiver from discharging the batteries.
4. Combination regulator switches supply -24 volts dc power to the various units.
5. A dc-to-dc converter and a filament power supply for each traveling-wave tube supply power at appropriate voltages to all elements of the traveling-wave tubes.

Electrical Power Requirements

The electrical power requirements of the spacecraft are summarized in Table II-12. Both command receivers and decoders are on continuously from prelaunch through orbiting. All of the other loads will be keyed on and off by command. For orbit determination and control, the

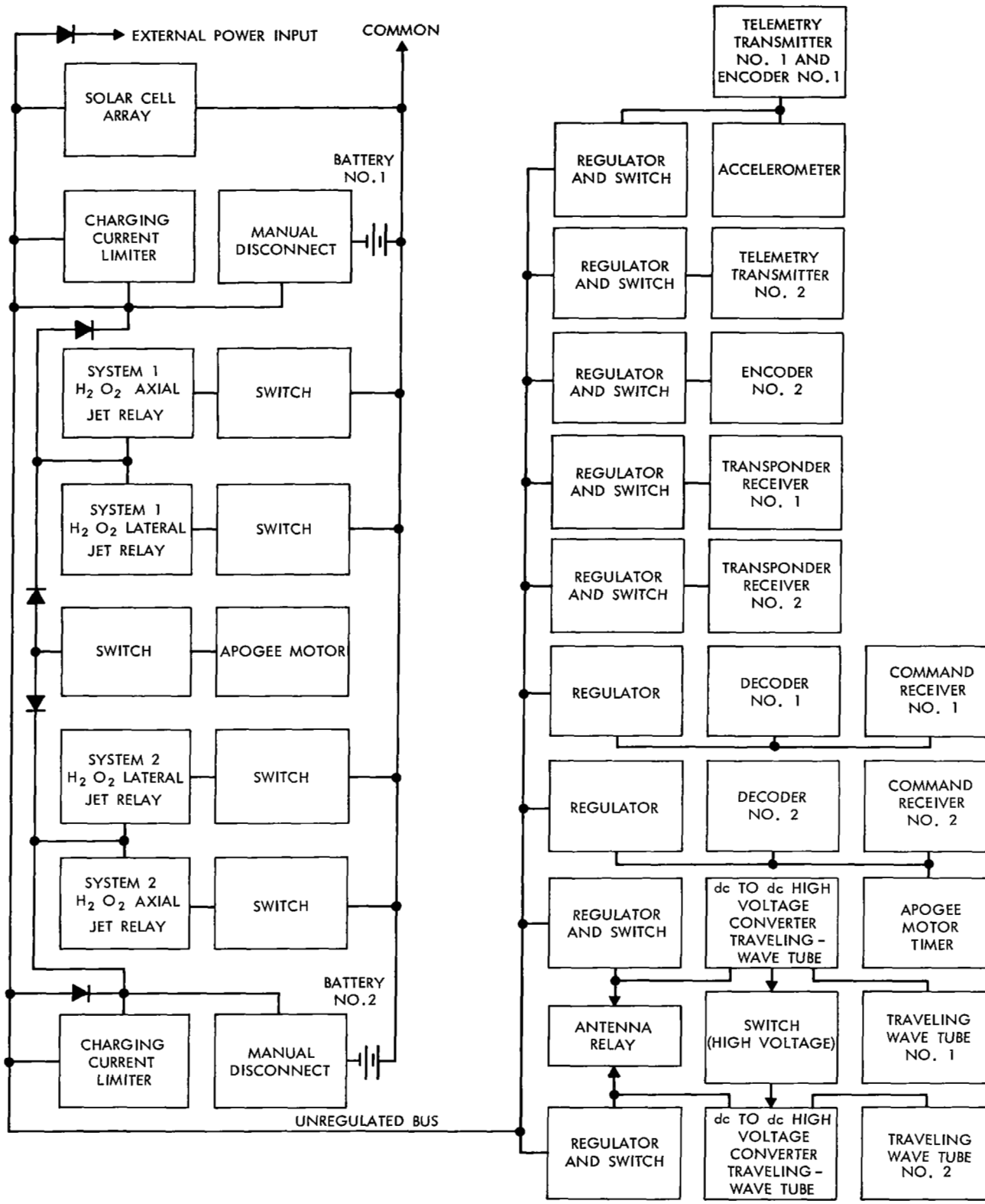

Figure II-17—Syncom power subsystem diagram.

Table II-12

Summary of Power Demands on Power Subsystem.

Load Condition	Power Demand in Watts at Regulated Bus, 24 volts
Continuous loads	
Two command receivers and two decoders	1.92
Keyed loads	
Telemetry subsystem 1 (telemetry transmitter, encoder 1, and accelerometer electronics)	7.5
Telemetry transmitter 2	0.7
Encoder 2	0.7
Transponder transmitter and high-voltage power supply*	13.2
Transponder electronics*	1.4

*Load indicated is for one of two similar units.

telemetry subsystem may be operated continuously. Prior to launch and up to the time after launching when the nose fairing is unfolded permitting illumination of the solar cells, the command receivers and one telemetry transmitter will be operated solely on battery power. The duration of this operation will be approximately 3 or 4 minutes.

When the satellite has been placed in its final orbit, either the transponder system or the telemetry system may be operated on command. When the satellite is eclipsed by the earth, only the command receivers will be operated on battery power.

Solar Cell Array

The silicon solar cells are N-P type with a true sunlight conversion of 9.92 percent in outer space (air mass zero). This efficiency includes the loss due to application of the 0.012-inch-thick glass coverslide. The outer surface of the slide has a magnesium fluoride antireflection coating vacuum deposit on its surface which reduces energy reflection from the slide in the 0.4 to 1.2-micron wavelength region. Five 1 by 2 cm cells are shingled together to form a module.

The solar cell modules are bonded to four 1/4-inch honeycomb panels which form the cylindrical external shell of the satellite. Each panel is 21.891 inches curved width by 15.5 inches high, providing an area of 339 $in.^2$ for module mounting. A total of 192 modules, or 16 parallel strings of 12 modules each, are mounted on each panel. Clearance is provided on the panel for the axial-jet nozzle.

Figure II-18 is a plot of solar array output voltage versus current with various load requirements noted on the graph. The curves are generated from tests of Syncom C solar array flight panel at Table Mountain on 17 March 1964.

Energy Storage System

The nickel-cadmium batteries provide (1) storage of electrical energy for operation during launching and during eclipse, and (2) energy capacity for pulse loads for apogee motor firings and operation of solenoids for the hydrogen peroxide system. The batteries consist of 22 hermetically sealed nickel-cadmium type "1/2 C" cells connected in series. The capacity of each battery is 0.77 amp-hr or 18.5 w-hr at an average discharge of 24 volts.

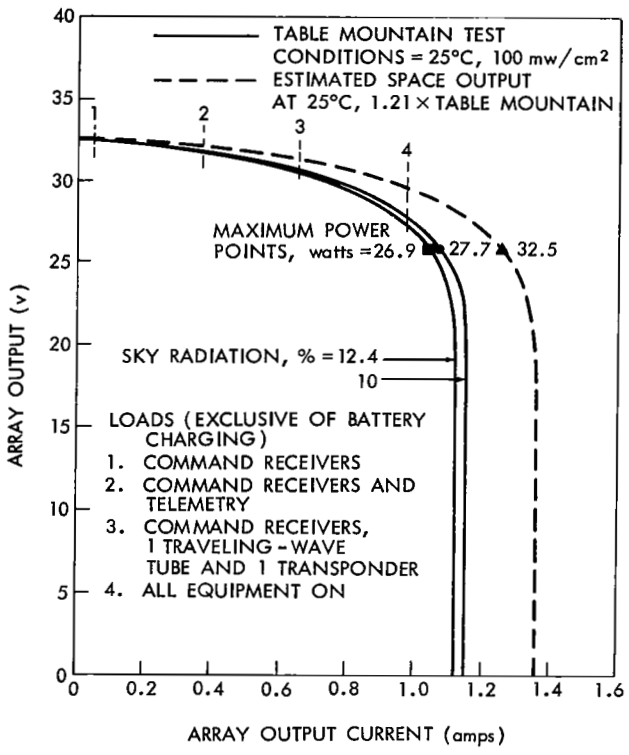

Figure II-18—Estimated solar array performance.

The battery has sufficient capacity to permit ground checks of all transmitters prior to launch and operation of one telemetry transmitter together with the command receivers until solar power becomes available after launch. A load of 8.6 watts, equivalent to the command receivers and one telemetry transmitter, can be sustained for a period of 2 hours at a battery depth of discharge not exceeding 50 percent.

Firing of the apogee motor requires a current surge of the order of 4 amperes for approximately 10 milliseconds for each igniter. Although this represents a high peak load, the resultant discharge in watt-hours of the battery is negligible.

In its 24-hour orbit, the satellite will be in full sunlight for most of its orbits in a year's time. During the equinoxes, the satellite will enter the earth's shadow. The maximum dark time is not expected to exceed 1.1 hours per day. During the eclipse time, the battery provides energy for operation of command receivers. Is is also possible to operate the telemetry subsystem during the eclipse without an appreciable battery discharge.

The two nickel-cadmium battery charging circuits, shown in Figure II-17, provide the charging current regulation essential for long-term reliable operation. Constant current charging at the minimum rate for reasonable battery recharge time will be employed wherever sufficient energy in excess of other load requirement is available from the solar cell array. A diode is used to bypass the charge regulation circuitry when battery power is required by the bus loads.

Regulators

The spacecraft contains nine series-type voltage regulators. Eight regulators maintain -24 volts ±1 percent at their output terminals for an input voltage variation between 25 and 26 volts,

as well as for normal variations in load current and temperature. Current capacities of all nine regulators will vary with the individual load requirements. As shown in Figure II-14 seven of these regulators also function as load switches. The two remaining regulators supply the loads which are continuously energized.

All nine regulators sense load current as a form of fault protection. The seven command-controlled regulators automatically shut off with excessive load current. They may be turned back on by command to see if the overload still persists. Curves of the output voltage versus current for each of the regulators are shown in Figure II-19.

DC-to-DC Converters

The power requirements of each traveling-wave tube are supplied by a dc-to-dc converter and a dc-to-ac converter. The dc-to-ac unit supplies filament power, while the other unit supplies power to the tube cathode, anode, and collector circuits. The tube helix is operated at ground potential. Each of the converters is a saturable core squarewave oscillator, with rectified outputs. Efficiencies are approximately 90 percent. The total load, consisting of one traveling wave tube and its associated power supplies, dissipates 13.2 watts. One command turns on the filament supply and a separate command turns on the high-voltage supply. A 4-minute delay circuit in the ground control station protects the tube from the destructive effects of cold cathode operation.

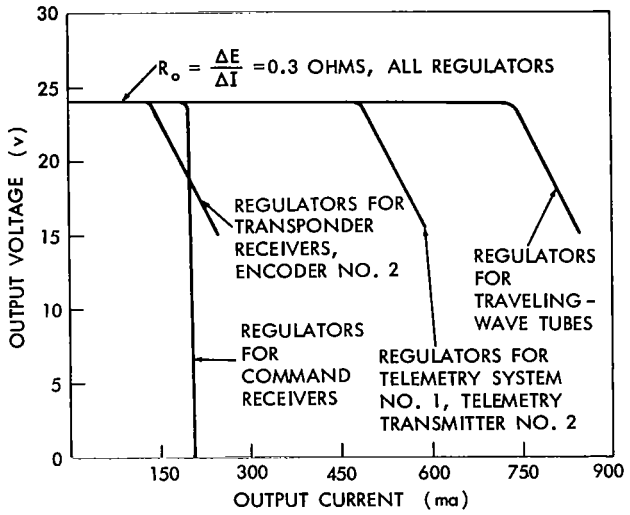

Figure II-19—Output voltage versus current characteristics.

The filament converter supplies constant current, regulated to ±1.8 percent. This reduces the thermal shock which would occur due to inrush current, if filament voltage were held constant. The hot filament dissipates between 1.2 and 1.8 watts. The high-voltage dc-to-dc converter has three outputs. This unit is not regulated, but has a very low output impedance. Traveling-wave tube voltage regulation requirements are met by close regulation of the -24 volt input.

STRUCTURAL DESCRIPTION

The spacecraft is composed of two structural units. The outer structure supports the solar panels, the majority of the electronics, and the control subsystem. An inner structure supports the apogee motor and the remaining electronics. An outline drawing of the spacecraft is shown in Figure II-20 and the general arrangement is shown in Figure II-21.

CENTER OF GRAVITY, INCHES	A
AT SEPARATION	12.74
AFTER BURNOUT	11.72
AFTER GAS DEPLETION	11.76

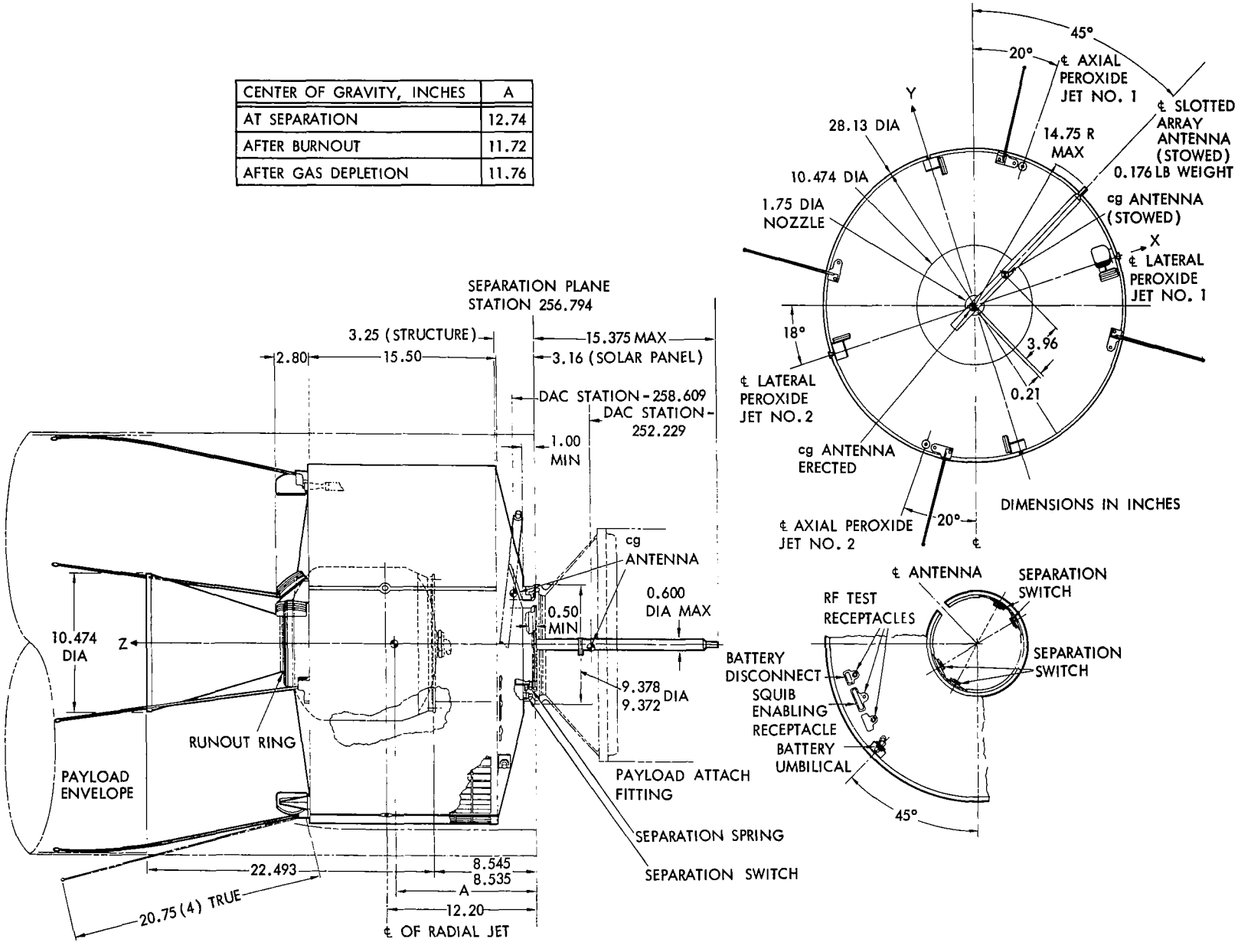

Figure II-20—Outline of Syncom 1 F2.

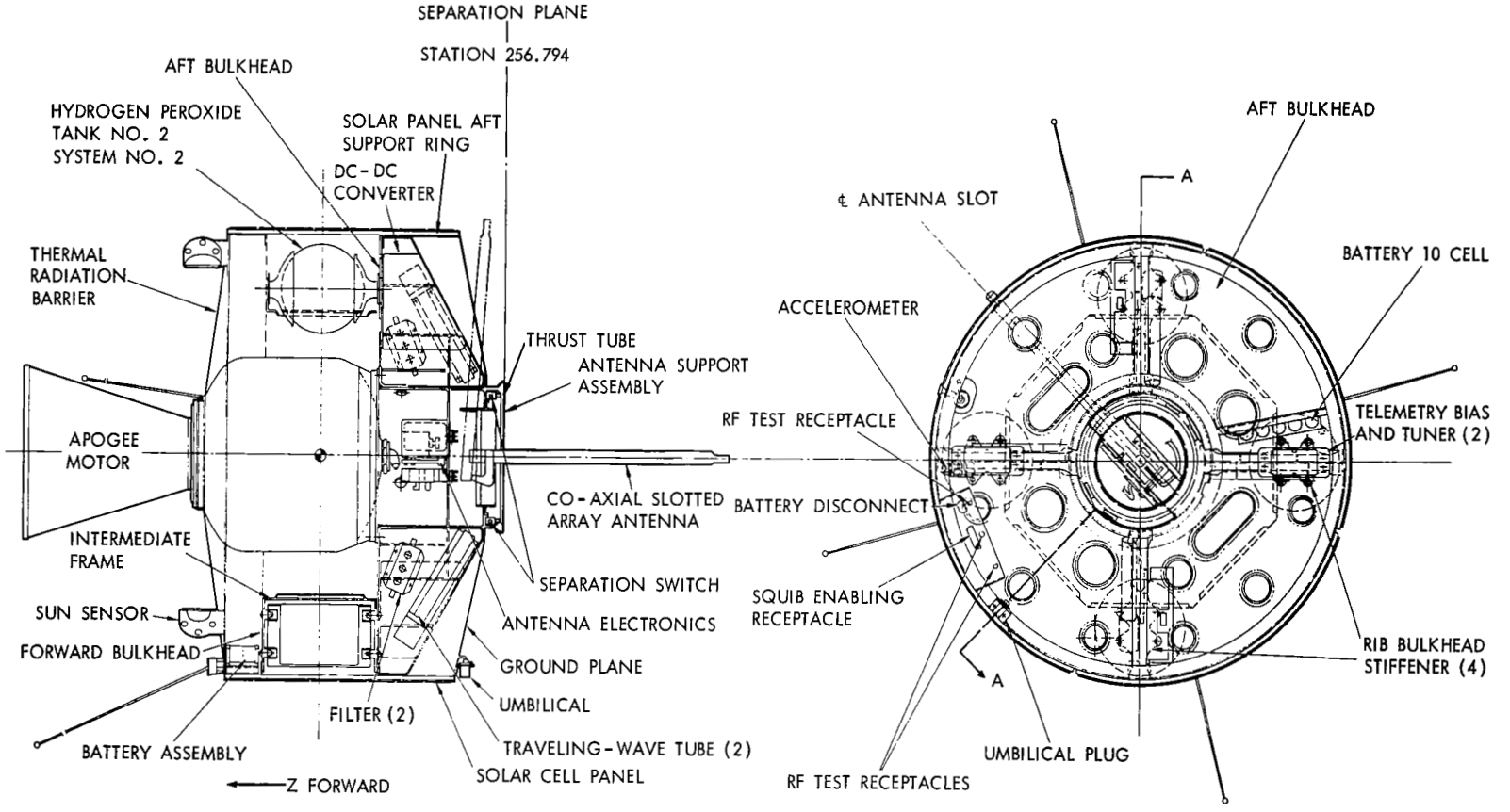

Figure II-21—General arrangement of Syncom 1 F2.

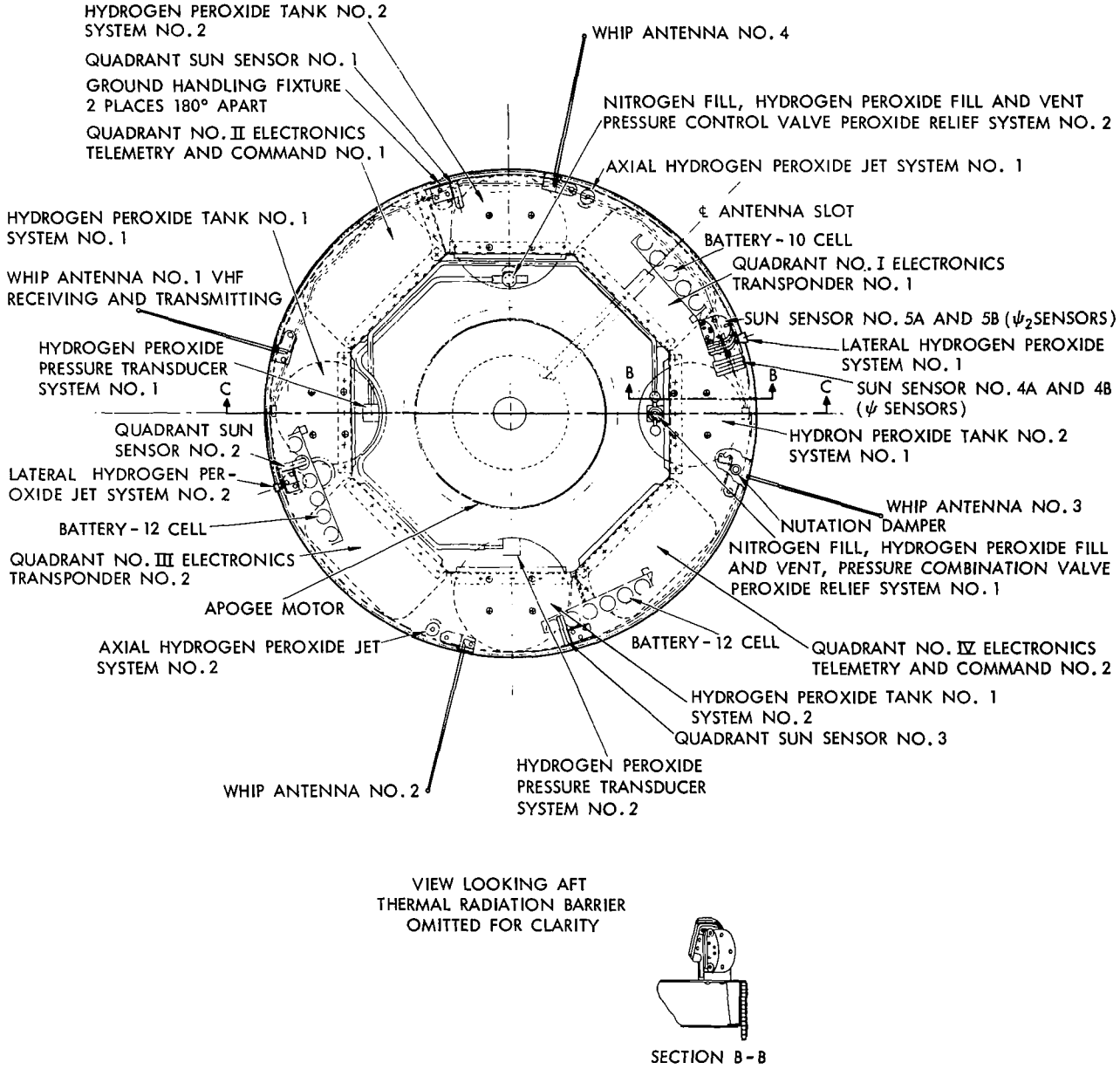

Figure II-21 (Continued)—General arrangement of Syncom 1 F2.

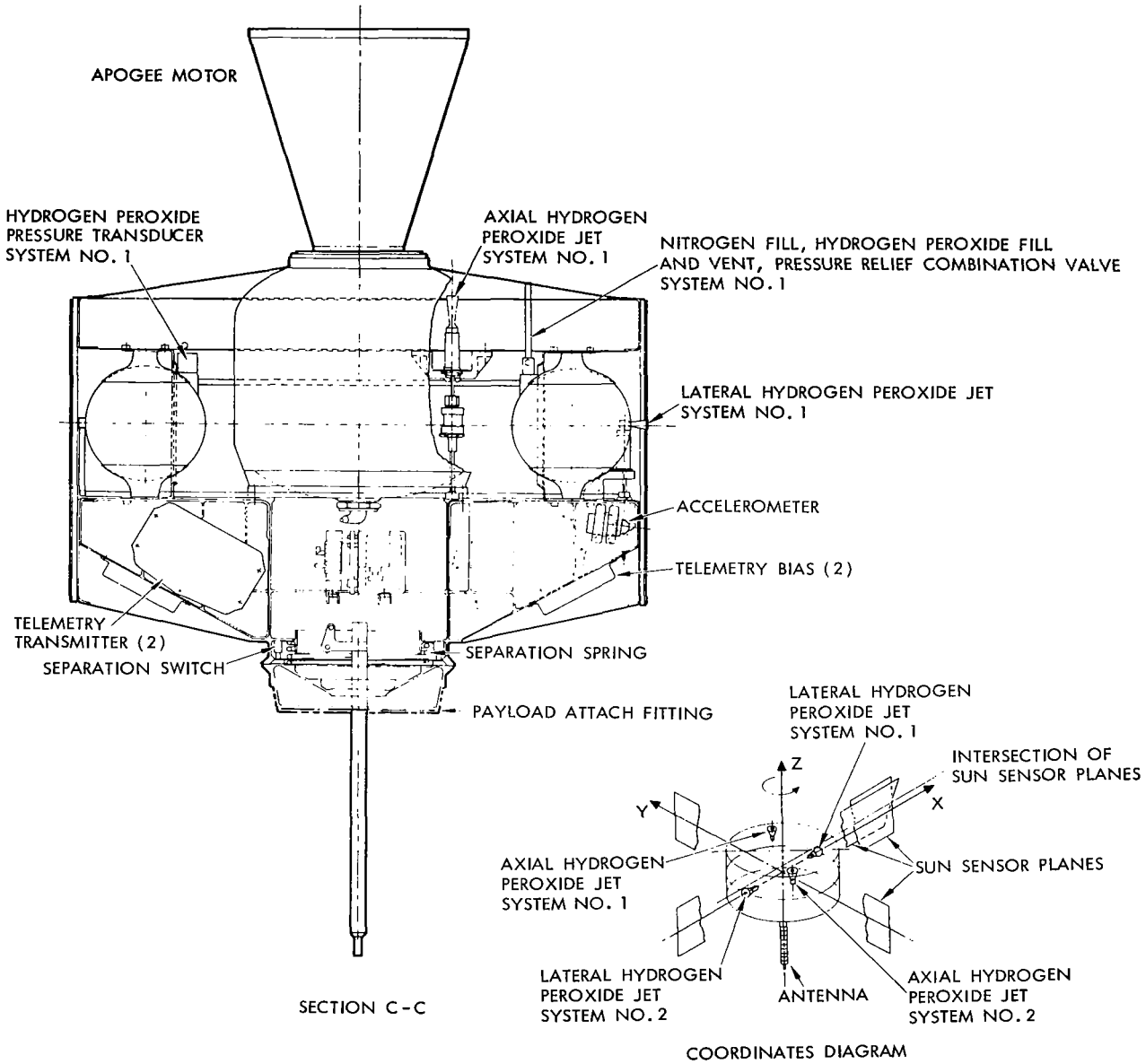

Figure II-21 (Continued)—General arrangement of Syncom 1 F2.

The outer structure attaches four honeycomb solar panels to a cylindrical support ring with four lightweight stiffening ribs located 90 degrees apart, providing the attachment to the inner structure. Steel inserts are bonded into the panels at the attach points to give added strength.

To satisfy the requirement that the ratio of the roll moment of inertia to the pitch moment of inertia be at least 1.10, it is required that the electronic equipment be packaged into small units and equally distributed as far out from the spin axis as possible. To avoid attaching the units

directly to the solar panels, a component-mounting bulkhead is provided. This consists of an octagonal box section and two thin bulkheads attached to the inner structural tube and the four stiffening ribs. A pair of cylindrical support rings, fore and aft, completes the outer structure. The forward ring carries the sun sensors, whip antenna, orientation jets, and the forward ends of the solar panels. The aft ring supports batteries and the aft ends of the solar panels. The octagonal frame mounts the electronic units, the hydrogen peroxide tanks, the nutation damper, and the velocity jets.

The inner structure consists of a machined magnesium ring with the payload attach fitting for mounting to the Delta third stage on one end and provisions for mounting the apogee motor on the opposite end. To allow for thermal expansion of the motor case, the motor is cantilevered from the forward end of the motor case using a four-lug mounting arrangement. Easy access to the attach nuts makes the alignment of the motor relatively simple.

Provisions are made to install the coaxial slot array antenna and its associated electronic package within the inner ring structure. The traveling-wave tubes are attached to the back of two of the stiffening ribs and the telemetry transmitters attached to the other two ribs. A ground plane on the aft end of a thermal radiation barrier on the forward face of the structure completes the enclosure of the components. A discussion of the thermal environment as it affects the structure is contained in the next section.

From the general arrangement shown in Figure II-21 it can be seen that accessibility to all of the units within the mounting frame is obtained by removing the appropriate solar panel. Removal of the ground plane gives access to the traveling-wave tubes and telemetry transmitters. The communications antenna and its electronics may be removed as a unit without any prior disassembly of the spacecraft. The hydrogen peroxide fill-and-drain fittings are accessible through ports in the radiation barrier. Further, a number of electrical test points are accessible with a minimum of disassembly.

The total weight, center of gravity, and mass moments of inertia about the roll and pitch axes of the spacecraft at separation from the booster, at apogee motor burnout, and at hydrogen peroxide burnout, are tabulated in Table II-13.

PROPULSION

To achieve a circular synchronous orbit, a velocity increment, in addition to the velocity imparted by the launch vehicle, must be given to the injected spacecraft at the apogee of the transfer ellipse. This increment is added largely by the apogee motor. However, additional velocity-correction capability must be available to achieve and maintain synchronism because of uncertainties which exist in the velocity increments imparted by both the launch vehicle and the apogee motor. The hydrogen peroxide gas control units provide this corrective capability.

The apogee motor that fits the general requirements of the Syncom spacecraft and mission is the JPL Starfinder motor. This motor was used successfully in the second (A-26) launch and will

Table II-13

Spacecraft Mass Properties Analysis.

Description	Weight (pounds)	Center of Gravity, Z-Z, (inches)	Moment of Inertia		
			Roll (slug-feet^2)	Pitch (slug-feet^2)	Ratio of Roll to Pitch
Final orbit condition*	73.32	11.68	1.68	1.31	1.28
Total at apogee burnout*	83.20	11.74	1.95	1.46	1.34
Payload at launch**	144.70				
Air buoyancy effect	0.06				
Payload at separation*	144.76	12.75	2.20	1.76	1.25

*Weight in vacuum.
**As weighed in air.

be used in the third launch. Figure II-22 shows the outline of the motor in Table II-14 lists its characteristics.

The thrust of the apogee motor is transmitted to the spacecraft through an attachment ring brazed to the forward hemispherical surface of the motor case. The ring is designed so that the motor may be displaced laterally during thrust alignment and dynamic balancing to optimize the system. No other contact, except for a thermal radiation barrier, exists between the motor and spacecraft structure or components.

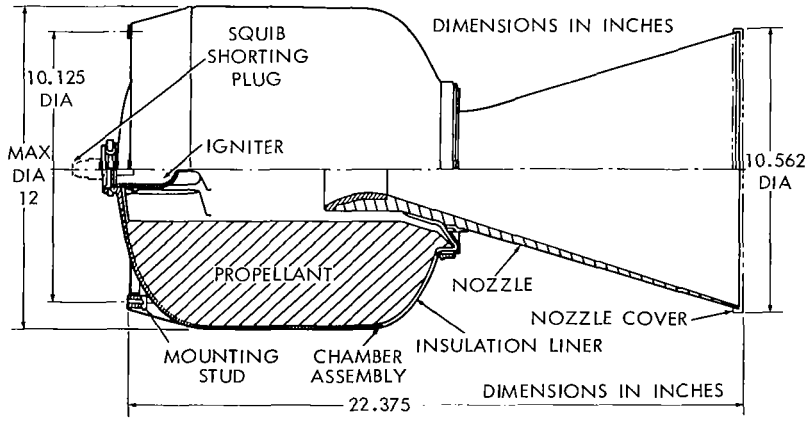

Figure II-22—Starfinder motor.

THERMAL CONSIDERATIONS

Thermal control of the Syncom satellite is accomplished purely by passive techniques. The structure and internal components of the spacecraft are closely coupled by thermal radiation to

Table II-14

Motor Characteristics (JPL Starfinder).

Dimensions	See Figure II-19	Performance (80°F)	
Total weight	71.00 pounds	Maximum thrust	1120 pounds
Inert weight	10.50 pounds	Maximum pressure	260 psi
Propellant weight	60.50 pounds	Burning time	19.7 seconds
Center of gravity		Total impulse	16,600 lb-sec
		Ignition system pressure	360 psia
Inert parts	8.5 inches aft of attach plane	Ignition time	0.013 second
Loaded assembly	6.0 inches aft of attach plane	I_{sp} (vacuum based on propellant weight)	274.2 lb-sec/lb
Dynamic unbalance		Case temperature	400°F
		Firing temperature limits	20 to 140°F
Inert parts before firing	Less than 1.0 oz-in.^{2}	Explosive classification	ICC jet thrust unit, Class B explosive
Inert parts after firing	Less than 5.0 oz-in.^{2}	Storage temperature limits	20 to 130°F
Loaded motor assembly	Less than 50 oz-in.^{2}	Estimated storage life	1 year at 80°F
Thrust misalignment	Less than 0.002 in/in.	Igniter	
Moment of inertia		Circuit	Two bridges in parallel
		Resistance	0.55 to 0.65 ohm
Loaded motor		Normal firing current	9 amperes at 24 to 30 volts dc
Roll	1308 lb-in.^{2}	No-fire current	1 ampere, 1 watt for 5 minutes each circuit
Pitch (about cg)	1648 lb-in.^{2}		
Empty motor			
Roll	163 lb-in.^{2}	Hazards classification	ICC Class B explosive
Pitch (about cg)	448 lb-in.^{2}	Autoignition temperature	850°F

the solar panels and decoupled from space through the use of low emittance end planes. Resulting temperature levels for structure and passive equipment within the spacecraft is 70 ±10°F during normal orbital operation.

Solar Panels

The external properties of the solar panels control, to a large extent, the average bulk temperature of the spacecraft. Based on the known thermal properties of the solar absorptance, IR emittance of the panels, and the spinning mode of operation of the vehicle, the solar panel temperatures vary from 55 to 85°F over the complete range of sun angles between ϕ = 70 degrees and ϕ = 110 degrees. During the maximum eclipse period of 70 minutes the solar panels are expected to drop in temperature to a minimum of -80°F.

Electronic Subsystem Equipment

Temperatures of electronic subsystem equipment are dependent on the spacecraft mode of operation. Some of the expected temperatures are given in Table II-15 for sun incidence angles of 70, 90, and 110 degrees.

During an eclipse transient condition, the electronics of the spacecraft will cool less rapidly than the solar panels and to a less severe minimum temperature. For the 70-minute eclipse, the telemetry transmitters will drop to a minimum of 20 °F.

Table II-15

Electronic Subsystem Estimated Temperatures (°F).*

Equipment	Inclination angle, ϕ (degrees)		
	70	90	110
Telemetry transmitters	65 to 100	75 to 110	80 to 115
Telemetry and command electronics	75 to 80	75 to 80	75 to 80
Traveling-wave tube	60 to 100	70 to 110	75 to 115

*Temperature range shown indicates nonoperating and operating conditions respectively.

Apogee Motor

The apogee motor temperatures are influenced strongly by the spacecraft bulk temperature and to some extent by the thermal coupling between the motor nozzle and space. The nozzle temperatures are a a strong function of solar angle. In general, the propellant grain temperatures will be between 50 and 100° F during normal steady-state orbital operation. During maximum eclipse periods of 70 minutes, the temperature will drop to no less than 40° F followed by warmup to steady state conditions within 3 to 4 hours after eclipse. During normal synchronous orbital operation, the nozzle temperatures will range between -30 and 90 °F as the solar angle on the vehicle varies from 110 degrees to 70 degrees.

Hydrogen Peroxide Unit

Storage limits for the hydrogen peroxide propellant have been specified to be 40 to 80° F. Because of the central location of the propellant tanks, the temperature during orbital operation will not be as greatly dependent on solar angle as some of the other subsystems. Normal orbital temperatures are expected to range from 69 to 78° F throughout the complete solar cycle.

During eclipse transients of 70 minutes, the tanks are expected to drop in temperature to 20° F. Warmup to steady state conditions is expected to take 3 to 4 hours following the eclipse.

CHAPTER III

LAUNCH AND ORBITAL MANEUVERS

Syncom III was shipped from the Hughes Aircraft Company facilities at El Segundo, California, to Cape Kennedy on 30 July 1964. Reported below are the prelaunch preparations made at the Cape and the vehicle and spacecraft performance during flight.

PREFLIGHT OPERATIONS

Shipment to T-4 Day

Syncom C was transported to Orlando, Florida, from Los Angeles on 30-31 July by commercial airlines. The spacecraft was then transferred from Orlando to Cape Kennedy in a closed-van truck and the temperature was controlled to approximately 70°F.

Immediately after arrival at the AE building a complete systems check was performed. All systems were normal. The spacecraft was again tested on August 3, 6, and 9 while waiting for the spin balance facility to be made available.

On the afternoon of 11 August, the spacecraft was moved to the Douglas spin balance facility and made ready for installation of the apogee motor. When this motor was delivered, a very small deep gouge was found on the casing curvature at the nozzle end. Because it could not be immediately determined just what, if any, effect this might have on the motor's performance, the decision was made to use the spare motor.

Temperature sensor 3 had been bonded to the apogee motor five days earlier. Now, unless the launch was delayed, not enough time remained for another sensor to be bonded to the spare motor because of the curing characteristics of the bonding material. The decision was made to launch without the sensor on the motor, but to mount the sensor in plug P-2061. P-2061 is located on the lower deck of quadrant IV and is the plug to which the apogee motor temperature sensor harness was intended to connect.

The spare apogee motor was installed in the spacecraft and centered to a total indicated runout of 0.0005 inch. At 0500 EST on 12 August, the spacecraft was ready to be mated with the third stage booster.

On 13 August, the spin balance of the third stage and payload was accomplished. Figure III-1 shows the spin balance operation. The third stage and payload were then made ready to be moved to the gantry.

On Friday morning, 14 August (T-4 Day), the third stage and payload were moved to the launch pad and installed on the boost vehicle. The T-4 Day All Systems Test was scheduled to start at 1230 EST; however, a rain storm with lightning moved in and the pad was cleared of all personnel. The rain continued until approximately 1545 EST. The test finally commenced with the start of the external power run at approximately 1630 EST, and was terminated after the internal power run at approximately 1830 EST. In general, all spacecraft and launch vehicle systems performed satisfactorily and no problems were encountered during the test.

One discrepancy was found in the spacecraft systems. The telemetry indication of transponder output power was lower than the value measured at the spacecraft antenna. Further checking after 1930 EST disclosed that the calibration curve of power output for traveling-wave tube 1 was 1.6db low and that for traveling-wave tube 2 was 1.0db low.

The foregoing activities are summarized in Table III-1.

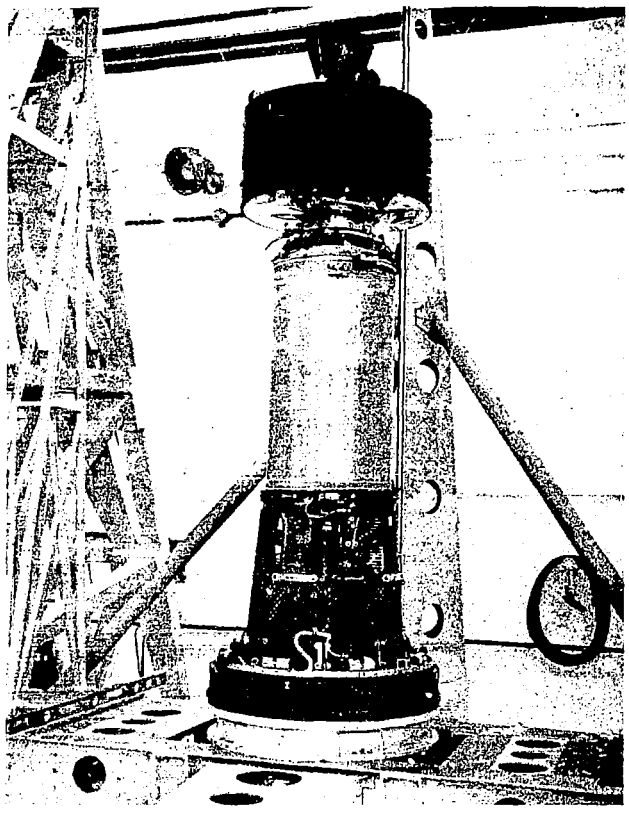

Figure III-1—Syncom III on X258 third stage during spin balance operation.

T-3 Day Operations

While conducting booster vehicle ordnance tasks on 15 August, low resistance paths of approximately 15 k ohms were observed between all pins of interstage connector J-59 (between first and second stages). It was determined that the primer had not fully dried before application of the potting when this connector was reworked at ETR for the installation of explosive nut circuits. This connector was changed and requalified. This problem necessitated rescheduling of the launch to 19 August.

T-1 Day Operation

The T-1 Day countdown was initiated on schedule at 0425 EST on 18 August. Engine checks commenced at 0430 EST, followed by spacecraft checks at 0435 EST and electrical systems checks at 0610 EST.

Spacecraft checks proceeded without incident until 0610 EST. At that time the ultrablitz flash unit was being used to exercise the sun sensors which start and stop the hydrogen peroxide control

Table III-1

Summary of Preflight Operations Through T-4 Day

Event	Date	Remarks
Spacecraft shipped to Cape Kennedy	30, 31 July	L.A. to N.Y.C., American Airlines, Flight 10 N.Y.C. to Orlando, Eastern Airlines, Flight 847 Orlando to Cape Kennedy via truck
Performance test	31 July	All O.K.
Functional check	3 August	All O.K.
Performance test	6 August	All O.K.
NASA visual inspection	6 August	Touch up on areas where gold coating had come off wiring
All systems test (RFI tests)	7 August	Y-1 on gantry – all O.K.
H_2O_2 system proof tested	7 August	Proof-tested to 200 psig H_2O_2 TM calibration checked
Performance test	9 August	All O.K.
Special leak check	10 August	No leaks
Moved to spin balance	11 August	
Apogee motor installed	11, 12 August	Small deep gouge found in motor casing. Motor rejected; spare installed in spacecraft. Total indicated runout 0.0005 inch.
S/C mated with third stage	12 August	
Spin balance	13 August	
Moved to gantry and placed on the boost vehicle	14 August (T-4 Day)	
All systems check	14 August (T-4)	Rechecked TWT power output. Discrepancy in power output TM calibrations noted.

jet. Once the control was started, however, a flash from the ultrabiltz flash unit would not always turn the jet off. It was found that the anomaly was caused by the high background illumination from the gantry lights. Sensor and control jet operation was satisfactory when the black curtains of the air-conditioning cover were lowered around the spacecraft.

Spacecraft checks were resumed and continued normally until a discrepancy was noted in the axial jet 2 leak rate at 0805 EST. When the leak detector used for the test was checked with a

calibrated leak, the leak detector sniffer probe was found to be malfunctioning. All four control jets were rechecked using a calibrated replacement sniffer probe and found to be within specification. Resolution of this problem caused approximately 90 minutes delay in the start of second stage propellant servicing.

T-0 Day Operations

The launch countdown was initiated at 1450 EST (T-895 minutes) on 18 August; however, actual countdown tasks were not started until 1620 EST because inclement weather necessitated clearing of all personnel from the pad area. The late start (90 minutes) of countdown tasks could not be made up before the start of the terminal countdown (T-35 minutes), and a 30-minute extension of the 60-minute built-in hold was required to complete all work. The main problem encountered during the countdown was with the nose fairing temperature sensor, which gave incorrect readings. The problem could not be corrected without postponing the launch operation, so a decision was made to launch without the sensors.

The spacecraft task was released at 1505 EST but thunderstorms moved in and the tower was cleared at 1515 EST. Spacecraft checks were resumed at 1650 EST. The spacecraft hydrogen peroxide servicing task was released at 1730 EST and completed at 1908 EST. Spacecraft RF checks were started at 1925 EST and satisfactorily completed at 2010 EST. Spacecraft ordnance installation began at 2155 EST and a spacecraft ordnance safety check was conducted at 2205 EST. The first group of T-0 Day spacecraft checks were completed at 2245 EST. Third-stage squib installation began at 2345 EST and was completed at 0110 EST 19 August.

In order to make up some of the time lost awaiting weather clearance and other problems, destruct checks and spacecraft preparations for fairing installation were conducted concurrently. Spacecraft preparations were completed and fairing installation began at 0135 EST.

At 0205 EST, it was discovered that the temperature probes inside the fairing did not function properly. It was decided that the loss of temperature sensors in the fairing did not constitute a major problem since a temperature sensor located in the second stage measures the temperature of the air coming from the same airconditioning duct that services the third stage. However, it was felt that a possible wiring error in the fairing could exist. Therefore, the wiring harness in the fairing was thoroughly checked out and no discrepancies were discovered.

The flight ordnance plug was installed in the spacecraft at 0301 EST; after an equipment inventory, the spacecraft personnel left the gantry.

Spacecraft RF checks were started again as soon as the gantry was moved back at 0615 EST. At 0658 EST spacecraft checks were completed.

At T-30 seconds, the spacecraft external power was reduced to the flight power level.

Liftoff (Figure III-2) occurred at 0715 EST, 1215 Z.

FLIGHT PERFORMANCE

The weather at T-0 was good. Surface winds were 4 knots at 280 degrees. The surface temperature was 25.5 °C, with a relative humidity of 90 percent. There was 0.3 cloud cover at 30,000 feet.

Upper air wind parameters are shown in Table III-2.

The sequence of events during the powered flight phase of the launch is shown in Table III-3, and Figure III-3 shows the rocket maneuvers performed to place the spacecraft in the desired transfer orbit.

Details of the trajectory achieved, and the vehicle and spacecraft performance are given in the sections that follow.

Trajectory Achieved

Initially, the Instantaneous Impact Point (IIP) Charts plot was about 0.5 n. mi. left of nominal until after ejection of the solid propellant motors; thereafter, the IIP plot remained on nominal track. MECO was on time, but SECO was about 8.5 seconds late. The IIP plot was running about 10 seconds slow when it passed through the Range Safety (African) gate. Based upon the C-band 0.18 radar data from the Cape 7094 computer, the estimated IIP of the first stage was 21 ° 40.070'N and 49 57.606'W. IIP data from the same source estimated second stage impact at 28 ° 33.197'S and 84 ° 48.671'E. Second-stage IIP based upon the 7.18 radar and Bermuda radar data from the GSFC computer was 28 ° 30.6'S and 85 ° 21.6'E.

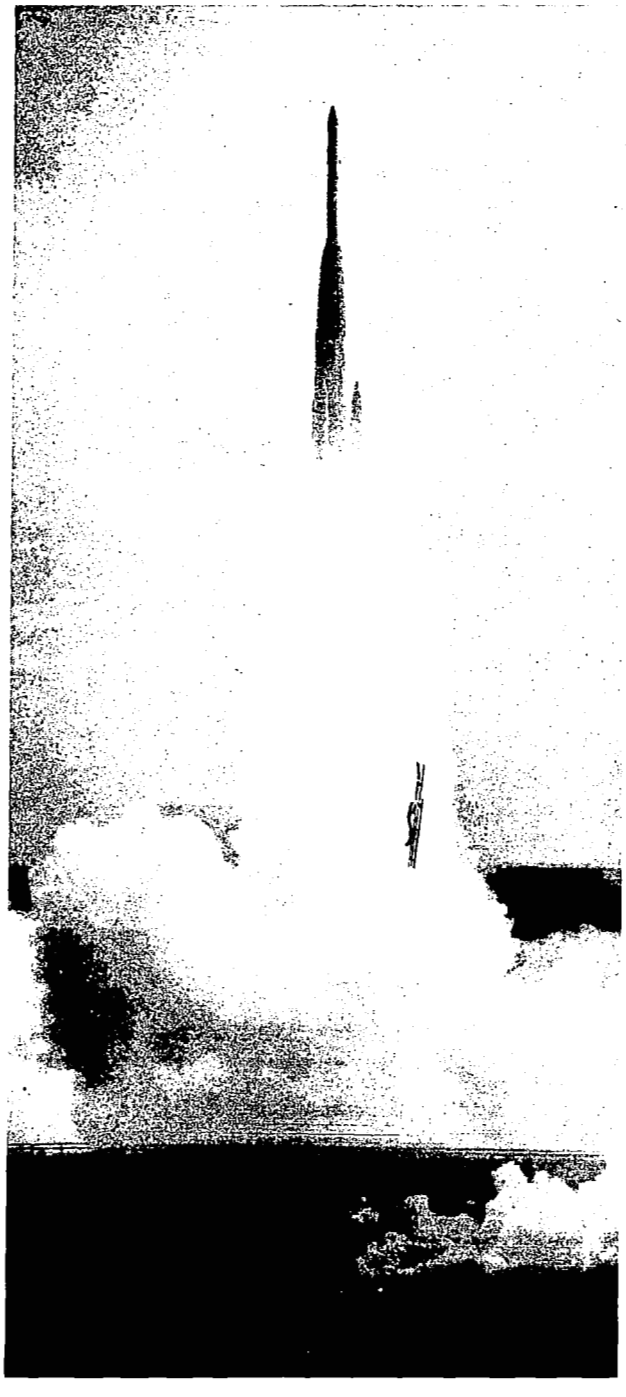

Figure III-2—Liftoff.

The present position charts of the vertical plane (launch area XZ-YZ) showed a smooth actual plot about midway between nominal and 3-sigma high. The ground plane computer showed a smooth actual plot about 0.4 n. mi. left of nominal XY and slightly high XH during first stage operation. The plot was on nominal XY but still showed

Table III-2

Upper Air Wind Parameters at T-0.

Altitude (feet)	Direction (degrees)	Speed (kt)	Shear (kt)
5,000	252	14	1
10,000	234	16	1
20,000	245	20	2
50,000	333	17	4
100,000	71	41	2

Table III-3

Sequence of Events During Powered Flight.

Event	Time	GMT
Liftoff	T + 0	1215:01.8
Solid motor separation	T + 71.1 sec	1216:12.9
Main engine cutoff (MECO)	T + 148.4	1217:30.2
Second-stage ignition	T + 152.4	1217:34.2
Jettison fairing	T + 163.9	1217:45.7
Second stage cutoff (SECO)	T + 324.4	1220:26.2
Western Electric guidance off	T + 379.7 (6:19.7 min)	1221:21.5
Spinup	T + 26:03.4	1241:05.2
Second/third-stage separation	T + 26:05.4	1241:07.2
Third-stage ignition	T + 26:10.2	1241:12
Third-stage burnout	T + 26:33.8	1241:34.8
Spacecraft separation	T + 27:36.8	1242:38.6

slightly high XY for the remainder of the flight (about 1 n. mi. high at MECO and 4 n. mi. high at SECO). The ground plane WECO source showed the actual plot about 0.5 n. mi. left of nominal XY until T + 280 seconds, then about 2 n. mi. right of XY thereafter. The XH plot showed slightly high until T + 280 seconds, then showed slightly low thereafter.

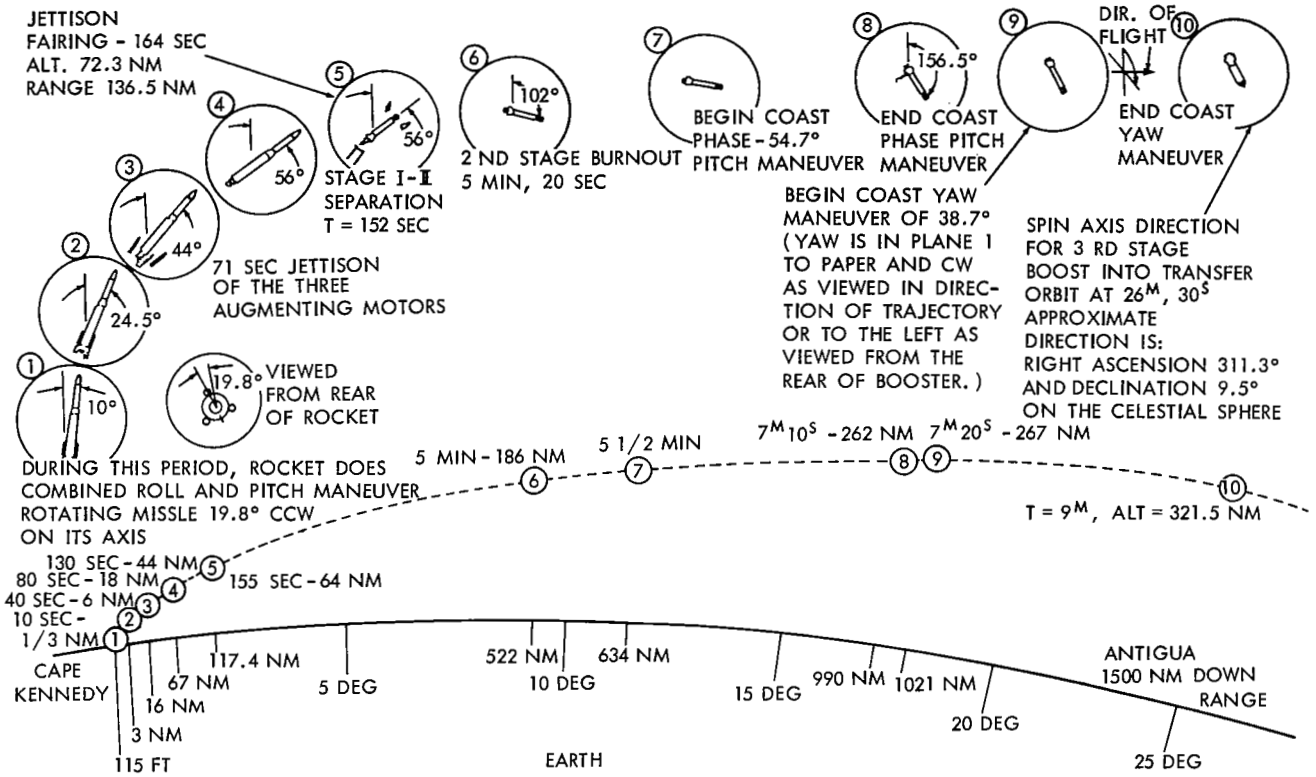

Figure III-3—Delta rocket maneuvers for Syncom III launch.

Vehicle Systems Performance

Propulsion

Preliminary data review indicates nominal first-stage performance. Total steady-state sea-level thrust was approximately 335,000 pounds at liftoff + 25 seconds. This nominal performance is reflected in solid motor chamber pressures, main engine chamber pressure, turbopump speed, turbine inlet temperature, and gas generator LOX injector pressure. First-stage burn time was nominal, with an apparent oxidizer depletion. Propellant utilization was indicated to be 99.7 percent with approximately 300 pounds of fuel remaining.

Solid booster performance was as expected. Chamber pressure rise was normal, the predicted burn time was achieved, and ejection of all three expended motor cases occurred as expected.

Second-stage performance was somewhat below nominal, with a steady, lower than nominal thrust of 7150 pounds for a burning period of 172 seconds. The burn time was 8 seconds longer than the predicted time of 164 seconds. SECO was commanded by Western Electric guidance with approximately 4 seconds of burn time remaining.

Preliminary spacecraft tracking data indicates nominal third stage operation. Verbal information from the range-tracking, ship doppler tracking station confirms normal operation with a burn time of approximately 21 seconds.

Guidance and Controls

The first stage performed satisfactorily. Liftoff transients were normal and compared favorably with a standard Delta.

Solid motor alignment was good and thrust misalignment of the main and vernier engines was negligible. Maximum roll control occurred during the max "Q" region (30 seconds). At approximately the same time, roll rate was 1.65 deg/sec. Maximum engine deflections during the max "Q" region were 0.94 degree pitch up and 0.85 degree yaw right. No abnormal disturbances occurred at either gain change, solid motor drop, or MECO.

WECO guidance, enabled at T + 80 seconds, started steering at T + 90 seconds. Initial steering orders were pitch down and yaw right. The last first stage WECO commands occurred at T + 138.9 seconds.

All first stage programmed times occurred as scheduled, and vehicle response to commanded inputs was normal.

The second-stage powered flight performance was also satisfactory. Thrust misalignment was less than 0.1 degree pitch down and 0.2 degree yaw left. All programmed events occurred on time. WECO steering, as received by the vehicle, appeared to be of low order. Initial WECO steering commands were pitch down and yaw left and occurred at MECO +14.5 seconds and terminated at MECO +170.5 seconds.

There was a first/second stage separation transient of 0.4 degree vehicle left and 0.6 degree vehicle down. All programmed events occurred on time and vehicle response to these commanded inputs was normal. Fairing ejection was on time and very little vehicle disturbance was noted. Second-stage battery and inverter voltages were good.

The coast flight phase was initiated at second-stage cutoff. SECO was commanded by WECO at MECO +176 seconds. Coast control was initiated by SECO and adequately damped the SECO open loop steering transients. WECO open loop steering commands commenced at M + 178.1 seconds and ended at M + 179.7 seconds. The yaw command was large (0.86 degree yaw left). The pitch command was less than 0.5 degree pitch down.

Spacecraft Performance

The Syncom III launch sequence is illustrated in Figure III-4, and Table III-4 summarizes the ground station acquisition times and command transmissions. Not indicated on the table is the fact that the Syncom ground station at the Cape tracked the spacecraft until T + 574 seconds at

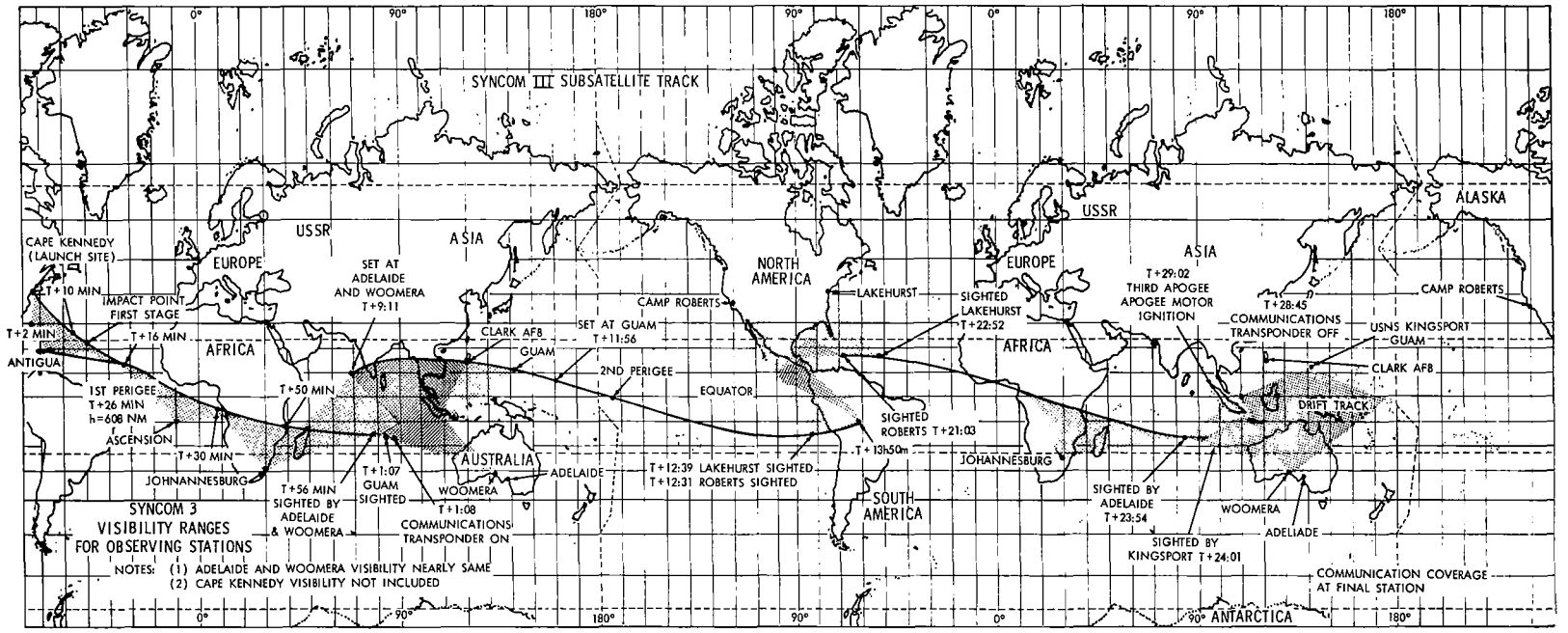

Figure III-4—Syncom III launch track.

Table III-4

Station Acquisition Summary.

Time (hrs GMT)	Time From Liftoff	Station	Remarks
1215	T + 0		Liftoff
1217	T + 2 minutes	GTCV	Acquired az. 195 el. 0.0 B L 100dbm
1225	T + 10 minutes	GTCV	Lost contact
1311	T + 56 minutes	ATAC	Acquired az. 270 el. 19 B L -118
1318	T + 1:03 hours	ATAC	Filament No. 2 ON (Command 9)
1319	T + 1:04	ATAC	Transponder Recvr. 2 ON (Command 11)
1322	T + 1:07	MKPT	Acquired az. 248 el. minimum B L -126
1323	T + 1:08	ATAC	Transponder high voltage ON (Command 13)
1323	T + 1:10	PHI	Acquired az. 226.4 el. 24.8 B L -131 POL 90
1329	T + 1:14	KPT	Acquired az. 242.8 el. 9.0 B L -131 POL-74
2126	T + 9:11	ATAC	Lost contact
2204	T + 9:49	KPT	Lost lock az. 276.9 el. 1.2 B L -143
2210	T + 9:50	MKPT	Data marginal el. 1.0
2251	T + 10:36	MKPT	Reacquired
2312	T + 10:57	KPT	Reacquired az. 280.5 el. 4.0 B L -133 POL -40
20 August			
0011	T + 11:56	MKPT	Lost contact
0015	T + 12:00	KPT	Lost track
0044	T + 12:29	GTCV	Acquired az. 203 el. minimum B L -135dbm
0046	T + 12:31	RBT	Acquired az. 158.8 el. 3.1 B L -113
0115	T + 13:00	TLH	Acquired az. 179.92 el. 18.0 B L -120 POL +58
0314	T + 14:59	GTCV	TM 2 ON (Commands 3 and 5)
0500	T + 16:45	GTCV	Reorientation maneuver (Command 21) Axial jet 1 -83 pulses
0918	T + 21:03	RBT	Lost track
1209	T + 23:54	ATAC	Acquired az. 272 el. 00 rec. level -127
1210	T + 23:55	PHI	Acquired az. 230.7 el. 9.7 B L -126 POL +112
1216	T + 24:01	MKPT	Acquired az. 273 el. (minimum) sig. level -135
1217	T + 24:02	KPT	Acquired az. 242.2 el. 0.8 B L -120
1315	T + 25:00	ATAC	TM 1 ON (Command 4)
1700	T + 28:45	ATAC	Transponder OFF (Command 14)
1700	T + 28:45	KPT	Secured az. 254.6 el. 41.6 B L -123 POL -40
1717	T + 29:02	ATAC	Fire apogee motor (Command 19)
1719	T + 29:04	MKPT	TM 2 ON (Commands 3 and 5)

Glossary

ATAC	Telemetry and Command Station, Adelaide, Australia
GTCV	Telemetry and Command Station, Lakehurst, New Jersey
KPT	Communications Terminal, USNS Kingsport, Guam
MKPT	Telemetry and Command Station, USNS Kingsport, Guam
PHI	Communications Terminal, Clark Field, Philippine Islands
RBT	Communications Terminal, Camp Roberts, California
TLH	Communications Terminal, Lakehurst, New Jersey

which time the radio horizon terminated the tracking. At that time, data were relayed to the Cape from the Antiqua and Ascension stations until they lost the signal at T + 2170 seconds. All spacecraft parameters were reported normal.

The paragraphs that follow briefly describe the acceleration history recorded during first, second, and third-stage powered flight, the power supply subsystem operation prior and just after spinup, and the reorientation and apogee firing which put the spacecraft in a near-synchronous equatorial orbit.

Powered Flight Acceleration History

Figure III-5 shows the plot of the spacecraft accelerometer output during the first and second-stage powered flight. Approximate calibration can be obtained from the 1 g indication as the vehicle stood on the pad prior to launch and the 0 g indication after second stage burnout.

Figure III-6 shows the accelerometer plot of the third-stage firing. It should be remembered that the accelerometer starts to saturate at approximately 14 to 15 g's.

Power Supply Subsystem Operation

The fairing was jettisoned at T + 2:44 minutes (T + 163.9 seconds) and spinup did not occur until T + 26:03 minutes. During the interim period, 23:19 minutes, one side of the spacecraft was

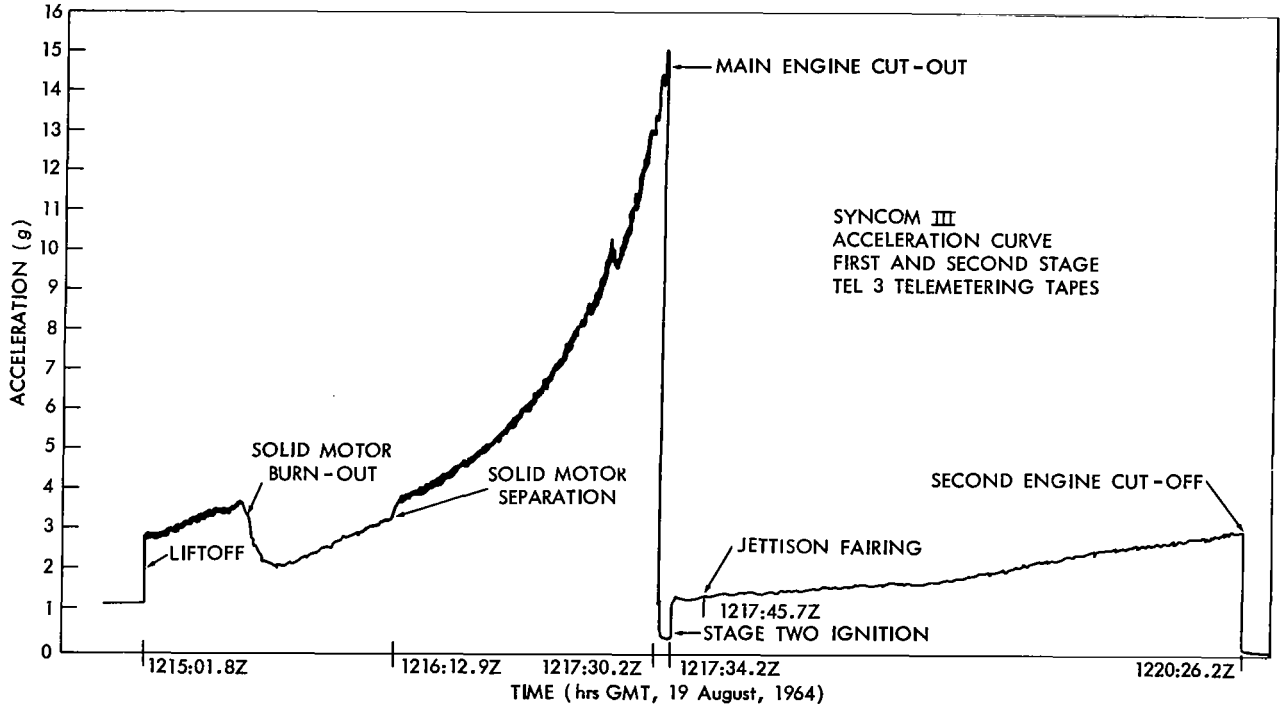

Figure III-5—Acceleration history of first- and second-stage firings.

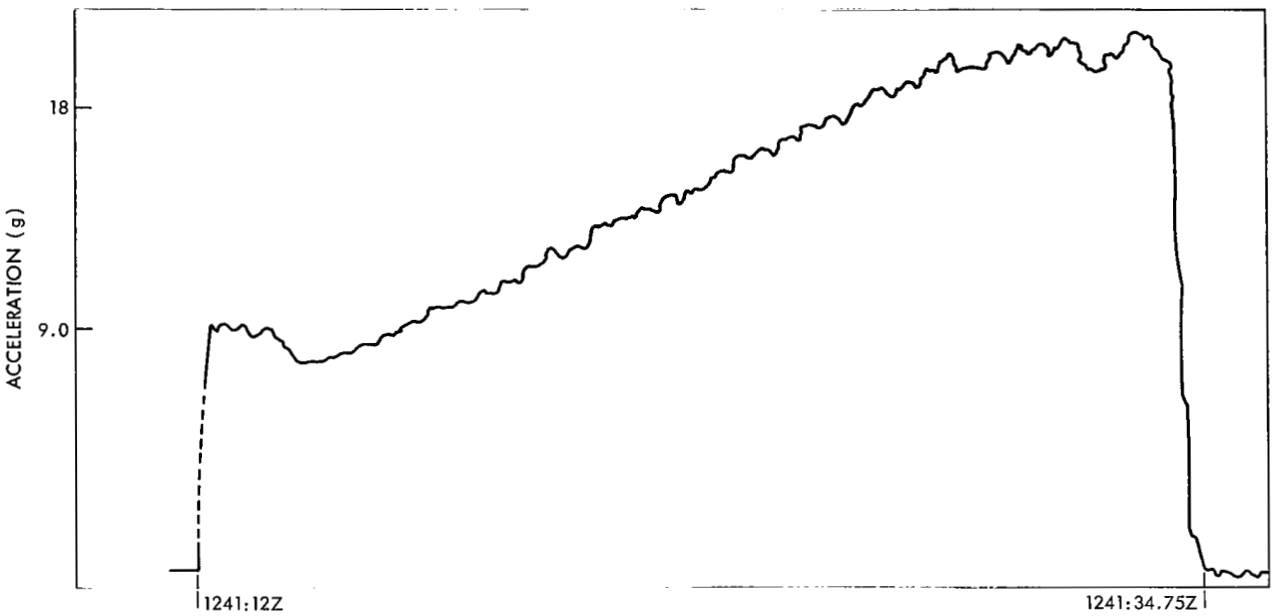

Figure III-6—Acceleration history of third-stage burning.

continuously exposed to the sun. The solar panels on this side were heated and consequently became less efficient. Figure III-7 shows the telemetry trace for the period just prior to and after spinup. Channel 7 represents the battery voltage, channel 8, the unregulated bus voltage. Prior to spinup, the power output from the solar panels was depreciated by this heating and the spacecraft had to draw current from the batteries.

After spinup, the unregulated bus voltage was modulated by power supplied alternately from the low-output hot panels and the high-output cold panels. The amplitude of this modulation was initially 5.5 volts but gradually decreased as the hot panel cooled. By 1306 Z, 25 minutes after spinup, the modulation disappeared and the unregulated bus voltage was riding 5.5 volts above the level it held prior to spinup.

Reorientation and Apogee Firing

Shortly after the satellite first became visible to the command station at Adelaide, Australia, it was apparent to the orbit control personnel at GSFC that the spacecraft sun angle data did not agree with the polarization data received. This was difficult to explain but the most probable solution seemed to be that the wiring of the ψ , ψ_2 sensors was reversed. To check this theory, the sign of the reported ψ_2 was changed and new calculations made; satisfactory correlation resulted. Secondly, as the spacecraft climbed to second apogee, telemetry system 2 was turned on to make use of the redundant ψ, ψ_2 sensors. The attitude as determined from telemetry 2 confirmed the theory that the ψ, ψ_2 sensors on telemetry system 1 were miswired. (See Appendix F for more details on this miswiring.)

It was also apparent at this time that a change of attitude of approximately 14 degrees had occurred somewhere near separation. The spacecraft accelerometer and the sun sensors provided the necessary information to later diagnose this anomaly as caused by coning after third-stage burnout. A detailed analysis of this nutation is contained in Appendix A.

At 0500 Z on 20 August while the spacecraft was at second apogee, a reorientation maneuver was performed to bring the attitude of the spacecraft into proper position for apogee motor firing. Because the objective was a stationary orbit, the attitude of the spacecraft at apogee motor firing had to be such that the thrust would not only produce a circular orbit but would also reduce the inclination to zero. This maneuver required 83 pulses of the axial jet 1.

At 1717 Z on 20 August, the Telemetry and Command Station at Adelaide, Australia fired the apogee motor. A plot of the accelerometer output is shown in Figure III-8.

The communications transponder was turned off 17 minutes prior to apogee motor firing so that it would not operate during the high temperature environment caused by the burning of the apogee motor.

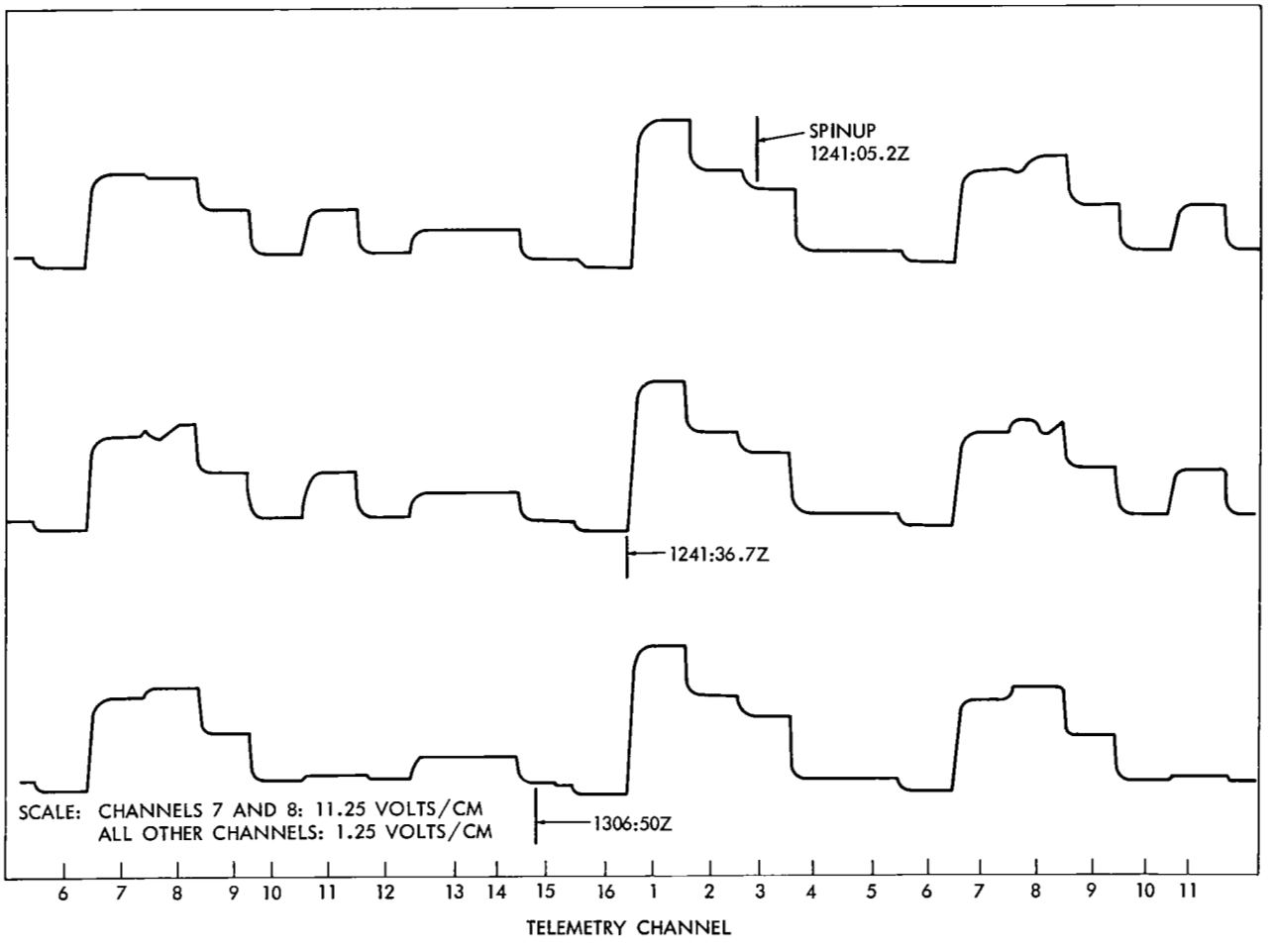

Figure III-7—Telemetry train indicating temporary solar panel degradation before spinup.

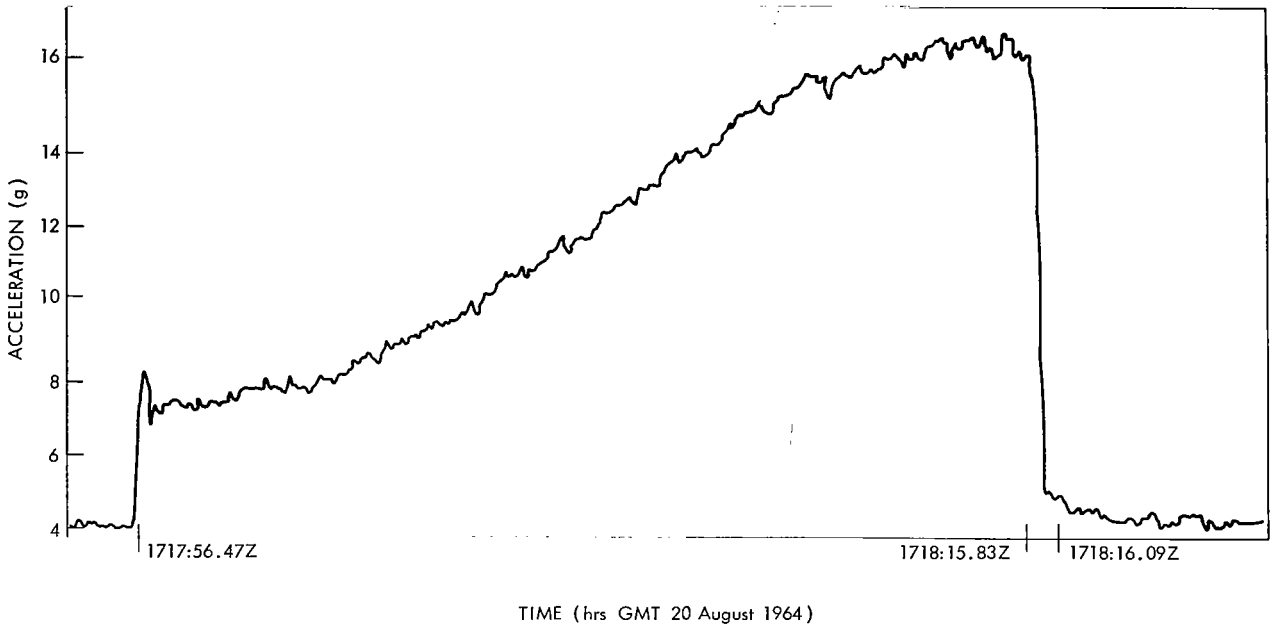

Figure III-8—Acceleration history of apogee motor firing as recorded at Adelaide, Australia Telemetry and Command Station.

Telemetry system 1 was ON at apogee motor firing and for two minutes thereafter to record the output of the accelerometer. Telemetry 2 was turned ON after two minutes to record the hydrogen peroxide tank mount and solar panel temperatures during the thermal cycle.

As seen in Figure III-9 the tank mount temperature went above the range of the sensor during a period of approximately four minutes. Normal transponder operations were again restored at 1953 Z.

The apogee motor firing was a complete success. The spacecraft was now in near-synchronous orbit and the inclination was reduced to less than 0.5 degree.

The orbital control maneuvers that positioned the spacecraft from this point are described in the next section of this report.

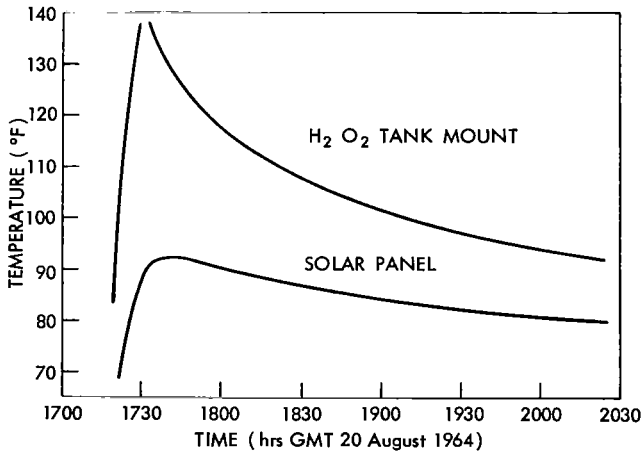

Figure III-9—Hydrogen peroxide tank mount and solar panel temperature history during apogee motor firing.

ORBITAL CONTROL PERFORMANCE

Summarizing the orbital maneuvers and control subsystem performance of Syncom III:

1. The spacecraft was synchronized at the desired 180 degrees longitude.

2. The transfer orbit and apogee motor boost were near-nominal; no mission degradation resulted from small deviations from predicted orbital parameters.
3. The spin axis attitude, after separation from the third stage, was different from the direction of the third-stage velocity increment by an unexpectedly large angle.
4. All of the orbit control modes exercised functioned properly.
5. There were no serious errors in any of the orbit maneuvers.
6. The specific impulses obtained from the control subsystem were nearly correct.
7. There were propellant flow-rate calibration errors but they did not seriously degrade mission results.
8. Orbit determination and prediction are limitations on the evaluation of small corrections (velocity corrections of 1 fps, for example).
9. Attitude determination within short intervals of time is limited by polarization angle measurement accuracy.

Definition of Parameters

Parameters referred to by symbols or groups of alphabetic characters in the discussion which follows are defined below.

Spacecraft Flight Parameters (Figure III-10)

The spacecraft flight parameters have been referred to a coordinate system where the X-axis lies in the Greenwich meridian and the equatorial plane at the epoch; the Y-axis is 90 degrees east, and the Z-axis is chosen to form a right-handed system.

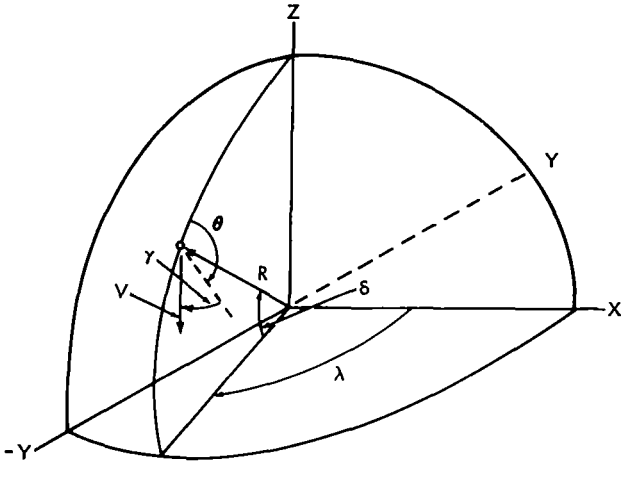

Figure III-10—Spacecraft flight parameters.

Latitude, δ Geocentric latitude (degrees) (+ north)

Longitude, λ Longitude (degrees) (+ west)

Radius, R Radius from the center of the earth (n. mi.)

Velocity, V Inertial velocity (fps)

Gamma, γ Vertical flight path angle of the velocity vector-degrees (positive if the spacecraft is moving away from the earth)

Azimuth, θ Azimuth angle of the velocity vector (0 degree to the north and increasing to the east)

Other Parameters

ϕ	Angle between the +Z spin axis direction and the sunline (Figure III-11)
ϕ_I	Initial ϕ
ϕ_F	Final ϕ
ψ_2	Spin phase angle between solar sensor pips; analytically, $\psi_2 = \sin^{-1}$ [tan 35°/tan ϕ]
ΔV	Magnitude of vector velocity increment (fps)
Resulting drift	Difference in longitude on two successive passes of the ascending node (i.e., when the subsatellite point crosses the Equator traveling from south to north); this quantity is positive if the drift is to the west
e	Eccentricity of the orbit
e_R	Resulting e after a maneuver
i	Orbital inclination (degrees)
i_R	Resulting i after a maneuver
a	Semi-major axis of the orbit (n. mi.)
a_R	Resulting a after a maneuver
Ω	Right ascension of ascending node (degrees)
Ω_R	Resulting Ω after a maneuver
Spin axis (attitude)	+Z spin-axis direction (i.e., the axis of rotation); the +Z axis is directed toward the apogee motor end of the satellite (see Figure III-11)
SARA	Right ascension of the +Z spin-axis direction (Figure III-12)
$SARA_R$	Resulting SARA after a maneuver
SADEC	Declination of the +Z spin-axis direction (Figure III-12)
$SADEC_R$	Resulting SADEC after a maneuver
ΔW	Amount of mass loss, (pounds)
Pulsing time	Total time required for a maneuver
Number pulses	Number of times the control jet was opened and closed for a maneuver
Precession phase	ψ_T, the angle from the projection of the sunline on the plane normal to the spin axis, to the average precession torque vector (positive in the sense of spin). Figure III-13 is a view of Syncom II with the +Z spin axis pointing out of the paper
POLANG	Polarization angle, the angle, measured about the line of sight, between the vertical plane containing the line of sight and the plane of the transponder signal (plane of electric vector and line of sight). If the polarization is vertical, the polarization angle is zero; if the plane of polarization is rotated clockwise from the vertical as seen from the station, the polarization angle is positive. POLANG has a range of -180 to +180 degrees, as the sense of direction of the spin axis, not observable in polarization angle measurements, is taken into account (Figure III-14).

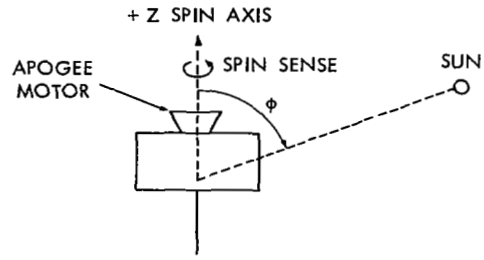

Figure III-11—Spin axis.

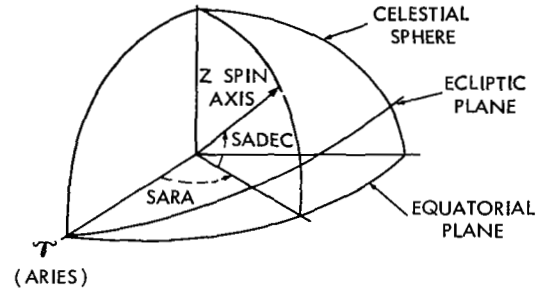

Figure III-12—Right ascension and declination.

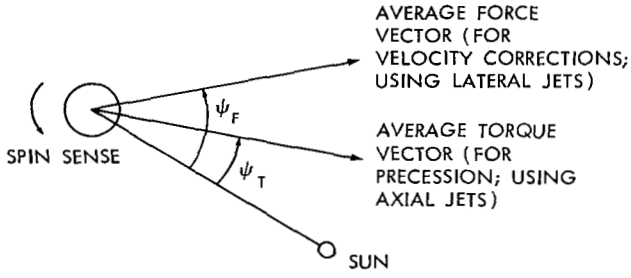

Figure III-13—Precession phase.

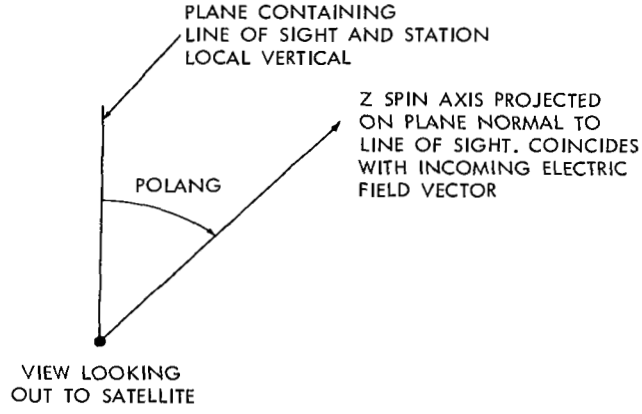

Figure III-14—Polarization angle.

P_I Initial H_2O_2 system pressure (psia)

P_F Final H_2O_2 system pressure (psia)

Control Subsystem Geometry

The geometry of the hydrogen peroxide unit, system 1, is shown in Figure III-15. The geometry of system 2 is the same as that of system 1 except for a 180 degree rotation around the spin axis.

Orbital Maneuvers

This discussion summarizes all of the orbital maneuvers which were made with Syncom III during the first 100 days in orbit.

The predicted on-times which appear in the following discussion were calculated to the nearest hundredth of a second, and then generally rounded off to the nearest whole second for execution of the maneuver. The predicted

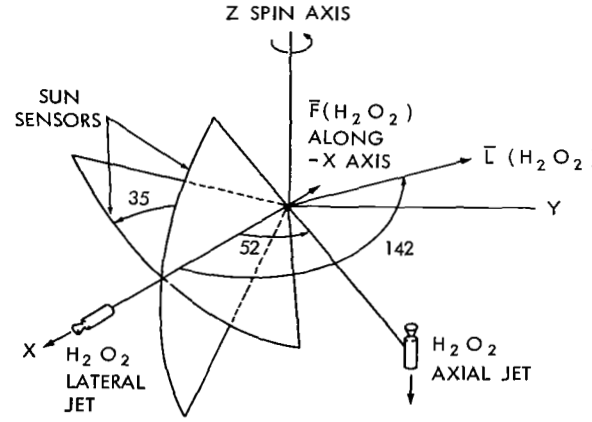

$(\psi_D)_{TORQUE} \cong 142 + 30 + 30 = 202$ deg

$(\psi_D)_{FORCE} \cong 180 + 30 + 30 = 240$ deg

$\left(\frac{60°}{2}\right)$ (30 msec TIME DELAY)

$\bar{L}$ = AVERAGE TORQUE VECTOR
$\bar{F}$ = AVERAGE FORCE VECTOR
ANGLES IN DEGREES

Figure III-15—Hydrogen peroxide unit geometry, System 1.

maneuver parameters are calculated based on the on-times before roundoff. It can be readily shown that this procedure introduces negligible error relative to the various other uncertainties (such as those in orbital elements and calibration data) associated with maneuver design. Rounded on-times are presented in parentheses.

Values of the right ascension of the ascending node (Ω) and inclination (i) included in the presentation indicate the uncertainty generally associated with the orbital plane. The NASA orbit determination group experienced much difficulty in establishing the orientation of the orbital plane; consequently, in general, there were uncertainties associated with maneuver design subsequent to apogee motor firing and the reported values of Ω and i have a low confidence level.

Transfer Orbit — 19 August, Epoch $12^h41^m35^s$*

The Thrust-Augmented Delta (TAD) booster vehicle placed Syncom III in a near-nominal transfer orbit (with slightly excess energy). Table III-5 gives predicted and actual flight parameters for this orbit (derived for the epoch).

Table III-5

Transfer Orbit Flight Parameters.

	Latitude	Longitude	Radius	Velocity	Gamma	Azimuth
Nominal†	-0.096	6.679	4049.78	31225.76	0.563	106.483
Actual††	-0.459	6.012	4043.63	31305.18	0.247	106.731

†Derived by the Douglas Aircraft Company prior to flight (DTO trajectory).

††Derived at the Goddard Space Flight Center from classic orbital elements supplied by the NASA orbit determination group. Data for the orbital solution consisted of range, range-rate, azimuth, elevation, and Minitrack direction cosines.

Spin Axis Attitude in the Transfer Orbit 19 August $12^h41^m35^s$ to 20 August $17^h17^m56^s$

After separation from the third-stage booster of the TAD, the most likely attitude of the spin axis corresponds to the direction of the third stage boost increment. Using the VINCEV** computer program to evaluate the third-stage parameters, the direction of the third stage, assuming a nominal second stage was:

		Predicted	Actual
SARA	=	240.07°	241.53°
SADEC	=	9.45°	8.69°

and by using the second-stage parameters as reported by BTL the direction was:

*The epoch corresponds to third stage burnout.

**The VINCEV computer program calculates the magnitude and direction of the imparted ΔV required to transfer from one orbit to another, based on knowledge of the orbital elements before and after a velocity correction.

	Predicted	Actual
SARA =	241.41°	242.69°
SADEC =	9.45°	9.28°

The latter values are more reliable, since the guidance of the vehicle took into account a change in expected third-stage performance relative to that used to derive the nominal (DTO trajectory). Since the derived direction of the third stage (and, therefore, supposedly the spin axis direction) was very close (1.3 degrees) to that predicted, the angle between the spin axis and the sunline, ϕ, was expected to be near the nominal 90 degrees. However, all T&C stations (GTCV, MKPT, and ATAC) were reporting 100.2 degrees. With this datum included with the POLANG data in the determination of the spin axis direction (ATTDET), a suitable solution could not be found (i.e., the residuals on the data were very large).

After several theories had been advanced to explain this behavior, two were tried. First, the sign of the reported ψ_2 was reversed and satisfactory convergence was achieved in the ATTDET computer program. Secondly, TM-2 was used to measure ψ_2 and the sign of the datum was opposite to that obtained from TM-1, conclusively verifying that ϕ was 79.8 degrees rather than 100.2 degrees.

The direction of the spin axis derived from the ATTDET computer program was:

SARA = 229.33° ($\pm$0.19)
SADEC = 3.51° ($\pm$0.26)

The angle between this direction and the direction of third-stage boost (using BTL input) was 14.47 degrees.

Since reorientation of the spin axis during the transfer orbit had been planned, no serious problems resulted from the "tip-off" experienced by Syncom III once the problem created by the erroneous ψ_2 indication had been resolved. The basic result was that the spin axis had to be precessed through 21.6 degrees rather than the nominal of approximately 9 degrees.

Spin Axis Direction for Apogee Motor Firing

The selection of the direction of the spin axis for apogee motor firing was made by the FUSIT 3 computer program. Basically, the direction was chosen such that even if there were large errors in the resulting direction for apogee motor firing, the requirement of a synchronous orbit could still be satisfied, with capability of achieving stationarity if the apogee boost were to be nearly nominal.

Reorientation of the spin axis took place near the second apogee of the transfer orbit. Reorientation mission parameters are given in Table III-6 and the effect of reorientation on the orbit is shown in Table III-7. The calibration data resulted in essentially perfect maneuvering of the spin axis. Therefore, there was no need to maneuver the axis again prior to apogee motor firing. This point is significant because if the resulting direction of the spin axis had been significantly off the desired direction, another correction would have been required before apogee

Table III-6

First Reorientation Maneuver Parameters – System 1

20 August $05^h 30^m 00^s$ to $05^h 31^m 01^s$.

	Pulsing Time	Number Pulses	Precession Angle	Precession Phase Angle	ΔW	ΔV	P_I **	P_F	ϕ_F	$SARA_R$	$SADEC_R$
Predicted	31.25 (31.0)	86	21.6	237.33	0.154	4.35	201	192	91.1	244.92	18.87
Actual	31.0	83	21.0	238.28*	0.155†	7.79	202	192	90.***	244.2 (±0.7)	18.7 (±0.4)

*Derived from the actual values for $SARA_R$ and $SADEC_R$.

**Since the maneuver parameters are generally derived several hours before the actual execution, the initial system pressure has to be estimated for the maneuver time.

***The ψ_2 pulses were too close together to obtain an accurate reading (i.e., ϕ_F could be $90° \pm 2°$).

†Weight used based upon the precession angle achieved.

motor firing. This could have resulted in more passes through the Van Allen belts, possibly resulting in degradation os spacecraft systems (i.e., power supply, etc.). (Subsequent to apogee motor firing, two more reorientations were performed, one with system 1 and one with system 2. Like the first, the subsequent two were near-perfect.)*

Table III-7

Effect of Reorientation on the Orbit.

	e_R	i_R	a_R	Ω_R
Predicted	0.7102	16.71	13984.0	330.5
Actual	0.7102	16.70	13983.5	330.6

Apogee Motor Firing – 20 August $17^h 17^m 56.25^s$ to $17^h 18^m 17.00^s$

Since the transfer orbit had slightly more energy than had been predicted prior to flight, an eastward drift rate after apogee motor firing could not be realized while making a near-optimum transfer to the near-synchronous orbit. Therefore, with the derived spin axis direction, it was expected that the impulse from the apogee motor would place Syncom III in an orbit which would be above synchronous energy (i.e., with a westward drift sense).

The spin axis direction was selected to accommodate this situation, however. With the derived direction, the impulse from the apogee motor would over-correct the inclination (i.e., change the ascending node by ~180 degrees) such that an axial jet correction, applied approximately 180 degrees away in the resulting orbit and in the same direction as the apogee motor, would produce an orbit with nearly zero inclination and with an eastward drift rate. Apogee motor firing took place as the satellite crossed the ascending node (on its third passage of the node). Maneuver parameters are given in Table III-8.

*A third reorientation was performed on 25 September, but was not evaluated due to a lack of data.

Table III-8

Maneuver Parameters for Apogee Motor Firing.

	ΔV	Burn Time	Resulting Drift	e_R	i_R	Ω_R	SARA	SADEC
Predicted	4808.9	19.7	2.99	0.0448	0.111	153.8	244.2	18.7
Actual	4822.5	20.75	3.28 3.32+	0.0438 0.0441+	0.208 0.544**	140.6 185.2**	245.1*	18.85*

*Derived from the VINCEV computer program.

**Actual value received from GSFC on 25 August. This indicates the order of difficulty which NASA had in determining the orbit.

First Axial Jet Velocity Correction — System 2

The impulse from the apogee motor produced an orbit very close to that which was predicted. Syncom III remained in this resulting orbit for 1-1/2 revolutions, at which time the axial engine was used to reverse the sense of the drift so that the objective longitude of 180 degrees would be approached. The parameters for this maneuver are given in Table III-9.

Combined Maneuver — Reorientation Followed by an Axial Jet Velocity Correction — System 2

The objectives of this maneuver were to:

1. Position the spin axis so that subsequent maneuvers (including final reorientation) would produce a zero inclination orbit.
2. Reduce the eastward drift rate to allow for more time to determine the plane of the orbit. Table III-10 gives the parameters for the reorientation maneuver and Table III-11 gives axial jet velocity correction parameters.

Table III-9

First Axial Jet Correction Parameters – 22 August $04^h54^m5.75^s$ to $04^h54^m13.65^s$ – $04^h55^m15.5^s$ to $04^h56^m50^s$.

	ΔV	Resulting Drift	ΔW	P_I	P_F	On-Time Sec	SARA	SADEC	e_R	i_R	Ω_R
Predicted	94.1	-6.242	1.59	208	139	110*	245.1**	18.85**	0.0256	0.033	140.3
Actual	102.8***	-7.12	1.69†	207	135	102.3			0.0253	0.307	221.6

*Since the actual on-time was 7.7 seconds shorter than the desired, the values tabulated in the above table are predictions for an on-time of 102.3 seconds.

**The direction of boost was derived from the VINCEV computer program for the apogee motor impulse.

***Based on resulting orbital period and assumed spin axis direction.

†Weight of peroxide used based on pressure drop.

Table III-10

Reorientation Maneuver Parameters 28 August $14^h 00^m 01^s$ to $14^h 00^m 54^s$.

	Pulsing Time	Number Pulses	Precession Angle	ΔW	ΔV	P_I	P_F	Ω_R	$SARA_R$	$SADEC_R$
Predicted	52.8 (53)	143	30.8	0.176	6.8	150	144.6	86.3	241.3	-11.0
Actual	53	142	31.0*	0.176**	***	149	144.7	88.0*	243.1	-11.4

*Based on the derived actual values of $SARA_R$ and $SADEC_R$.

**Assumed to be the predicted ΔW (because the resulting spin axis direction was accurate, and of uncertainties in pressure readings, i.e., P_I could easily have been 150).

***Unable to evaluate because of the combined maneuver.

Table III-11

Axial Jet Velocity Correction Parameters

28 August $14^h 07^m 40.8^s$ to $14^h 08^m 13.4^s$.

	ΔV	Resulting Drift	ΔW	P_I	P_F	On Time	SARA	SADEC	e_R	i_R	Ω_R
Predicted	25.2	-3.6*	0.420	144.6	133.5	31.94 (32)	241.3	-11.0	0.0170	0.113	133.0
Actual	***	-3.3	0.470**	144.7	131	32.6	243.1	-11.4	0.0175	0.312	25.7

*This drift rate accounts for the predicted ΔV from the reorientation part of the maneuver.

**Based on pressure drop and realized change in orbital energy.

*** Unable to evaluate because of the combined maneuver. However, the VINCEV program derived a total ΔV for the two maneuvers of ~39 fps, which is approximately correct to explain the larger change in orbital energy which was realized.

"Maneuver" to Reduce the Pressure in System 1 31 August $16^h 58^m 10.35^s$

GSFC officials did not wish to test the pressure release valves at this early date and therefore scheduled this "maneuver" to reduce the pressure in system 1. The axial engine was exercised in the continuous mode for 3.7 seconds reducing the pressure from 231 to 225 psia. Then, at $17^h 47^m 15.4^s$, the lateral engine was exercised in the continuous mode for 7.7 seconds reducing the pressure to 214 psia.

The lateral engine impulse did not have any particular effect on the orbit since it was used in the continuous mode for an integer number of revolutions. However, the impulse from the axial engine did increase the energy of the orbit. The combined parameters for the above operation are given in Table III-12.

Third Spin Axis Reorientation — System 1 3 September $18^h 00^m 00.4^s$ to $18^h 00^m 11.2^s$ $18^h 01^m 00.2^s$ to $18^h 02^m 14.9^s$

Prior to this maneuver the attitude of the satellite was such that 24-hour communications could not be realized. The objective of this maneuver was to orient the spin axis normal to the

Table III-12

Combined "Maneuver" Parameters.

	ΔV	ΔW	Resulting Drift	e_R	i_R	Ω_R
Predicted	5.7		-2.97	0.0168	0.317	25.7
Actual	5.6**	0.270*	-2.98	0.0171	0.128	141.8

*Based on actual pressure drop.
**Based on change in predicted versus actual drift rates.

equatorial plane, thus providing 24-hour service. This maneuver was required because of urgent military communication needs, and was not scheduled far enough in advance to permit an accurate determination of the initial attitude. Since the spin axis was not known to within several degrees prior to the maneuver, at least this much error was expected in the result. The actual initial attitude was computed after the maneuver took place. Table III-13 gives the parameters for this maneuver.

First Lateral Jet Velocity Correction — System 1

By the time this maneuver was made Syncom III had drifted east of the International Date Line, being at 178 degrees west longitude at maneuver time. This was planned as a feature of the maneuver sequence, since the first lateral jet maneuver was designed to raise the perigee to the synchronous radius, thus producing a westward drift rate. Parameters for this maneuver are given in Table III-14.

The maneuver was low by 14.9 percent (VINCEV). This reflected in the perigee radius, which was not raised to the synchronous radius, being low by 66 n. mi.

To achieve a stationary orbit at 180 degree longitude from this point in the maneuver sequence, three more velocity corrections, occurring at about 12 hour intervals, would have to be made. This mode was deemed unreasonable from the standpoint of available manpower; therefore, only two more maneuvers were planned. The first, to occur 12 hours later, was to reduce the drift rate such that one orbital period subsequently (36 hours) Syncom could be synchronized at a mean longitude of 180 degrees.

Second Lateral Jet Velocity Correction — System 1

This maneuver was designed to reduce the westward drift rate such that one orbital period subsequent to the maneuver time Syncom III would be in position to be synchronized at a mean longitude of 180 degrees. Maneuver parameters are given in Table III-15.

Third Lateral Jet Velocity Correction — System 1

This maneuver was designed to synchronize Syncom III at a mean longitude of 180 degrees. Maneuver parameters are given in Table III-16. The initial synchronous orbit was established on

Table III-13

Third Reorientation Maneuver Parameters.

	Pulsing Time	Number Pulses	Precession Angle	ΔW	ΔV	P_I	P_F	ϕ_F	$SARA_R$	$SADEC_R$	e_R	i_R	Ω_R
Predicted	85.9 (86)	231	80.0	0.386	22.8	220	199	97.4	ϕ	-90.			
Actual	85.5	233	81.4	0.365*	23.4	218	198	99.6	25.**	-86.6	0.0157	0.128	147.2

*Based on pressure drop and resulting attitude.

**In the region of ±90 degrees for SADEC, the value of SARA is ill-defined; therefore large discrepancies are expected.

Table III-14

Lateral Jet Correction Parameters 10 September $10^h30^m00^s$ to $10^h34^m39^s$.

	ΔV	Resulting Drift	Pulsing Time	Number Pulses	ΔW	P_I	P_F	e_R	i_R	Ω_R	$SARA_R$	$SADEC_R$
Predicted	53.1	2.781	279.17 (279)	760	1.167	216	168	0.0052	0.139	10.5	5.4***	-85.1***
Actual	46.3	2.058	279	758	1.104**	215	169	0.0065	0.125	7.2	*	*

*Not determined due to insufficient data.

**Based on pressure drop.

***Computed after the maneuver based on change in ϕ and direction of impulse.

Table III-15

Lateral Jet Correction Parameters – 10 September $22^h45^m00^s$ to $22^h46^m07^s$.

	ΔV	Resulting Drift	Pulsing Time	Number Pulses	ΔW	P_I	P_F	e_R	i_R	Ω_R	$SARA_R$	$SADEC_R$
Predicted	9.62*	0.984	67.2 (67)†	182	0.259	166	158	0.0046	0.122	7.9	3.5††	-84.9††
Actual	9.68**	1.011	67	182	0.259	166	158	0.0046	0.096	22.0	***	***

*Based on results of the previous maneuver, the ΔV which was used to deduce the on-time for this maneuver was 1.1488 times the predicted tabular value. (This procedure compensated for calibration errors.)

**Based on period of resulting orbit.

***Not determined due to insufficient data.

†An error was made when calculating the total impulse required for the maneuver. The geometry factor for pulsed operation was omitted. Fortunately, this aided in achieving a near-perfect maneuver because the correction factor based on the previous maneuver in error by about this same amount at the lower pressure. In effect, the errors cancelled. Note the ** footnote on the next maneuver where a factor of 1.1137 was used for design. If the on-time for this maneuver had been derived based on the factor of 1.1137, an on-time of 68.1 seconds would have been used. This would have been a good on-time to used since the actual of 67.2 seconds which was used produced an under-shoot.

††Computed after the maneuver based on change in ϕ and direction of the impulse.

Table III-16

Lateral Jet Correction Parameters – 11 September $22^h40^m00^s$ to $22^h41^m08^s$.

	ΔV	Resulting Drift	Pulsing Time	Number Pulses	ΔW	P_I	P_F	e_R	i_R	Ω_R	$SARA_R$	$SADEC_R$
Predicted	9.26**	ϕ*	67.7 (68)	184	0.255	159	151	0.0028	0.094	23.9	-14.6†	-84.0 †
Actual	9.11	0.008	68	185	0.257***	160	151	0.0028	0.095	20.2		

*The actual drift rate used in the calculations, which are based on the period corresponding to the osculating semi-major axis, was 0.014 degree/orbit and was selected to compensate for perturbations due to the sun, moon, triaxiality, and oblateness, thus producing a mean drift rate of 0. deg/orbit.

**Based on results of the previous maneuver, the ΔV which was used to deduce the on-time for this maneuver was 1.1137 times the predicted tabular value.

***Based on actual on-time and pressure drop.

†Computed after the maneuver based on change in ϕ and direction of the impulse.

11 September and had an eccentricity of 0.0028. With this eccentricity, the daily excursion in longitude was 179.68 to 180.32 degrees west with a mean value of 180.00 degrees. The excursion in latitude was ±0.095 degree (i.e., equal to the orbit inclination).

Combined Maneuver – Reorientation Followed by Orbital Inclination Adjustment Using the Axial Engine – System 1

The objectives of this combined maneuver were to:

1. Position the spin axis normal to the equatorial plane (i.e., the +Z direction along the southward normal).
2. Adjust the orbital inclination such that one week subsequently (allowing for perturbations due to the sun and moon), the orbit could be made stationary using the lateral engines.

Reorientation maneuver parameters are given in Table III-17 and orbital inclination adjustment parameters are given in Table III-18.

Table III-17

Reorientation Maneuver Parameters 25 September $22^h50^m00^s$ to $22^h50^m6.8^s$

$22^h50^m40^s$ to $22^h50^m41.8^s$.

	Pulsing Time	Number Pulses	Precession Angle	ΔW	ΔV	P_I	P_F	ϕ_F	$SARA_R$	$SADEC_R$
Predicted	8.6	23	5.67	0.049	1.8*	163	161.6	89.2	ϕ	-90.0
Actual	8.6	23	††	0.049***	†	164	163	**	††	††

*Includes a factor of 1.5 for higher ΔV realized when using this mode of maneuvering.

**The T&C stations were unable to read ϕ since the ψ and ψ_2 pulses are superimposed at 90 degrees.

***Assumed to be the predicted due to uncertainty in pressure reading.

†Unable to evaluate because of the combined maneuver and uncertainties in orbital data.

††Not evaluated due to lack of data.

Table III-18

Axial Jet Orbital Inclination Adjustment 25 September $02^h57^m00^s$ to $02^h57^m22.5^s$.

	ΔV	On-Time	Resulting Drift	ΔW	P_I	P_F	e_R	i_R	Ω_R
Predicted	21.0*	22.5	-0.03	0.335	161.6	152	0.0028	0.017	280
Actual	†	22.5	-0.069	**	163	154	0.0028	0.006***	270

*The ΔV required to obtain the desired inclination was 22.8 fps. However, 1.8 fps should have been obtained from the reorientation part of the maneuver.

**Not computed due to uncertainty in pressure.

***The resulting inclination differs from the predicted by the amount of uncertainty in the initial inclination.

†Unable to accurately evaluate due to uncertainties in the orbital elements.

Three Maneuvers to Establish a Near-Stationary Orbit — System 1

The purpose of this series of three maneuvers was to establish a circular orbit at 179.97 degrees west longitude with an initial drift rate of 0.011 degree per orbit west. Achievement of such an orbit would cause Syncom III to remain within 0.03 degree of the desired longitude of 180 degrees west for the maximum period of time, 22.2 days, without additional corrections.

To accomplish the maneuvers in a reasonable period of time, the three were designed and executed without intermediate orbit determination. Table III-19 summarizes the three maneuvers.

Table III-19

Data on Maneuvers to Establish Near-Stationary Orbit.

Maneuver Number	Maneuver Number	ΔV	Resulting Drift	Pulsing Time	Number Pulses	ΔW	P_I	P_F	e_R	i_R
Predicted 1	October 1 $08^h51^m00^s$ $08^h51^m46.3^s$	6.273	0.596	46.3 (46.3)*	127 (127)*	0.185	160 (160)*	155 (155)*		
Predicted 2	October 1 $20^h50^m00^s$ $20^h50^m50.2^s$	6.652	-0.116	50.2 (50.2)	138 (138)	0.195	154 (153)	149 (148)		
Predicted 3	October 2 $08^h48^m00^s$ $08^h48^m10.4^s$	1.185	0.011	10.3 (10.4)	28 (29)	0.052	149 (148)	148 (147)	0	0.04
Actuals for After Maneuver Number 3			0.0025						0.00016**	0.058

*Numbers in parentheses are actuals.

**Mean eccentricity after reduction using perturbation scheme. See HAC IDC 2280.03/157.

Seventh Lateral Jet Velocity Correction — System 2

By the time this maneuver was made the triaxial force had caused the drift sense to change to eastward and the satellite had drifted to 0.4 degree to the east of the International Date Line. Since it was desired to keep the vehicle near 180 degree longitude, this maneuver was designed to produce a westward drift such that the vehicle would drift to 0.03 degree west of the Date Line and at such time the triaxial force would again reverse the drift sense; the result being that the satellite would remain within 0.03 degree of the date line for a maximum length of time without further correction. The lateral jet correction parameters are given in Table III-20.

Data on propellant utilization is summarized in Table III-21.

Table III-20

Lateral Jet Correction Parameters 30 October $17^h01^m30^s$ to $17^h01^m35.2^s$.

	ΔV	Resulting Drift	Pulsing Time	Number Pulses	ΔW	P_I	P_F	e_R
Predicted	0.57	0.030	4.2	11	0.025	201	200	0.00006
Actual	0.98**	0.075***	5.2	14	0.043††	†	†	0.00013

*As in previous velocity corrections the factor of 1.1137 was applied to the desired ΔV for the calculation of ON time. (i.e., the assumption being that systme 1 and system 2 are the same.)

**1) Derived from the resulting net change in drift rate.
2) An error in the actual ΔV was expected since in-flight calibration had not been performed on System 2 in the pulsed mode.

***Mean drift rate; accounting for the sun, the moon, and oblateness.

†Not reported.

††Based on actual ΔV.

Table III-21

Summary of Propellant Utilization.

System 1	System 2	Maneuver Time	Comments
4.90 pounds	4.92 pounds	19 August	Initial loading
0.155		20 August	First reorientation
	1.69	22 August	First axial jet correction
	0.176	28 August	Second reorientation
	0.470	28 August	Second axial jet correction
0.270		31 August	"Maneuver" to release pressure
0.365		3 September	Third reorientation
1.104		10 September	First lateral jet correction
0.259		10 September	Second lateral jet correction
0.257		11 September	Third lateral jet correction
0.049		25 September	Fourth reorientation
0.335		25 September	Orbit inclination adjustment
0.185		1 October	Fourth lateral jet correction
0.195		1 October	Fifth lateral jet correction
0.052		2 October	Sixth lateral jet correction
	0.043	30 October	Seventh lateral jet correction
1.674 remains	2.541 remains (as of 30 October)		
(3.226 used)	(2.379 used)		

CHAPTER IV

COMMUNICATION TEST RESULTS

INTRODUCTION

This chapter presents a report prepared by the U. S. Army Satellite Communications Agency in accordance with the NASA/SATCOM Experimental Test Plan, Revision B, dated 21 March 1964; the NASA/GSFC Operations Plan 6-64 for the A-27 Syncom III Spacecraft, and the DCA Syncom II and Syncom III Implementation Test Plan. The report contains the final analysis of the results of Syncom III tests with the main emphasis on multichannel testing. (A separate series of tests involving two-way VHF communications with aircraft is described in Chapter VII.)

The evaluation of the Syncom III system provides an analysis of the multichannel capability of the system, including such parameters as signal-plus-noise-to-noise vs. communication receiver carrier levels, amplitude and phase delay characteristics, intermodulation characteristics, telephony characteristics (articulation and intelligibility), signal-plus-noise-to-noise distribution, and multichannel teletype characteristics. The system performance characteristics are used as a basis to determine the multichannel capability of the Syncom III system.

It should be noted that the Syncom III tests were performed mainly in a half duplex or loop configuration and the results may be considered valid for this type of operation. In considering multiple accesses through the spacecraft, the half duplex results must be degraded to allow for the inherent M-A losses of approximately 4db.

Also included in this report is a discussion of the digital data transmission characteristics using biphase modulation techniques and discussion of the 50-kc transponder characteristics of the Syncom III system. Initial testing of the 50-kc transponder was from collection of ETP test data was completed by 7 May 1965. As of 30 June 1965 the Syncom III spacecraft has logged over 6037 hours of communication time and approximately 132 hours of range and range-rate measurements.

The communications performance of the Syncom III spacecraft resulting from the experimental test program demonstrated the capability of providing adequate communications for up to two voice channels (or 32 channels of teletype) of tactical quality in full duplex operation. Results show that the system will support four voice channels of half duplex communications albeit at greatly degraded levels.

Test results disclosed that the modifications of the ground stations to incorporate the AN/TCC-3 equipment did not effect any significant change in the single channel performance. Therefore, single channel results appearing in previous Syncom reports are considered valid and representative.

BASEBAND DESCRIPTION

During the period from November 1964 to March 1965, the AN/TCC-3 equipment was installed in the ground stations. The terminal modifications in conjunction with the AN/TCC-3 were to

provide increased operational flexibility and provisions for trading off threshold for additional channels or channel improvement if warranted by the received signal levels. Up to five 4-kc baseband channels and up to 10 modulation indices may be selected for both the modulator and demodulator by the console operator.

Tables IV-1 and IV-2 show a complete layout of the available modulation indices, bandwidths, channel capacities and demodulator characteristics. Below is a list of the new modes of operation which were tested and their intended application.

Table IV-1

Multichannel Indices and IF Bandwidths.

Baseband Channel Capacity	Baseband width	IF Bandwidth for Given Modulation Index (M)		
		M = 1 (no FB)	M = 4 (FB)	M = 10 (FB)
1	4 kc	10 kc	23 kc	23 kc
2	8 kc	33 kc	33 kc	60 kc
3	12 kc	33 kc	60 kc	----
5	20 kc	60 kc	60 kc	----

Table IV-2

Demodulation Characteristics.

Baseband Channel Capacity	Baseband width	Available Deviation Ratio	Demodulator Characteristics		
			M = 1	M = 4	M = 10
1	4 kc	1, 4, 10	FM	FMFB	FMFB
2	8 kc	1, 4, 10	FM	FMFB	FMFB
3	12 kc	1, 4	FM	FMFB	----
5	20 kc	1, 4	FM	FMFB	----

Mode	Function
1-4; 1-1	4-kc maximum deviation and 4-kc baseband. The IF bandwidth is 10 kc. This mode provides communications under conditions of low input carrier-to-noise ratios.
1-10; 1-10	40-kc maximum deviation and 4-kc baseband. The IF bandwidth is 23 kc and FM with feedback is employed. This mode provides the advantages of a high modulation index system at lower input carrier-to-noise ratios than possible with conventional FM receiver.
2-4; 2-4	32-kc maximum deviation and 8-kc baseband. The IF bandwidth is 33 kc and FM with feedback is employed. This mode provides two multiplexed voice channels of communications under conditions of low input carrier-to-noise ratios.
2-10; 2-10	80-kc maximum deviation and 8-kc baseband. The IF bandwidth is 60 kc and FM with feedback is employed. This mode provides the advantage of a high modulation index system employing two multiplexed voice channels of communications.

Mode	Function
3-4; 3-4	48-kc maximum deviation and 12-kc baseband. The IF bandwidth is 60 kc and FM with feedback is employed. This mode provides three multiplex channels when a relatively good input carrier-to-noise ratio is available.
5-4; 5-4	80-kc maximum deviation and 20-kc baseband. The IF bandwidth is 60 kc and FM with feedback is employed. This mode provides five multiplexed voice channels of communications.

TECHNICAL TEST EVALUATION

Signal-Plus-Noise-to-Noise vs. Communications Level

The signal-plus-noise-to-noise vs. communication carrier level is one of the basic fundamental relationships used in determining the performance of a communication system. The initial approach, therefore, in evaluating the Syncom III system was to accumulate the data required to establish the signal-plus-noise-to-noise vs. communication level relationship for each of the various operating modes in single channel operation. In addition, this relationship was also determined for the various 4-kc baseband channels using the AN/TCC-3 in each of the appropriate operating modes. A great amount of test time was devoted to recording enough measurements to provide statistical reliability to each of the resulting signal-plus-noise-to-noise vs. carrier level relationships for the various system configurations. The data from each series of tests were plotted as scatter diagrams which were used to fit curves of signal-plus-noise-to-noise vs. communication carrier level.

The test procedures employed in the single channel tests (test code 13) are described in the Experiment Test Plan (ETP), revision B. Essentially, the tests were performed by feeding 1 kc input test tone at -10dbm directly to the modulator from a test tone generator and transmitting it at various power levels. The initial transmitter power is set at 16 kw and is lowered in 3db steps until the receive system breaks lock. These tests were performed in the six operating modes described earlier. Multichannel testing required using the basic test code 13 procedure but loading the other baseband channels. Figures IV-1 through IV-19 show the relationship of signal-plus-noise-to-noise vs. communication carrier for the various operating modes at Camp Roberts, Clark AFB, and the USNS Kingsport. It should be noted, however, that the nature of the experimental testing produced a wide dispersion in the scatter diagrams which formed the basis for the fitted curves of Figures IV-1 through IV-19. Figure IV-20 illustrates a typical scatter diagram with fitted curve. Statistical comparison of the fitted curves for the three stations indicate that the dispersion encountered at Camp Roberts was fairly low, for the Kingsport it was somewhat higher, but still not critical, and for the Philippines it was relatively high. Investigation and analysis indicated that the following were significant contributors to the spread of data.

During the test period, the Philippine station was involved primarily in operational type traffic and participated only periodically in experimental testing. This produced fewer data points and a poor testing environment.

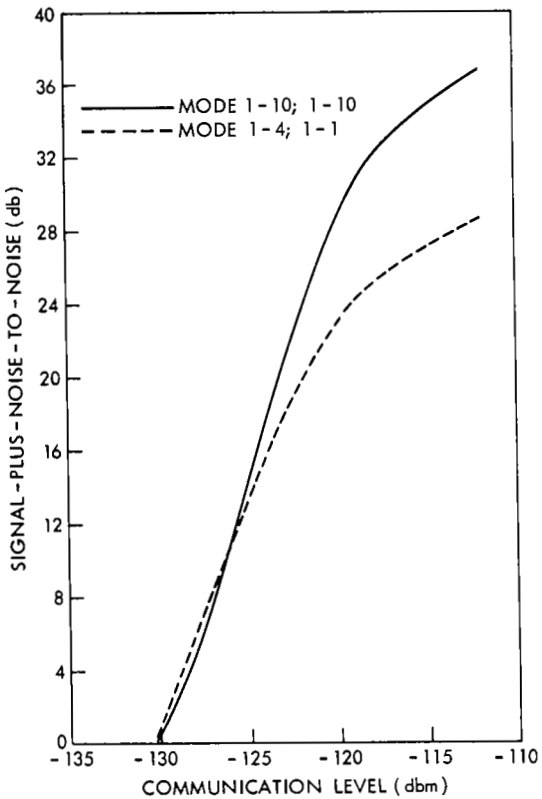

Figure IV-1—Signal-plus-noise-to-noise vs. communication level, modes 1-4, 1-1 and 1-10; 1-10—Camp Roberts.

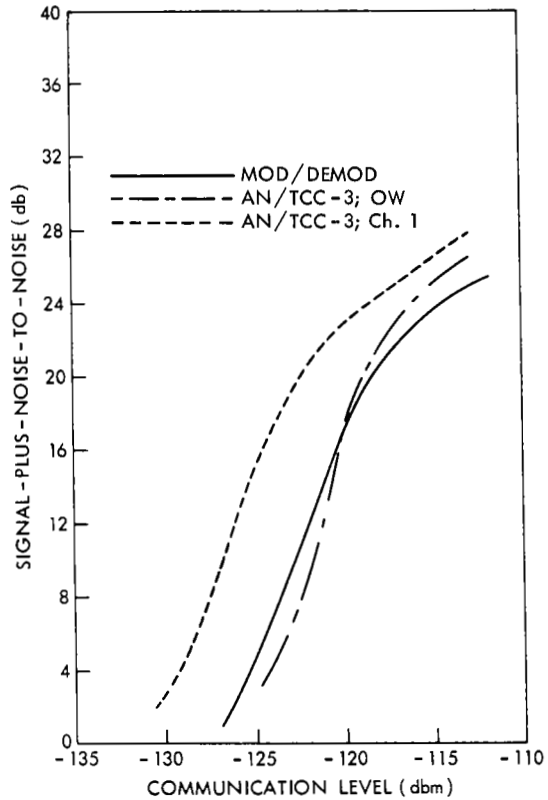

Figure IV-2—Signal-plus-noise-to-noise vs. communication level, mode 2-4; 2-4; mod/demod; AN/TCC-3 (OW and ch. 1)—Camp Roberts.

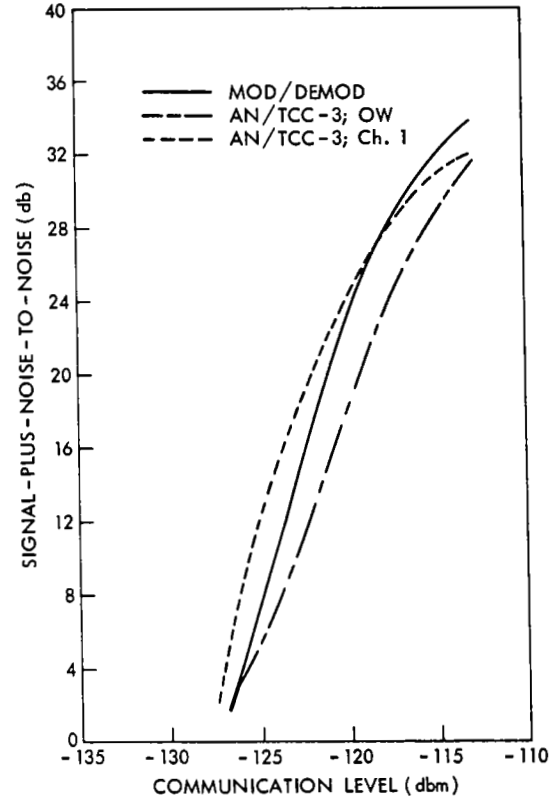

Figure IV-3—Signal-plus-noise-to-noise vs. communication level, mode 2-10; 2-10; mod/demod; AN/TCC-3 (OW and ch. 1)—Camp Roberts.

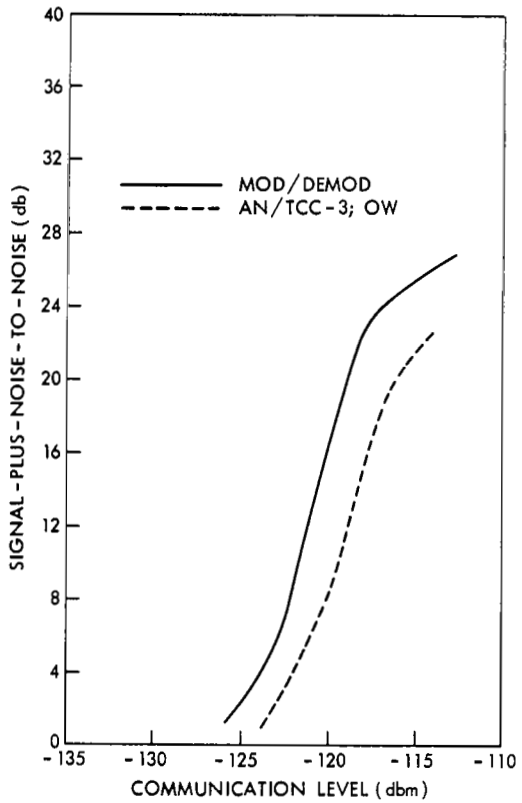

Figure IV-4—Signal-plus-noise-to-noise vs. communication level, mode 3-4; 3-4; mod/demod; AN/TCC-3 (OW)—Camp Roberts.

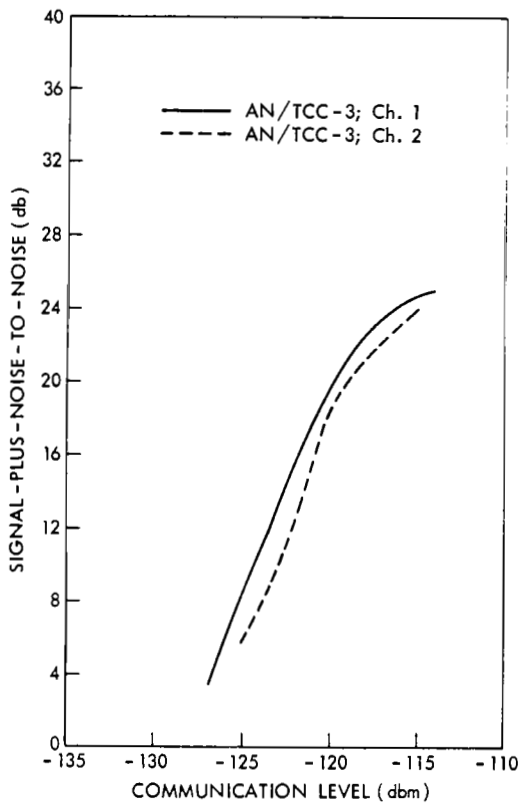

Figure IV-5—Signal-plus-noise-to-noise vs. communication level, mode 3-4; 3-4; AN/TCC-3 (ch. 1 and ch. 2)—Camp Roberts.

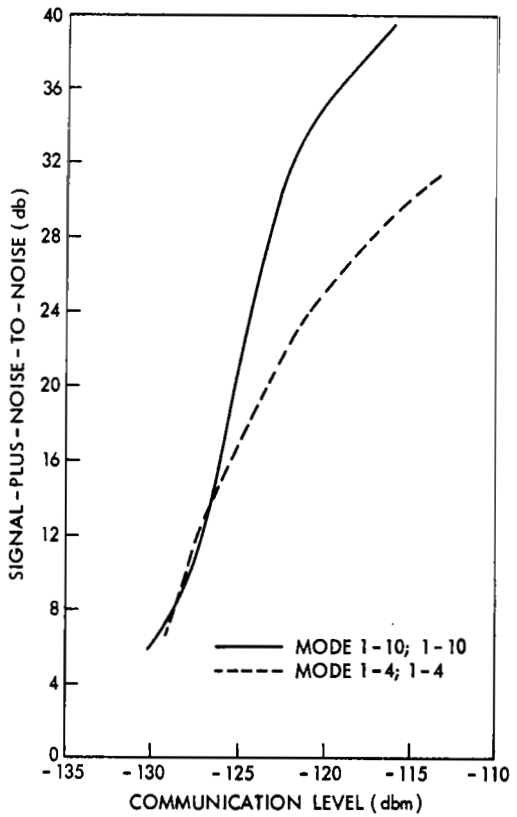

Figure IV-6—Signal-plus-noise-to-noise vs. communication level, modes 1-4; 1-1 and 1-10; 1-10—Philippines.

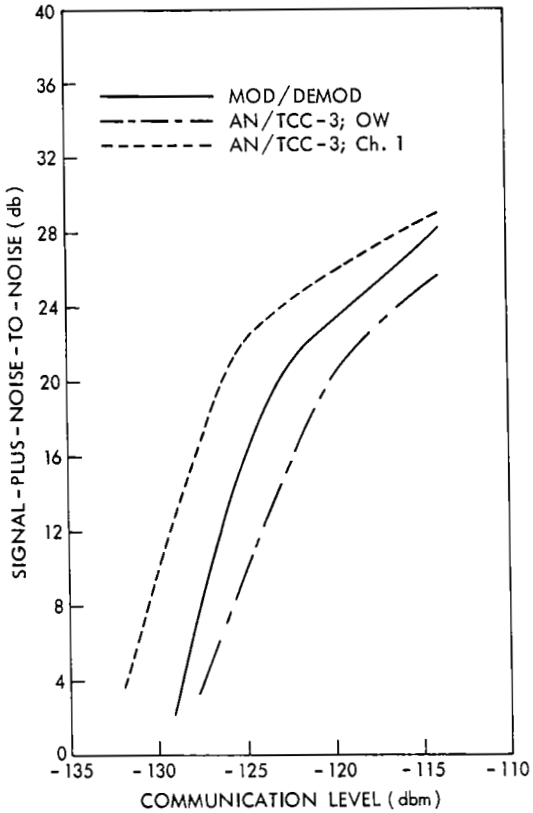

Figure IV-7—Signal-plus-noise-to-noise vs. communication level, mode 2-4; 2-4; mod/demod; AN/TCC-3 (OW and ch. 1)—Philippines.

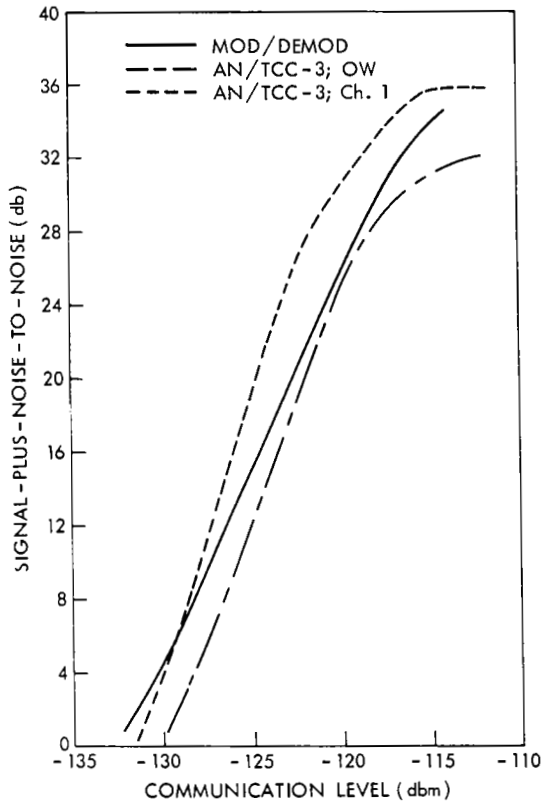

Figure IV-8—Signal-plus-noise-to-noise vs. communication level, mode 2-10; 2-10; mod/demod; AN/TCC-3 (OW and ch. 1)—Philippines.

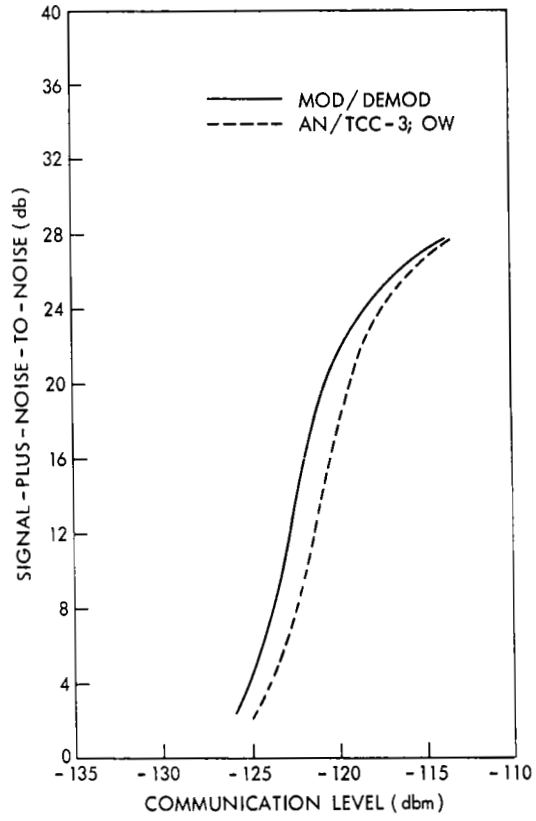

Figure IV-9—Signal-plus-noise-to-noise vs. communication level, mode 3-4; 3-4; mod/demod; AN/TCC-3 (OW)—Phillipines.

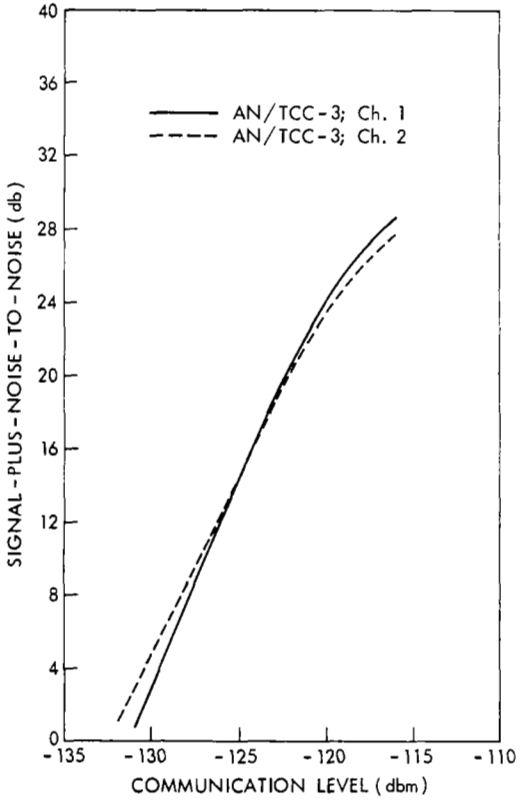

Figure IV-10—Signal-plus-noise-to-noise vs. communication level, mode 3-4; 3-4; AN/TCC-3 (ch. 1 and ch. 2)—Philippines.

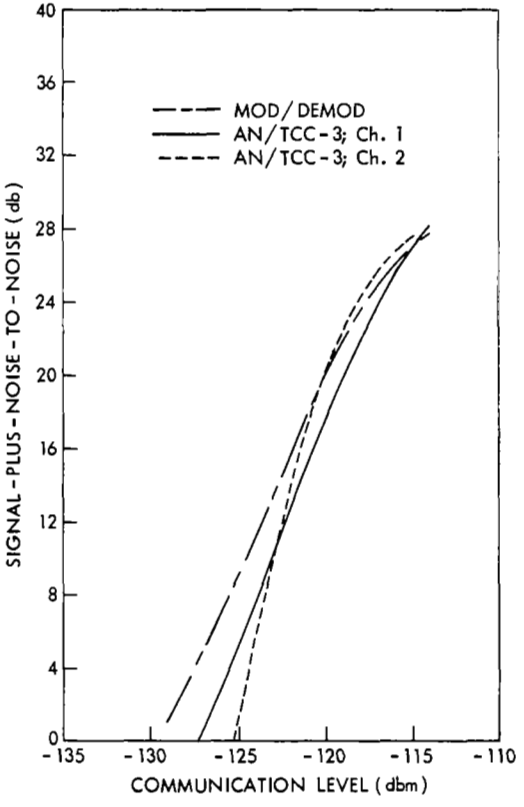

Figure IV-11—Signal-plus-noise-to-noise vs. communication level, mode 5-4; 5-4; mod/demod; AN/TCC-3 (ch. 1 and ch. 2)—Philippines.

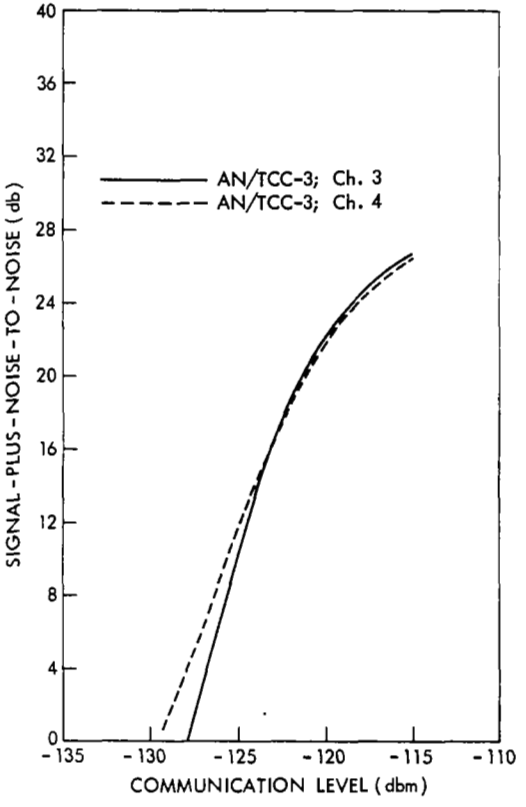

Figure IV-12—Signal-plus-noise-to-noise vs. communication level, mode 5-4; 5-4; AN/TCC-3 (ch. 3 and ch. 4)—Philippines.

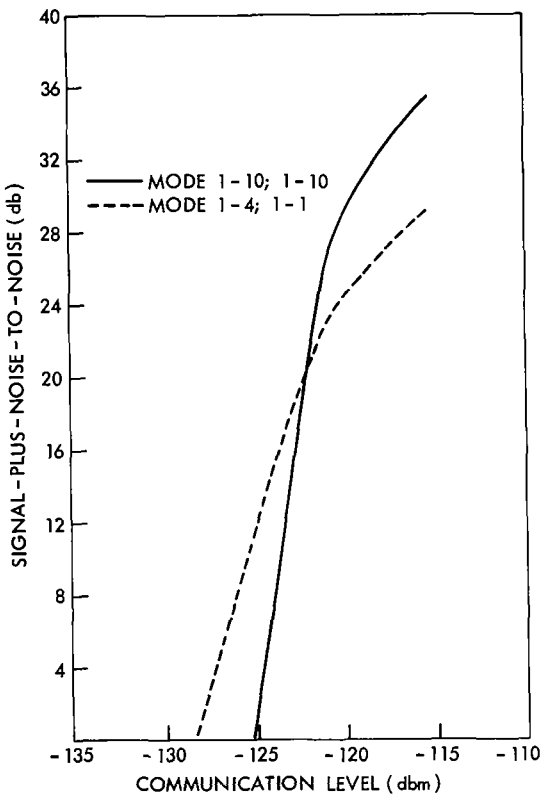

Figure IV-13—Signal-plus-noise-to-noise vs. communication level, modes 1-4; 1-1 and 1-10; 1-10—Kingsport.

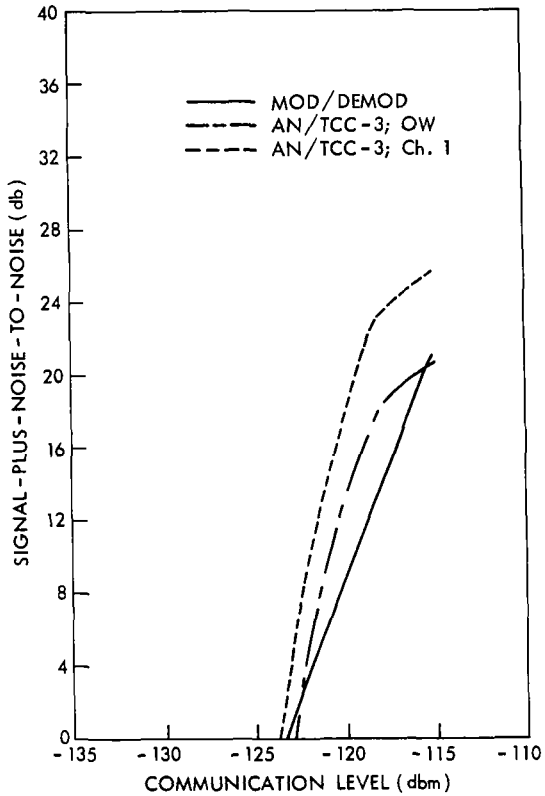

Figure IV-14—Signal-plus-noise-to-noise vs. communication level, mode 2-4; 2-4; mod/demod; AN/TCC-3 (OW and ch. 1)—Kingsport.

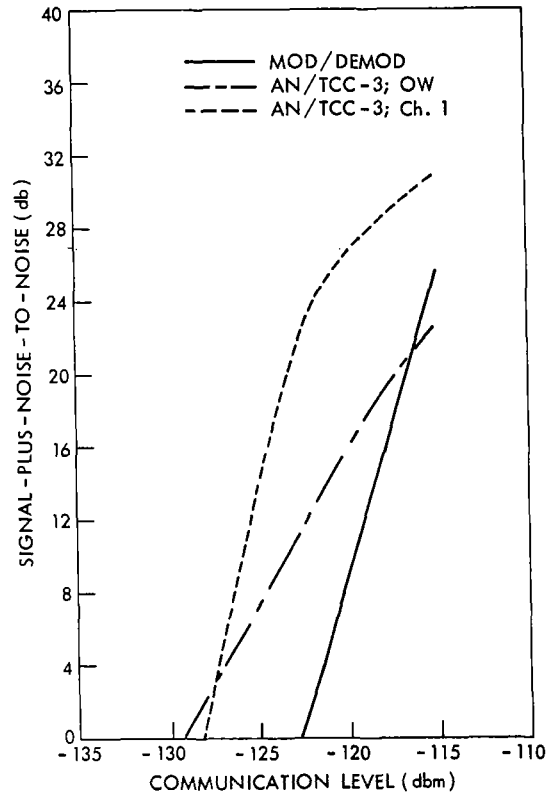

Figure IV-15—Signal-plus-noise-to-noise vs. communication level, mode 2-10; 2-10; mod/demod; AN/TCC-3 (OW and ch. 1)—Kingsport.

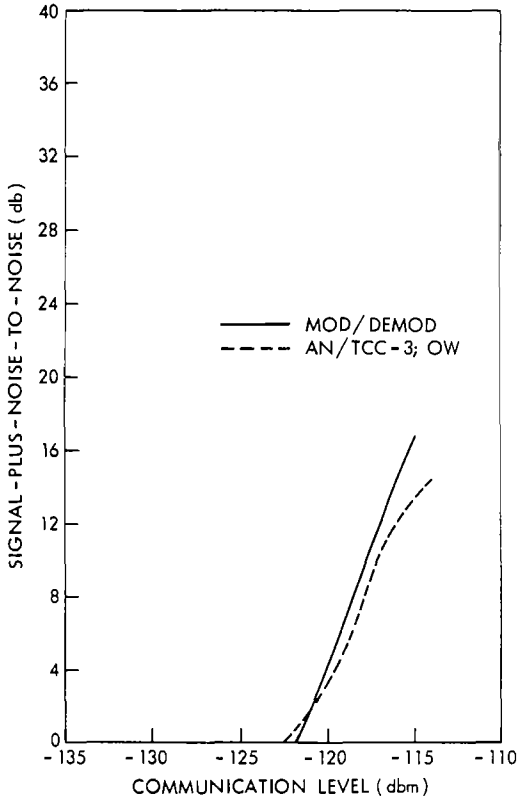

Figure IV-16—Signal-plus-noise-to-noise vs. communication level, mode 3-4; 3-4; mod/demod; AN/TCC-3 (OW)—Kingsport.

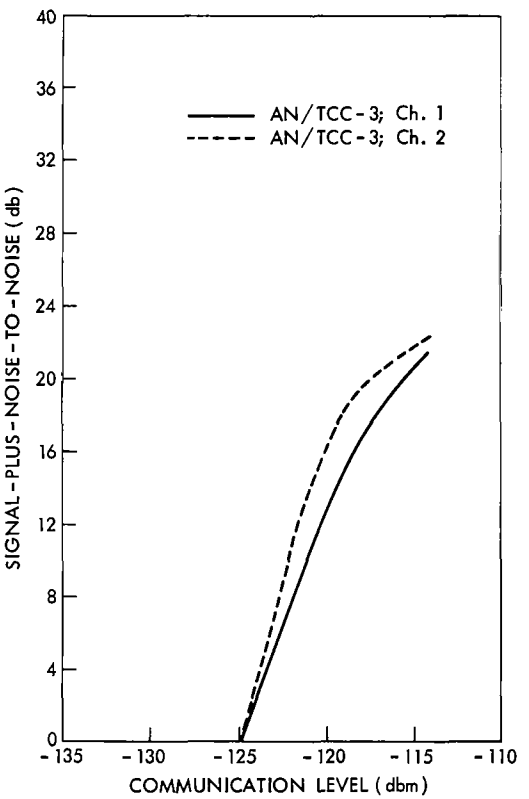

Figure IV-17—Signal-plus-noise-to-noise vs. communication level, mode 3-4; 3-4; AN/TCC-3 (ch. 1 and ch. 2)—Kingsport.

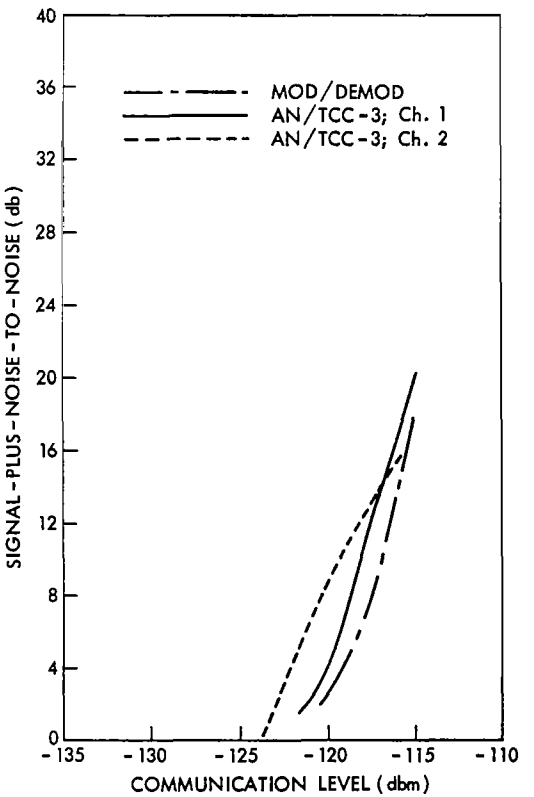

Figure IV-18—Signal-plus-noise-to-noise vs. communication level, mode 5-4; 5-4; mod/demod; AN/TCC-3; (ch. 1 and ch. 2)—Kingsport.

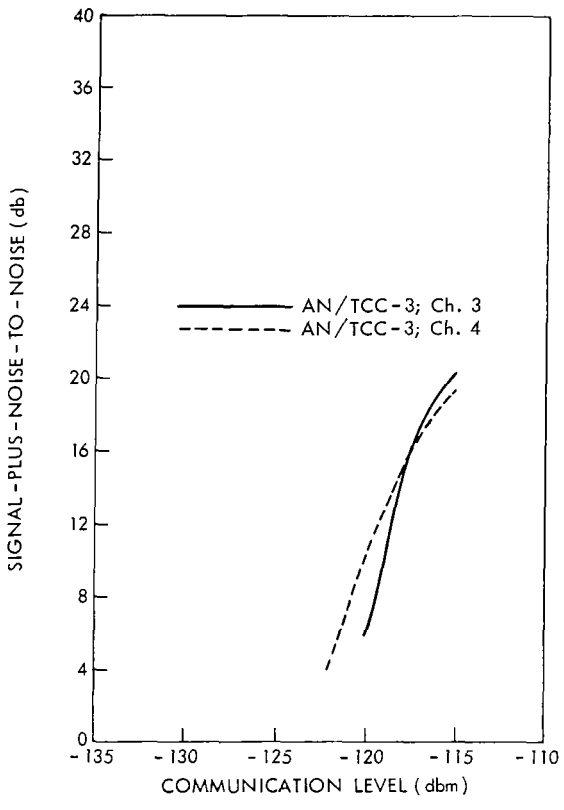

Figure IV-19—Signal-plus-noise-to-noise vs. communication level, mode 5-4; 5-4; AN/TCC-3 (ch. 3 and ch. 4)—Kingsport.

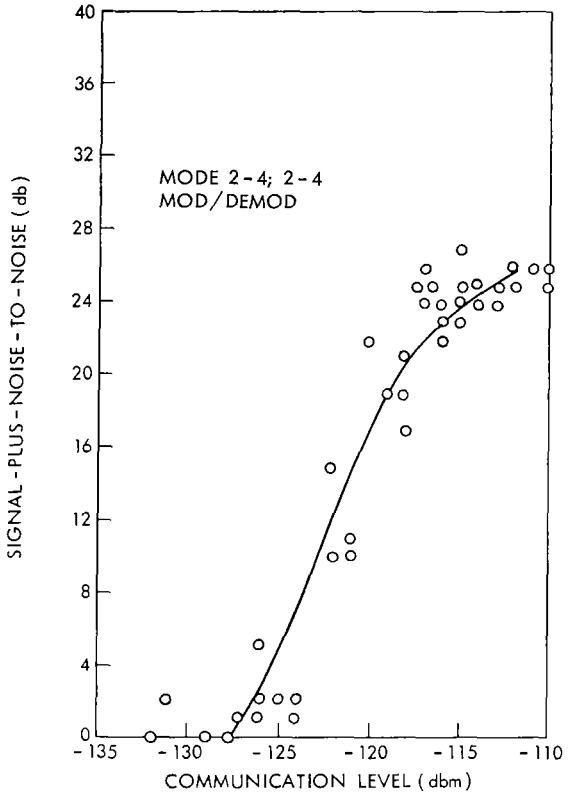

Figure IV-20—Signal-plus-noise-to-noise vs. communication level; curve fitted to scatter points.

The station operating personnel were not sufficiently trained for a test program of this magnitude, and quite often failed to follow the stringent procedures required for good test data.

In the area of threshold and below, it is expected that the dispersion will be significant.

The modification of the stations to utilize the AN/TCC-3 equipment introduced the problem (inherent with AN/TCC-3 operation) of nonconsistent alignment from test to test.

The fact that Camp Roberts had much lower dispersion (or standard deviations) lends much credulence to 1 and 2 above since Roberts acted as the pilot test station and operated with the best trained and most experienced crew. In addition, it should be further noted that the fitted curves represent the mean curves and when used in conjunction with other statistical values, such as the distribution of signal-plus-noise-to-noise ratios (Tables IV-4 through IV-6), care should be taken to make comparisons with corresponding mean values only.

Also included in the investigation of system signal-plus-noise-to-noise vs. communication level is a comparison of curves from data measured before the station modification in the narrow/narrow mode (i.e., 4-kc deviation, 4-kc baseband, 10-kc IF bandwidth and peak clipping at an audio

frequency above 1-kc) and the wide/narrow with feedback mode (i.e., 40-kc maximum deviation, 4-kc baseband, 17-kc IF bandwidth) with the curves from data measured in the 1-4, 1-1 and 1-10; -10 modes after the station modification. Results shown in Figures IV-21 and IV-22 are for the Camp Roberts station and they show the two systems to be comparable.

Intermodulation

This test, as it was performed, is not described in the ETP. Briefly, it consisted of loading all the baseband channels of the AN/TCC-3 with equal levels using incoherent test tones and measuring the signal-plus-noise-to-noise in each channel with the other channels loaded. The test was performed in a half duplex or loop configuration and the transmitter power was adjusted to 16 kw to provide optimum signal-plus-noise-to-noise ratios. The test tone levels were increased in 2db steps from -16dbm to -4dbm and the signal-plus-noise-to-noise was measured in each step. Intermodulation is determined when the slope of the curve of signal-plus-noise-to-noise versus input level deviates from a 1 to 1 relationship. To determine the effect of the different subsystems on overall intermodulation, the test was performed with the AN/TCC-3 back-to-back, with the AN/TCC-3 modulator/demodulator back-to-back, with the AN/TCC-3 modulator/demodulator through the collimation tower and finally with the complete system through the

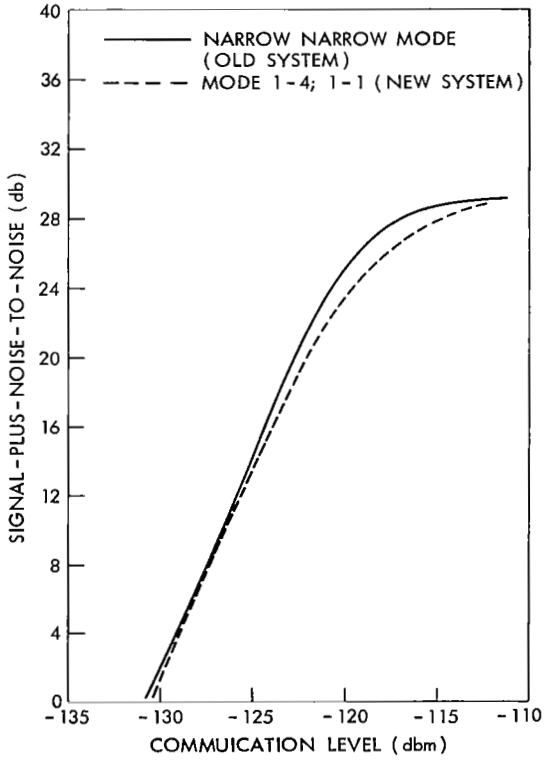

Figure IV-21—Signal-plus-noise-to-noise vs. communication level, modes 1-4; 1-1 and NN—Camp Roberts.

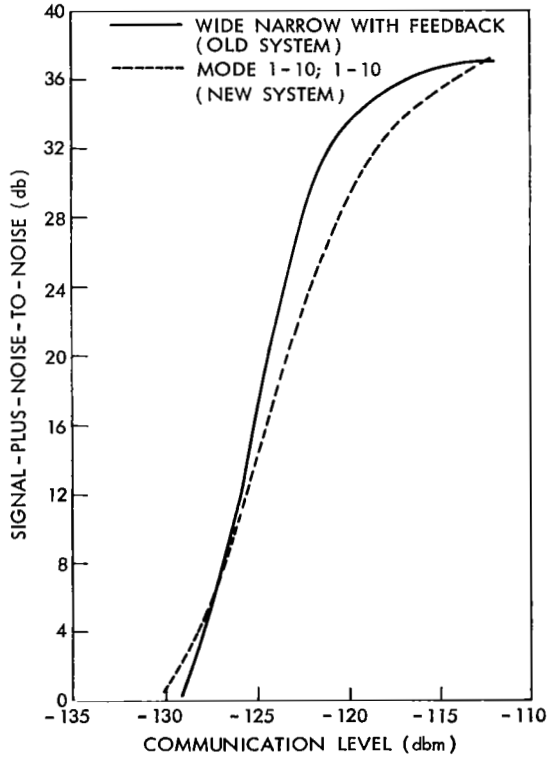

Figure IV-22—Signal-plus-noise-to-noise vs. communication level, modes 1-10; 1-10; WNFB—Camp Roberts.

satellite. Figures IV-23 through IV-25 show the results of intermodulation test performed with the AN/TCC-3 connected back-to-back at Camp Roberts. These curves show the optimum signal-plus-noise-to-noise ratio that can be expected. Figures IV-26 and IV-27 show the intermodulation due to the AN/TCC-3 and the non-linearity of the modulator/demodulator. Figures IV-28 through IV-30 show the intermodulation due to the simulator in conjunction with the AN/TCC-3 and the modulator/demodulator. As is expected, very little degradation is due to the transponder. Figures IV-31 through IV-42 show the results of intermodulation due to the satellite in conjunction with the AN/TCC-3 and the modulator/demodulator. Again, very little is added by the satellite; however, the optimum signal-plus-noise-to-noise is now determined by the downlink power budget. It should be noted that the intermodulation and noise mostly falls into the lower order channels. The system is designed for a nominal rms test tone level of -10dbm and in most cases the test results show that this is the optimum level from an intermodulation standpoint; however, the curves show that for mode 5-4; 5-4 operation, the input level of the individual channels should be about 4db lower than the nominal design input level of -10dbm. The input level should be derated from the nominal based on the statistical nature of the type of signal being used in an actual operational condition. For example, if voice were used the input would be derated to 11db below the nominal -10dbm (i.e. -21dbm).

Frequency Response and Phase Delay

The frequency response and phase delay measurements were performed in accordance with the procedures in the U. S. Army Satellite Communications Agency's Syncom Evaluation Report, dated 1 August 1964. Tests were performed in two categories: (1) those where measurements were derived at the input and output of the modulator/demodulator, and (2) those where measurements were derived at the input and output of the AN/TCC-3. All tests were performed at the Camp Roberts station. Figures IV-43 through IV-47 show the frequency response and phase delay characteristics of the system with the input to the modulator and the output of the demodulator. The modulator and demodulator are connected back-to-back at the 60-Mc point. Figures IV-48 through IV-54 show the frequency response and phase delay characteristics of the 4-kc baseband channels of the AN/TCC-3 with the modulator/demodulator connected back-to-back at the 60-Mc point. Figures IV-55 through IV-61 show the frequency response and phase delay characteristics with input to AN/TCC-3 through the spacecraft. Normally, the frequency and phase delay characteristics are determined by the baseband equipment. It is believed that the difference between the modulator/demodulator tests and the spacecraft tests is due to equipment alignment differences between the two tests and not due to the spacecraft characteristics.

The AN/TCC-3 receiver includes provisions to equalize the non-linear frequency response of up to 40 miles of spiral four cable. This equalization is accomplished by three controls (bulge, flat and slope) which vary the frequency response of a filter network inserted at the input of the receiver. Since employment of the TCC-3 as a multiplex equipment in the SATCOM link terminals obviated any requirement to operate with spiral four cable, elimination of the equalization network appeared possible. Multichannel operation during the Syncom Test Program indicated that retention of the equalization network complicated the performance of tests by requiring that each TCC-3 be equalized for flat response prior to commencement of testing.

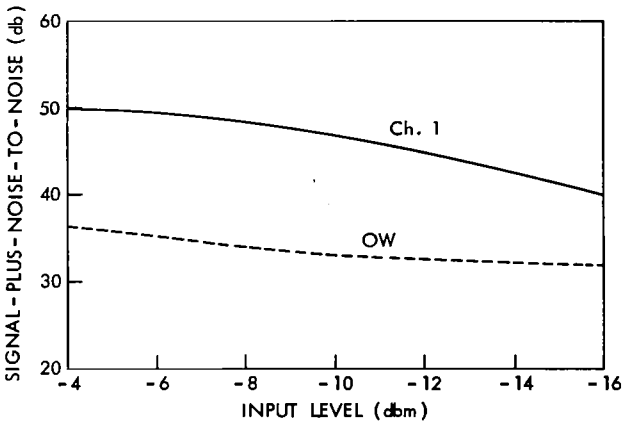

Figure IV-23—Intermodulation; signal-plus-noise-to-noise vs. input level, AN/TCC-3 back-to-back; mode 2-4; 2-4—Camp Roberts.

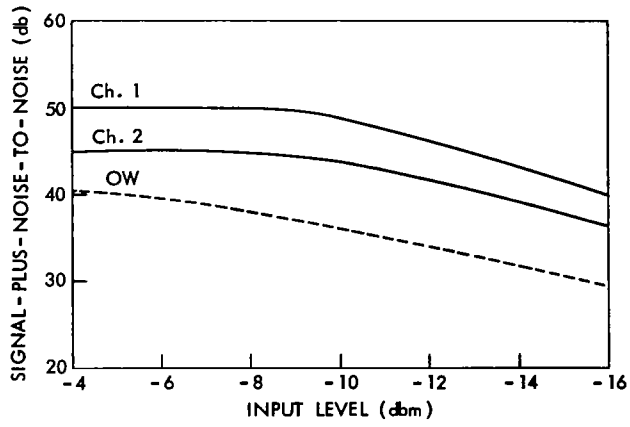

Figure IV-24—Intermodulation; signal-plus-noise-to-noise vs. input level, AN/TCC-3 back-to-back; mode 3-4; 3-4—Camp Roberts.

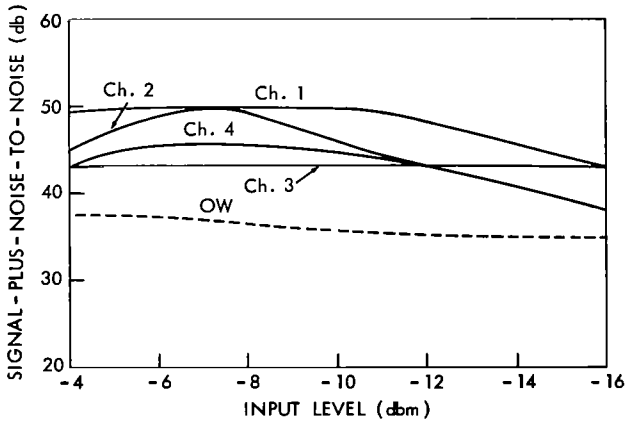

Figure IV-25—Intermodulation; signal-plus-noise-to-noise vs. input level, AN/TCC-3 back-to-back; mode 5-4; 5-4—Camp Roberts.

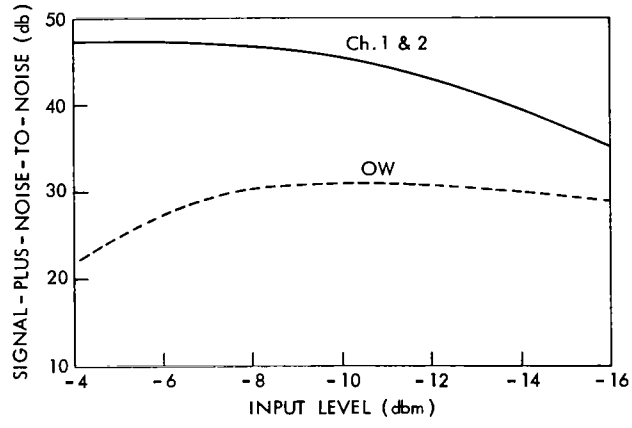

Figure IV-26—Intermodulation; signal-plus-noise-to-noise vs. input level, AN/TCC-3 mod/demod; mode 3-4; 3-4—Camp Roberts.

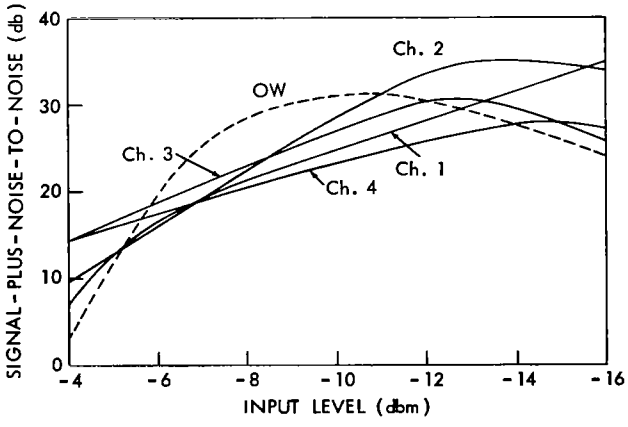

Figure IV-27—Intermodulation; signal-plus-noise-to-noise vs. input level, AN/TCC-3 mod/demod; mode 5-4; 5-4—Camp Roberts.

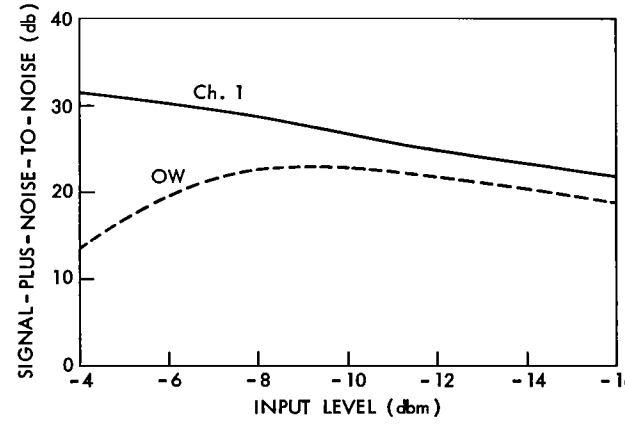

Figure IV-28—Intermodulation; signal-plus-noise-to-noise vs. input level, collimation tower; mode 2-4; 2-4—Camp Roberts.

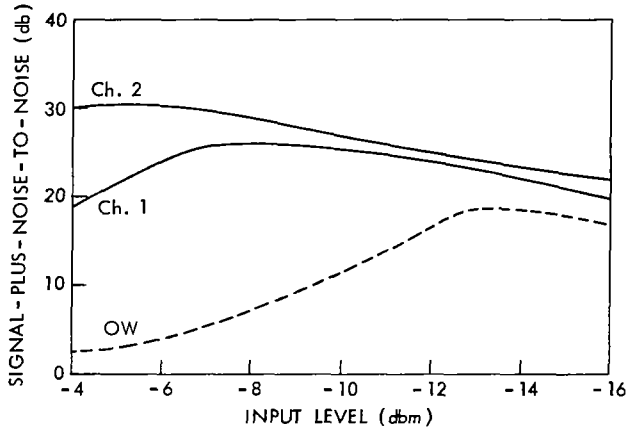

Figure IV-29—Intermodulation; signal-plus-noise-to-noise vs. input level, collimation tower; mode 3-4; 3-4—Camp Roberts.

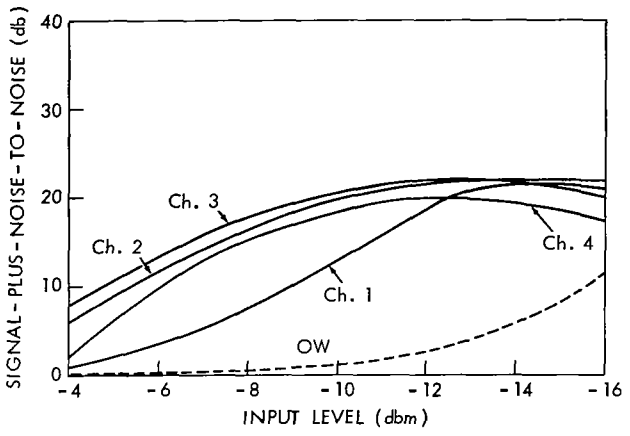

Figure IV-30—Intermodulation; signal-plus-noise-to-noise vs. input level, collimation tower; mode 5-4; 5-4—Camp Roberts.

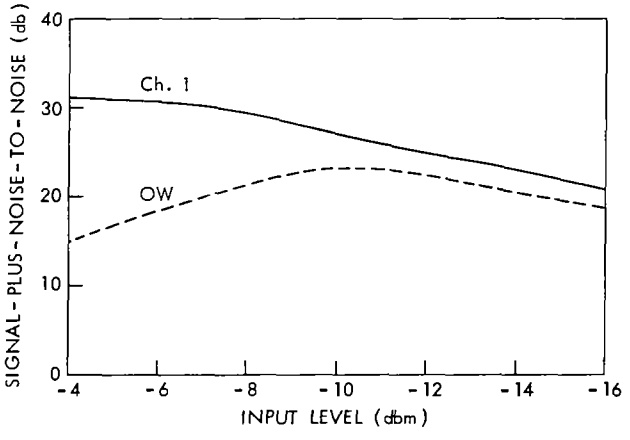

Figure IV-31—Intermodulation; signal-plus-noise-to-noise vs. input level, mode 2-4; 2-4—Camp Roberts.

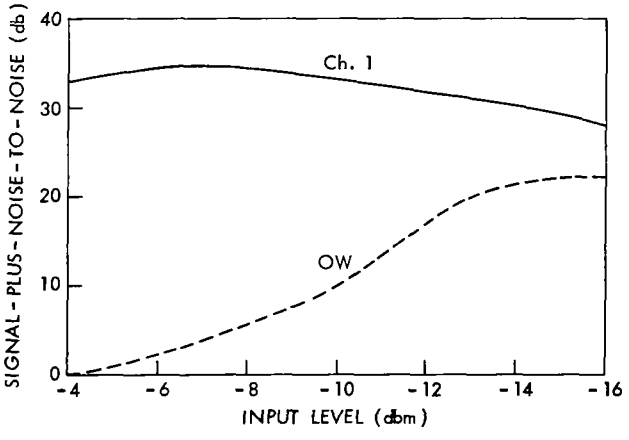

Figure IV-32—Intermodulation; signal-plus-noise-to-noise vs. input level, mode 2-10; 2-10—Camp Roberts.

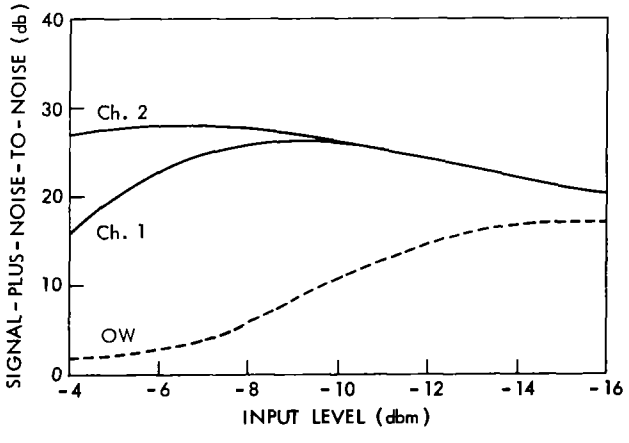

Figure IV-33—Intermodulation; signal-plus-noise-to-noise vs. input level, mode 3-4; 3-4—Camp Roberts.

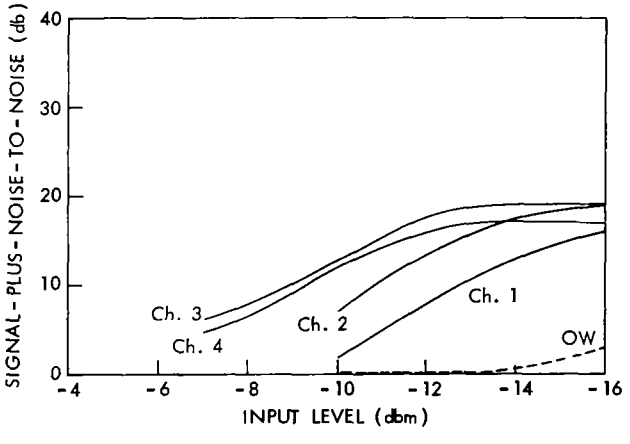

Figure IV-34—Intermodulation; signal-plus-noise-to-noise vs. input level, mode 5-4; 5-4—Camp Roberts.

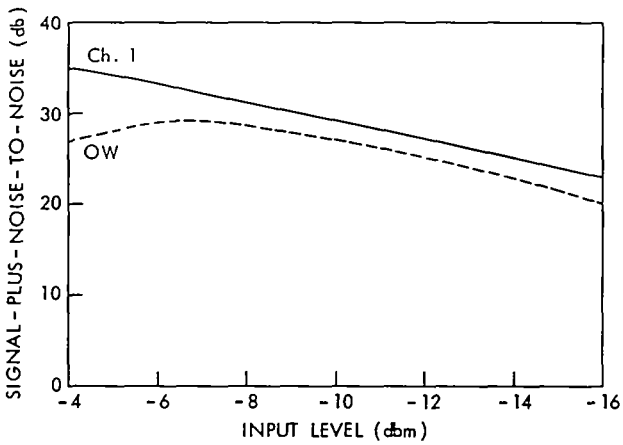

Figure IV-35—Intermodulation; signal-plus-noise-to-noise vs. input level, mode 2-4; 2-4—Philippines.

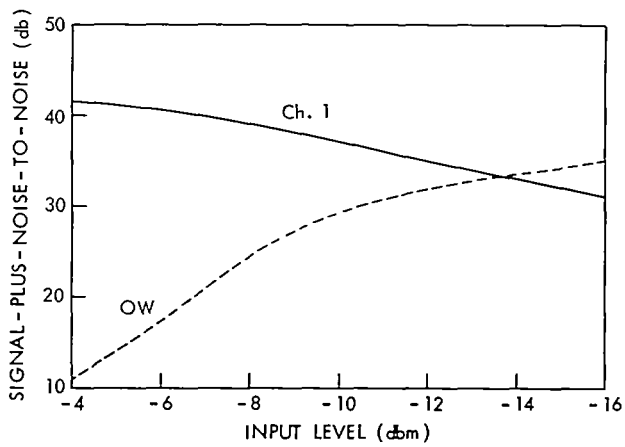

Figure IV-36—Intermodulation; signal-plus-noise-to-noise vs. input level, mode 2-10; 2-10—Philippines.

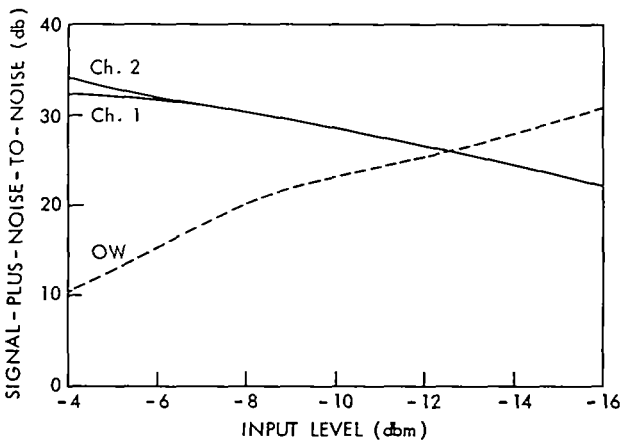

Figure IV-37—Intermodulation; signal-plus-noise-to-noise vs. input level, mode 3-4; 3-4—Philippines.

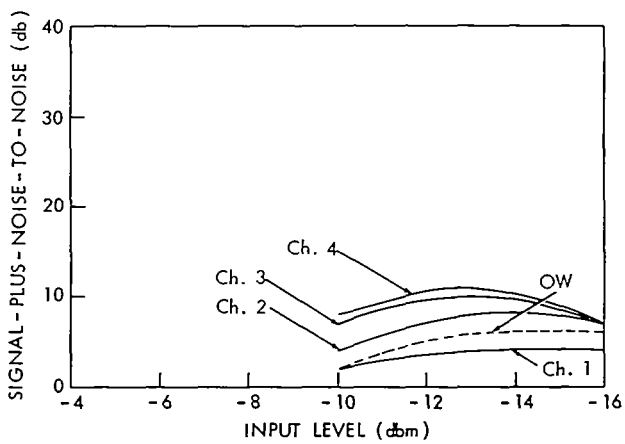

Figure IV-38—Intermodulation; signal-plus-noise-to-noise vs. input level, mode 5-4; 5-4—Philippines.

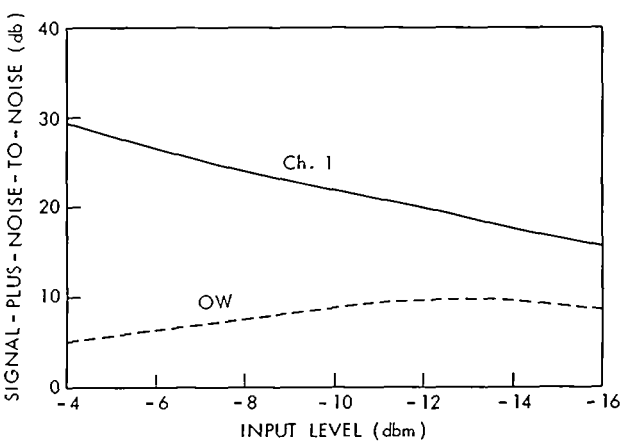

Figure IV-39—Intermodulation; signal-plus-noise-to-noise vs. input level, mode 2-4; 2-4—Kingsport.

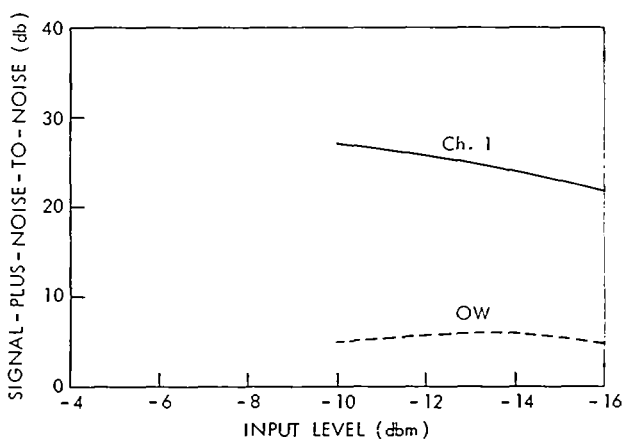

Figure IV-40—Intermodulation; signal-plus-noise-to-noise vs. input level, mode 2-10; 2-10—Kingsport.

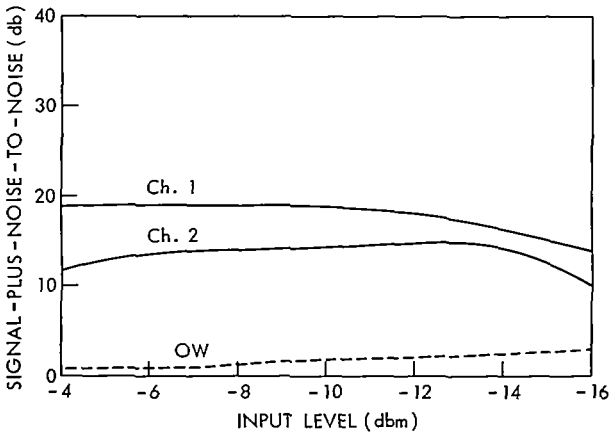

Figure IV-41—Intermodulation; signal-plus-noise-to-noise vs. input level, mode 3-4; 3-4—Kingsport.

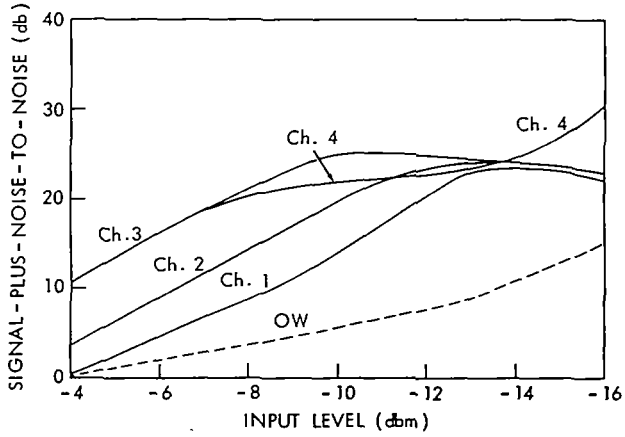

Figure IV-42—Intermodulation; signal-plus-noise-to-noise vs. input level, mode 5-4; 5-4—Kingsport.

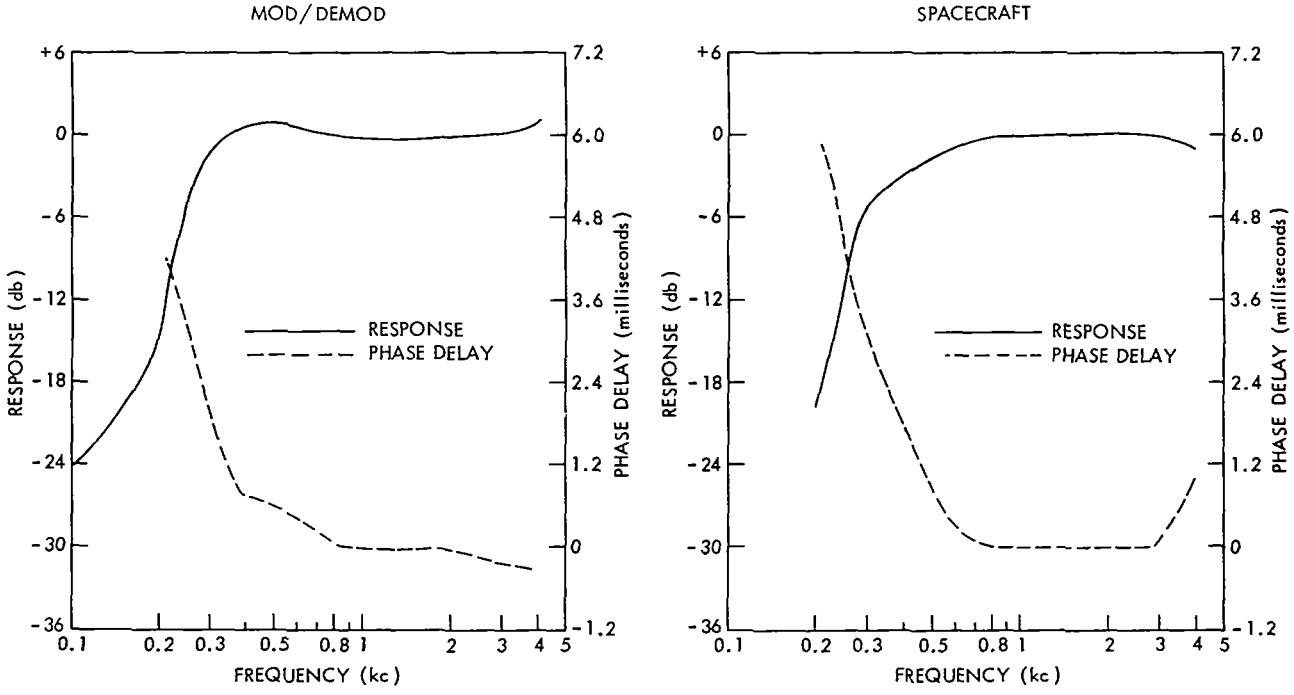

Figure IV-43—Amplitude and phase delay, mode 1-4; 1-1; mod/demod and spacecraft—Camp Roberts.

Furthermore, the equalization controls do not have a clearly defined zero, or flat, setting and consequently, the flatness achieved depends on operator skill and varies from station-to-station and even from test-to-test for the same TCC-3 if the sets were re-equalized between tests. As a consequence of operation with the TCC-3 during the Syncom Test Program, removing or by-passing the spiral four line equalization network in the TCC-3 receiver appears desirable. Further study has been undertaken and appropriate recommendations will be made for future programs.

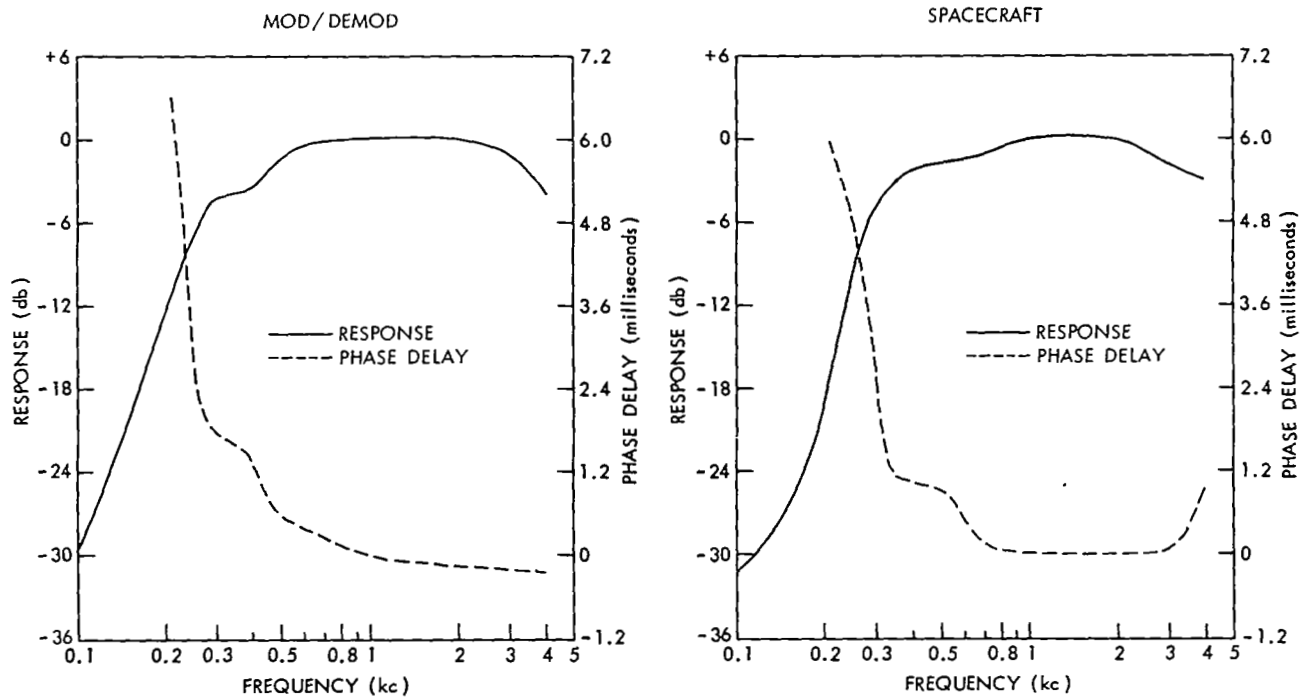

Figure IV-44—Amplitude and phase delay, mode 1-10; 1-10; mod/demod and spacecraft—Camp Roberts.

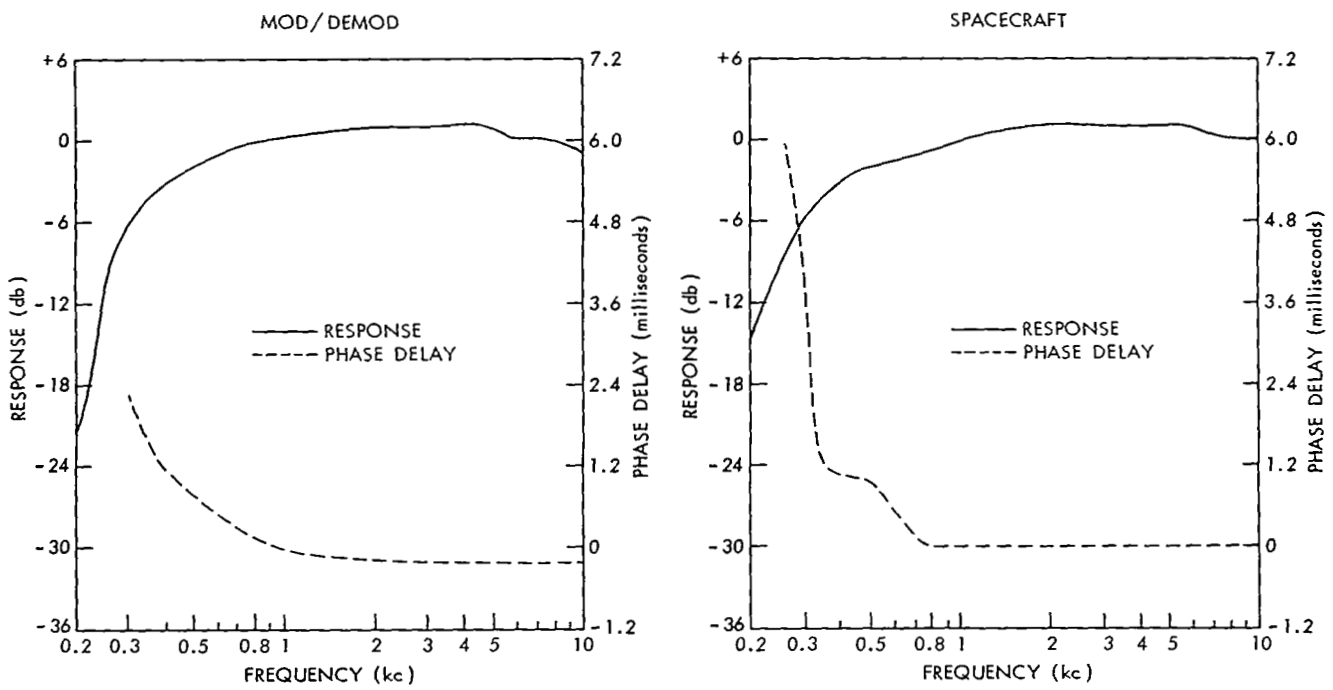

Figure IV-45—Amplitude and phase delay, mode 2-4; 2-4; mod/demod and spacecraft—Camp Roberts.

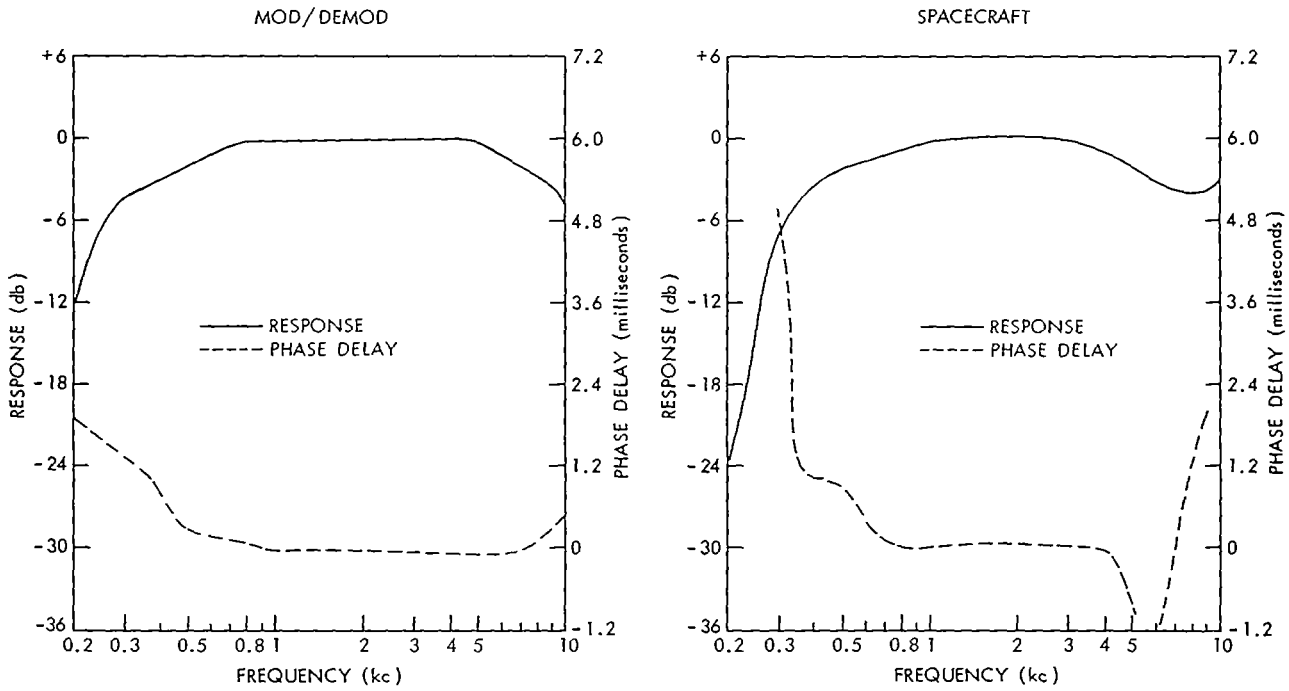

Figure IV-46—Amplitude and phase delay, mode 2-10; 2-10; mod/demod and spacecraft—Camp Roberts.

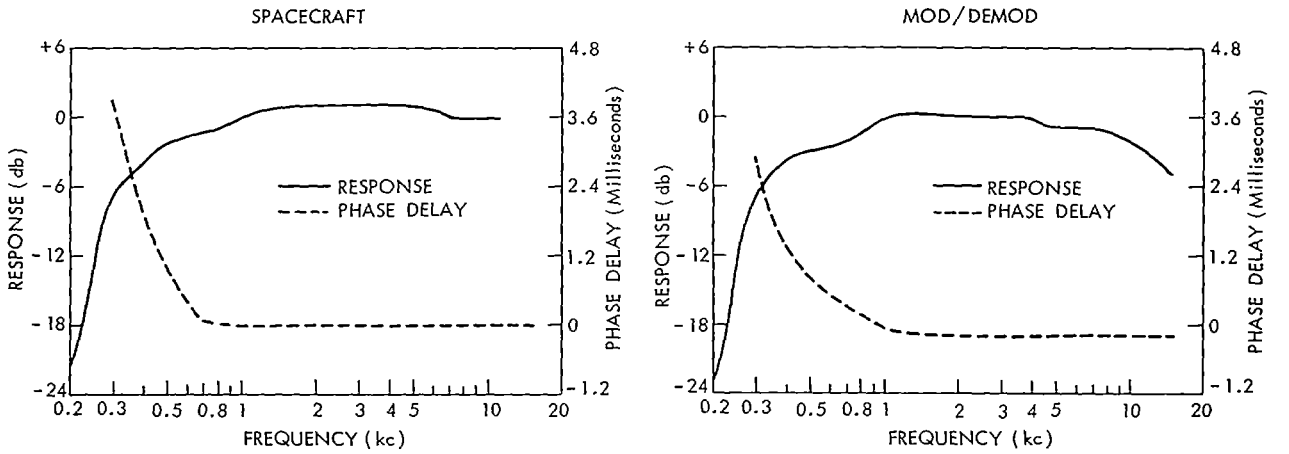

Figure IV-47—Amplitude and phase delay, mode 5-4; 5-4; mod/demod and spacecraft—Camp Roberts.

The frequency and phase delay curves of the AN/TCC-3 4 kc channels 1-4 reveal that the baseband response of the satellite link exceeds the requirements of MIL STD 188B for a 6,000 n.mi. reference circuit. If, however, the satellite links were to meet the specification of high quality data grade circuits such as Autodin, additional delay equalization would be necessary for each channel.

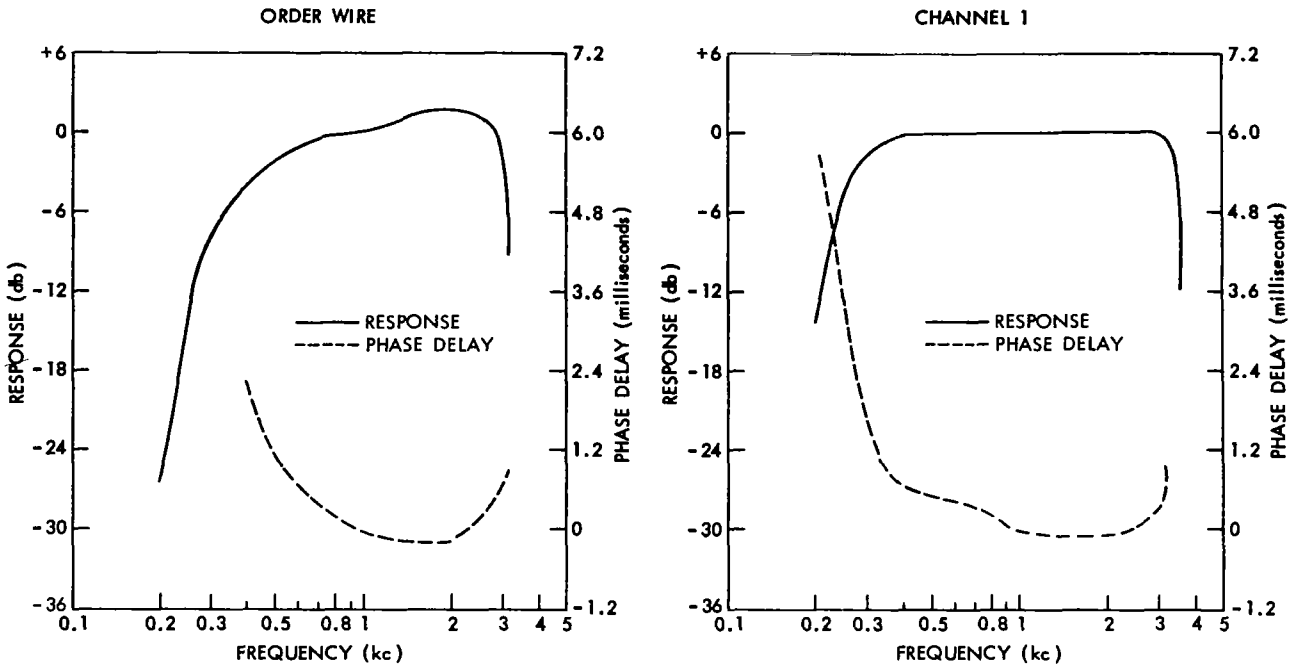

Figure IV-48—Amplitude and phase delay, mode 2-4; 2-4; mod/demod, AN/TCC-3 (OW and ch. 1)—Camp Roberts.

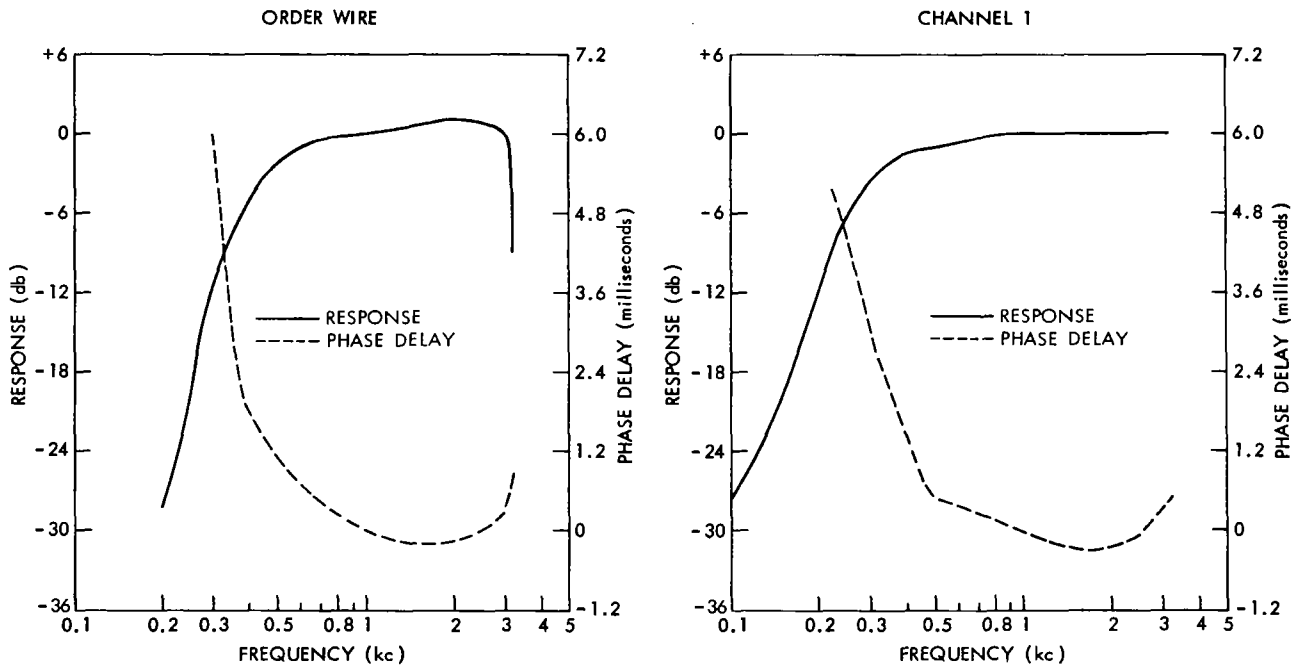

Figure IV-49—Amplitude and phase delay, mode 2-10; 2-10; mod/demod; AN/TCC-3 (OW and ch. 1)—Camp Roberts.

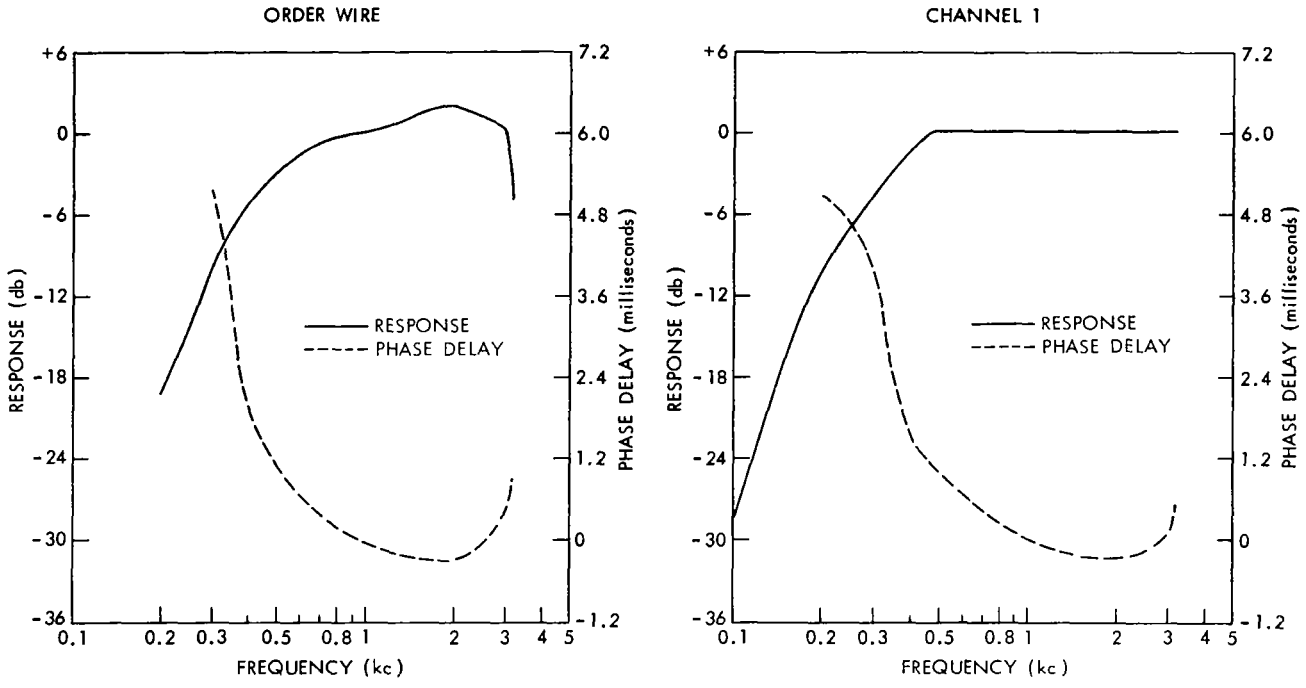

Figure IV-50—Amplitude and phase delay, mode 3-4; 3-4; mod/demod; AN/TCC-3 (OW and ch. 1)—Camp Roberts.

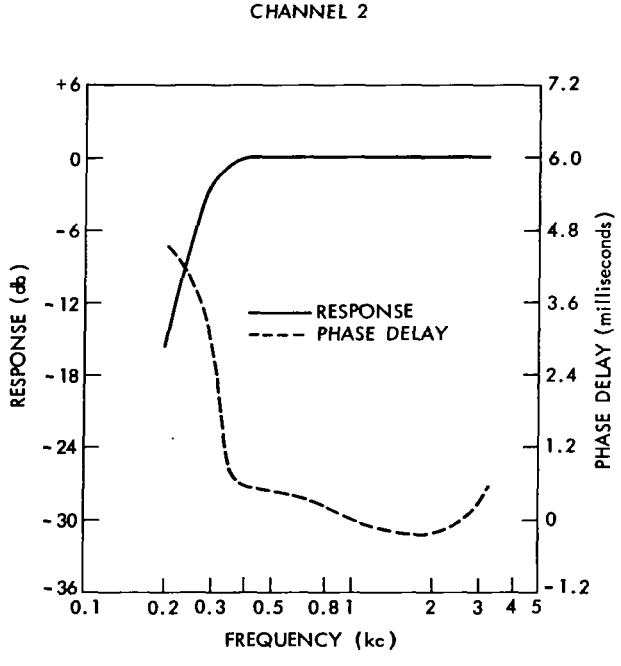

Figure IV-51—Amplitude and phase delay, mode 3-4; 3-4; mod/demod; AN/TCC-3 (ch. 2)—Camp Roberts.

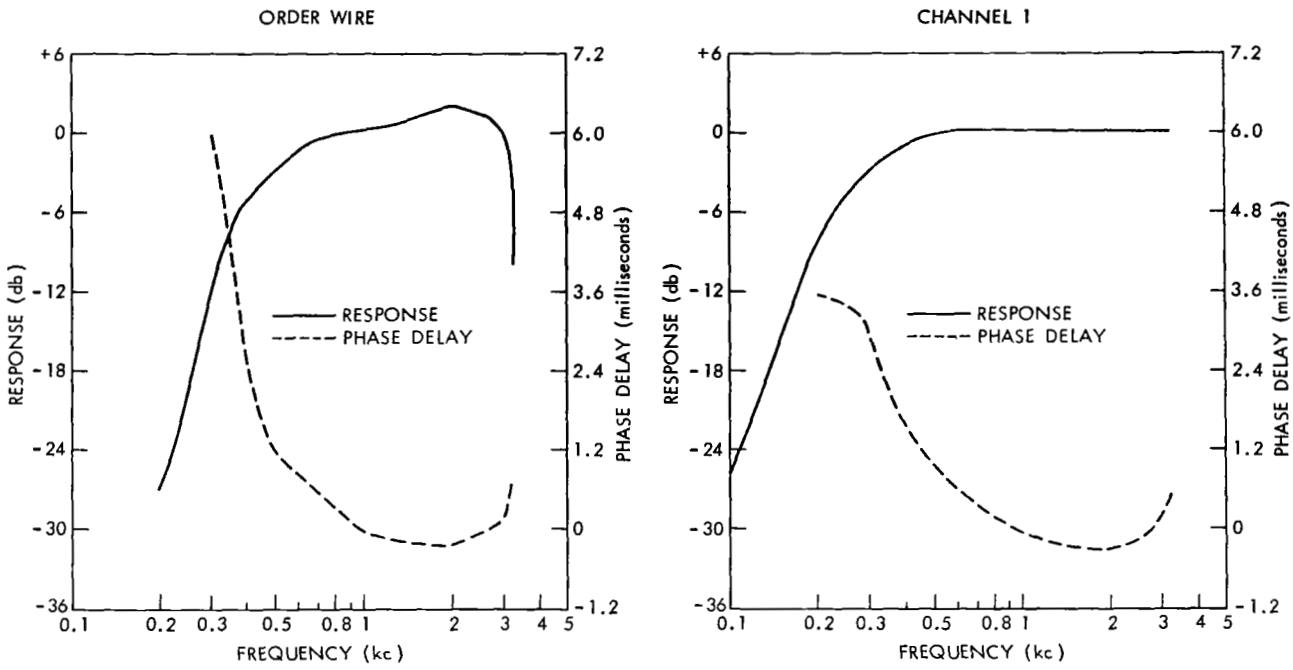

Figure IV-52—Amplitude and phase delay, mode 5-4; 5-4; mod/demod; AN/TCC-3 (OW and ch. 1)—Camp Roberts.

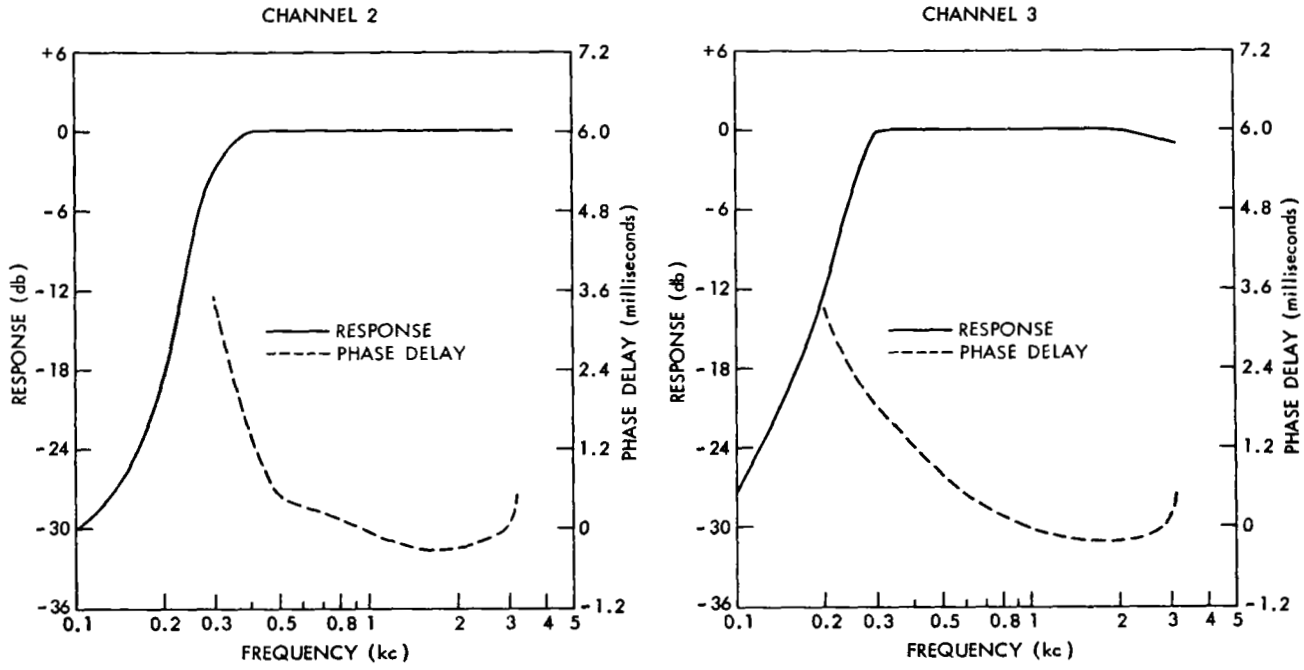

Figure IV-53—Amplitude and phase delay, mode 5-4; 4-5; mod/demod; AN/TCC-3 (ch. 2 and ch. 3)—Camp Roberts.

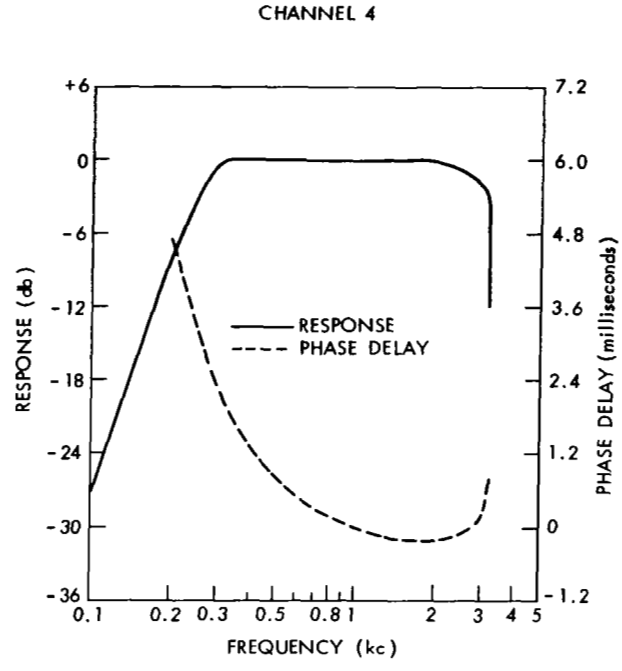

Figure IV-54—Amplitude and phase delay, mode 5-4; 5-4; mod/demod; AN/TCC-3 (ch. 4)—Camp Roberts.

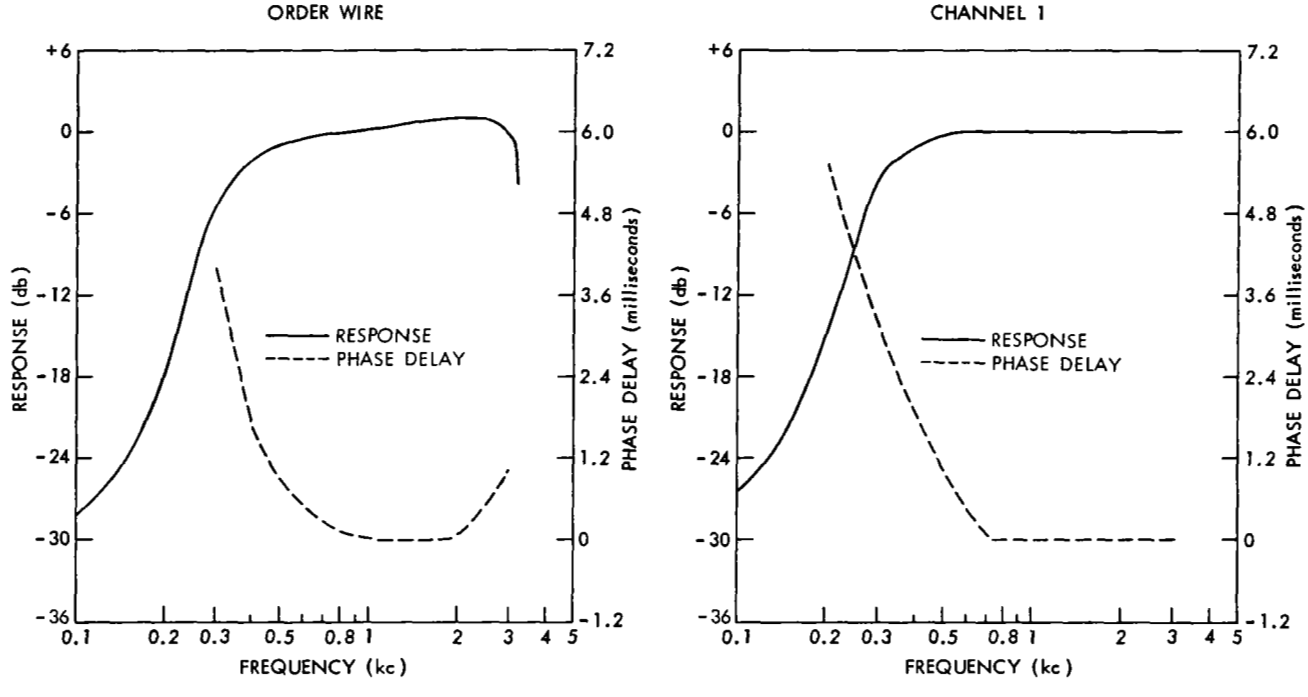

Figure IV-55—Amplitude and phase delay, mode 2-4; 2-4; spacecraft AN/TCC-3 (OW and ch. 1)—Camp Roberts.

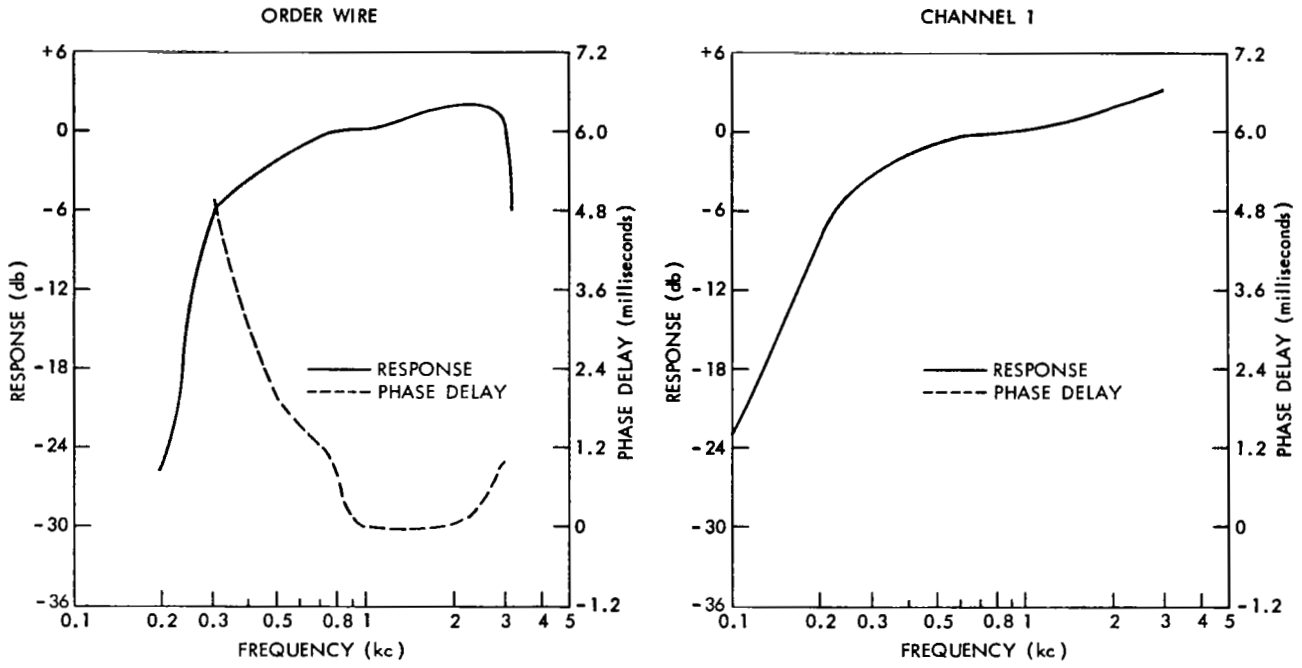

Figure IV-56—Amplitude and phase delay, mode 2-10; 2-10; spacecraft; AN/TCC-3 (OW and ch. 1)—Camp Roberts.

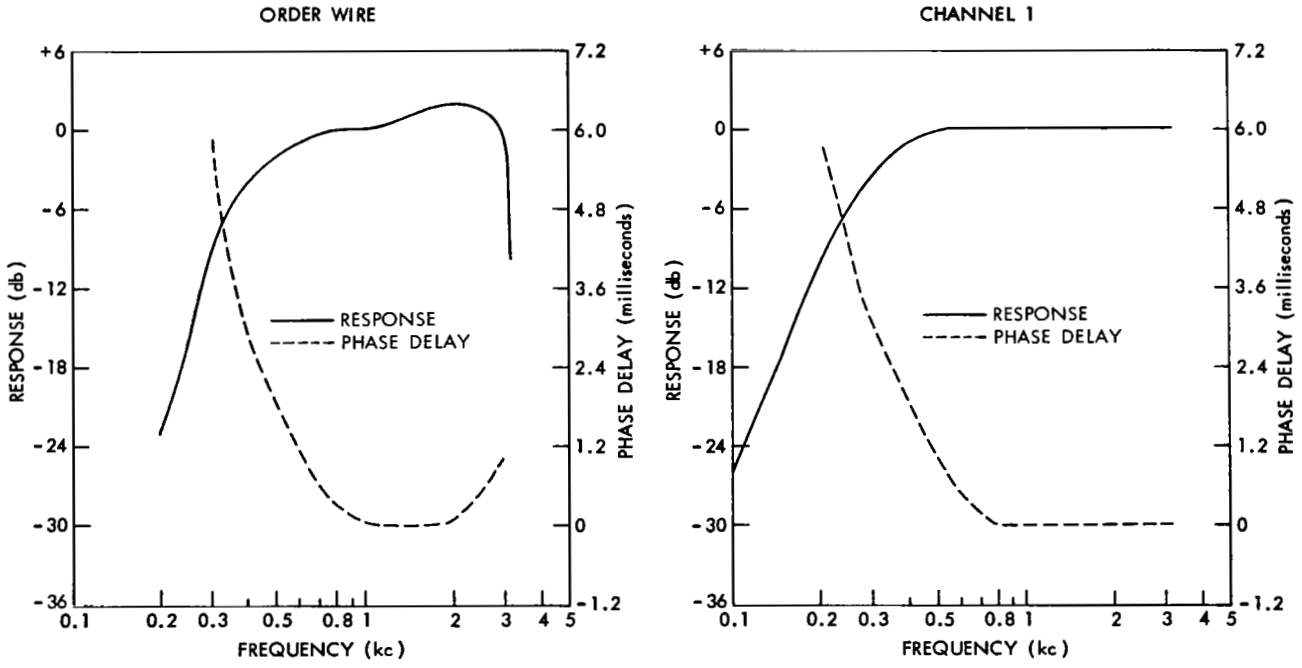

Figure IV-57—Amplitude and phase delay, mode 3-4; 3-4; spacecraft; AN/TCC-3 (OW and ch. 1)—Camp Roberts.

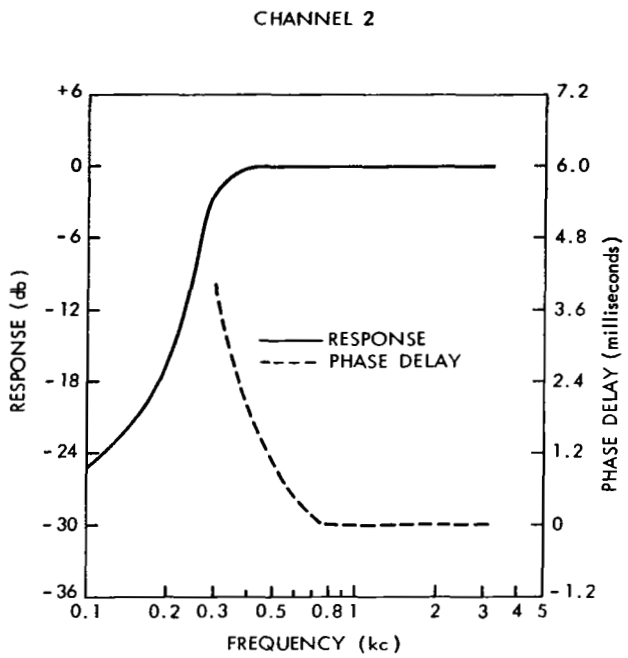

Figure IV-58—Amplitude and phase delay, mode 3-4; 3-4; spacecraft; AN/TCC-3 (ch. 2)—Camp Roberts.

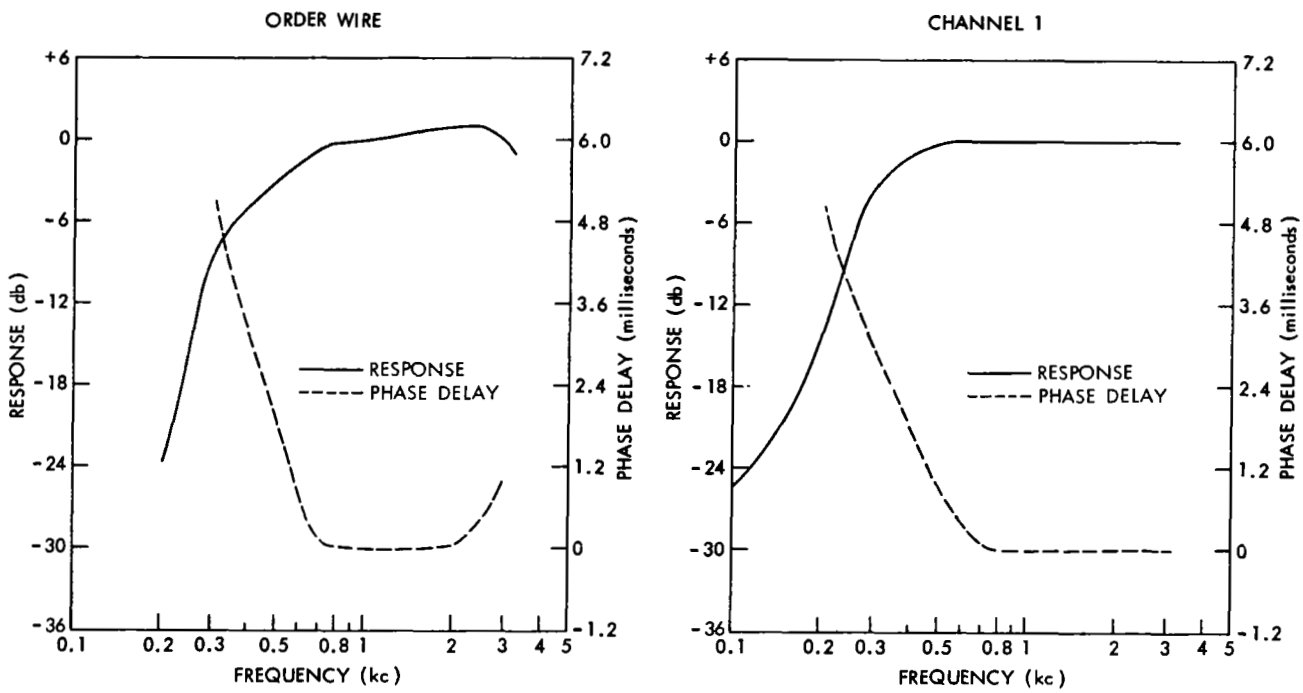

Figure IV-59—Amplitude and phase delay, mode 5-4; 5-4; spacecraft; AN/TCC-3 (OW and ch. 1)—Camp Roberts.

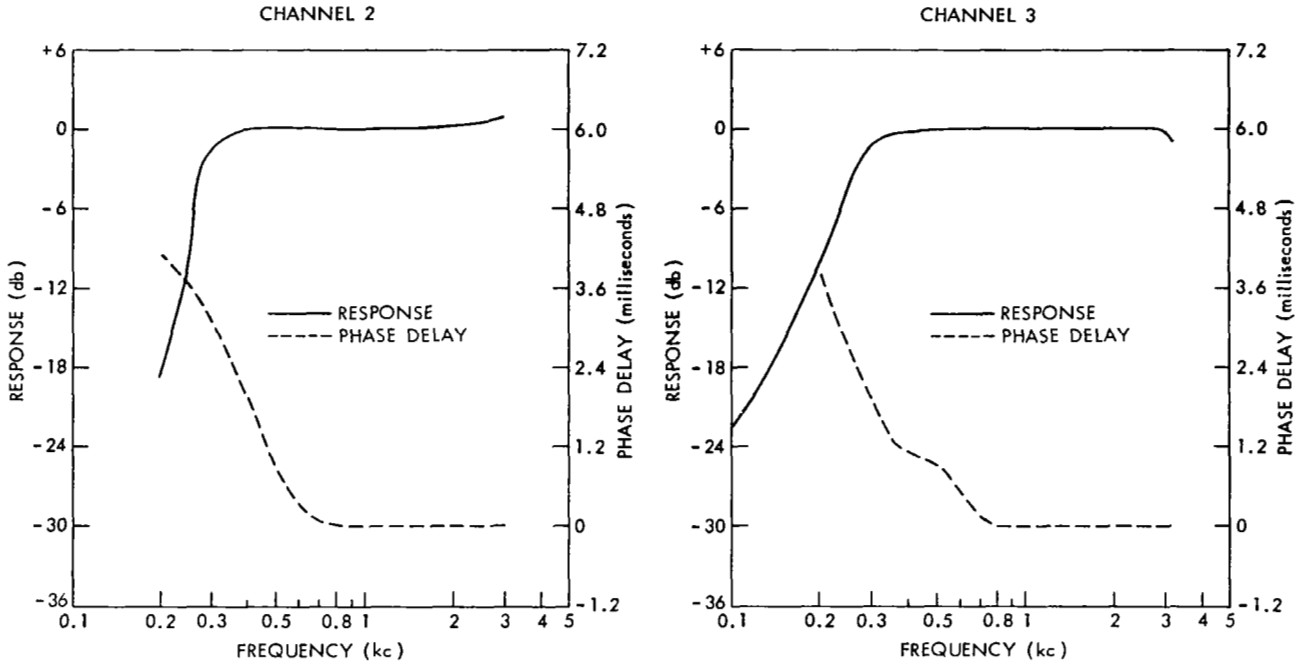

Figure IV-60—Amplitude and phase delay, mode 5-4; 5-4; spacecraft; AN/TCC-3 (ch. 2 and ch. 3)—Camp Roberts.

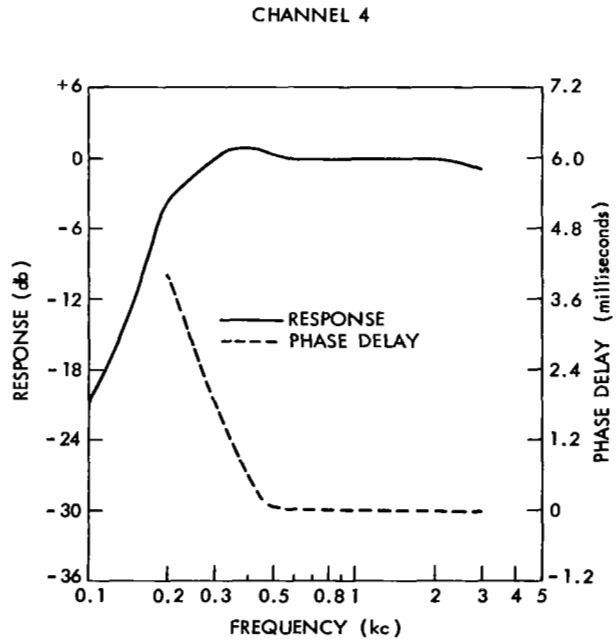

Figure IV-61—Amplitude and phase delay mode 5-4; 5-4; spacecraft; AN/TCC-3 (ch. 2 and ch. 3)—Camp Roberts.

50-kc Slot, 10-Mc Transponder

During the month of October 1964, technical characteristics tests were performed on the 50-kc transponder using the Camp Roberts station. These tests were conducted to determine the bandwidth, the transfer characteristics, the signal-plus-noise-to-noise versus communication level using the 50-kc transponder, and the transponder local oscillator stability. Figure IV-62 shows the spacecraft 50-kc slot bandpass characteristics. The 1db bandwidth, as measured using two methods, varied from 69 kc to 73 kc and the 3db bandwidth varied from 89 kc to 87 kc. The 1db and 3db points are referenced to the center of the response curve; however, there is a large hump of about 3db which is approximately 30 kc below the center. Since this hump is approximately 30 kc wide, if it is possible to shift the ground transmitter frequency by using a synthesizer, we can take advantage of this irregular shape. The measured bandwidth compares with the prelaunch data which shows the 3db bandwidth as being 81.9 kc after the thermal vacuum test made on 7 April 1964. However, pre-spin balance test results on 6 August showed the 3db bandwidth as being 48 kc. Evaluation would indicate that the bandwidth characteristics of the crystal filter are unstable. The effects of the hump in the bandwidth will be more pronounced when transmitting at power levels below saturation.

Figure IV-63 shows the transfer characteristics of the 50-kc slot. Results of this test show that the 50-kc transponder can be saturated with approximately 50 watts using the Camp Roberts station. The transmission characteristics of the Camp Roberts station are described in previous Syncom Evaluation Reports. By using these characteristics, it is possible to determine the power required to saturate the transponder when using stations with different transmission characteristics, such as smaller antennas and different line losses. The 50 watts required to saturate the 50-kc transponder is approximately 16db below the power required to saturate the 5-Mc transponder. If the bandwidth of the 50-kc transponder is actually 89 kc and the bandwidth of the 5-Mc transponder is actually 4.6 Mc (refer to Syncom Evaluation Report, dated 30 November 1964), then the theoretical power required to saturate the 50-kc transponder should be approximately 17.1db below that required to saturate the 5-Mc transponder.

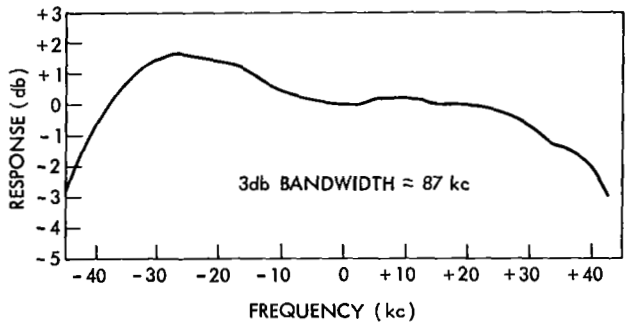

Figure IV-62—Spacecraft bandpass characteristics—50 kc slot—Camp Roberts.

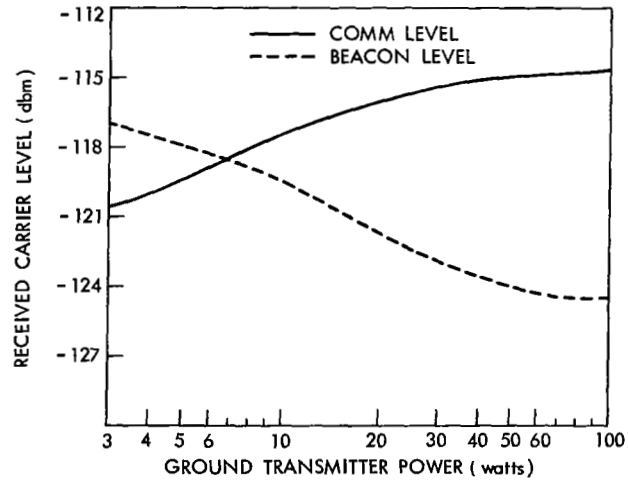

Figure IV-63—Spacecraft transfer and characteristics, 50 kc slot—Camp Roberts transmitting and receiving.

Figure IV-64 shows the results of the signal-plus-noise-to-noise versus the communication level using the 50-kc transponder. The results of this test show that the maximum signal-plus-noise-to-noise ratios obtained using the 50-kc transponder are: narrow-narrow mode -29.5db; wide-narrow mode -37db; and wide-narrow with feedback -36db. These values compare quite favorably with maximum signal-plus-noise-to-noise ratios obtained using the 5-Mc transponder.

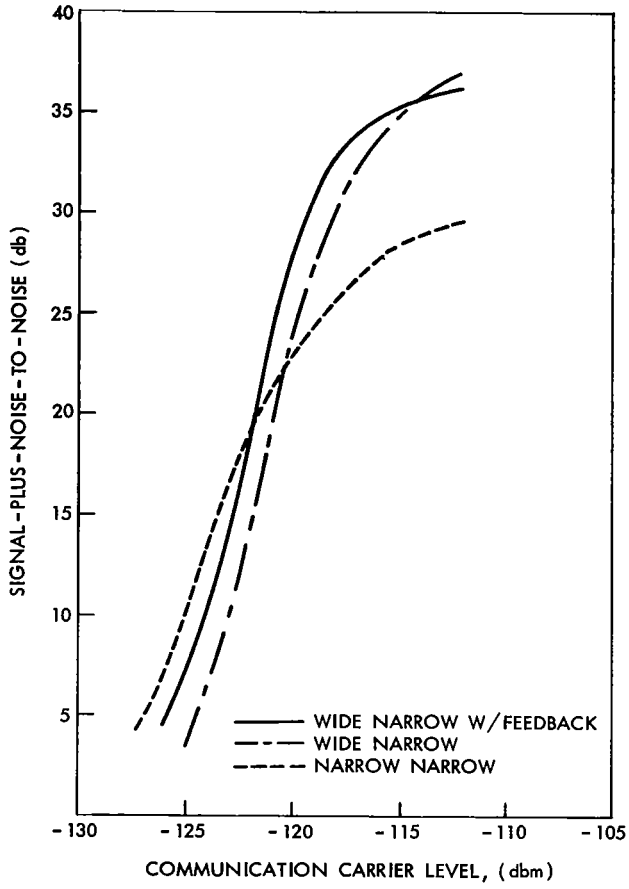

Figure IV-64—Signal-plus-noise-to-noise vs. communication level, 50 kc slot—Camp Roberts.

The actual spacecraft oscillator frequency and the long-term stability were determined using methods described in the NASA/U. S. Army SATCOM Agency Experiment Test Plan, revision B, dated 21 March 1964. From these measurements it was possible to determine where the nominal ground station channel 2 lies within the 50-kc slot. Results show that the local oscillator frequency is 28.891 Mc ±1 cps. This test was performed over a 4-1/2 hour period. Prelaunch data shows the local oscillator frequency as being 28.891,744 on the 6th of August, 1964. By using the measured spacecraft oscillator frequency and the nominal ground transmitter frequency for channel 2, it is observed that the nominal channel 2 frequency is 17.608 kc from the measured center of the 50-kc bandwidth.

PERFORMANCE TEST EVALUATION

Signal-Plus-Noise-to-Noise Distribution

The measurement which best describes system performance, while also providing a basis for comparison with other systems, is the signal-plus-noise-to-noise ratio. Ultimately, almost all of the operating characteristics may be related to this quantity. Using mathematical curve fitting techniques, frequency distribution curves were plotted to yield the signal-plus-noise-to-noise ratio to be expected for a given percentage of transmissions, for each 4-kc baseband channel and each mode of operation. In order to increase statistical confidence in the curves, a large quantity of controlled data is required for each 4-kc baseband mode. Figures IV-65 to IV-69 show the signal-plus-noise-to-noise distribution curves for modes 1-4, 1-1; 1-10, 1-10; 2-4, 2-4; 2-10, 2-10; 3-4,

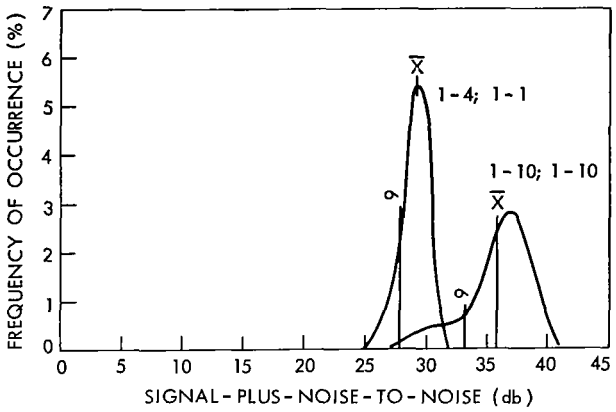

Figure IV-65—Frequency of occurrence vs. signal-plus-noise-to-noise, modes 1-4; 1-1 and 1-10—Camp Roberts.

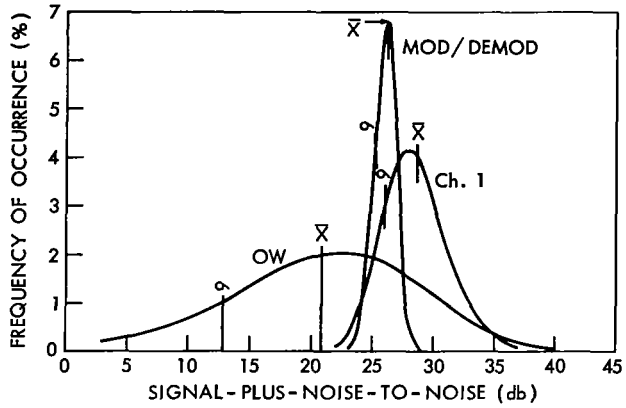

Figure IV-66—Frequency of occurrence vs. signal-plus-noise-to-noise, mode 2-4; 2-4; mod/demod; AN/TCC-3 (OW and ch. 1)—Camp Roberts.

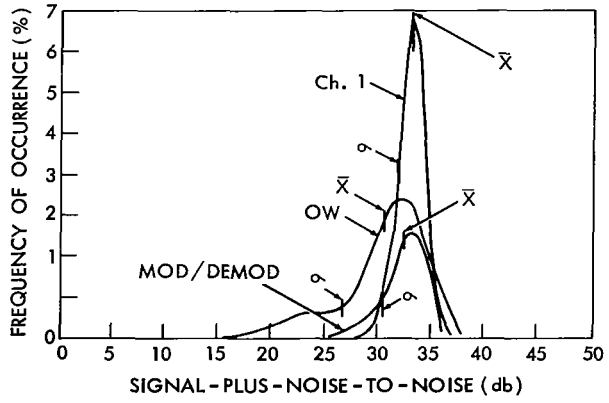

Figure IV-67—Frequency of occurrence vs. signal-plus-noise-to-noise, mode 2-10; 2-10; mod/demod; AN/TCC-3 (OW and ch. 1)—Camp Roberts.

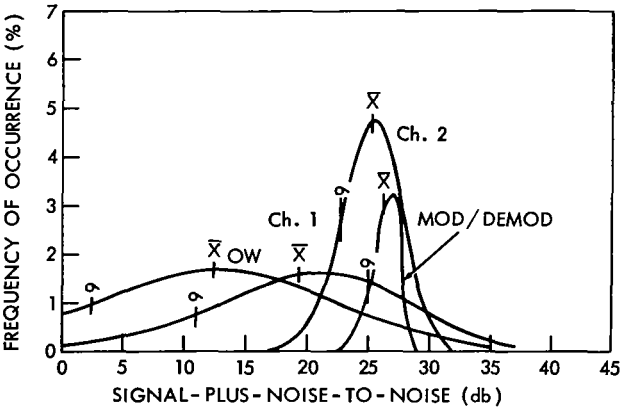

Figure IV-68—Frequency of occurrence vs. signal-plus-noise-to-noise; mode 3-4; 3-4; mod/demod; AN/TCC-3 (OW, ch. 1, ch. 2)—Camp Roberts.

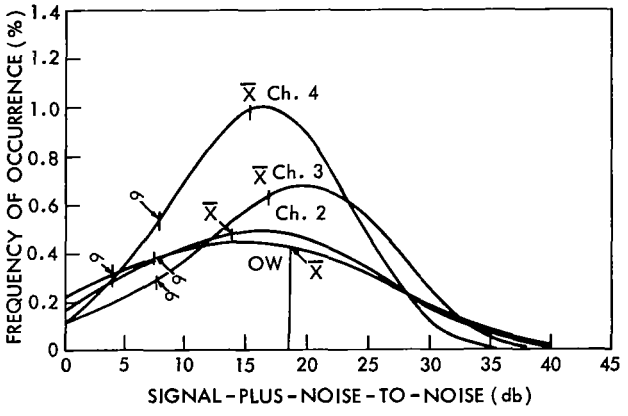

Figure IV-69—Frequency of occurrence vs. signal-plus-noise-to-noise; mode 5-4; 5-4; AN/TCC-3 (OW, ch. 2, ch. 3, ch. 4)—Camp Roberts.

3-4; and 5-4, 5-4 for Camp Roberts. Similar curves have been plotted for the Philippines and the Kingsport. The results of the statistical analysis for the three stations are summarized in Tables IV-3 through IV-5. These tables may be used to make predictions of future system performance for various combinations of stations, operating modes and baseband channels. The figures under the columns titled "84% db" and "90% db" are worst case situations and should be interpreted as the minimum signal-plus-noise-to-noise ratio (in db) which can be

Table IV-3

Signal-Plus-Noise-to-Noise Distribution, Camp Roberts.

Mode	Channel	Mean (db)	Standard Deviation (db)	1.282 Standard Deviation (db)	84% Expected Occurrence (db)	90% Expected Occurrence (db)
1-4, 1-1	Mod/Demod	29.00	1.10	1.41	27.90	27.59
1-10, 1-10	Mod/Demod	35.73	2.54	3.25	33.19	32.48
2-4, 2-4	Mod/Demod	26.00	.89	1.14	25.11	24.86
2-4, 2-4	OW	20.85	7.89	10.11	12.96	10.74
2-4, 2-4	Ch. 1	28.56	2.67	3.42	25.89	25.14
2-10, 2-10	Mod/Demod	32.50	2.06	2.64	30.44	29.86
2-10, 2-10	OW	30.42	3.73	4.78	26.69	25.64
2-10, 2-10	Ch. 1	33.04	1.24	1.59	31.80	31.45
3-4, 3-4	Mod/Demod	26.22	1.13	1.44	25.09	24.78
3-4, 3-4	OW	12.45	9.90	12.69	2.55	—
3-4, 3-4	Ch. 1	19.31	8.31	10.65	11.00	8.66
3-4, 3-4	Ch. 2	25.21	2.44	3.13	22.77	22.08
5-4, 5-4	Mod/Demod	25.67	1.11	1.42	24.56	24.25
5-4, 5-4	OW	18.78	11.18	14.33	7.60	4.45
5-4, 5-4	Ch. 1	13.78	12.18	15.61	1.60	—
5-4. 5-4	Ch. 2	14.78	10.70	13.71	4.08	1.07
5-4, 5-4	Ch. 3	16.86	9.05	11.60	7.81	5.26
5-4, 5-4	Ch. 4	15.39	7.39	9.47	8.00	5.92

expected to occur 84 percent and 90 percent of the time, respectively. For example, the signal-plus-noise-to-noise ratio which can be expected 84 percent of the time using mode 1-4; 1-1 for Camp Roberts is 27.9db or better, and the signal-plus-noise-to-noise ratio which can be expected 90 percent of the time is 27.59db or better.

It should again be noted that these curves are for half duplex or loop configurations. If the mean signal-plus-noise-to-noise ratio is at least 5db above the FM threshold, the distribution curves could be adjusted for full duplex operation, assuming equal signal strengths at the spacecraft, by shifting the curve to the left by approximately 4db; however, in the case of multichannel operation, the mean signal-plus-noise-to-noise ratio is not above FM threshold; hence, the multiple access performance using these signal-plus-noise-to-noise distributions cannot be predicted.

Telephony Performance

A good overall indicator of telephony performance is provided by human listener panel intelligibility ratings. However, these measurements are costly and even under the best of conditions

Table IV-4

Signal-Plus-Noise-to-Noise Distribution, Kingsport.

Mode	Channel	Mean (db)	Standard Deviation (db)	1.282 Standard Deviation (db)	84% Expected Occurrence (db)	90% Expected Occurrence (db)
1-4, 1-1	Mod/Demod	24.90	7.40	9.48	17.50	15.42
1-10, 1-10	Mod/Demod	31.90	6.20	7.94	25.70	23.96
2-4, 2-4	Mod/Demod	15.80	7.00	8.97	8.80	6.83
2-4, 2-4	OW	11.50	9.10	11.66	2.40	—
2-4, 2-4	Ch. 1	22.30	6.90	8.84	15.40	13.46
2-10, 2-10	Mod/Demod	21.30	6.70	8.58	14.60	12.72
2-10, 2-10	OW	16.60	7.60	9.74	9.00	6.86
2-10, 2-10	Ch. 1	28.20	3.90	4.99	24.30	23.21
3-4, 3-4	Mod/Demod	11.90	6.20	7.94	5.70	3.96
3-4, 3-4	OW	7.00	5.70	7.30	1.30	—
3-4, 3-4	Ch. 1	16.20	5.90	7.56	10.30	8.64
3-4, 3-4	Ch. 2	19.00	7.00	8.97	12.00	10.03
5-4, 5-4	Mod/Demod	12.20	6.70	8.58	5.50	3.62
5-4, 5-4	OW	10.10	5.20	6.66	4.90	3.44
5-4, 5-4	Ch. 1	13.10	7.70	9.87	5.40	3.23
5-4, 5-4	Ch. 2	14.60	6.20	7.94	8.40	6.66
5-4, 5-4	Ch. 3	15.50	6.10	7.82	9.40	7.68
5-4, 5-4	Ch. 4	14.50	4.10	5.25	10.40	9.25

they are somewhat subjective and dependent upon panel selection, training, and experience. Another problem which existed in the intelligibility evaluation of the multichannel capability of the Syncom system was the limited number of different word lists to be presented to the listener panel. The limited number of word lists plus the large number of repetitions produced listener panel memory and hence, an upward bias in the resulting scores. Therefore, the multichannel telephony testing for Syncom III was confined mainly to the use of the voice interference analysis set (VIAS) which is an electronic method of analyzing the voice performance. Earlier Syncom evaluation reports have verified the excellent correlation between the listener panel and VIAS results in determining telephony performance capability. As described in previous Syncom evaluation reports, the quality of voice communication is evaluated by first determining the mathematical relationship between the articulation index and signal-plus-noise-to-noise ratio, and then relating these correlations back to the expected signal-plus-noise-to-noise as determined from the distribution curves. The word or sentence intelligibility can be determined by using Kryter's curves of intelligibility versus articulation index and the sentence intelligibility which can be expected 84 percent or 90 percent of the time can be determined. Figures IV-70 and IV-71 show the relationship of the

Table IV-5

Signal-Plus-Noise-to-Noise Distribution, Philippines.

Mode	Channel	Mean (db)	Standard Deviation (db)	1.282 Standard Deviation (db)	84% Expected Occurrence (db)	90% Expected Occurrence (db)
1-4, 1-1	Mod/Demod	29.40	7.20	9.23	22.20	20.17
1-10, 1-10	Mod/Demod	32.60	12.60	16.15	20.00	16.45
2-4, 2-4	Mod/Demod	19.00	9.40	12.05	9.60	6.95
2-4, 2-4	OW	16.60	9.50	12.18	7.10	4.42
2-4, 2-4	Ch. 1	25.90	9.40	12.05	16.50	13.85
2-10, 2-10	Mod/Demod	25.90	5.10	6.53	20.80	19.37
2-10, 2-10	OW	25.20	10.80	13.84	14.40	11.36
2-10, 2-10	Ch. 1	29.10	9.90	12.69	19.20	16.41
3-4. 3-4	Mod/Demod	18.70	9.40	12.05	9.30	6.65
3-4, 3-4	OW	11.60	9.40	12.05	2.20	—
3-4, 3-4	Ch. 1	21.60	6.60	8.46	15.00	13.14
3-4, 3-4	Ch. 2	22.90	8.70	11.28	14.20	11.62
5-4, 5-4	Mod/Demod	18.10	9.90	12.69	8.20	5.41
5-4, 5-4	OW	14.40	12.50	16.02	1.90	—
5-4, 5-4	Ch. 1	14.20	11.90	15.25	2.30	—
5-4, 5-4	Ch. 2	16.30	11.50	14.74	4.80	1.56
5-4, 5-4	Ch. 3	17.40	9.80	12.56	7.60	4.84
5-4, 5-4	Ch. 4	17.40	9.00	11.53	8.40	5.87

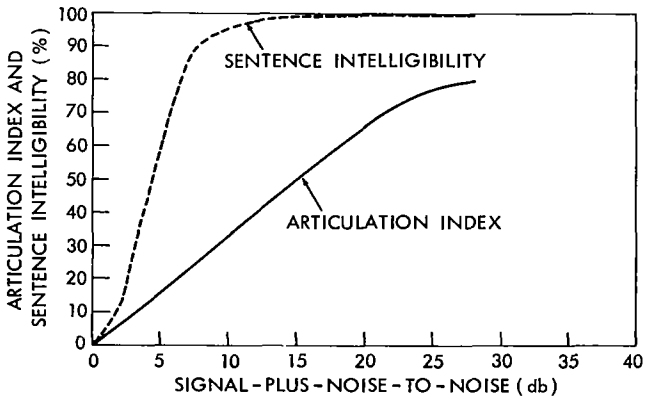

Figure IV-70—Articulation index and sentence intelligibility vs. signal-plus-noise-to-noise; mode 1-4; 1-1—Camp Roberts.

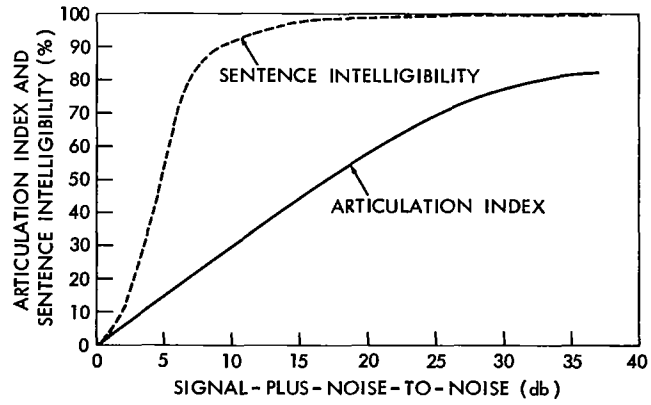

Figure IV-71—Articulation index and sentence intelligibility vs. signal-plus-noise-to-noise, mode 1-10; 1-10—Camp Roberts.

signal-plus-noise-to-noise vs. articulation index and sentence intelligibility as derived from Kryter's curves for modes 1-4, 1-1 and 1-10, 1-10 for Camp Roberts. Figures IV-72 to IV-82 show the relationship of signal-plus-noise-to-noise vs. articulation index and sentence intelligibility as derived from Kryter's curves for the individual 4-kc baseband channels of the AN/TCC-3 for modes 2-4, 2-4; 2-10, 2-10; 3-4, 3-4; and 5-4, 5-4. By referring to the tape scenario of test code 06 (Figure IV-83), it is noted that these results simulate actual traffic loading of the channels. Table IV-6 summarizes the results which may be used to make predictions of future telephony performance for various combinations of stations, operating modes, and baseband channels. Another word of caution is that these expected performances are for a half duplex or loop configuration and will be reduced for duplex operation. In fact, multichannel operation may be impossible in full duplex operation.

Teletype

The approach employed in the statistical analysis of teletype is identical to that employed in the telephony analysis. Tests were performed which have resulted in correlation between signal-plus-noise-to-noise ratio vs. teletype error for each of the many combinations of multiplex operations in the multichannel AN/TCC-3. As mentioned in earlier reports, the available test time severely limited the amount of data which could be accumulated for each of the combinations. Therefore, statistical confidence in the curves derived, especially in modes 3-4 and 5-4, is necessarily low. Furthermore, early data on the expected levels of signal-plus-noise-to-noise ratio, which were subsequently substantiated (see Tables IV-3 through IV-5), indicated that the system would not support 3- or 4-channel operation since modes 3-4 and 5-4 would, based upon the derived statistics, be below threshold for a significant percentage of operation. Hence, emphasis was placed upon testing of teletype in the two channel modes of AN/TCC-3 operation which the system is capable of supporting.

The problems of analysis were further aggravated by the desirability of evaluating each of the 16 channels of multiplex teletype individually. This resulted in a 16-fold increase in the number of combinations. As mentioned in earlier reports, the even numbered (or lower frequency) channels of the 16 channel transmissions are inferior to the odd numbered (or higher frequency) channels because of the poor low frequency response and the effects of spin modulation. It is found, however, that when the AN/TCC-3 is introduced, these factors do not effect the low frequency channels as much as in the single channel case.

Since an exhaustive discussion of all of the combinations of teletype transmissions would require presentation of approximately 1000 curves, representative samples (Figures IV-84 through IV-89) have been chosen to illustrate the capability which can be expected for the feasible two channels of operation.

It should be noted that the signal-plus-noise-to-noise ratios of the 16-channel teletype are in-channel measurements (i.e., $S+N/N$ as measured in a bandwidth of 170 cps). In previous Syncom evaluation reports the teletype error was correlated with the signal-plus-noise-to-noise ratio as measured in a 3-kc bandwidth. In order to interpret Figures IV-84 through IV-89, and to make

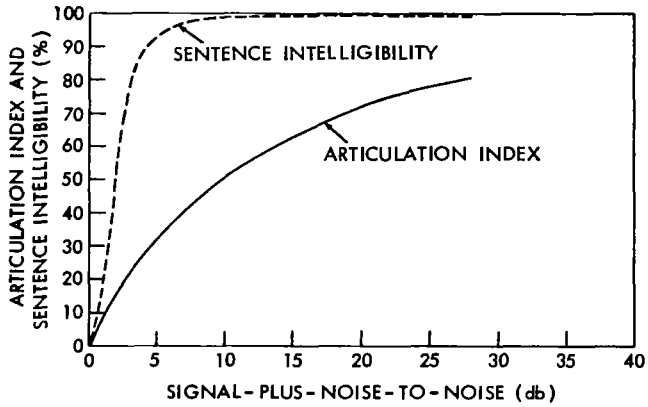

Figure IV-72—Articulation index and sentence intelligibility vs. signal-plus-noise-to-noise, mode 2-4; 2-4; AN/TCC-3 (OW)—Camp Roberts.

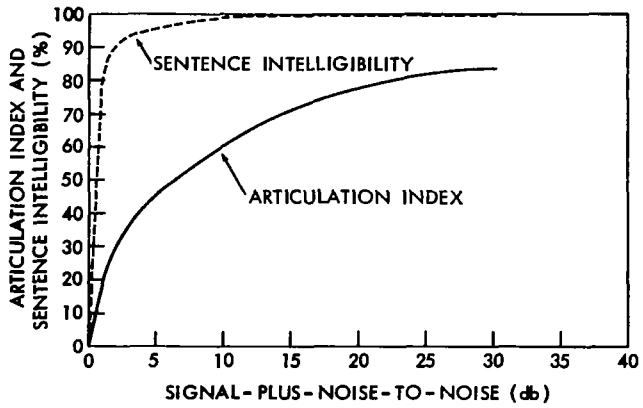

Figure IV-73—Articulation index and sentence intelligibility vs. signal-plus-noise-to-noise, mode 2-4; 2-4; AN/TCC-3 (ch. 1).

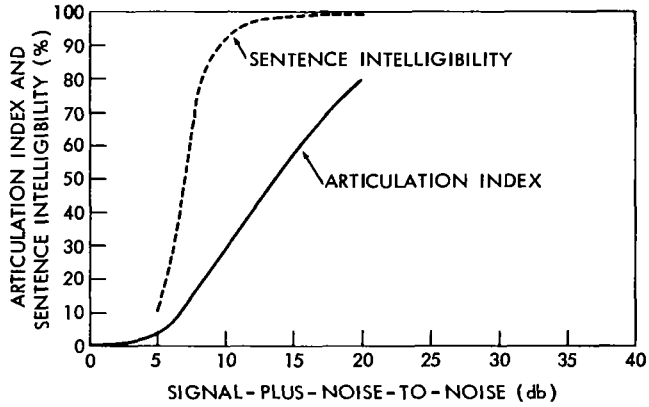

Figure IV-74—Articulation index and sentence intelligibility vs. signal-plus-noise-to-noise, mode 2-10; 2-10; AN/TCC-3 (OW).

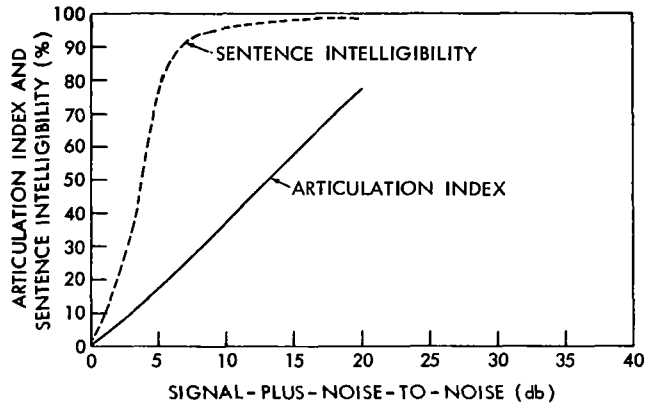

Figure IV-75—Articulation index and sentence intelligibility vs. signal-plus-noise-to-noise, mode 2-10; 2-10; AN/TCC-3 (ch. 1).

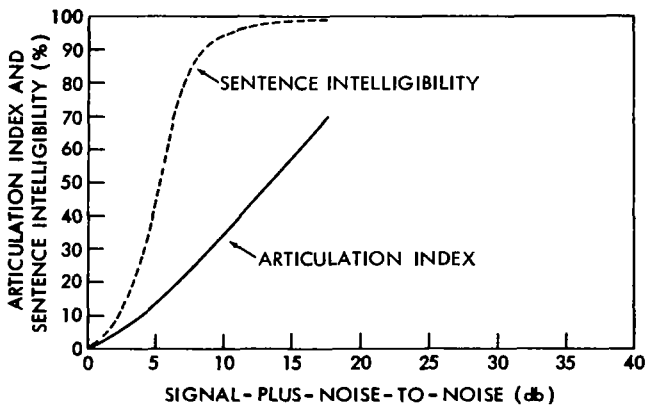

Figure IV-76—Articulation index and sentence intelligibility vs. signal-plus-noise-to-noise, mode 3-4; 3-4; AN/TCC-3 (OW).

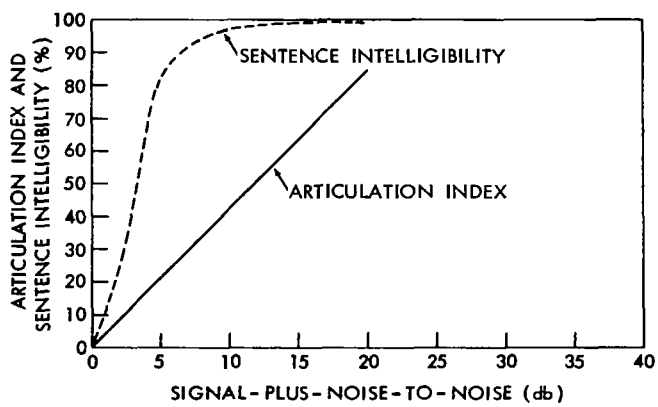

Figure IV-77—Articulation index and sentence intelligibility vs. signal-plus-noise-to-noise, mode 3-4; 3-4; AN/TCC-3 (ch. 1).

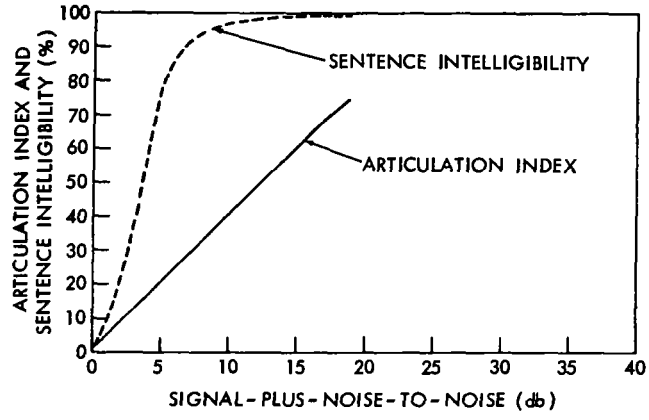

Figure IV-78—Articulation index and sentence intelligibility vs. signal-plus-noise-to-noise, mode 3-4; 3-4; AN/TCC-3 (ch. 2).

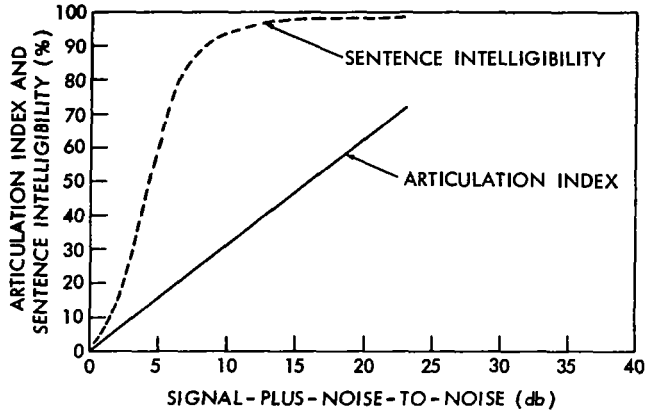

Figure IV-79—Articulation index and sentence intelligibility vs. signal-plus-noise-to-noise, mode 5-4; 5-4; AN/TCC-3 (ch. 1).

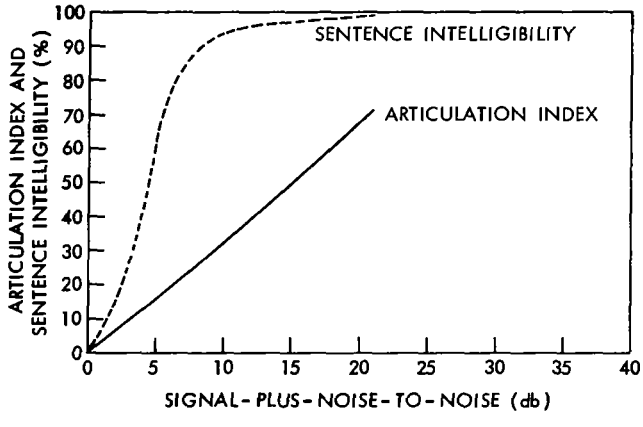

Figure IV-80—Articulation index and sentence intelligibility vs. signal-plus-noise-to-noise, mode 5-4; 5-4; AN/TCC-3 (ch. 2).

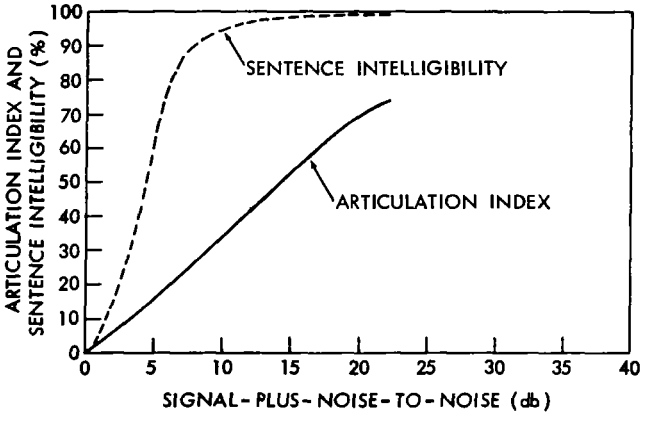

Figure IV-81—Articulation index and sentence intelligibility vs. signal-plus-noise-to-noise, mode 5-4; 5-4; AN/TCC-3 (ch. 3).

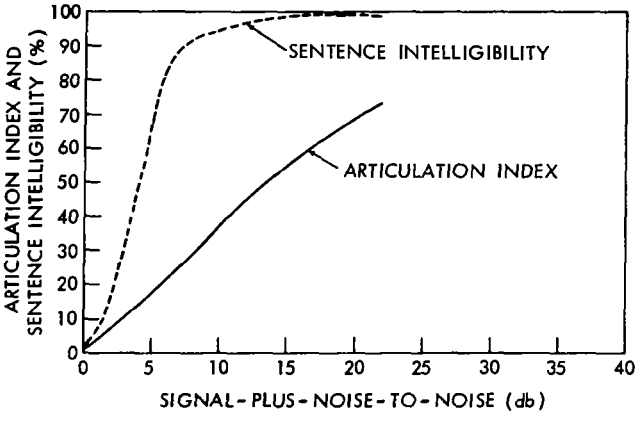

Figure IV-82—Articulation index and sentence intelligibility vs. signal-plus-noise-to-noise, mode 5-4; 5-4; AN/TCC-3 (ch. 4).

predictions on teletype performance which may be expected in the future, it is necessary to adjust the signal-plus-noise-to-noise distribution curves which are derived from data measured in a 3-kc bandwidth. The adjustment factor is derived by subtracting the ratio of the bandwidths (3000 cps/170 cps = 17.64) from a derating factor which approximates the signal degradation. Since the ratio of bandwidths is 17.64 or approximately 12.4db and an average derating factor is in the order of 15db, the overall adjustment which must be made to Tables IV-3 through IV-5 is 2.6db (15db minus 12.4db). As an example, the 1.28 sigma or 90 percent

Test Title: Multichannel Voice

Test Code: 06

Running Time: Approx. 21 minutes

Tape No. 6.6

Item No.	Description	Time
1	Announcement: Test Code Zero - Six. Running time approximately 21 minutes.	:05
2	Quiet	:15
3	1 kc Tone (Track 1 only)	1:00
4	Quiet	:15
5	1 kc Tone (Track 3 only)	1:00
6	Quiet	:15
7	1 kc Tone	2:00
8	Quiet	:15
9	400 cps	:30
10	Quiet	:15
11	3 kc Tone	:30
12	Quiet	:15
	Tracks 1 and 5 Only	
13	VIAS modulation	1:00
14	Quiet	:15
15	Word List #4 on Track 1; #2 on Track 5	3:50
16	Quiet	:15
17	Word List #5 on Track 1; #3 on Track 5	3:50
18	Quiet	1:15
19	1 kc Tone	1:00
20	Quiet	:30
	Tracks 3 and 7 Only	
13	16 - channel telegraphy: FOX message	3:15
14	Telegraph reversals	2:00
15	Quiet	:15
16	16 - channel telegraphy: FOX message	2:00
17	Quiet	:10
18	16 - channel telegraphy (Mark)	2:35
19	Quiet	1:00
20	1 kc Tone	:30
	********	
21	Quiet	:15
22	1 kc Tone	1:00
23	Quiet	:15
24	Announcement: This concludes Test Code Zero - Six	:05

Engineering Notes to Test Code 06, Tape No. 6.6

1. VIAS modulation, word lists and 16 - channel telegraph signal are recorded at the average rms level of item 3.
2. Unless otherwise indicated, the data is recorded on tracks 1, 3, 5 and 7 simultaneously.
3. The individual channel level for the 16 - channel telegraph signal is 15db below the level of the calibration tone (item 3).
4. Word lists #2 and #3 are 3:25
5. Items 13 through 20 on tracks 1 and 5 are simultaneous with Items 13 through 20 on tracks 3 and 7.

Figure IV-83—Multichannel test tape scenario.

Table IV-6

Expected Vias-Derived Articulation Index and Sentence Intelligibility Camp Roberts.

Mode	Channel	84% Articulation Index	84% Sentence	90% Articulation Index	90% Sentence
1-4, 1-1	Mod/Demod	.79	99%	.79	99%
1-10, 1-10	Mod/Demod	.80	99%	.79	99%
2-4, 2-4	OW	.57	98%	.51	98%
2-4, 2-4	Ch. 1	.82	100%	.82	100%
2-10, 2-10	OW	>.80	≈100%	>.80	≈100%
2-10, 2-10	Ch. 1	>.79	≈100%	>.79	≈100%
3-4, 3-4	OW	.06	12%	—	—
3-4, 3-4	Ch. 1	.46	98%	.36	95%
3-4, 3-4	Ch. 2	>.75	≈100%	>.75	≈100%
5-4, 5-4	Ch. 1	.05	10%	—	—
5-4, 5-4	Ch. 2	.12	40%	.03	6%
5-4, 5-4	Ch. 3	.27	90%	.18	69%
5-4, 5-4	Ch. 4	.28	91%	.21	79%

expected occurrence case for channel one of mode 2-10, 2-10 at Camp Roberts as given by Table IV-3, is 31.45db. This value is now adjusted by subtracting the adjustment factor (31.45db - 2.6db) to obtain the adjusted value (28.85db) which may be used to obtain expected teletype performance. To carry out the final step of our example, the value of teletype error corresponding to 28.85db S + N/N is obtained for Figure IV-84. It can be seen that the teletype error which can be expected 90 percent of the time will be less than 1 percent. Repeating the above procedure for all combinations of two channels, AN/TCC-3 operation shows that less than 1 percent error is representative of three stations operating in the system.

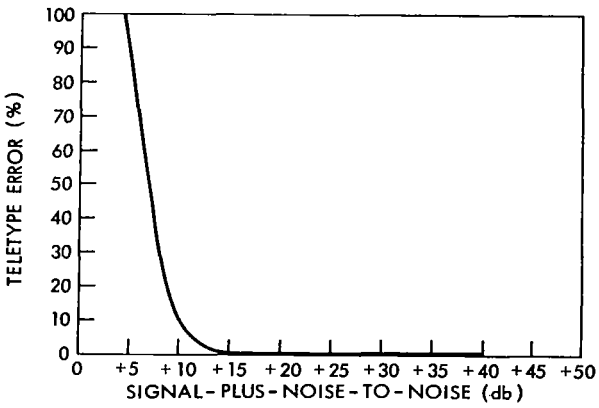

Figure IV-84—Signal-plus-noise-to-noise vs. teletype error; mode 2-10; 2-10; AN/TCC-3 (OW); TTY ch. 2—Camp Roberts.

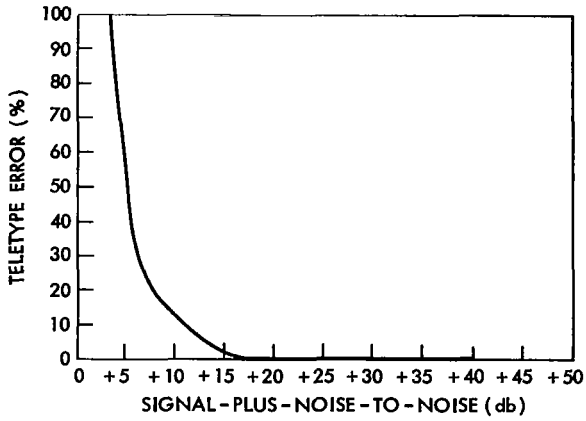

Figure IV-85—Signal-plus-noise-to-noise vs. teletype error; mode 2-10; 2-10; AN/TCC-3 (OW); TTY ch. 9—Camp Roberts.

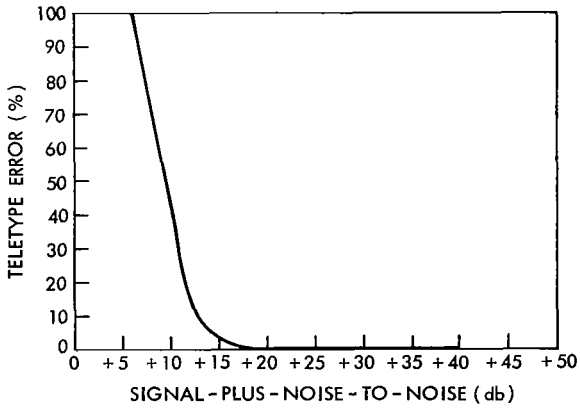

Figure IV-86—Signal-plus-noise-to-noise vs. teletype error; mode 2-10; 2-10; AN/TCC-3 (OW); TTY ch. 16—Camp Roberts.

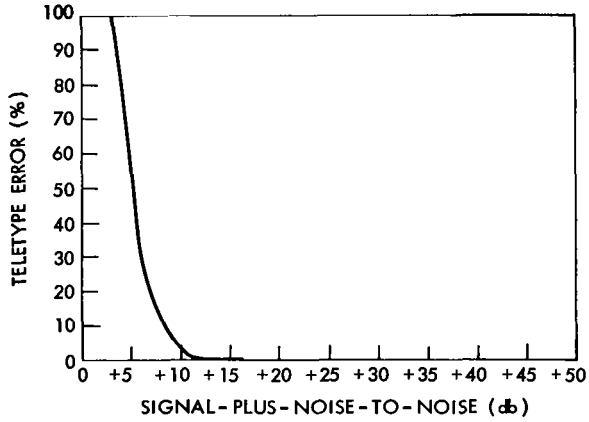

Figure IV-87—Signal-plus-noise-to-noise vs. teletype error; mode 2-10; 2-10; AN/TCC-3 (ch. 1); TTY ch. 2—Camp Roberts.

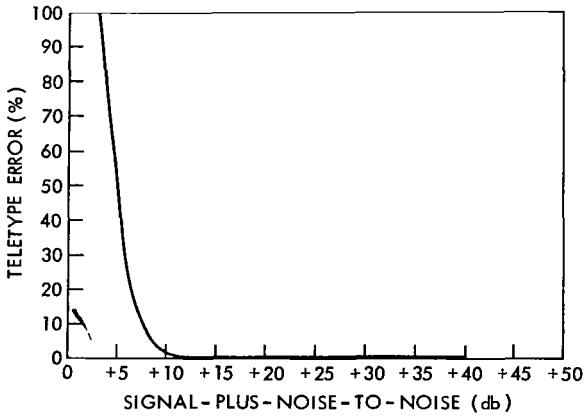

Figure IV-88—Signal-plus-noise-to-noise vs. teletype error, mode 2-10; 2-10; AN/TCC-3 (ch. 1); TTY ch. 9—Camp Roberts.

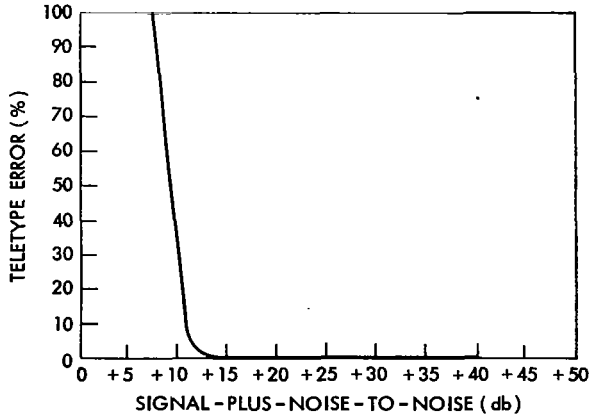

Figure IV-89—Signal-plus-noise-to-noise vs. teletype error, mode 2-10; 2-10; AN/TCC-3 (ch. 1); TTY ch. 16—Camp Roberts.

BIBLIOGRAPHY

"Evaluation of SYNCOM Modulator-Demodulator Analysis System Performance," The Bendix Corporation, November 30, 1962.

French, N. R., and Steinberg, J. C., "Factors Governing Intelligibility of Speech Sounds," *J. Acoust. Soc. Amer.* 19(1) January 1947.

Gleason, T. R., Tobias, W. T. and Keyes, R. G., "Communication Operations with Syncom II," 1964 IEEE Convention Record.

Grim, W. M., Jr., "The Voice Interference Analysis Set, An Instrument for Evaluating the Performance of a Voice Communication Channel," General Electronic Laboratories, Inc., November 1961.

Kryter, K. D., "Proposed Methods for the Calculation of the Articulation Index," ESD TDR-62-35 Report No. 906, Bolt, Beranek and Newman, Inc., October 1961.

Kryter, K. D., "The Validity of the Articulation Index," ESD TDR-62-35, Bolt, Beranek and Newman, Inc., October 1961.

Maresca, P. T., "Satellite Communications Ground Station," Paper No. C. P. 63-1115, presented to IEEE Summer General Meeting, 1963, Toronoto, Canada.

"NASA/U. S. Army SATCOM Agency Experiment Test Plan, Revision A," U. S. Army Satellite Communications Agency, Fort Monmouth, New Jersey, March 21, 1964.

"NASA/U. S. Army SATCOM Agency Experiment Test Plan, Revision B," U. S. Army Satellite Communications Agency, Fort Monmouth, New Jersey, March 21, 1964.

Norsell, P. E., "Syncom," *Astro. and Aero. Eng.* 1(8):76-78, September 1963.

Silverman, G. Lockett, J. W., and Cittadino, J. C., "Results of SYNCOM II Communications Experiments," IEEE Convention Record, March 1964.

"Syncom Acceptance Test Report for Syncom Satellite Communications Transportable Ground Terminal," SYN 63-12-01, The Bendix Corporation, Bendix Radio Division, June 15, 1963.

"Syncom C System Summary," Contract NAS5-1560, Hughes Aircraft Company, Space Systems Division, April 1964.

"Syncom Evaluation Report," U. S. Army Satellite Communications Agency, Fort Monmouth, New Jersey, August 1, 1964.

"Syncom Evaluation Report," U. S. Army Satellite Communications Agency, Fort Monmouth, New Jersey, December 20, 1963.

"Syncom Evaluation Report," U. S. Army Satellite Communications Agency, Fort Monmouth, New Jersey, July 26—September 23, 1963.

"Syncom II and III Evaluation Report," U. S. Army Satellite Communications Agency, Fort Monmouth, New Jersey, November 30, 1964.

Tobias, W. T., Locket, J. W. and Cittadino, J. C. "Results of Intelligibility and Articulation Experiments Using the Syncom II Satellite," GLOBECOM VI 1964, U. S. Army Satellite Communications Agency, Fort Monmouth, New Jersey.

CHAPTER V

SPACECRAFT PERFORMANCE

Telemetry data reduction and analysis for Syncom III has been continuing since launch. This analysis has revealed the following:

1. All modes of spacecraft operation, except the quadrant mode, have been exercised, and all performed successfully. The sun sensor $\psi - \psi_2$ reading is reversed in telemetry system 1. The cause has not been determined, but the reading can be used by simply reversing the polarity.
2. Spin rate is almost constant. Spin changes occurred during hydrogen peroxide engine operations, but were well within tolerable limits.
3. Electrical power supply degradation is much less than that experienced by Syncom II, and indications are that a much extended life can be expected.
4. Hydrogen peroxide systems indicate a continual pressure rise.
5. Spacecraft temperatures are slightly higher than predicted but are not expected to rise to a damaging level.

TELEMETERED DATA

Analysis of all the factors involved results in the conclusion that Syncom III telemetered data are accurate within ±2 percent, based on root mean square evaluation of the contributing errors. Telemetry data analysis is based primarily on magnetic and paper strip chart recordings of data recorded at various ground stations. In addition, the "quick look" telemetry data or VCO (voltage controlled oscillator) readings have been utilized. The magnetic tapes have been processed to allow each decommutated segment of the telemetry pulse train to be plotted separately on scaled paper at low speeds. With the use of calibrated overlays, the telemetry data can be read out directly. Any point or time in question can then be identified and rerecorded in the original high speed pulse train form for more thorough investigation. The accuracy with which the spacecraft parameters can be determined is limited to a degree by the following factors:

1. Circuitry tolerances relating to calibration or reference voltages.
2. Stability of the subcarrier oscillator.
3. Effect of various load and voltage conditions on telemetered data.
4. Calibration and accuracy of the transducers.
5. Ability to accurately read and reduce the telemetry data.

A theoretical analysis of the reference voltage circuitry and the subcarrier oscillator was made to determine the effects of the first three factors on telemetry accuracy. It was concluded that the contribution is about ±1 percent.

TEMPERATURE

Four temperature sensors are mounted on the spacecraft as follows:

No. 1. On rib between quadrants 1 and 2, on opposite side from traveling-wave tube 2.

No. 2. On forward bulkhead (apogee motor nozzle end) just above the hydrogen peroxide system 2 tank between quadrants 3 and 4.

No. 3. On the aft bulkhead on quadrant 4, about four inches outboard of the apogee motor mounting ring (originally planned for apogee motor).

No. 4. Imbedded in the rear of a solar panel just outboard from hydrogen peroxide system 1 tank between quadrants 1 and 4 and about 5 inches from lateral engine 1.

Sensors 1 and 3 are monitored by encoder 1, and 2 and 4 by encoder 2.

Very precise data were not available from the sensors for three reasons in addition to those previously mentioned as effecting data accuracy in general.

1. Accuracy of the calibration of the sensors. Curves had been drawn for temperature variations from 30 to 80 degrees, the temperatures the spacecraft had been subjected to during acceptance testing. The temperatures actually encountered were sometimes outside this range, and the curves had to be extrapolated at a loss in accuracy.
2. Telemetry 1, which transmits sensors 1 and 3 values, is used very little. Not enough points have been obtained to determine trends.
3. The spacecraft entered solar eclipses, ranging in length from 18 to approximately 70 minutes, 45 times during the period covered by this report. The caused considerable variation of the temperature and made steady-state trends difficult to perceive. Eclipses commenced on 1 September and ended 15 October.

During an eclipse, the spacecraft temperature began to fall toward the almost zero absolute surrounding it. The solar panel temperature falls below range of the calibration curves (10°F) in approximately 10 minutes. It then requires 6 hours in the sunlight for this temperature to return to the level prior to the eclipse.

Aft Bulkhead Temperature: Sensor 3

The original plan was to have a temperature sensor mounted on the forward end of the apogee motor. One was bonded to the motor and the bonding material was allowed to cure. Then, just

prior to mounting the motor in the spacecraft, a defect was noted in the motor casing. Sufficient time did not remain to bond the sensor to a new motor, so it was potted into the plug and mounted on the aft bulkhead in the original sensor harness socket.

However, this sensor is monitored by telemetry system 1, and because system 1 was only used for 3 minutes immediately after apogee fire, and for only few short periods since then, no conclusions can be made from temperature conditions indicated by this sensor.

Traveling-Wave Tube Temperature: Sensor 1

This sensor is monitored by telemetry system 1 also. As in the case of sensor 3, very little data were received from sensor 1. Also, each time telemetry 1 was operating traveling-wave tube 1 was on, so the actual traveling-wave tube 2 temperature has never been monitored.

Solar Panel Temperature

Prior to liftoff, the solar panel temperature (Figure V-1) was approximately 80°F. The first data, taken 15 hours after launch when telemetry system 2 was turned on indicated 66°F. At this time, the spin axis was approximately in the equatorial plane, with a sun angle of 79 degrees. The apogee motor was then fired, heating up the panels to 93°F. The temperature then fell to 66°F, a value it held until approximately 23 September. It rose to 73°F on 15 October, continued rising to 78°F on 23 October and then fell to a steady 75°F on about 27 October.

It appears that three factors-eclipse time, sun angle, and distance from the sun—have predominant control of the spacecraft temperature.

After apogee motor firing, the closing on the sun was compensated for by the decreasing sun angle and increasing eclipse time to hold the temperature, exclusive of eclipse transient effects, at a stable 66 degrees. After 23 September, the decreasing range to sun and decreasing eclipse time overcame the increasing angle of incidence of the sunlight on the solar panel, causing the temperature to rise. It appears also that the sun, now approaching the south end of the spacecraft (the apogee motor nozzle), causes a temperature rise in the solar panel due to the energy absorbed by the nozzle.

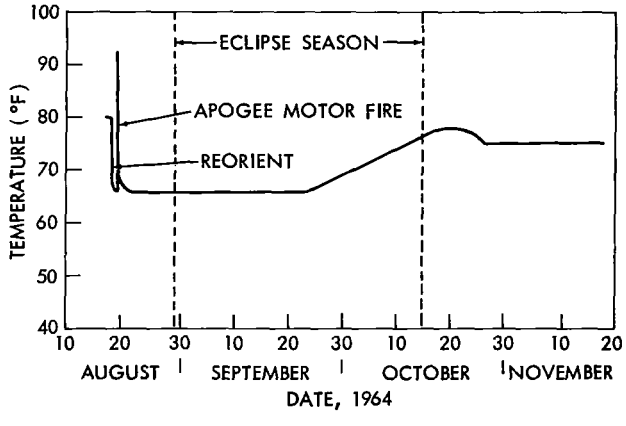

Figure V-1—Solar panel temperatures versus date.

Hydrogen Peroxide Tank Mount Temperature (Figure V-2)

The hydrogen peroxide tank mount temperature sensor is mounted behind a system 2 tank on the forward side (apogee motor nozzle end) of the forward bulkhead.

The first data after launch indicated no change from the 80°F at launch. Reorientation of the spacecraft from the initial sun angle of 79.9 to 90 degrees caused the temperature to drop, but before it reached its lowest point, the apogee motor was fired causing the temperature to rise to 140°F. In the following 18 hours, the temperature fell to 72°F, at which time the sunline was perpendicular to the solar panels, and the sun was more than the mean distance away.

As the spacecraft moved with the earth around the sun, its spin axis approximately in the equatorial plane, the sunline moved toward the apogee motor nozzle end and the temperature rose to 75°F.

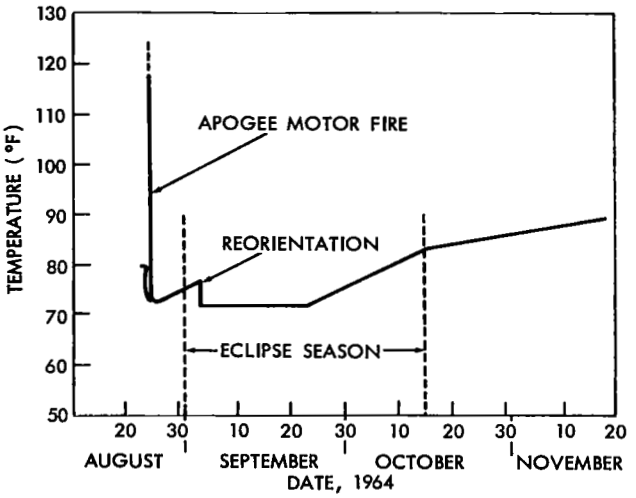

Figure V-2—Hydrogen peroxide tank mount temperature history.

On 3 September, the spin axis was reoriented to approximately perpendicular to the equatorial plane. This shifted the sun angle to 100 degrees, which, along with the eclipse season which began a daily cycle on 1 September, reduced the temperature to 72°F.

Increasing eclipse time, decreasing sun angle, and range to the sun held the temperature constant until 25 September. At this time, a reorientation maneuver brought the spin axis more precisely perpendicular to the equatorial plane. The combined effect of reducing eclipse periods, decreasing distance to the sun, and decreasing sun angle produced an increasing temperature of a little more than 1/2 degree per day.

It appears that the dominant parameter affecting the hydrogen peroxide tank mount temperature is sun angle. The apogee motor nozzle acts as a blackbody and absorbs increasing amounts of heat energy as the sun angle decreases.

Figure V-3 shows the effect of the solar eclipses on the temperature of the hydrogen peroxide tank mount. Shown are temperature provides during eclipse number 3 on 3 September, number 9 on 9 September, and number 45 on 15 October. Eclipse number 3 was approximately 35 minutes long and caused the temperature to fall rapidly to a temperature of 30°F. It then took approximately 15 hours for the temperature to rise back to its initial state. This initial state was 77°F because the sun angle was decreasing, and the apogee motor nozzle was absorbing more energy.

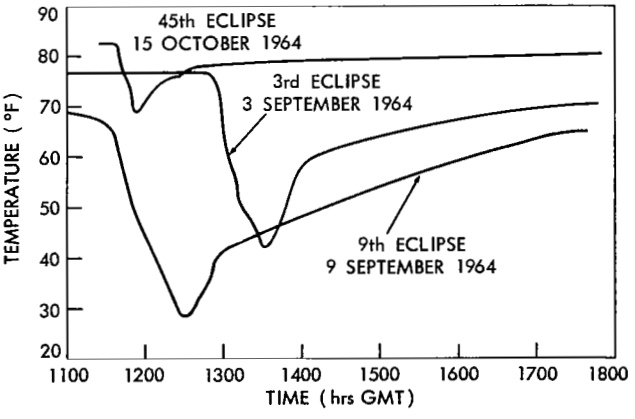

Figure V-3—Hydrogen peroxide tank mount temperature during eclipses.

Before the next eclipse, the spacecraft was reoriented, bringing the sun angle to 100 degrees, and dropping the temperature to 72°F.

The temperature returned after each daily eclipse to 72°F until 23 September. Then, because of decreasing eclipse time, decreasing sun distance, and decreasing sun angle, the temperature began to rise.

By the time of the last eclipse of 15 October, the temperature prior to entering the eclipse was 83°F. The duration of the last eclipse was only 19 minutes and the temperature dropped to only 69°F.

The eclipses shown in Figure V-3 do not center about the same time as the spacecraft was still moving relative to Greenwich. It was not brought to a longitudinal stop until 11 September.

HYDROGEN PEROXIDE SYSTEM PRESSURE

Each hydrogen peroxide system pressure is separately monitored by a transducer composed of a wire-wound potentiometer whose center arm is moved by a mechanism sensitive to differential pressure.

After the hydrogen peroxide systems had stabilized following pressure rises due to apogee motor firing heat, it became obvious that the pressure in each system was steadily increasing. This presented a different picture than did Syncom II whose pressure had remained constant.

The rate of pressure increase was proportional to the amount of fuel in the system (note decreasing slope after each fuel consumption of Figures V-4 and V-5) and increased with temperature rise. To preclude the loss of pressure in the event of possible failure of the relief valve to reseat, the pressure was deliberately reduced before venting pressure was reached by actuating both the axial and lateral engines of system 1 on 31 August.

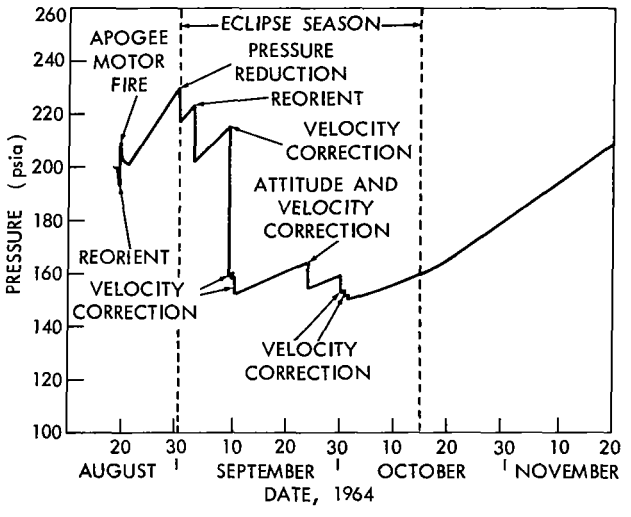

Figure V-4—Hydrogen peroxide system 1 pressure.

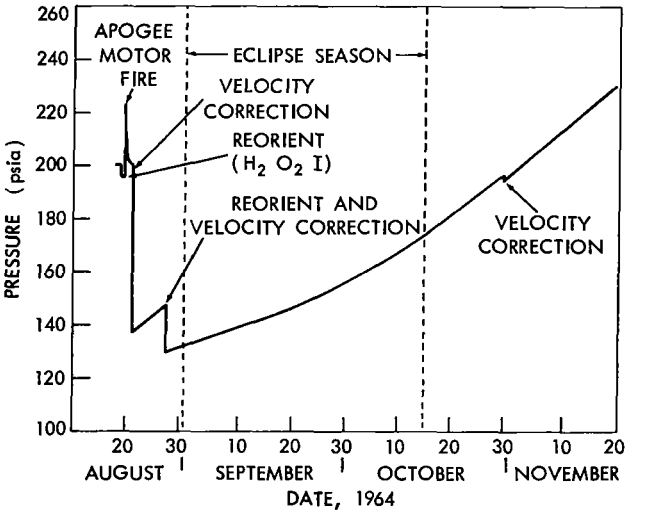

Figure V-5—Hydrogen peroxide system 2 pressure.

If the pressure rises continue at the present rate, system 1 should reach relief valve pop-off pressure of approximately 265 psia on or about 5 January, and system 2 should reach this value about 12 December. It is planned to allow the relief valve to operate. The escaping gases are vented through an anti-reaction tube to preclude any attitude or velocity change.

Hydrogen Peroxide System 1 Pressure (Figure V-4)

System 1 was filled with 4.90 pounds of hydrogen peroxide and pressurized to 200 psia prior to launch. At second apogee of the transfer orbit, this system was used to reorient the spacecraft to the desired attitude for apogee motor. At apogee motor fire, the increased temperature caused a temporary pressure rise to 210 psia. The pressure then fell to 200 psia and began to climb at a rate of approximately 3.5 psia per day. This build-up is attributed to a slow, continuing decomposition of the hydrogen peroxide.

On 31 August, NASA ordered a pressure reduction precautionary maneuver in which 0.270 pound of fuel was dumped through the motor valves to reduce the pressure from 231 to 217 psia.

The effect of each maneuver and the continuing pressure build-up is shown. The rate of pressure rise is constant with a constant temperature, but increases at a rate of approximately 1.6 for each 10-degree rise in temperature.

The pressure rise is sensitive to tank temperature which in turn appears to be quite sensitive to sun angle. Heat absorbed through the apogee motor nozzle increases as the sun angle decreases.

Hydrogen Peroxide System 2 Pressure (Figure V-5)

System 2 was filled with 4.92 pounds of hydrogen peroxide and pressurized to 200 psia prior to launch. Pressure build-up was detected after the first use of the system. Because system 2 has not been used as much as system 1, its pressure build-up has been at an uninterrupted rate and should reach pressure relief valve pop-off pressure in December.

Unregulated Bus

Figure V-6 represents the nominal bus voltage since launch under a load of approximately one ampere provided by one transponder and one telemetry system.

Variations caused by load variations and temperature variations are not shown, but are of interest, however. During eclipse, the unregulated voltage falls to the battery voltage, throwing the load to the battery. The panels cooled during the eclipse with a corresponding increase in efficiency. Then, for the first instant back in the sun, their output was above 36 volts, the approximate saturation of the telemetry monitor. In 10 to 15 minutes, the voltage fell back to a nominal level somewhat dependent on load.

The bus voltage, when the unregulated load is at the smallest level that can be monitored (353 ma: telemetry + command receivers), averages 31.3 volts.

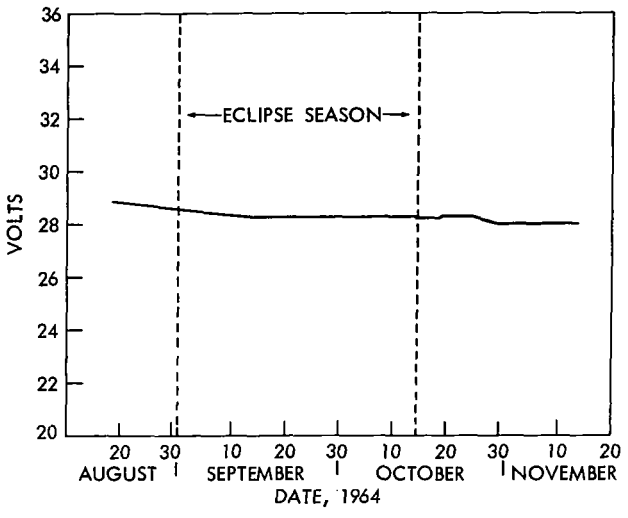

Figure V-6—Syncom III bus voltage.

Again referring to Figure V-6, the drop in voltage level can be attributed to three factors:

1. Solar panel degradation due to radiation damage.
2. Increased solar panel temperature.
3. Angle of light incidence.

On 9 September before the 11th eclipse and for the remaining eclipse season, telemetry was turned off during eclipses (transponders were turned off during all eclipses), and the bus voltage level held constant. Beginning 15 October, both telemetry and transponder systems were left on continually for the next five days, causing a 0.1 volt bus drop. From 20 October to 25 October, telemetry was on for only one hour a day, and the bus increased 0.1 volt. From 25 October to the present, the load has been relatively constant at one ampere (one telemetry system and one transponder), and the bus has stabilized at 28 volts.

Battery Voltage (Figure V-7)

Two batteries, each consisting of 22 hermetically sealed nickel cadmium cells connected in series, supply power to the spacecraft whenever the solar panels are shadowed. This occurred prior to fairing separation and during each eclipse.

Prior to launch, the cells were fully charged. In orbit, their state of charge is dependent on spacecraft power load requirements and solar panel charging.

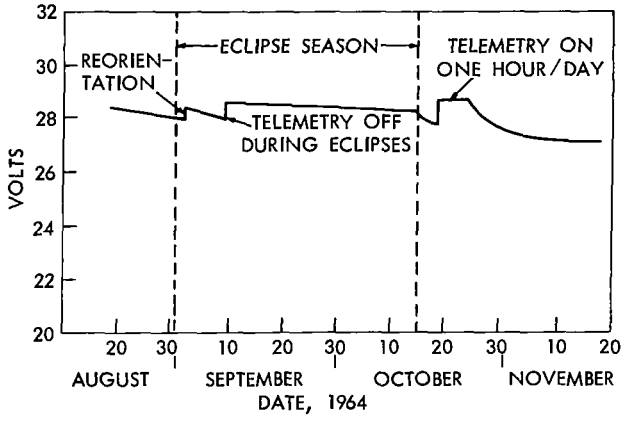

Figure V-7—Syncom III battery voltage.

The plot of battery voltage shows the initial fall-off as the spacecraft was operated almost continually. At reorientation, a better sun angle on the solar panels raised the bus voltage, but the added drain on the batteries for the approximate one hour each day as they carried the entire load while the spacecraft was in eclipse caused a more rapid fall-off. To decrease this load, telemetry was turned off during eclipses commencing 10 September.

The battery terminal voltage dropped gradually until after the last eclipse. The

telemetry and transponder were then left on continually. The poorer sun angle and warmer solar panels caused the battery voltage to drop until 20 October. On this day, the telemetry was turned off except for one hour per day to determine the effects of an operating telemetry on the spacecraft temperature. On 25 October, both telemetry and transponder were left on full time, and the battery voltage has gradually fallen to approximately 27 volts.

SPIN SPEED

Initial spin speed produced by third stage spin-up was 166 rpm. The operation of the hydrogen peroxide engines and the firing of the apogee engine has changed the speed, as shown in Figure V-8.

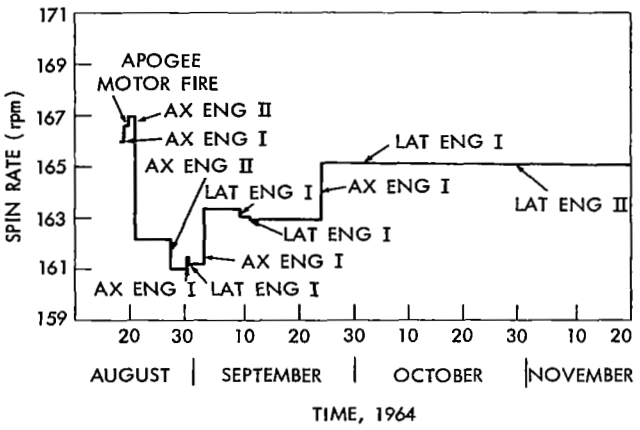

Figure V-8—Syncom III spin speed.

This change in speed is the result of the force vector of the engine not passing exactly through or parallel to the axis of rotation. During acceptance testing, the engines were aligned within design limits.

Plotting spin speed on a reduced scale (Figure V-9) gives a better indication of the spin speed changes relative to the operating limits of the spacecraft. The upper limit line represents the maximum spin speed for structural considerations. The lower limit line represents the minimum spin speed for stability considerations and operation with the present ground control equipment.

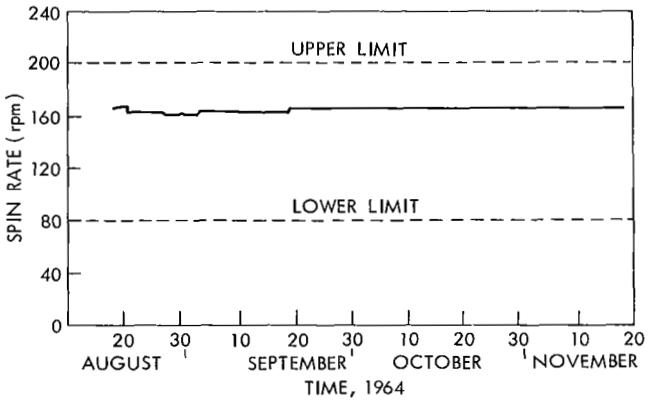

Figure V-9—Spin speed versus time with upper and lower limits.

SUN ANGLE

Sun angle (Figure V-10) is the angle between the spacecraft spin axis and the sunline measured from the apogee motor end. Shown is a plot of sun angles as seen by the spacecraft. This angle is determined from telemetry by measuring the $\psi_1 - \psi_2$ angle and converting according to the following relationship:

$$\cot \phi = \sin \psi_2 \cot 35^\circ ,$$

$$\phi = \text{sun angle} .$$

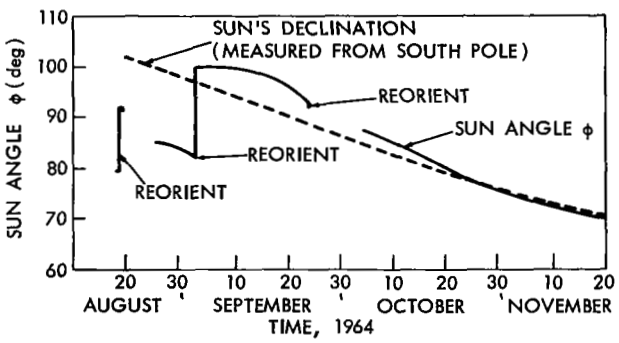

Figure V-10—Syncom III sun angle measurements.

CHAPTER VI

TELEVISING THE OLYMPICS FROM JAPAN TO THE U. S., CANADA, AND EUROPE

The coincidence of the availability over the Pacific Hemisphere of Syncom III, with its ability to relay television signals, and the Olympic Games in Japan presented an attractive opportunity to bring the attention of the world to the revolution in communication being wrought by synchronous satellites. The televising of the Olympics live from Japan to the United States had been under consideration both in Japan and the United States since NASA's decision to locate Syncom III over the Pacific. Much informal investigation and discussion had been carried on among interested agencies.

Near mid-1964, the Space Council reviewed a proposed program for live TV coverage of the Olympics and found it to be in the national interest. The Council suggested the Communications Satellite Corporation (Comsat) as the appropriate U. S. agency to coordinate the program and endorsed the utilization of various U. S. government facilities for the program.

Comsat set about organizing the program as a non-profit endeavor and obtained funding from interested sponsors. Among those expressing interest were the Canadian Broadcasting Corporation and the European Broadcasting Union. The latter company, which distributes program material to the whole of Europe (Eurovision), found that it could bring the events to its audience at a much earlier time (the same day as their occurrence and at prime viewing time) by combining transmission via Syncom III and microwave link from Tokyo to Montreal, Canada, with fast jet aircraft transport from Montreal to Europe. These organizations arranged with Comsat to purchase transmission time for Olympic program material.

The entire program arranged by Comsat is outlined in Comsat's filing with the Federal Communications Commission (FCC). The report that follows describes the transmissions that took place, the transmitting and receiving equipment used in the program, and lastly, provides a few photographs illustrative of the program material transmitted and a tabulation of receiving, antenna pointing angles attesting to the stationarity of Syncom III's orbit.

TRANSMISSION ACTIVITY

Between 17 September and 24 October, a daily period of three to four hours was devoted to the transmission of video material from the Radio Research Laboratory at Kashima, Japan, via

Syncom III to Point Mugu, California. The total number of separate scheduled transmission attempts was approximately 48. All were successful except the one attempted on 25 September, which was terminated by a typhoon in Japan (that forced stowing of the antennas to prevent damage to them). From 17 September through 9 October, the transmissions consisted primarily of four-hour periods of test patterns and still picture material for station adjustments.

During the period 10 October through 24 October, approximately three hours of Olympic Games video program material (from video tape) was transmitted daily from Kashima to Point Mugu. (Voice was transmitted via cable and voice and sound were synchronized by addition of time delay to the voice circuits.) Some material, including the opening day ceremonies in Tokyo, were shown (via microwave relay link) in real time in the eastern United States. Figure VI-1 shows the routing of signals in their passage about the world.

The quality of the video received on all transmissions to Point Mugu was outstanding as judged by technical and subjective measurement standards. On most viewers' sets it was not distinguishable in quality from most other program material, though it was reprocessed many times after

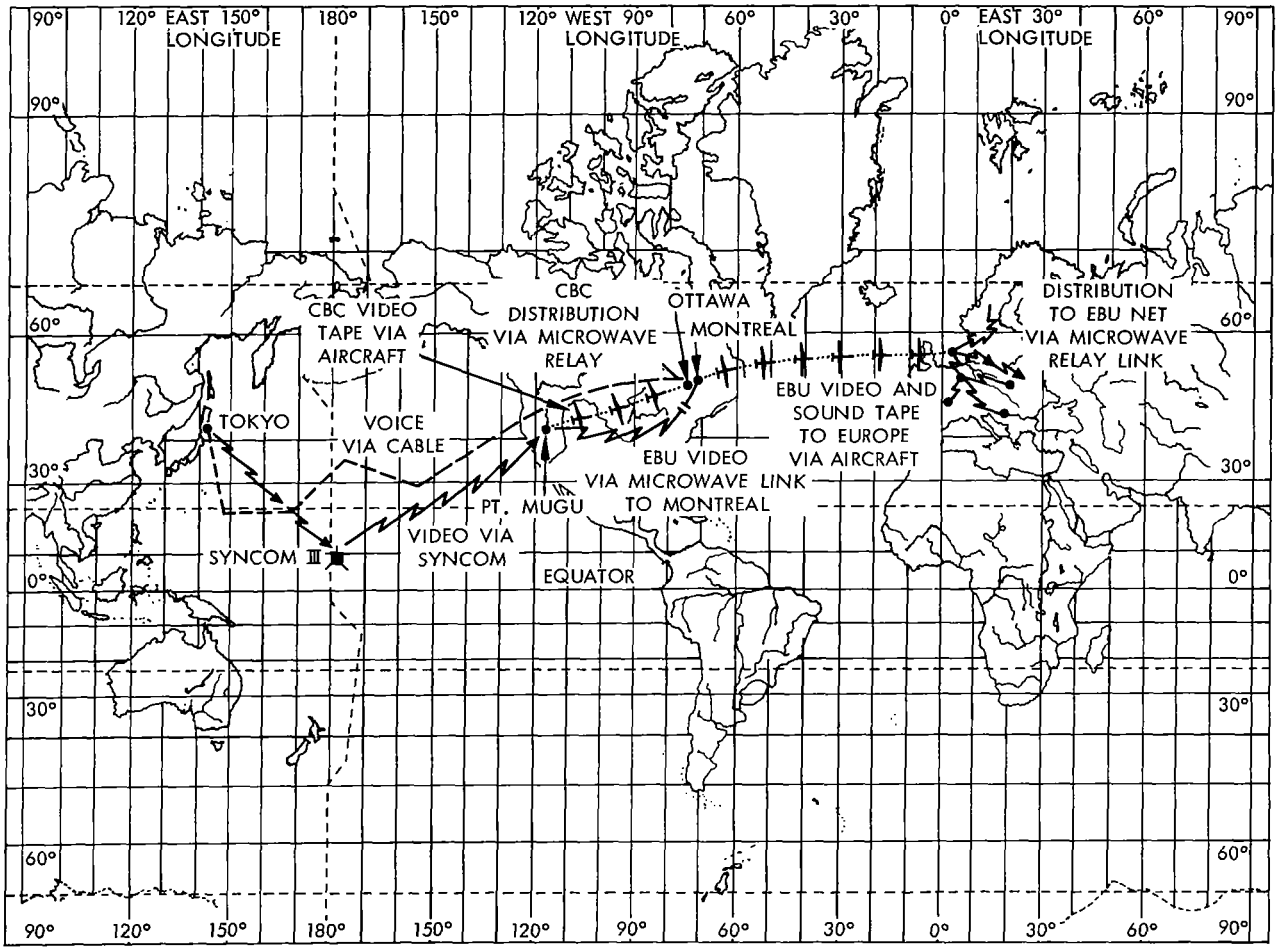

Figure VI-1—Olympic TV signal routing.

its initial receipt at Point Mugu with the normal degradations attendant on such processing steps.

Figure VI-2 shows the schedule of transmissions and test activity during the month of October. Several important points are illustrated.

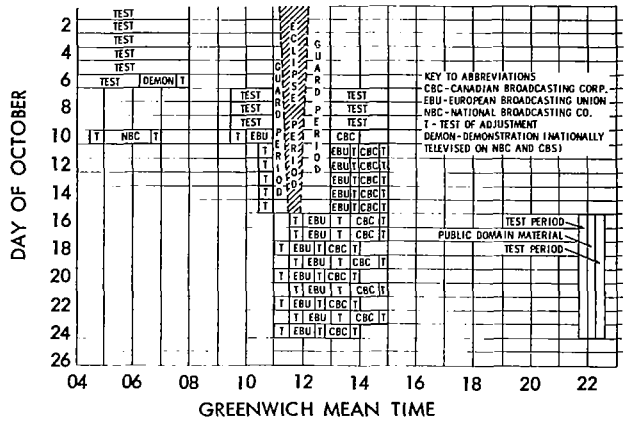

Figure VI-2—Olympic TV transmission schedule.

The schedule required by the European Broadcasting Union to provide effective exploitation of Syncom-relayed material was governed by the relative geographic position of Europe and Japan and by the time required for editing the material and transporting it to Europe. These factors, along with the restraints imposed by other users of the satellite, dictated a time of transmission of the material through the satellite which coincided with the eclipse time of Syncom III on the days shown in Figure VI-2. It was necessary to interrupt transmissions during the eclipse period to allow the satellite to be turned off. No deteriorating effects of the shadow transit on the relayed video were observed.

Transmissions were sent at various times of day as illustrated. The time of day did not affect the quality of the video or the noise levels of the receiving system. This conclusion was drawn from observation by the operating personnel and can be confirmed by comparing Table VI-7, which lists the receiving system's performance over several days, with the schedule (Figure VI-2).

The test periods indicated on the schedule were used for acquisition of the satellite (primarily at the transmitting end where pointing tests were conducted with both the receiving and transmitting antennas to obtain optimum illumination of Syncom by the transmitter) and for adjusting the modulation parameters. Signal-to-noise and carrier-to-noise measurements were made during each test period.

The schedule was adhered to 100 percent of the time, except for five minutes of program material and ten minutes of test time lost on 14 October due to a failure in the transmitter. All transmitted video material was judged acceptable by the exhibiting agencies. This performance attests to the dependability of communication by synchronous-orbit satellites.

TRANSMITTING SYSTEM

Kashima Transmitting Station

Program material, selected and edited by the United States, Canadian and European recipients, was processed by NHK (Japan Broadcasting Company) in its studios in Tokyo, and sent via microwave link to the Kashima transmitting station (Figure VI-3). This station, owned by Japan's Radio

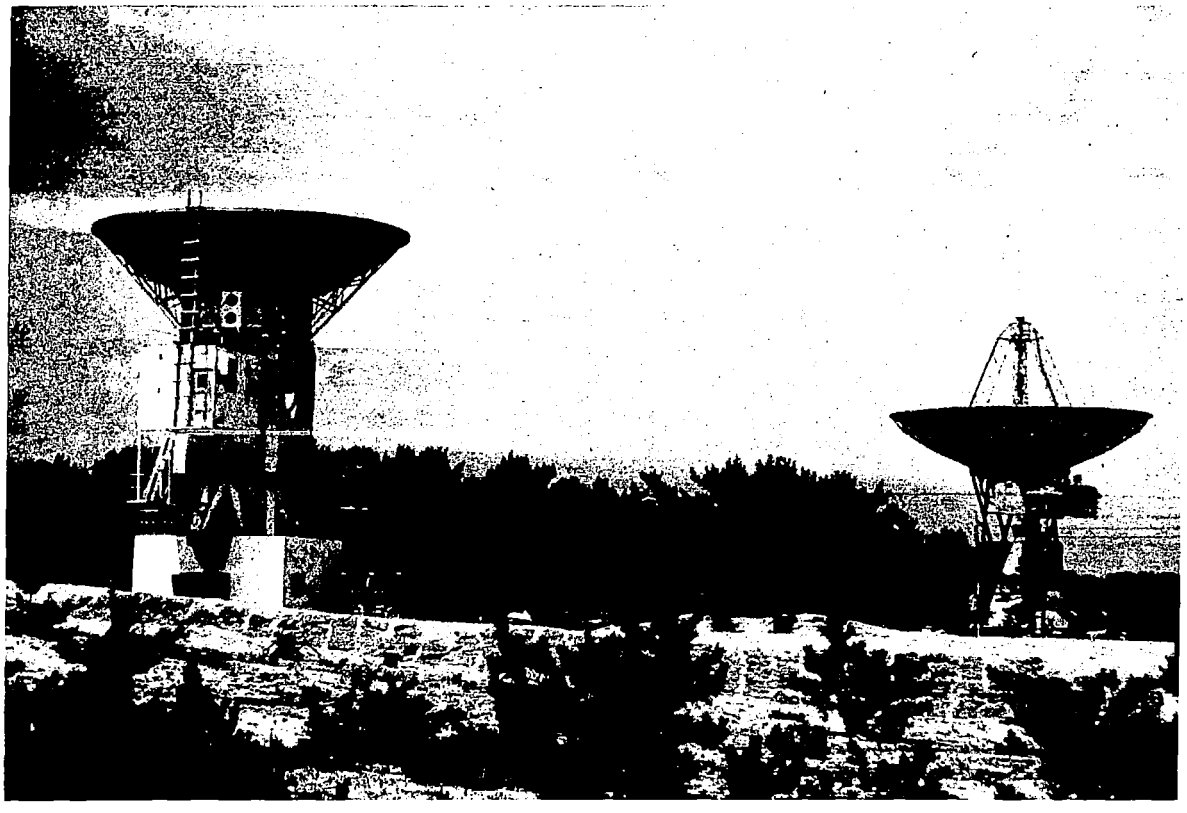

Figure VI-3—Transmitting site at Kashima (10-meter transmitting antenna at left; 30-meter receiving antenna at right).

Research Laboratory, was made available for transmitting Olympic program material by the Japanese Government. NHK coordinated Japanese activities associated with the transmissions. Figure VI-4 is a block diagram of the transmitting and receiving equipment used at Kashima, Japan. Table VI-1 lists the principal transmitting and receiving characteristics.

The first tests in the series were loop tests where the signal was transmitted by Kashima to the satellite and received from the satellite by the Kashima receiving system. Table VI-2 lists typical results obtained in a day's TV transmission test. Table VI-3 is another set of data taken during a day's loop testing. It shows the effects of power reduction at the transmitter on carrier-to-noise and signal-to-noise ratios.

The Kashima receiver uses a cooled parametric amplifier, achieving an equivalent noise temperature of about 60 K. At this noise temperature, the signal-to-noise characteristics were not as good as those at Point Mugu but were considered acceptable for unusual program material.

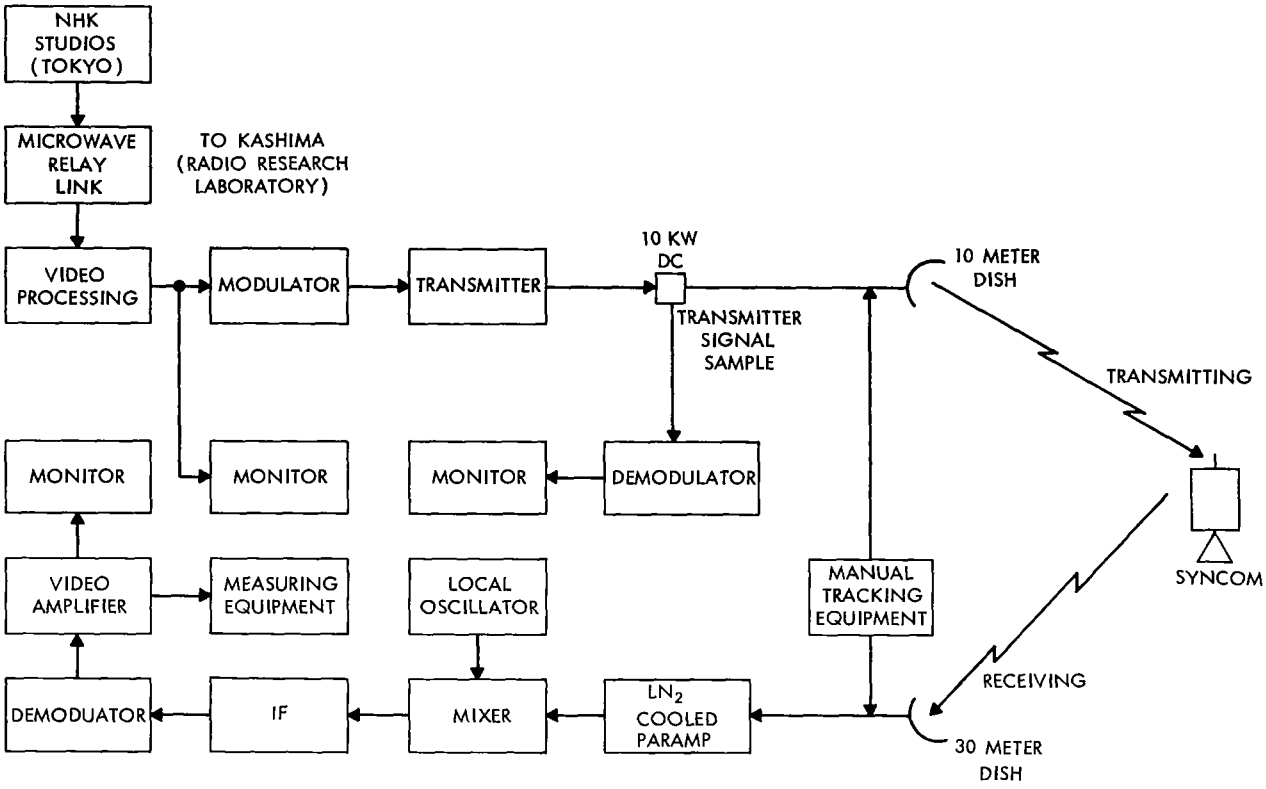

Figure VI-4—Block diagram of transmitting and receiving equipment in Japan.

Table VI-1

Characteristics of RRL (Kashima) Transmit-Receive System.

Transmitter	
Antenna	10 meter dish 55.0-db gain
Transmitter power	1 to 10 kw (variable) 7 kw, normal
Transmitter frequency	7359.4232 Mc
Bandwidth	10 Mc
Pointing	Manual control
Receiver	
Antenna	30 meter dish 51.5db gain
Pointing	Manual control
Preamplifier	Paramp, liquid nitrogen cooled
Receiving frequency	1812.2170 Mc (nominal)
Equivalent noise temperature	60°K (approximate)

Table VI-2

Parameters Observed at Kashima During the 30th TV-Transmission Test via Syncom III on 23 October 1964.

TM	RP	SY	FD	EM	CF	BF	IF	C/N	S/N	PQ
2148	7	B4	7.5	14	300	2.5	11	7.0	32.6	Passable
2220	7	B4	7.5	14	300	2.5	11	6.9	32.2	Passable

Abbreviated Notation

TM	Time (GMT)
BF	Baseband frequency (max) in Mc
CF	Crossover frequency of emphasis in kc
C/N	Carrier-to-noise ratio in db
EM	Emphasis in db
FD	Frequency deviation (p-p) in Mc
IF	IF bandwidth of receiver in Mc
PQ	Picture quality
RP	Radiated power in kw
S/N	Signal-to-noise ratio in db (DAP picture/rms noise, unweighted)
SY	System of TV transmission— B-4, 60 fields per second, positive Synchronizing pulse, amplitude compression

Table VI-3

Effects of Radiated Power on C/N and S/N at Kashima During the 9th TV Transmission Test via Syncom III on 11 October 1964.

TM	RP	SY	FD	EM	CF	BF	IF	C/N	S/N	PQ
1048	10	B4	7	14	300	2.5	11	6.8	29.3	Passable
1305	10	—	0	—	—	—	—	6.3	—	—
1454	1	B4	7	14	300	2.5	11	5.9	25.6	—
1454	2	B4	7	14	300	2.5	11	6.2	28.1	—
1455	3	B4	7	14	300	2.5	11	6.5	29.4	—
1455	4	B4	7	14	300	2.5	11	6.6	30.2	—
1456	5	B4	7	14	300	2.5	11	6.7	30.9	—
1456	7	B4	7	14	300	2.5	11	6.8	31.4	—
1457	10	B4	7	14	300	2.5	11	6.9	31.8	—

Abbreviated Notation

TM	Time (GMT)
BF	Base-band frequency (max) in Mc
CF	Crossover frequency of emphasis in kc
C/N	Carrier-to-noise ratio in db
EM	Emphasis in db
FD	Frequency deviation (p-p) in Mc
IF	IF bandwidth of receiver in Mc
PQ	Picture quality
RP	Radiated power in kw
S/N	Signal-to-noise ratio in db (DAP picture/rms noise, unweighted)
SY	System of TV transmission— B-4, 60 fields per second, positive Synchronizing pulse, amplitude compression

Modulation Technique

The Syncom III transponder is an angle-modulated system. Therefore, the video signals were transmitted in a frequency modulation form. The relatively narrow bandpass of Syncom III raised some important technical questions concerning the frequency spectrum of video baseband and the signal processing methods to be used to obtain the best signal-to-noise ratios. These problems were solved using the techniques described in the following paragraphs.

The basic energy content of the video signal lies in the lower frequency portion of the video baseband. The higher frequency components contribute primarily to better resolution of fine picture detail and contain very little spectral energy, the actual amount being somewhat proportional to frequency but depending considerably on the spectral content of the picture being transmitted. Noise signals, on the other hand, are uniformly distributed over the bandpass occupied by the video modulation. In low signal level situations such as in the transponder receiver and in the ground receiver, the noise has a tendency to swamp out the high video frequencies and cause a noisy picture lacking in detail.

The noise problem in other satellite systems has been attacked by the fundamentally good method of using large frequency deviations when modulating the transmitting carrier. Since the noise in a well-limited FM receiver causes small frequency deviations in the carrier, the signal components compete favorably with the noise at the FM demodulator. This method requires a wideband communication system (20 megacycles or more) and is not suited to Syncom III because of the latter's relatively narrow bandwidth (about 10 megacycles). Therefore, another approach was necessary.

The predominance of noise in the higher video frequency regions can be effectively overcome by pre-emphasis of the video higher frequency components before they are applied to the transmitter modulator. Pre-emphasis is achieved by a passive filter network (which actually depresses signal power at the lower frequencies relative to the highs according to a prescribed relationship). It was chosen as a technique for noise suppression in the Syncom III video transmission system. Various networks were tried experimentally to determine appropriate pre-emphasis characteristics for the system. The amount of pre-emphasis is related to the deviation bandwidth available and the amount of frequency deviation characteristic of the modulator. Therefore, the bandwidth of Syncom III entered in the selection of the pre-emphasis technique.

The video signal with its synchronizing components is an amplitude signal in which a large fraction of the amplitude is devoted exclusively to the synchronizing pulse. When this amplitude signal is used to frequency-modulate a transmitter, the synchronizing portion of the signal uses up a considerable portion of any bandwidth available for transmission of the FM signal. It thus competes with the video for the bandwidth space and limits the permissible deviation of the video signal components, thereby reducing the possibility of improving signal-to-noise ratio by use of higher index FM.

In commercial transmission practice, the sophisticated equipment used makes it possible (and reasonable) to remove the transmitted synchronizing pulse completely and replace it with a newly

generated synchronizing pulse of more precise shape, salvaging only the video from the transmitted information. This practice was exploited in the Syncom III system to make more deviation bandwidth available for video transmission. The carrier frequency, situated at the low end of the passband, was "clamped" to the "dark" or "pedestal" level of the video. A two-megacycle sine wave train (tone burst) was substituted for the synchronizing pulses, one maximum for the train being held at the clamp level, the other maximum being in the direction of "bright" video. Since the frequency deviation in an FM system is somewhat proportional to modulating signal amplitude, this substitution permitted more deviation bandwidth for the video components of the signal, thereby improving the signal-to-noise ratio substantially. After demodulation at the receiver end, standard synchronizing information generated from the two-megacycle tone bursts was added to the video to form a new composite signal. Figure VI-5 illustrates the substitution process.

Selection of the pre-emphasis characteristic and the modulation deviation factor is dependent on still another factor which is the subjective evaluation of the viewer. The nature of the video signal and the interplay of noise and picture detail permit deviation of some of the high frequency picture components beyond the passband of the system without detection of their loss by the viewer. This "over-deviation" permits greater frequency deviation of the main energy components of the picture and consequent further improvement in the signal-to-noise ratio.

The final selection of pre-emphasis and deviation factor is dependent, then, on subjective evaluation and is an exercise in comparing various combinations of these factors under various

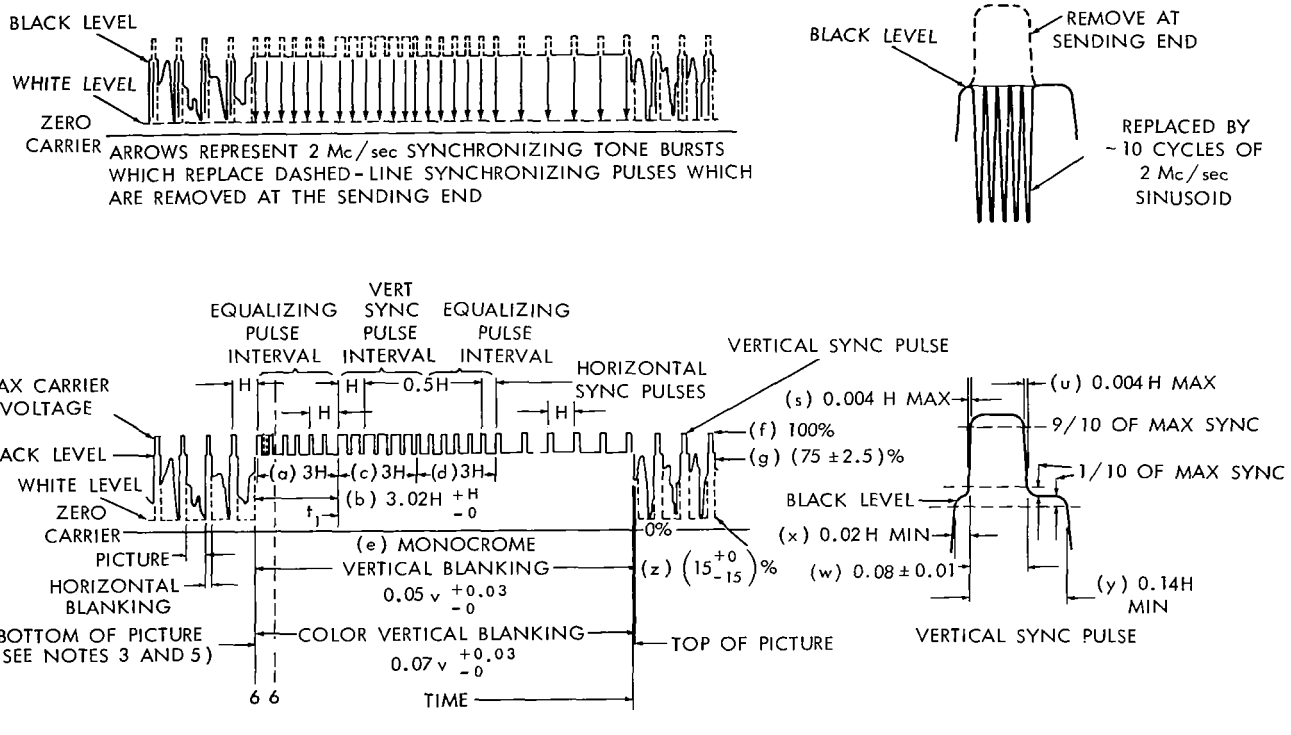

Figure VI-5—Sinusoid pulse train substitution for synchronizing pulses.

noise conditions. In the day-to-day transmission activity it was feasible to adjust these factors for the prevailing noise conditions, the program material, and the system parameters to achieve very acceptable results.

RECEIVING SYSTEM

Point Mugu Receiving Station

The Point Mugu receiving station consisted of the TAA-2 telemetry receiving system, made available to Comsat by the Department of the Navy and modified to suitable configuration. Figure VI-6 is a block diagram of the Point Mugu receiving station.

The primary features of the Point Mugu station were its 85-foot reflector (Figure VI-7), and its very low system-equivalent-noise-temperature (less than 38°K at elevation angles of 15 degrees), which permitted the achievement of relatively high carrier-to-noise and signal-to-noise ratios with the relatively low effective radiated power of Syncom.

The low equivalent noise temperature of the receiving system was achieved by:

1. Using feed with a very narrow pattern and low sidelobes resulting in very low "spill-over" of signals from the reflecting dish. This feed combined with the very narrow beam pattern of the large parabolic reflector kept sidelobe noise to a very low level.

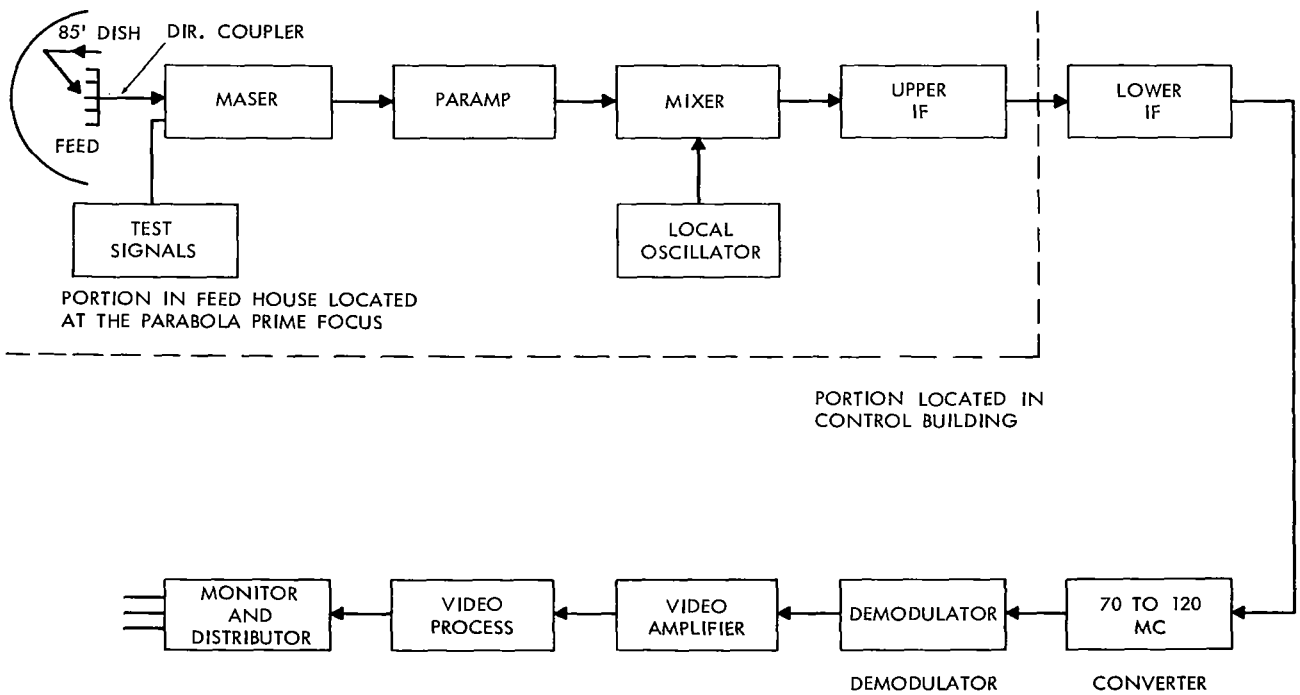

Figure VI-6—Block diagram of Olympic television receiving system Point Mugu, California.

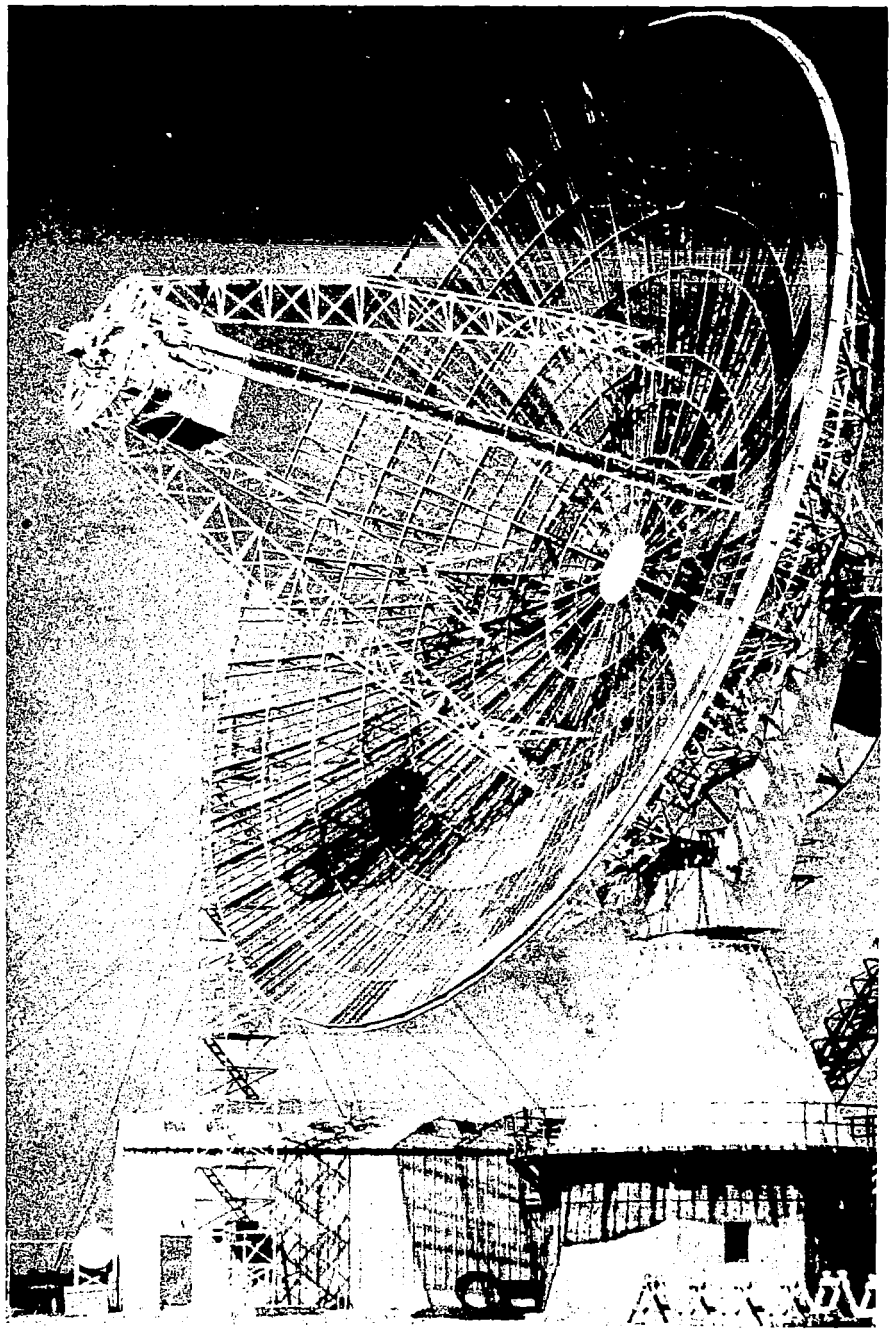

Figure VI-7—Receiving antenna and adjacent control house at Point Mugu, California.

2. Placing the principal receiver elements at the prime focus of the reflector and using a very short, low-loss transmission line between the feed and the maser first amplifier to keep the loss-generated noise contribution low.

3. Using a high-gain (about 26db) traveling-wave maser amplifier, cooled in a bath of liquid helium which contributed, with its coupling circuits, only thirteen to fifteen degrees of equivalent noise temperature.

4. Following the maser with a low-noise (T_k° = 110), high-gain (approximately 21db) parametric amplifier to drive the low-noise converter stage.

5. Using a relatively narrow bandpass (10 Mc) IF strip to reduce noise from the unused (for modulation) bandpass of the system.

The site of the antenna also offered some natural advantage. The antenna was located some three hundred yards from the shore and looked at Syncom III over the open ocean. The small amount of man-made noise in the sea direction and the lower "ground" noise from the sea surface aided in obtaining low equivalent noise temperatures.

Table VI-4 lists the estimated noise contributions of various elements of the receiving system. Figure VI-8 is a graph of the system equivalent noise temperature as a function of antenna elevation angle. Tables VI-5, VI-6, and VI-7 summarize receiving performance characteristics observed during the period of Olympic program transmissions. Table VI-7 shows a high degree of uniform performance although there was considerable variation in weather conditions (fog and cloud cover) during the period. Also significant relative to the uniformity is the fact that only one front end service adjustment was made during the period. (The paramp pump was readjusted on 21 October.)

Table VI-4

Noise Contributions of "Front-End" Components.

Component		Contributed Equivalent Noise Temperature (°K)
T_{A^*}	(antenna)	15
T_L	(transmission line temperature)	6
T_M	(maser)	14
T_I	(noise from temperature instrumentation)	1
T_{F_1}	(paramp and mixer)	1
T_S	(sum of above—the predicted system temperature)	37
T_{S_a}	(the actual average system temperature measured)	37.7

*Calculated using antenna and feed pattern. Remaining data calibrated by Hughes Primary Standards Laboratory.

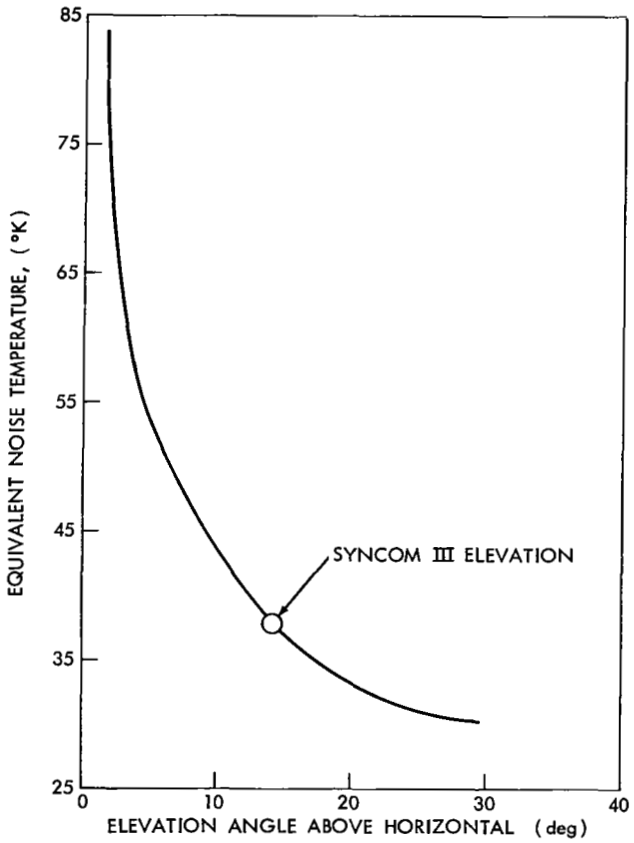

Figure VI-8—Noise temperature versus elevation angle.

Table VI-5

Carrier Level and Carrier-to-Noise Ratio (C/N) Measured Through Various Bandpass Filters.

Bandpass (Mc)	4.0	5.0	6.3	8.0	10.0	12.0
C/N (db)	15.3	14.8	14.1	13.8	13.2	13.0
Carrier level (dbm)	-101.4	-101.0	-100.6	-100.0	-99.6	-98.8

Notes:
1. Average of 70 measurements between 9/26 and 10/24.
2. Variation of values of carrier level with bandpass reflects errors contributed by excess noise in the wider bands.
3. Average noise temperature 37.7°K at 15 degrees elevation angle and 5 degrees off the satellite in azimuth.

Table VI-6

Signal-to-Noise Ratio (S/N) as a Function of Modulation Parameters.

Baseband (Mc)	Frequency Deviation (Mc)	Pre-Emphasis (db)	Signal/Noise
2.5	6	14	32
2.5	7	14	34
2.5	8	14	35

Notes:
1. Average of 70 measurements between 9/26 and 10/24.
2. Average noise temperature 37.7°K at 15 degrees elevation angle and 5 degrees off the satellite in azimuth.
3. Special emphasis, as noted in modulation discussion, was used.

Table VI-7

Receiver Performance Characteristics Point Mugu Station.

Date, October	Time (hrs Z)	Deviation (Mc)	S/N (db)	C/N (db)	Carrier Lead (dbm)	Temperature (°K)
23	2200	7.5	35	13.3	-99.5	38.9
	1440	7.5	35	12.7	-100.2	37.9
22	2200	7.0	34	13.3	-99.2	38.6
	1400	8.0	35	12.9	-99.5	37.9
21	2100	8.0	34	12.7	-100.3	38.3
	1200	8.0	35	12.2	-100.4	38.6
20	2100	7.5	34	12.5	-100.1	37.5
	1400	7.5	34	11.4	-101.3	39.3
18	2100	6.0	32	14.6	-98.1	39.8
17	1400	7.0	34	13.2	-99.7	37.5
16	1200	6.5	34	13.5	-99.4	36.9
	2140	6.0	32	13.4	-99.4	37.8
15	2200	6.0	32	14.3	-98.7	37.1
14	1245	6.3	33	14.8	-98.1	37.5
13	1500	—	34	14.3	-98.7	36.5
12	1300	7.0	34	13.5	-99.4	37.4

Notes:

S/N → p-p signal to rms noise
S/N average value ≅ 34db measured using stair step test pattern.
Baseband video signal 2.5 Mc
Carrier received at 1812.2 Mc

Front End Components

Figure VI-9 is a block diagram of the Point Mugu receiver front end comprising the feed antenna, transmission lines, maser, and parametric amplifier. All these components, housed in the small feedhouse shown at the focal point of the 85-foot antenna previously shown in Figure VI-7, are described below.

Feed Antenna and Transmission Line

The feed antenna, shown in Figure VI-10, is a flat, round-plate structure having a series of concentric, hoop-like rings which act as chokes to distribute the antenna currents so that the pattern is within 4db across the face of

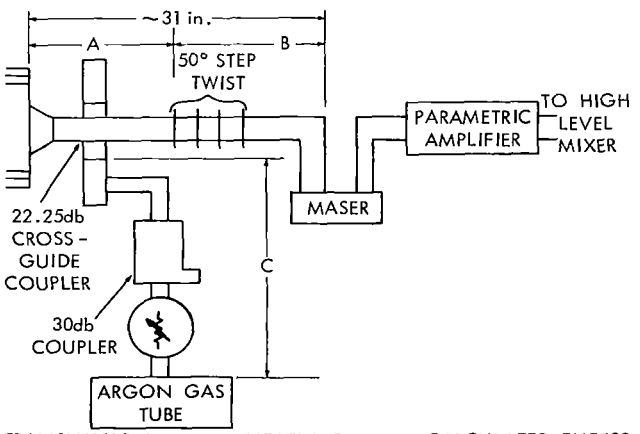

TRANSMISSION LINE	MEASURED ATTENUATION	CALCULATED EXCESS TEMPERATURE
A	A 0.05db ± 0.02	3.5 ± 1.5°K
B	B 0.05db ± 0.02	3.5 ± 1.5°K
C	C 0.87db ± 0.02	NOT APPLICABLE

Figure VI-9—Waveguide component attenuations and related equivalent excess noise temperature.

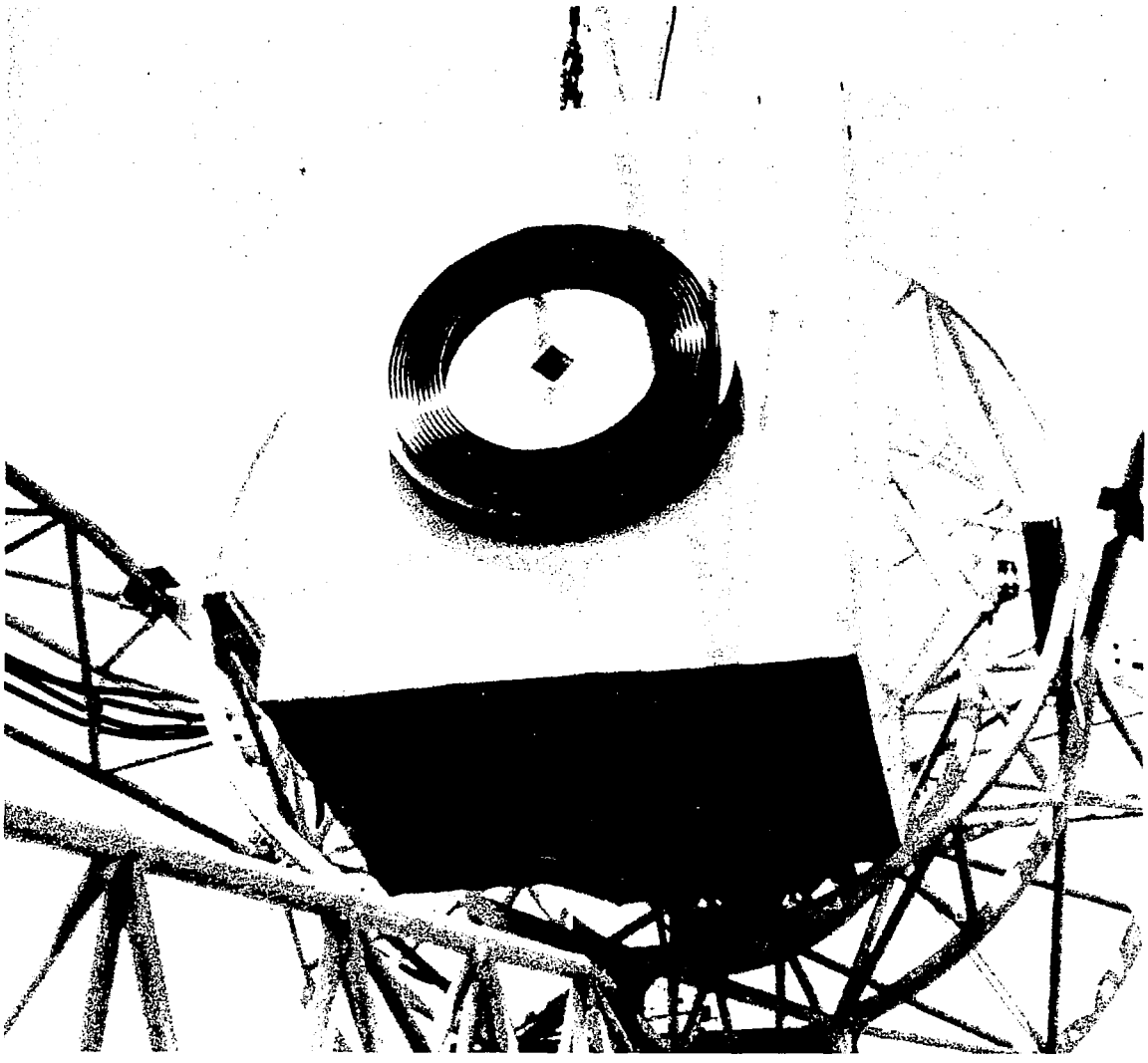

Figure VI-10—Antenna feed house mounted in place.

the dish and thereafter drops very sharply (see Figure VI-11 which is the E plane power pattern taken on the feed). The 85-foot reflecting dish has an F/D ratio of 0.425, which places the focal point at 36 feet and the dish edges at 61 degrees from the central axis as seen from the focal point. Therefore, the feed intercepts very little "spill-over" energy (that is, very little energy which does not arrive at the feed via the paraboloid reflector, meaning that the antenna has very small sidelobes).

An antenna pointed toward the sky receives most of its noise energy from the sidelobes since, unlike the main lobe which intercepts noise energy of the relatively cold sky, the sidelobes usually intercept the relatively warm ground and the man-made terrestrial noise sources. The special feed characteristics are in large measure responsible for the low system equivalent noise temperature achieved with the Point Mugu antenna.

The efficiency of an antenna is a measure of its maximum gain relative to the maximum theoretical gain of the antenna. A high efficiency antenna collects more signal from the source and thereby yields a higher signal-to-noise ratio than a less efficient antenna (assuming equal sidelobe noise contributions). The efficiency of a paraboloid antenna system depends primarily on the ability of the feed to collect signal uniformly from all parts of the reflector. The design chosen for this feed is particularly well suited to produce high antenna efficiency because its pattern has relatively constant magnitude across the face of the reflector. Calculations and confirming measurements indicate that the feed is approximately 57 percent efficient.

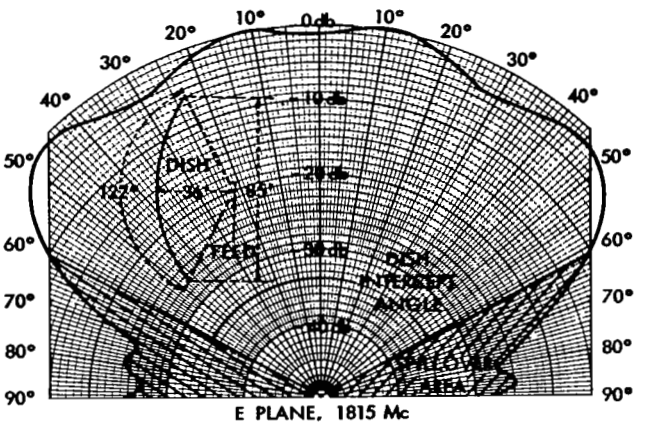

Figure VI-11—Feed-antenna relative power pattern showing relative uniformity of reflector illumination and sharp power density reduction beyond edges of paraboloid reflector.

The polarization of the feed is linear as is the polarization of the satellite. To maximize the received signal, the feed was rotated about its central axis to match the feed polarization angle to the apparent polarization angle of the satellite as seen by the feed. The feed waveguide was matched physically to the maser waveguide by a tuned step-twist (which has the very short dimensions advantageous to this application). Great care was exercised in the design and fabrication of the twist to keep its losses and mismatch as low as possible. Its insertion loss was kept down to 0.05db. Figure VI-12 shows the apparent polarization angle seen at Point Mugu as a function of longitudinal placement of the satellite. For placement at 180 degrees longitude, the graph indicates an angle of 52.5 degrees. (The angle for which the twist was designed was 50 degrees. At design freeze time the exact final longitude was not known.) Figure VI-12 does not include the diurnal variation of approximately 10 degrees (shown in Figure VI-13) caused by Faraday rotation as the signal passes through the ionosphere. The diurnal variation of 10 degrees produces a maximum signal variation of about 0.1db shown in Figure VI-14.

A conventional cross-guide directional coupler is provided for insertion of signal and noise for system calibration and noise temperature measurements. The coupler provides 22.25db of isolation between the direct and coupled input channels.

The total length of the transmission line from the feed plate to the maser waveguide input flange is only 31 inches.

Maser

The key element in the low noise receiving chain is the traveling-wave maser which was developed by the Microwave Electronics Corporation, Palo Alto, California, from a design previously prepared for the Goldstone deep space tracking facility.

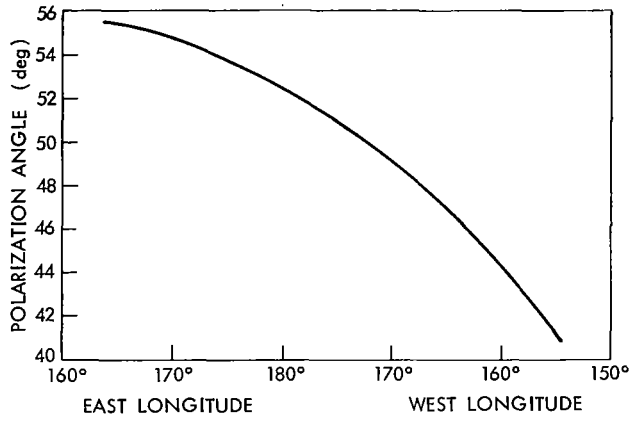

Figure VI-12—Polarization angle at Point Mugu for Syncom III at various longitudes.

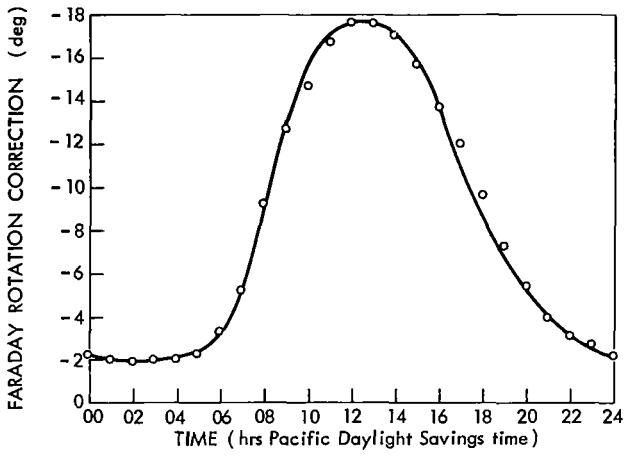

Figure VI-13—Diurnal variation caused by Faraday rotation.

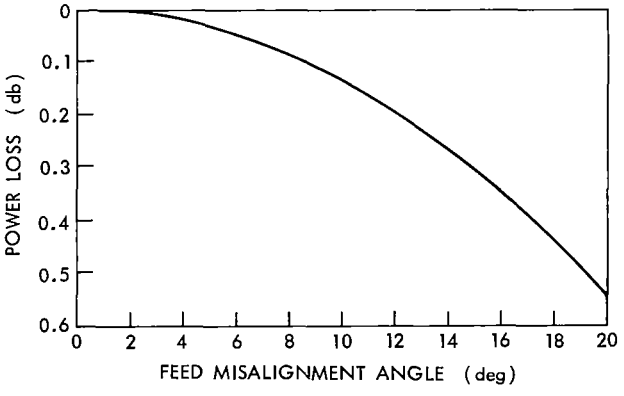

Figure VI-14—Received power loss resulting from misalignment of antenna feed with polarization vector.

It utilizes a chromium-doped aluminum oxide (ruby) amplifying element in a "typical" traveling-wave circuit. At liquid helium temperatures, the paramagnetic chromium ions in the ruby are permitted four paramagnetic quantum states of energy represented in Figure VI-15. Following maser operation theory, the three lowest energy states are used in the manner illustrated to establish the particular operating frequency of this maser (thus qualifying it for identification under the commonly used terminology "three level ruby maser").

The ruby element is coupled to the signal with a "comb" type of slow-wave structure which is dielectric end-loaded to widen the bandwidth. These elements are enclosed in a conventional waveguide section. The comb propagates a circular polarized wave. Oscillation of the amplifier is prevented by placement of ytterium-iron-garnet absorption elements along the comb structure at points of magnetic field maxima of the reflected wave, where they will absorb the reflected energy, thus reducing it below the level necessary to sustain oscillation.

The pump power is coupled to the ruby by the cavity effect of the waveguide.

Figures VI-16 and VI-17 show, respectively, the basic elements of the amplifying portion of the traveling-wave maser and their positional relationship and the actual maser elements. Figure VI-18 shows this maser head attached to the low temperature extension which is necessary for placing the maser in the proper physical relationship to the cooling fluid and magnetic field.

The cross section sketch of Figure VI-19 illustrates the placement of maser and extension head in the liquid helium dewar and the magnet. Figure VI-20 shows the complete maser assembly ready for installation.

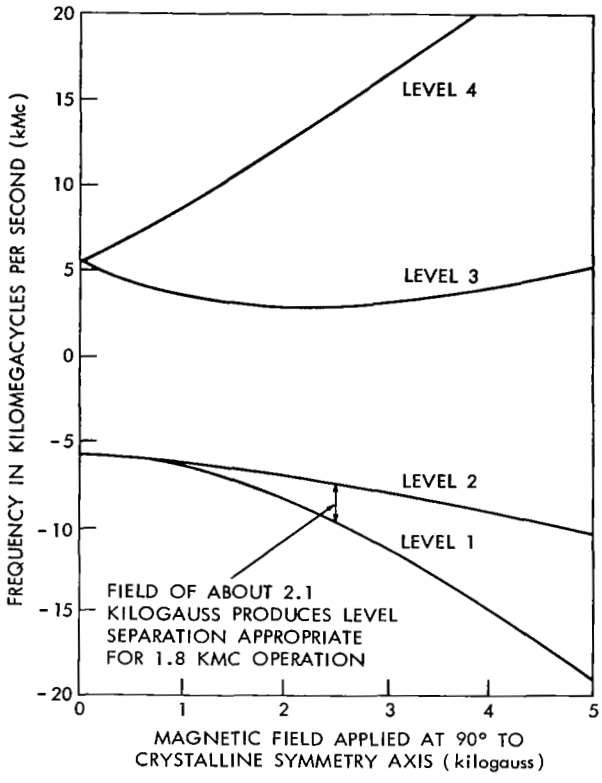

A. EFFECT OF MAGNETIC FIELD ON ENERGY LEVEL SEPARATION

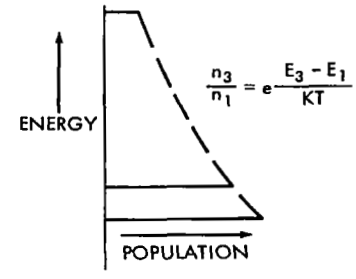

B. POPULATION DISTRIBUTION VERSUS ENERGY LEVEL AT THERMAL EQUILIBRIUM

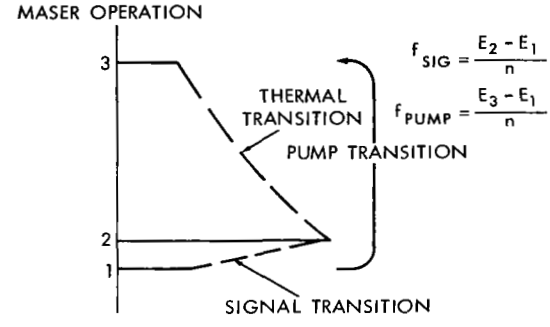

C. POPULATION INVERSION DUE TO PUMP-POWERED TRANSITION (LEVEL 1-3) AND THERMAL TRANSITION (LEVEL 3-2), WHICH LEADS TO MASER AMPLIFICATION IN SIGNAL TRANSITION (LEVEL 2-1).

Figure VI-15—Energy diagram showing fundamentals of maser operation.

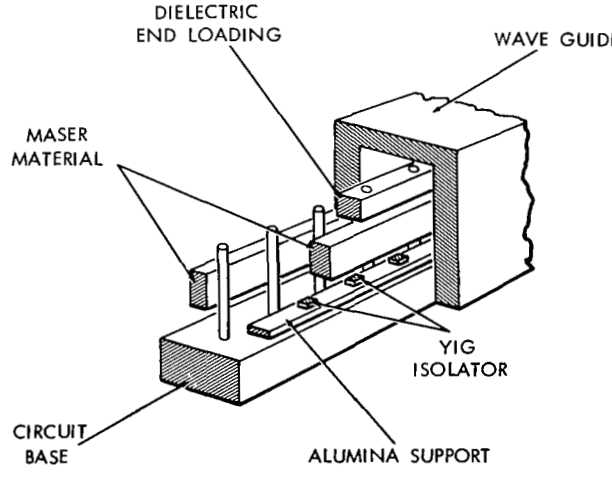

Figure VI-16—Placement of components within traveling wave maser structure.

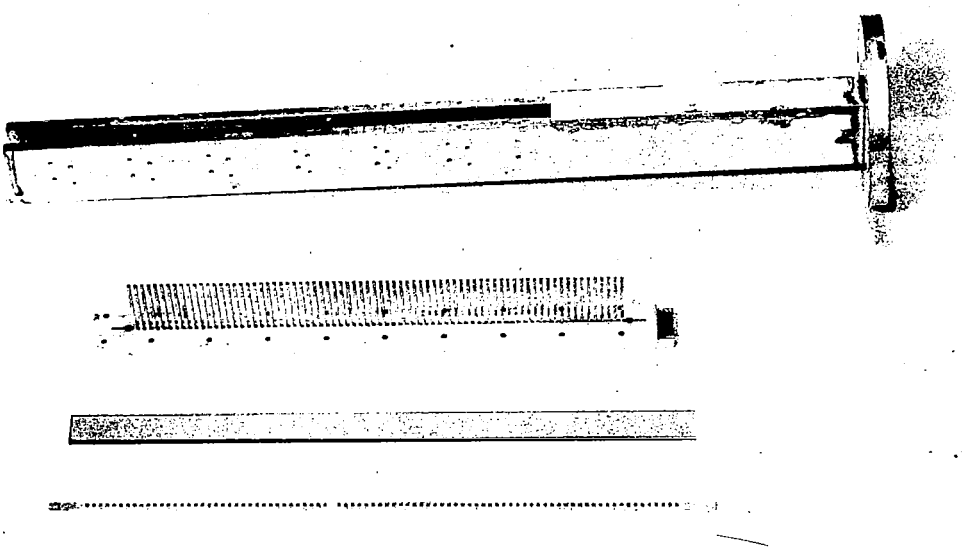

Figure VI-17—Traveling-wave maser amplifier components.

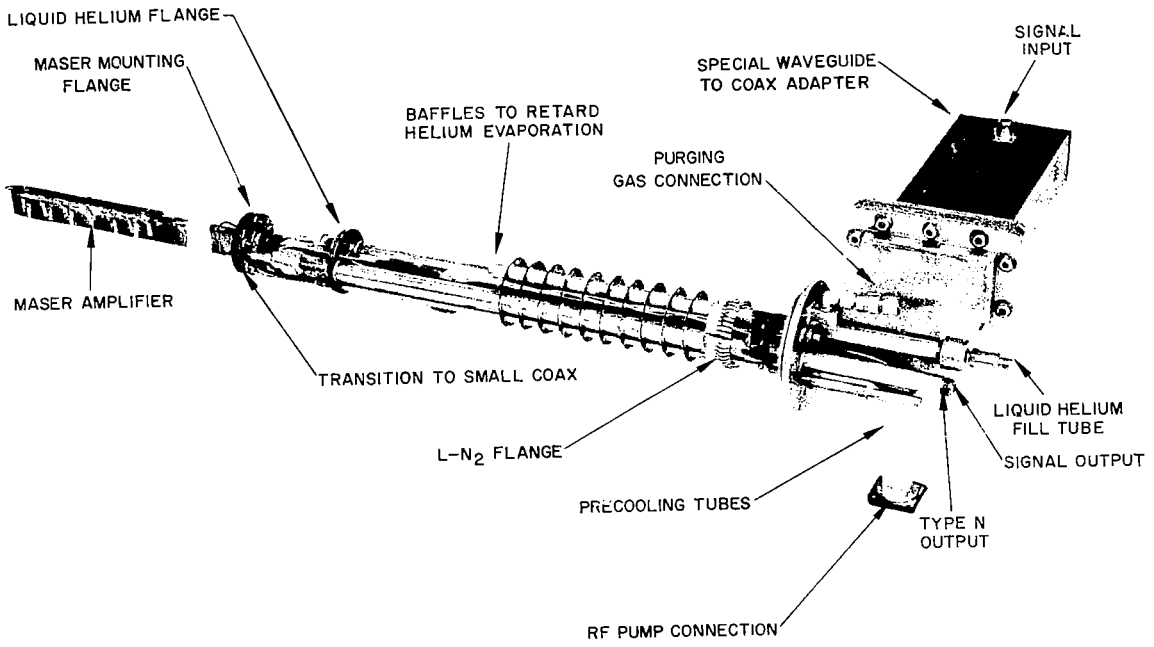

Figure VI-18—Low temperature extension head with maser attached with component identification.

Table VI-8 enumerates the characteristics of the maser and Figure VI-21 shows the gain versus bandwidth of the maser. Figure VI-22 shows the maser gain as a function of tuning range. Tuning is accomplished by varying the current in differential field coils placed around the permanent magnet which provides the primary magnetizing field.

The block diagram of Figure VI-23 shows the maser position in the receiving system and identifies its controls and supporting elements. As shown in the diagram, the principal status indicators and the operating controls are not installed in the feedhouse but in the control building adjacent to the antenna.

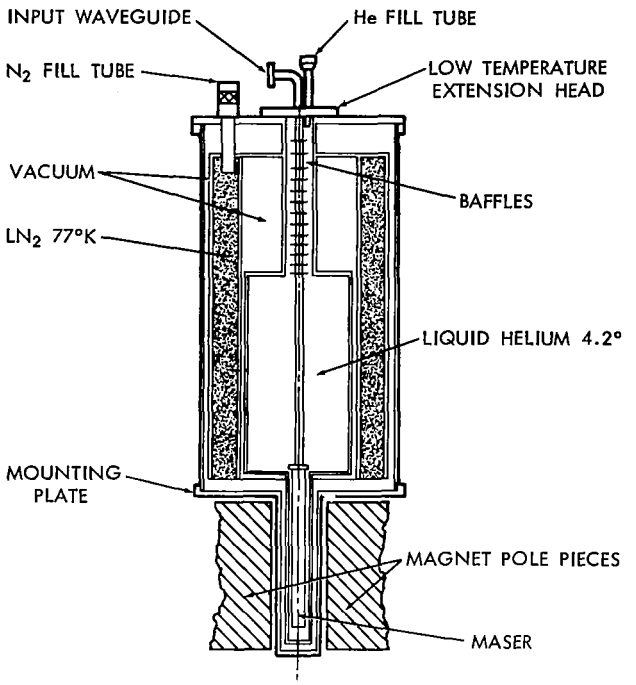

Figure VI-19—Cross section of inner portion of liquid helium storage dewar with maser installed.

Parametric Amplifier

To further reduce the effects of mixer noise on the receiving system signal-to-noise ratio, a parametric amplifier was used, following the maser, to obtain an additional 20db of gain at the carrier frequency prior to mixing. Operating at room temperature, the amplifier had an equivalent noise temperature of about 125°K.

The amplifier is of the typical two-cavity, single-port, negative resistance, non-degenerate variety, coupled to the input and output circuits through a four-port circulator. It is pumped by a reflex klystron oscillator operating at 17.5 Gc. The amplifier bandwidth is about ±11 megacycles and the center frequency tuning range is about twenty-five megacycles.

The amplifier with its klystron pump was located in the feedhouse adjacent to the maser output port, to keep noise contributions of the transmission line circuits as low as possible. Figure VI-24 is a photograph of the parametric amplifier.

Converter and IF Amplifier

Subsequent to the low-noise RF amplifiers, the elements of the receiving system are conventional. The converter consists of a diode mixer with the local oscillator signal derived from a crystal oscillator and varactor multiplier chain. The intermediate frequency is 70 Mc. The IF amplifier consists of two sections, one of which was located in the feedhouse, with the mixer, adjacent to the parametric amplifier to bring the received signal to a high power level before transmission through the long coaxial line carrying the signal from the antenna feed house to the

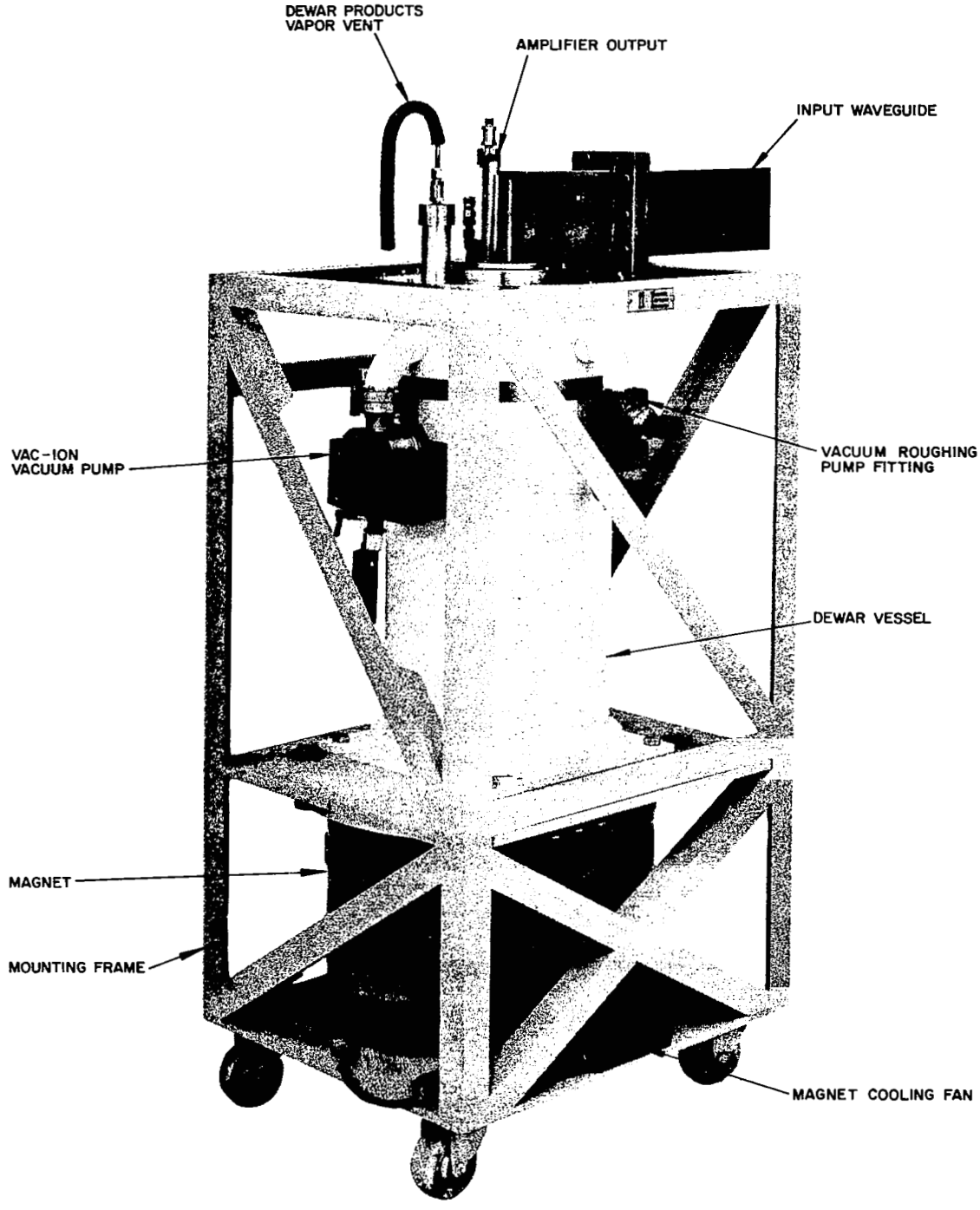

Figure VI-20—Maser assembly containing magnet in lower compartment, helium dewar with low-temperature extension head installed.

Table VI-8

Maser Characteristics.

Noise temperature at 1814 Mc	13 degrees T_K 15 degrees (overall)
Gain	
at 1809	23.0db
at 1814	25.3db
at 1819	23.5db
Bandwidth (maser)	
2db at about 1814 Mc	±5.0 Mc
at about 1764 Mc	36.5db down
3db at about 1814 Mc	12.5 Mc
at about 1864 Mc	40.5db down
VSWR maser input at 1814 ±5 Mc	Less than 1.5
VSWR maser output at 1814 ±5 Mc	Less than 1.5
System gain stability at 1814 Mc for 10 minutes	Less than ±0.05db
Saturation level (input)	-66dbm
Pump power	30 mw
Pump frequency	11.900 Gc
Pump power stability	0.1 mw/°C
Pump frequency stability	14 kc/°C
Magnetic field (approximate)	2150 gauss
Magnet trimming current	2.55 amps
Dewar run time	More than 30 hours

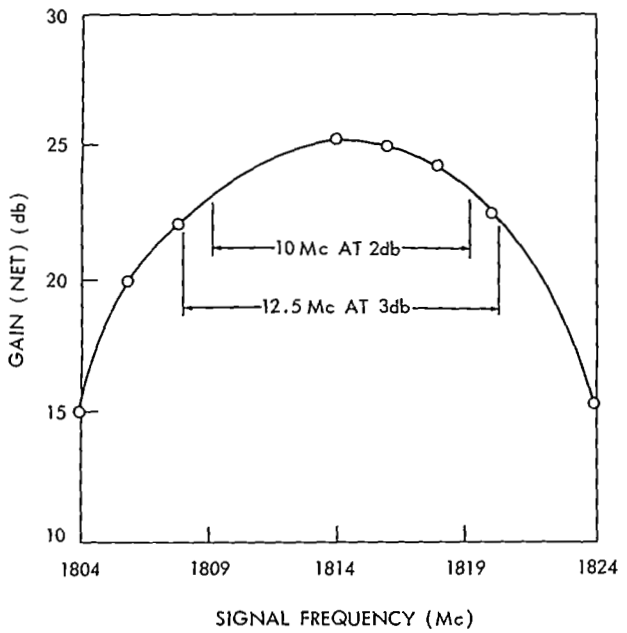

Figure VI-21—Gain versus instantaneous bandwidth operating at center frequency of 1814 Mc with pump power of 50 mw.

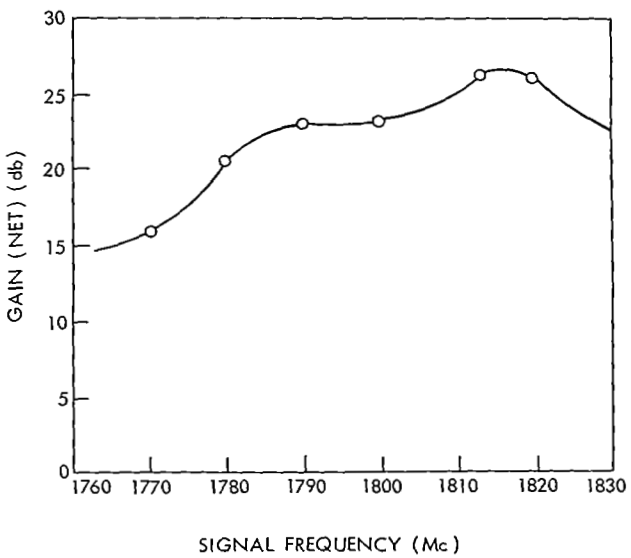

Figure VI-22—Gain versus tuning range for maser amplifier.

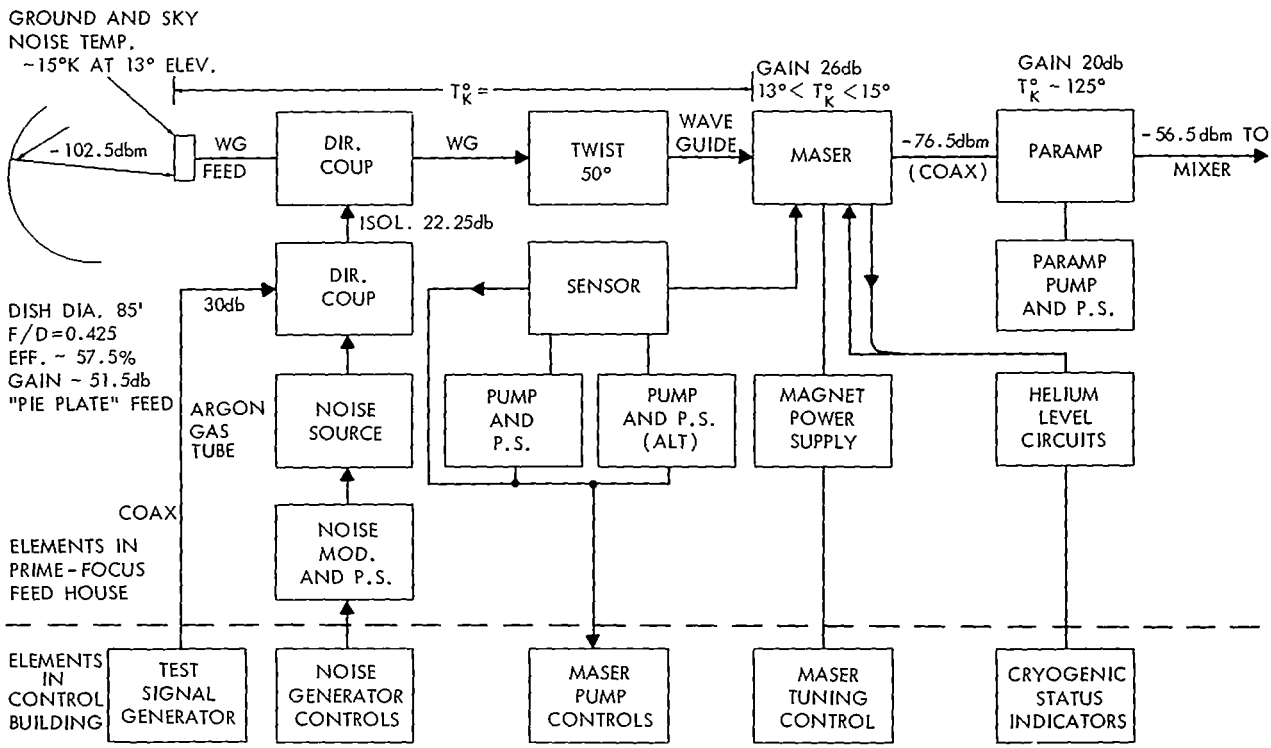

Figure VI-23—Olympics television receiver low noise front end and pre-amplifier.

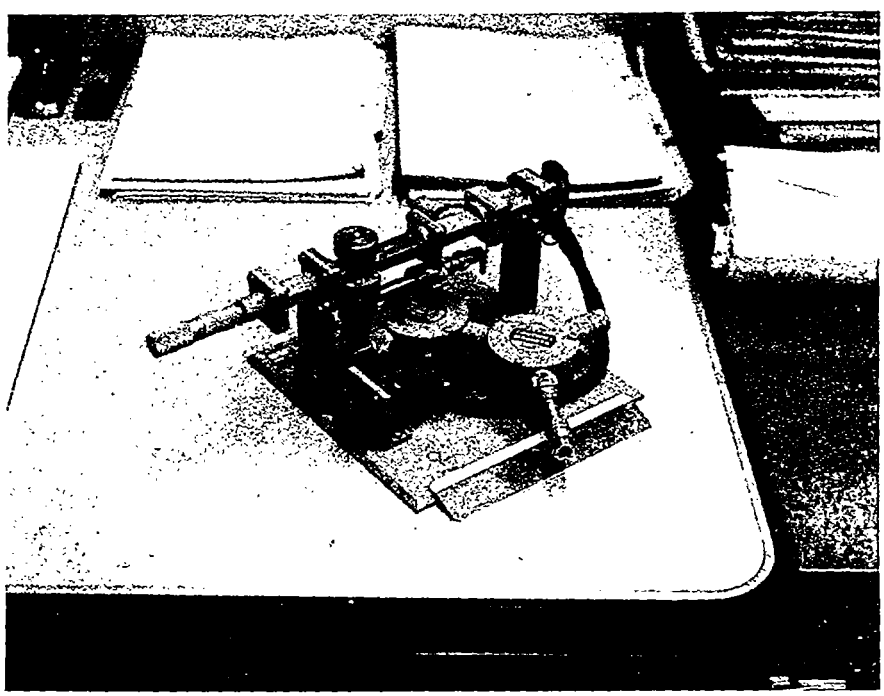

Figure VI-24—Parametric amplifier.

demodulation equipment in the control house. This is a further design step to reduce noise in the system. Manual gain control was used on the feedhouse section of the IF; manual and automatic gain control were used on the control-house section. The IF system block diagram, Figure VI-25, shows the arrangement of the IF system elements and enumerates some of the system parameters. In video systems, transmission-line impedance matching is an important consideration in preventing delay distortion. The 200-foot transmission line from the feedhouse to the receiving building was matched by terminating each end in an attenuating pad of the appropriate impedance level. This simple effective method was made possible by the considerable excess gain available in the system.

The IF system was arranged for use with bandpass filters of various bandwidths for selecting optimum signal-to-noise ratios. Five filters covering the range from 4 to 10 Mc (at 3db point) were provided. Four-pole, Tchebycheff-formula design was used to provide the filters with relatively steep band edges.

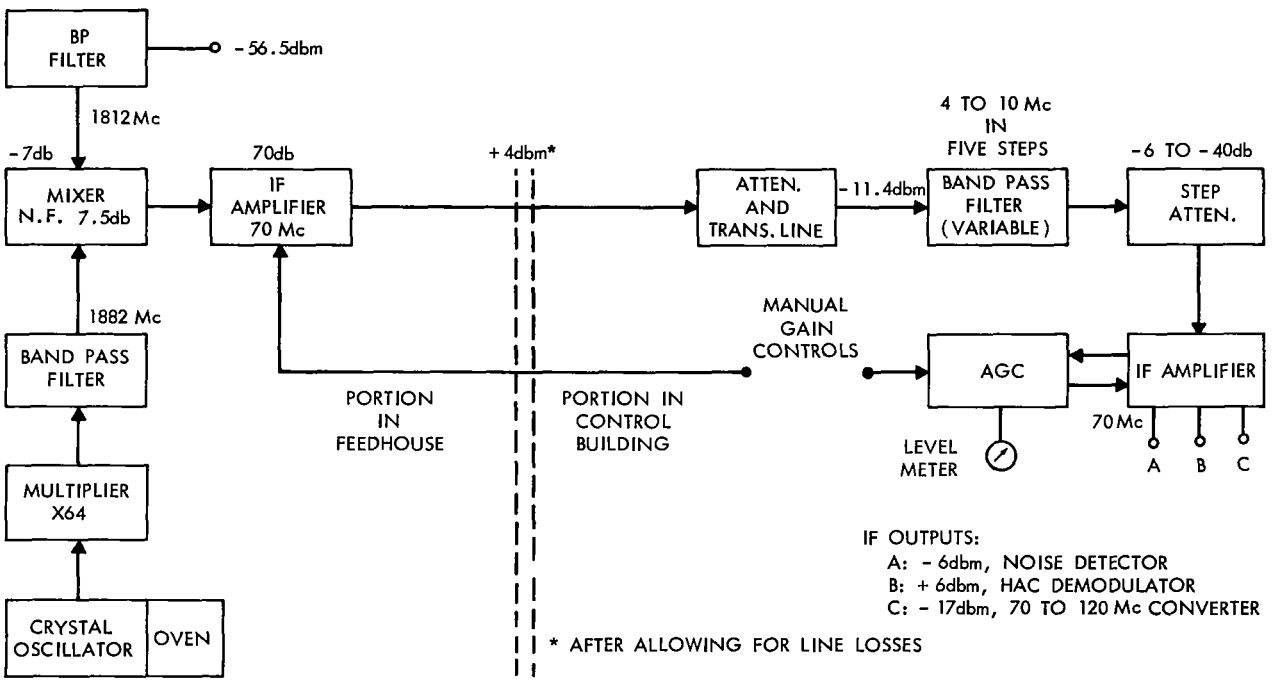

Figure VI-25—Olympics television receiver intermediate frequency amplifier.

Baseband Equipment

A conventional wideband FM discriminator was used for video demodulation during reception of Olympic program material. Subsequent to demodulation, the signal was processed by the video processing equipment provided by Japan Broadcasting Corporation (NHK). Processing consisted of several steps, including removing the synchronizing signal tone bursts and replacing them with standard synchronizing pulses. In another step, the pre-emphasized signal was restored to its

original character by appropriate de-emphasis equipment. Noise cancelling circuits were used to remove noise spikes from the composite video.

Two different phase-lock loop demodulators were provided as alternates to the conventional discriminator. At the beginning of the program it was not clear that low equivalent noise temperatures and high antenna efficiency could be achieved with certainty. Therefore, the expected signal-to-noise ratio for the video signals was somewhat indeterminate. No extensive comparison of the viewing qualities of the available modulation-demodulation schemes for FM transmission were available at that time, but the phase-lock loop demodulator theoretically appeared to have a definite advantage over the conventional FM discriminator at low signal-to-noise ratios. These considerations led to the decision to provide phase-lock loop demodulators, which were readily available, as demodulator alternatives. Figure VI-26 represents the configuration of the baseband equipment.

During preliminary tests on the system, it was determined conclusively that the subjectively "best" pictures were achieved with a video composite consisting of pre-emphasized video, positive synchronizing tone burst (as previously described), deviation of some of the high frequency components beyond the IF passband, and demodulation by means of the wideband conventional discriminator. The phase-lock loop demodulators did not hold phase-lock well under these conditions, the synchronizing tone bursts probably causing the loss of lock. Their amplitudes were large compared to the amplitude of the 2-Mc video signal components, and caused instantaneous phase excursions beyond the tracking capacity of the phase-lock loop.

The phase-lock loop demodulators did perform well in early test transmissions of conventional video composites. A definitive comparison of the technique of phase-lock loop demodulation versus

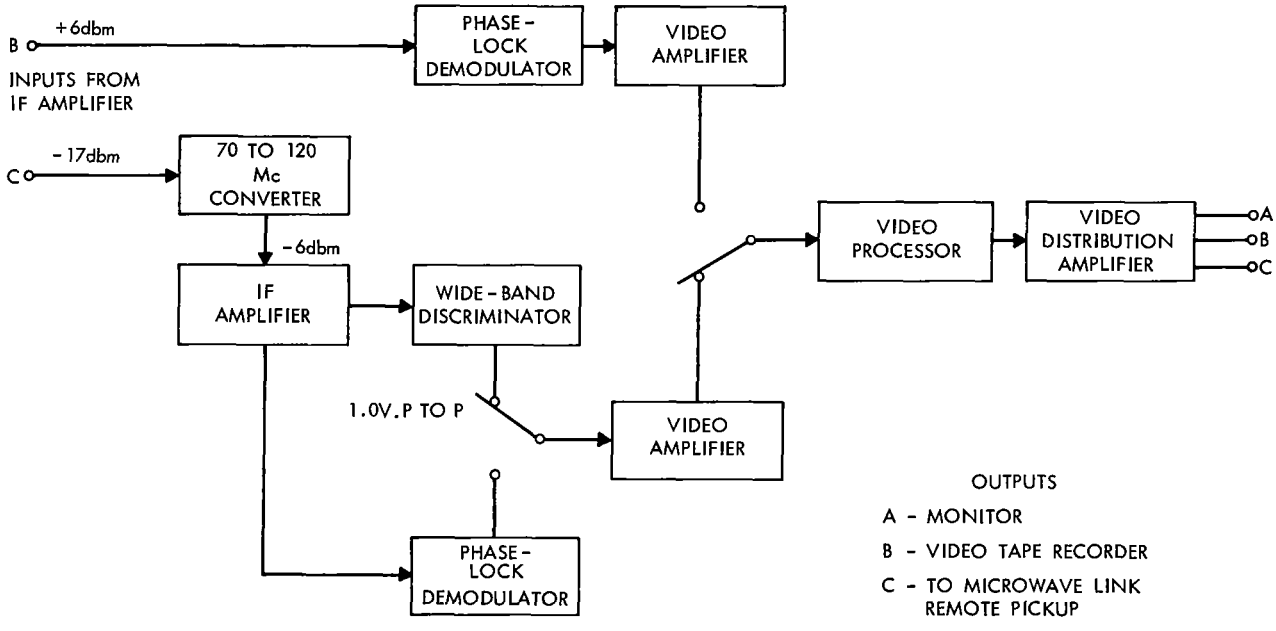

Figure VI-26—Simplified block diagram of Olympics television receiver baseband equipment.

the technique of over-deviation and demodulation by a conventional demodulator, however, was not made. In both schemes, pre-emphasis/de-emphasis techniques showed a definite advantage and were usable to about the same extent. Also, where over-deviated components were removed by the IF passband (and not by the characteristics of the phase-locked loop passband), the advantages seemed about equal. However, the phase-locked loop has the characteristic that signal (or noise) phase rates high enough to unlock the loop cause black or white spots of unusual intensity to appear on the video screen. While these spots are not necessarily objectionable, they are a phenomenon not normally observed on TV screens and an observer accustomed only to conventional TV demodulation systems might find them annoying. The scheme of pre-emphasis and over-deviation utilizing a conventional discriminator presents the picture characteristic of standard television except that the detail (and the noise) represented by the over-deviation does not appear. In normal viewing from a short distance, this loss of detail is far out-weighed by the improved noise reduction.

TYPICAL VIDEO PROGRAM MATERIAL

Figures VI-27 and VI-28 show typical video material received during the transmissions. Figure VI-27 illustrates the test patterns and typical "still" pictures used for test and adjustment. Figure VI-28 illustrates some of the more dramatic live material received.

ANTENNA TRACKING EXPERIENCE AT POINT MUGU

The first deep nulls of the Point Mugu antenna pattern were at approximately 0.5 degree off the pattern peak. Such a narrow beam antenna derives a primary advantage from a "stationary" satellite. Not only would a moving satellite radically complicate the receiving system, but it would require constant operator attention and many involved precautions to prevent motion modulation of the received signal. In contrast, the operators at Point Mugu were able to acquire the satellite quickly in a manual operating mode, set the antenna brakes, shut down the antenna drive, and perform other duties. The operations were hardly more taxing than operating a remote, fixed microwave relay terminal.

The satellite was acquired by pointing the antenna (as indicated by the direction dials on the control console) toward the predicted direction of Syncom III, then moving the antenna vernier position controls until the transmitted satellite signal appeared "peaked" on a spectrum analyzer and carrier-level meter. During the early tests, the antenna was "peaked" several times during a test. This practice was soon discontinued, however, because the satellite did not drift enough during a four hour program to have a discernable effect on signal strength. Thereafter the antenna ordinarily was peaked at the start of a test period and left in place except for moving it for equivalent noise temperature measurement purposes. The average time for acquisition and peaking (after having slewed to the approximate position of Syncom) was about one minute.

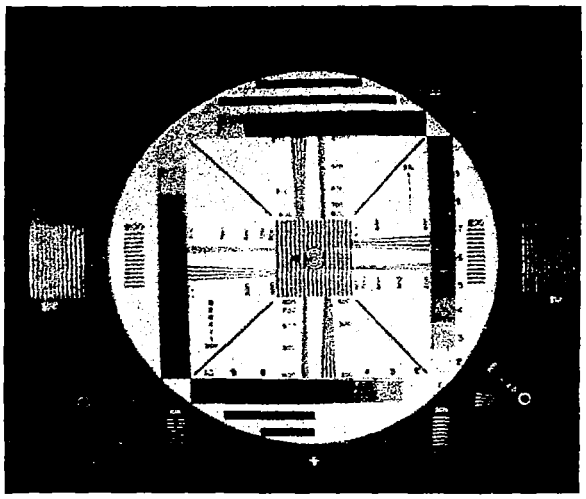

a. RTMA test pattern transmitted on 21 September in American standard form without benefit of any special processing except pre-emphasis. Black dot near center comes from flaw in Video pickup tube.

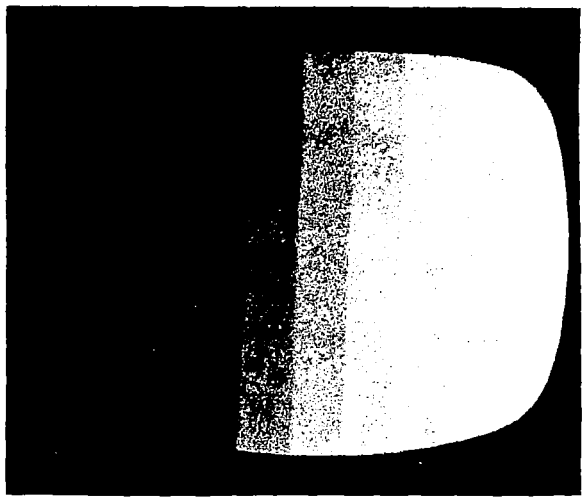

b. "Stair-step" pattern used in measuring Video signal-to-noise ratio. On "A" scan this pattern has appearance of side view of flight of stairs; hence, the name "stair step."

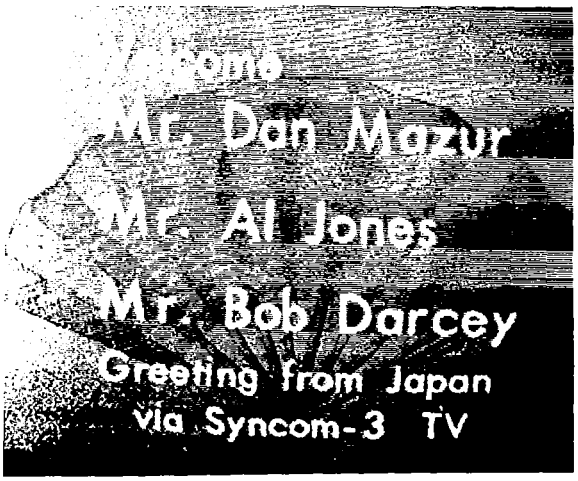

c. Greetings transmitted to NASA visitors during station test period.

d. Action shot showing announcer counting with voice and fingers to synchronize video with sound (which arrived via cable).

Figure VI-27—Typical early test transmission.

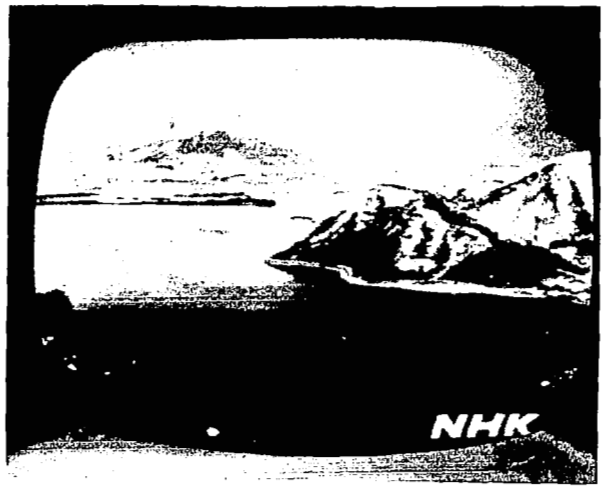

a. "Travelogue" scene of Japan.

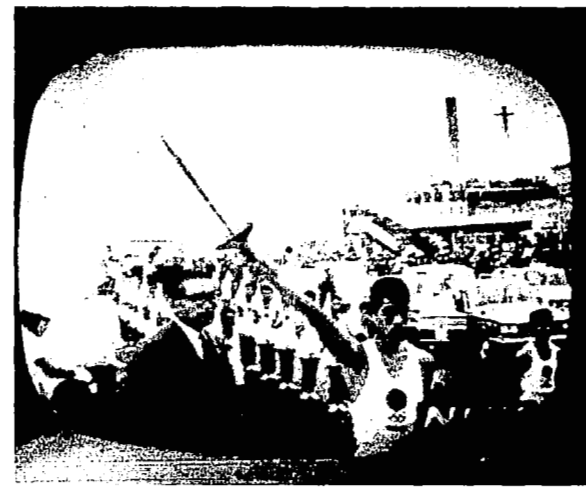

b. Beginning of processing carrying Olympic torch from Tokyo Airport to Olympic Stadium.

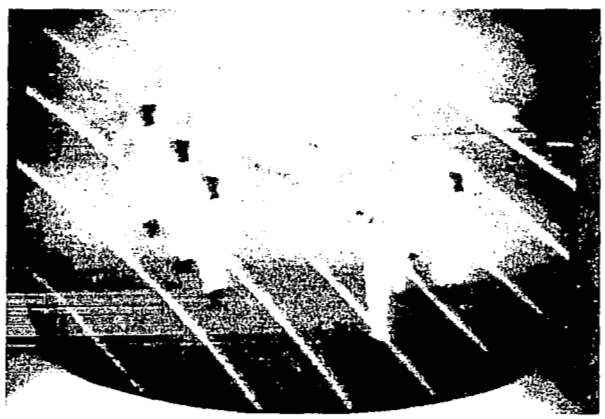

c. Japanese sailors leading opening day Olympic parade carrying Olympic flag.

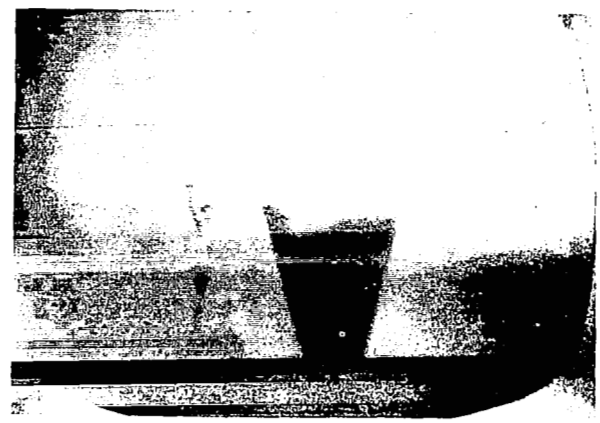

d. Lighting Olympic Torch as seen by TV camera across Olympic stadium.

Figure VI-28—Test program and opening day scenes received during Olympic TV program.

Table VI-9 lists all the acquisition positions recorded during October. The recorded numbers include small boresight errors and uncertainty errors in the pointing system and are tabulated here only to demonstrate the positional stability of Syncom III.

Table VI-9

Positions of Syncom III as Seen by Point Mugu Antenna.

Date, October	Time (Ms GMT)	Azimuth Angle (degrees)	Elevation Angle (degrees)
6	04:05	252.55	15.13
6	06:15	252.55	15.18
7	09:38	252.60	15.22
8	09:40	252.60	15.18
8	13:17	252.60	15.20
8	14:32	252.62	15.21
9	09:40	252.60	15.15
11	03:50	252.60	15.22
13	10:34	252.55	15.24
13	23:45	252.45	15.15
14	12:50	252.55	15.21
14	23:48	252.53	15.23
15	13:30	252.53	15.21
15	22:50	252.50	15.25
16	21:50	252.50	15.20
17	11:38	252.50	15.20
18	11:00	252.45	15.27
—	No Further Data Recorded		

CHAPTER VII

VHF COMMUNICATIONS EXPERIMENTS

Several tests were conducted during the period as part of a program to demonstrate the feasibility of establishing two-way communications with commerical aircraft via a synchronous satellite. PAA, NASA, Bendix, Boeing, FAA, ATA, and Hughes cooperated in these experiments.

On 21 September, a Pan American Hawaiian flight successfully received and recorded Syncom III telemetry signals. On 16 November, the Syncom III telemetry and command equipment was used as a VHF transponder for teletype transmissions between receiving and transmitting terminals at the Hughes Malibu facility. On 22 November, teletype messages were successfully transmitted from the NASA Telemetry and Command trailer at Camp Roberts, California to a Pan American flight enroute to Hawaii. These tests are briefly described below.

THE MALIBU EXPERIMENT

In the Malibu experiment, the normal telemetry and command equipments of Syncom III were utilized as a VHF transponder by making use of the 9.745-kc controller audio tone.

Figure VII-1 is a block diagram of the test set-up and Figure VII-2, a photograph of the terminal equipment. A standard 60-wpm teletype machine was used to generate mark and space signals for a breadboard teletype modulator. The modulator can generate CW tones selectable at either 9670 or 9820 cps or can generate tones at each frequency time shared sequentially at 22 millisecond intervals or in accordance with the mark space input from the teletype machine. The tones were used to amplitude-modulate a Collins 242F-5 VHF transmitter, which in turn was used to drive a Viking Johnson 6N2 linear RF amplifier. The amplitude-modulated 148-Mc carrier was transmitted to Syncom III via a 14db circular polarized YAGI antenna, received by Syncom, demodulated, and the signal passed through the 300-cps wide bandpass filter centered at 9745 cps. This signal, when of sufficient strength, gates off normal Syncom telemetry and directly phase modulates the 136-Mc telemetry transmitter. The phase-modulated 136-Mc carrier was transmitted to earth, received on a 14db circular polarized YAGI antenna, passed through a narrow band filter, and phase detected by a Defense Electronics TMR-6 receiver. The narrow band cavity filter was required to prevent receiver overloading by the 148-Mc transmitted signal. The output of the receiver was used to drive two pieces of equipment: a teletype demodulator driving a standard teletype machine to reproduce the original transmitted message; and a narrow band filter (4 cps) centered at the telemetry calibrate frequency of 13.5 kc used for initial acquisition of the satellite. The telemetry data was recorded on a strip recorder. Table VII-1 lists the system

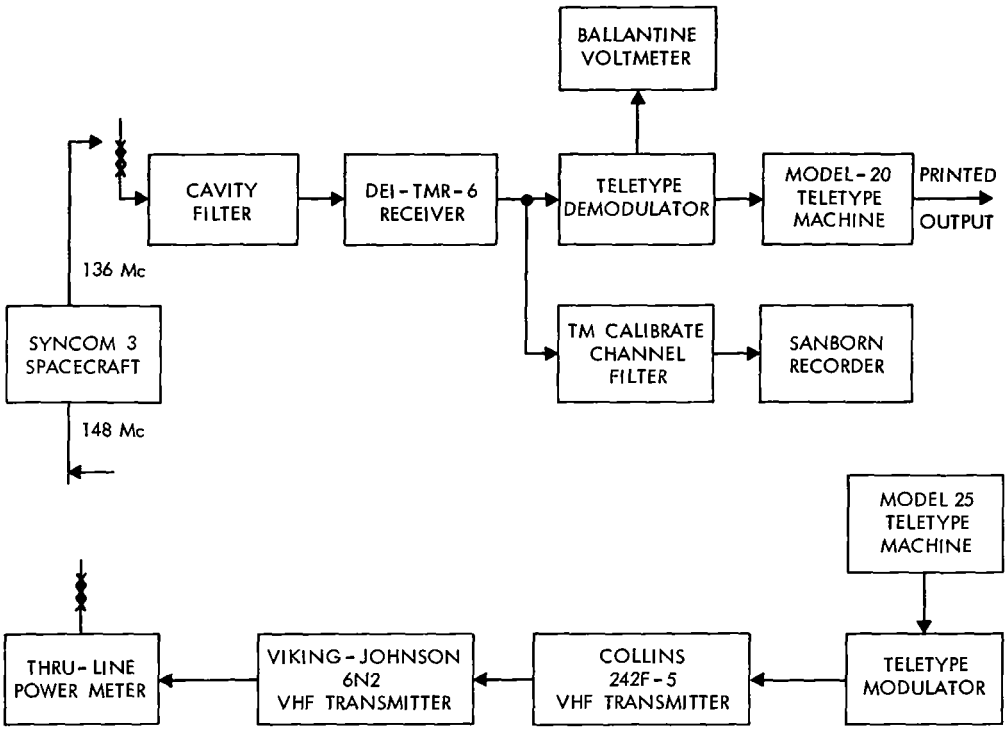

Figure VII-1—Malibu VHF teletype communications test block diagram.

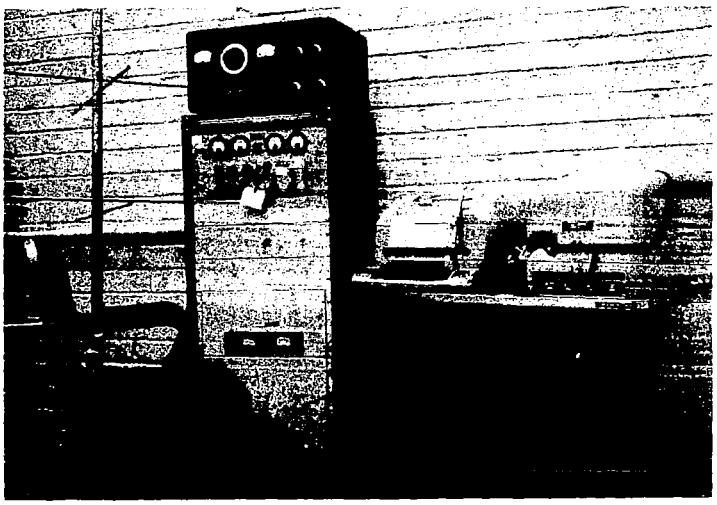

Figure VII-2—Terminal equipment used in the Malibu experiment.

parameters for the predicted ground-to-spacecraft link, and Table VII-2, those for the predicted spacecraft-to-ground link.

A number of tests were run to check out the terminal and on 16 November an error test was made to prove the link. Figure VII-3 shows 70 lines of teletype sent at 4:30 in the afternoon. During

Table VII-1

Calculated Parameters for the Ground-to-Spacecraft Link.

Ground transmitter (50 watts)	+ 17dbw
Ground antenna	+ 14db
Cable losses	- 0.5db
Effective radiated power	+ 30.5dbw
Free space loss	-168.0db
Spacecraft antenna gain	- 3db
Duplex loss	- 3db
Polarization loss	- 3db
Spacecraft cable loss	- 2db
Total losses	-179.0db
Signal power at spacecraft receiver input	-148.5dbw
Noise at receiver terminals:	
Receiver noise power density	-228.6dbw
Receiver bandwidth (60 kc)	47.8db
$T = \frac{T_G}{L} + \frac{(L-1)}{L}(290)$	
$+ (F-1)(290) = 1250 =$	+ 31.0db
Receiver noise power	-149.8dbw
Signal-to-noise in IF	+ 1.3db
Signal-to-noise ratio out of demodulator	0.0db
Signal-to-noise at telemetry transmitter modulator (300 cps bw)	
$= (M^2)(S/N)\left(\frac{B_{IF}}{2B_{tone}}\right) =$	+ 20.0db

this test at 200 watts transmitted power, only five errors were made, yielding a bit error rate of 1.4×10^{-4}. The signal-to-noise ratio in each teletype filter bandwidth was 18 to 20db, in close agreement with the 18.6db S/N predicted. Then transmitter power was reduced to 50 watts and the

Table VII-2

Calculated Parameters for the Spacecraft-to-Ground Link.

Power applied to spacecraft antenna	+ 1.0dbw
Spacecraft antenna gain	- 3.5db
Ground antenna gain	+ 14.0db
Space attenuation	-167.5db
Cable loss on the ground	- 1.0db
Polarization loss	- 3.0db
Signal at preamp input	-160.0dbw
Receiver noise figure	3.5db
Receiver noise power	228.6dbw/°C/cps
$T_{eff} = \frac{T_G}{L} + \frac{L-1}{L}(290) + (F-1)(290)$	
$= \frac{870}{1.26} + \frac{0.26}{1.26}(290) + 1.25(290)$	
$\square$ 1121° =	30.5db
Noise power density	-198.1dbw/cps
Modulation loss:	
a. Carrier -3.5db	
b. Signal 0.0db	
C/N in receiver IF (60 kc)	- 13.2db
C/N in tracking loop (20 x 2)	+ 18.6db
S/N at filter output (40 x 2)	+ 19.1db
S/N in filter output considering both up and down links	+ 18.6db

modulator unit was retuned for maximum signal-to-noise ratio. (It tended to drift during the tests as its temperature increased from transmitter heat.) Figure VII-4 shows 73 error-free lines which were sent during this test, indicating that the modulator-demodulator had been temporarily detuned during the previous test.

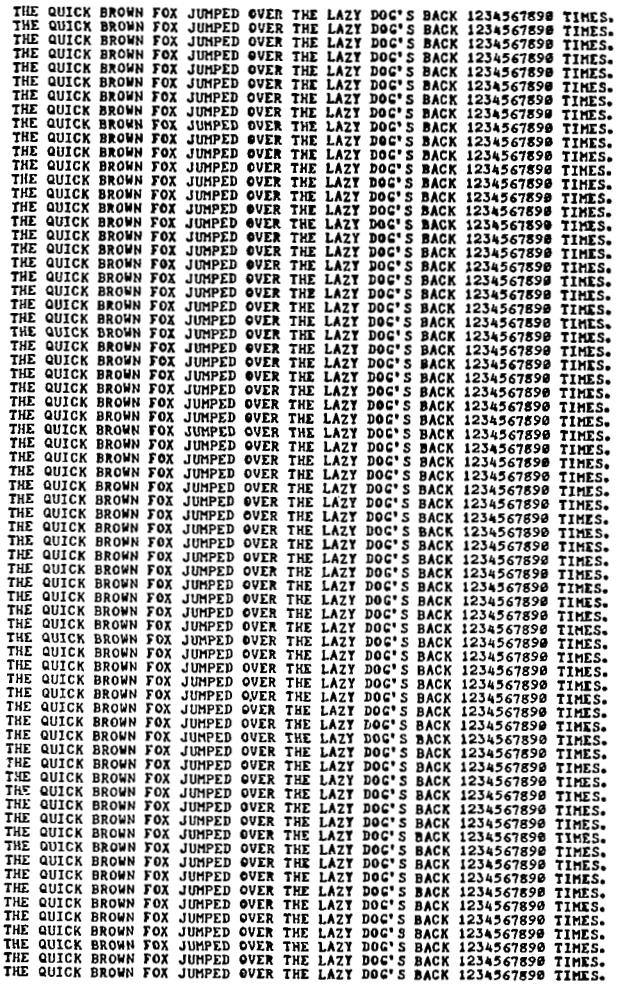

a. To Syncom at 200 watts.

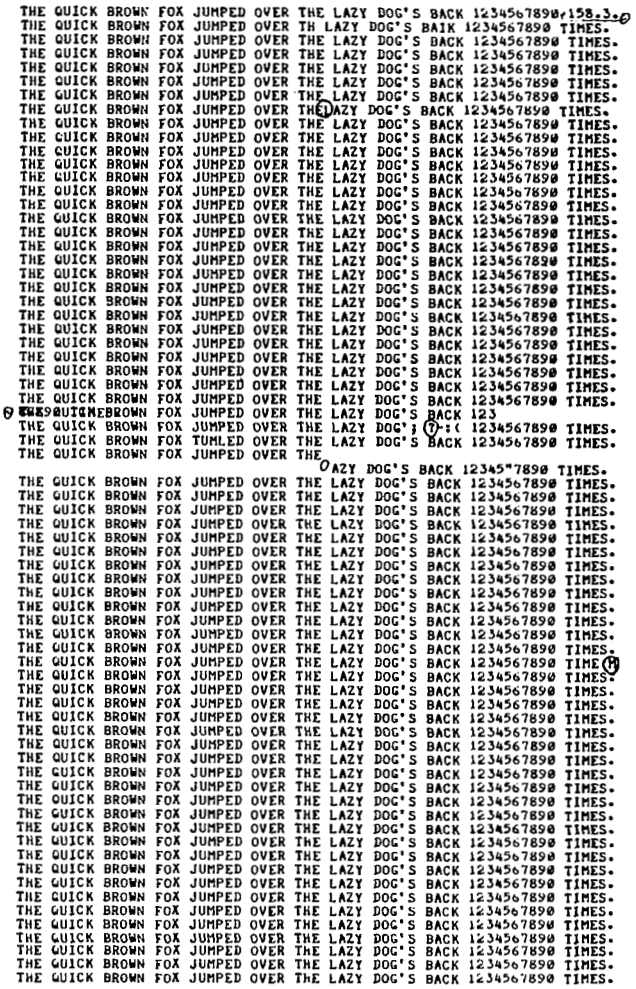

b. Received from Syncom at 200 watts.

Figure VII-3—Teletype transmission.

When transmitter power was reduced to 20 watts, the messages were completely garbled. At 40 watts transmitted power, the messages were somewhat better, but still poor. The abrupt change in loop performance as a function of transmitter power occurs because, as indicated earlier, there is essentially a threshold which the transmitted signal must exceed to gate off telemetry and directly modulate the telemetry transmitter. Also, it was noted that there exists a slight dip in satellite receiver antenna gain once per revolution, causing the satellite to gate off the execute tone once per revolution at marginal uplink signal levels.

Because of the excellent results of the transmission test at the low power of 50 watts, a weather message was then transponded through the satellite. Figure VII-5 shows the message sent. This message was repeated many times without error. These tests clearly demonstrated the feasibility of satellite communication from small inexpensive terminals.

```
THIS MESSAGE IS BEING SENT THRU THE SYNCOM THREE SPACECRAFT WITH
50 WATTS OF TRANSMITTED POWER THRU A CIRCULARLY POLARIZED YAGI. THE
RECEIVER ANTENNA IS ALSO A CIRCULARLY POLARIZED YAGI WITHOUT A PREAMP.

THE QUICK BROWN FOX JUMPED OVER THE LAZY DOG'S BACK 1234567890 TIMES.
THE QUICK BROWN FOX JUMPED OVER THE LAZY DOG'S BACK 1234567890 TIMES.
THE QUICK BROWN FOX JUMPED OVER THE LAZY DOG'S BACK 1234567890 TIMES.
THE QUICK BROWN FOX JUMPED OVER THE LAZY DOG'S BACK 1234567890 TIMES.
THE QUICK BROWN FOX JUMPED OVER THE LAZY DOG'S BACK 1234567890 TIMES.
THE QUICK BROWN FOX JUMPED OVER THE LAZY DOG'S BACK 1234567890 TIMES.
THE QUICK BROWN FOX JUMPED OVER THE LAZY DOG'S BACK 1234567890 TIMES.
THE QUICK BROWN FOX JUMPED OVER THE LAZY DOG'S BACK 1234567890 TIMES.
THE QUICK BROWN FOX JUMPED OVER THE LAZY DOG'S BACK 1234567890 TIMES.
THE QUICK BROWN FOX JUMPED OVER THE LAZY DOG'S BACK 1234567890 TIMES.
THE QUICK BROWN FOX JUMPED OVER THE LAZY DOG'S BACK 1234567890 TIMES.
THE QUICK BROWN FOX JUMPED OVER THE LAZY DOG'S BACK 1234567890 TIMES.
THE QUICK BROWN FOX JUMPED OVER THE LAZY DOG'S BACK 1234567890 TIMES.
THE QUICK BROWN FOX JUMPED OVER THE LAZY DOG'S BACK 1234567890 TIMES.
THE QUICK BROWN FOX JUMPED OVER THE LAZY DOG'S BACK 1234567890 TIMES.
THE QUICK BROWN FOX JUMPED OVER THE LAZY DOG'S BACK 1234567890 TIMES.
THE QUICK BROWN FOX JUMPED OVER THE LAZY DOG'S BACK 1234567890 TIMES.
THE QUICK BROWN FOX JUMPED OVER THE LAZY DOG'S BACK 1234567890 TIMES.
THE QUICK BROWN FOX JUMPED OVER THE LAZY DOG'S BACK 1234567890 TIMES.
THE QUICK BROWN FOX JUMPED OVER THE LAZY DOG'S BACK 1234567890 TIMES.
THE QUICK BROWN FOX JUMPED OVER THE LAZY DOG'S BACK 1234567890 TIMES.
THE QUICK BROWN FOX JUMPED OVER THE LAZY DOG'S BACK 1234567890 TIMES.
THE QUICK BROWN FOX JUMPED OVER THE LAZY DOG'S BACK 1234567890 TIMES.
THE QUICK BROWN FOX JUMPED OVER THE LAZY DOG'S BACK 1234567890 TIMES.
THE QUICK BROWN FOX JUMPED OVER THE LAZY DOG'S BACK 1234567890 TIMES.
THE QUICK BROWN FOX JUMPED OVER THE LAZY DOG'S BACK 1234567890 TIMES.
THE QUICK BROWN FOX JUMPED OVER THE LAZY DOG'S BACK 1234567890 TIMES.
THE QUICK BROWN FOX JUMPED OVER THE LAZY DOG'S BACK 1234567890 TIMES.
THE QUICK BROWN FOX JUMPED OVER THE LAZY DOG'S BACK 1234567890 TIMES.
THE QUICK BROWN FOX JUMPED OVER THE LAZY DOG'S BACK 1234567890 TIMES.
THE QUICK BROWN FOX JUMPED OVER THE LAZY DOG'S BACK 1234567890 TIMES.
THE QUICK BROWN FOX JUMPED OVER THE LAZY DOG'S BACK 1234567890 TIMES.
THE QUICK BROWN FOX JUMPED OVER THE LAZY DOG'S BACK 1234567890 TIMES.
THE QUICK BROWN FOX JUMPED OVER THE LAZY DOG'S BACK 1234567890 TIMES.
THE QUICK BROWN FOX JUMPED OVER THE LAZY DOG'S BACK 1234567890 TIMES.
THE QUICK BROWN FOX JUMPED OVER THE LAZY DOG'S BACK 1234567890 TIMES.
THE QUICK BROWN FOX JUMPED OVER THE LAZY DOG'S BACK 1234567890 TIMES.
THE QUICK BROWN FOX JUMPED OVER THE LAZY DOG'S BACK 1234567890 TIMES.
THE QUICK BROWN FOX JUMPED OVER THE LAZY DOG'S BACK 1234567890 TIMES.
THE QUICK BROWN FOX JUMPED OVER THE LAZY DOG'S BACK 1234567890 TIMES.
THE QUICK BROWN FOX JUMPED OVER THE LAZY DOG'S BACK 1234567890 TIMES.
THE QUICK BROWN FOX JUMPED OVER THE LAZY DOG'S BACK 1234567890 TIMES.
THE QUICK BROWN FOX JUMPED OVER THE LAZY DOG'S BACK 1234567890 TIMES.
THE QUICK BROWN FOX JUMPED OVER THE LAZY DOG'S BACK 1234567890 TIMES.
THE QUICK BROWN FOX JUMPED OVER THE LAZY DOG'S BACK 1234567890 TIMES.
THE QUICK BROWN FOX JUMPED OVER THE LAZY DOG'S BACK 1234567890 TIMES.
THE QUICK BROWN FOX JUMPED OVER THE LAZY DOG'S BACK 1234567890 TIMES.
THE QUICK BROWN FOX JUMPED OVER THE LAZY DOG'S BACK 1234567890 TIMES.
THE QUICK BROWN FOX JUMPED OVER THE LAZY DOG'S BACK 1234567890 TIMES.
THE QUICK BROWN FOX JUMPED OVER THE LAZY DOG'S BACK 1234567890 TIMES.
THE QUICK BROWN FOX JUMPED OVER THE LAZY DOG'S BACK 1234567890 TIMES.
THE QUICK BROWN FOX JUMPED OVER THE LAZY DOG'S BACK 1234567890 TIMES.
THE QUICK BROWN FOX JUMPED OVER THE LAZY DOG'S BACK 1234567890 TIMES.
THE QUICK BROWN FOX JUMPED OVER THE LAZY DOG'S BACK 1234567890 TIMES.
THE QUICK BROWN FOX JUMPED OVER THE LAZY DOG'S BACK 1234567890 TIMES.
THE QUICK BROWN FOX JUMPED OVER THE LAZY DOG'S BACK 1234567890 TIMES.
THE QUICK BROWN FOX JUMPED OVER THE LAZY DOG'S BACK 1234567890 TIMES.
THE QUICK BROWN FOX JUMPED OVER THE LAZY DOG'S BACK 1234567890 TIMES.
THE QUICK BROWN FOX JUMPED OVER THE LAZY DOG'S BACK 1234567890 TIMES.
THE QUICK BROWN FOX JUMPED OVER THE LAZY DOG'S BACK 1234567890 TIMES.
THE QUICK BROWN FOX JUMPED OVER THE LAZY DOG'S BACK 1234567890 TIMES.
THE QUICK BROWN FOX JUMPED OVER THE LAZY DOG'S BACK 1234567890 TIMES.
THE QUICK BROWN FOX JUMPED OVER THE LAZY DOG'S BACK 1234567890 TIMES.
THE QUICK BROWN FOX JUMPED OVER THE LAZY DOG'S BACK 1234567890 TIMES.

THE FOLLOWING IS TRANSMITTED AT TWENTY WATTS


THE FOLLOWING IS TRANSMITTED AT THIRTY WATTS
THE QUICK BROWN FOX JUMPED OVER THE LAZY DOG'S BACK 1234567890 TIMES.
THE QUICK BROWN FOX JUMPED OVER THE LAZY DOG'S BACK 1234567890 TIMES.
THE QUICK BROWN FOX JUMPED OVER THE LAZY DOG'S BACK 1234567890 TIMES.
THE QUICK BROWN FOX JUMPED OVER THE LAZY DOG'S BACK 1234567890 TIMES.


THE FOLLOWING IS BEING TRANSMITTED AT FORTY WATTS
THE QUICK BROWN FOX JUMPED OVER THE LAZY DOG'S BACK 1234567890 TIMES.
THE QUICK BROWN FOX JUMPED OVER THE LAZY DOG'S BACK 1234567890 TIMES.
THE QUICK BROWN FOX JUMPED OVER THE LAZY DOG'S BACK 1234567890 TIMES.
THE QUICK BROWN FOX JUMPED OVER THE LAZY DOG'S BACK 1234567890 TIMES.
THE QUICK BROWN FOX JUMPED OVER THE LAZY DOG'S BACK 1234567890 TIMES.
THE QUICK BROWN FOX JUMPED OVER THE LAZY DOG'S BACK 1234567890 TIMES.
THE QUICK BROWN FOX JUMPED OVER THE LAZY DOG'S BACK 1234567890 TIMES.
THE QUICK BROWN FOX JUMPED OVER THE LAZY DOG'S BACK 1234567890 TIMES.
```

a. To Syncom 3.

```
THIS MESSAGE IS BEING SENT THRU THE SYNCOM THREE SPACECRAFT WITH
50 WATTS OF TRANSMITTED POWER THRU A CIRCULARLY POLARIZED YAGI. THE
RECEIVER ANTENNA IS ALSO A CIRCULARLY POLARIZED YAGI WITHOUT A PREAMP.

THE QUICK BROWN FOX JUMPED OVER THE LAZY DOG'S BACK 1234567890 TIMES.
THE QUICK BROWN FOX JUMPED OVER THE LAZY DOG'S BACK 1234567890 TIMES.
THE QUICK BROWN FOX JUMPED OVER THE LAZY DOG'S BACK 1234567890 TIMES.
THE QUICK BROWN FOX JUMPED OVER THE LAZY DOG'S BACK 1234567890 TIMES.
THE QUICK BROWN FOX JUMPED OVER THE LAZY DOG'S BACK 1234567890 TIMES.
THE QUICK BROWN FOX JUMPED OVER THE LAZY DOG'S BACK 1234567890 TIMES.
THE QUICK BROWN FOX JUMPED OVER THE LAZY DOG'S BACK 1234567890 TIMES.
THE QUICK BROWN FOX JUMPED OVER THE LAZY DOG'S BACK 1234567890 TIMES.
THE QUICK BROWN FOX JUMPED OVER THE LAZY DOG'S BACK 1234567890 TIMES.
THE QUICK BROWN FOX JUMPED OVER THE LAZY DOG'S BACK 1234567890 TIMES.
THE QUICK BROWN FOX JUMPED OVER THE LAZY DOG'S BACK 1234567890 TIMES.
THE QUICK BROWN FOX JUMPED OVER THE LAZY DOG'S BACK 1234567890 TIMES.
THE QUICK BROWN FOX JUMPED OVER THE LAZY DOG'S BACK 1234567890 TIMES.
THE QUICK BROWN FOX JUMPED OVER THE LAZY DOG'S BACK 1234567890 TIMES.
THE QUICK BROWN FOX JUMPED OVER THE LAZY DOG'S BACK 1234567890 TIMES.
THE QUICK BROWN FOX JUMPED OVER THE LAZY DOG'S BACK 1234567890 TIMES.
THE QUICK BROWN FOX JUMPED OVER THE LAZY DOG'S BACK 1234567890 TIMES.
THE QUICK BROWN FOX JUMPED OVER THE LAZY DOG'S BACK 1234567890 TIMES.
THE QUICK BROWN FOX JUMPED OVER THE LAZY DOG'S BACK 1234567890 TIMES.
THE QUICK BROWN FOX JUMPED OVER THE LAZY DOG'S BACK 1234567890 TIMES.
THE QUICK BROWN FOX JUMPED OVER THE LAZY DOG'S BACK 1234567890 TIMES.
THE QUICK BROWN FOX JUMPED OVER THE LAZY DOG'S BACK 1234567890 TIMES.
THE QUICK BROWN FOX JUMPED OVER THE LAZY DOG'S BACK 1234567890 TIMES.
THE QUICK BROWN FOX JUMPED OVER THE LAZY DOG'S BACK 1234567890 TIMES.
THE QUICK BROWN FOX JUMPED OVER THE LAZY DOG'S BACK 1234567890 TIMES.
THE QUICK BROWN FOX JUMPED OVER THE LAZY DOG'S BACK 1234567890 TIMES.
THE QUICK BROWN FOX JUMPED OVER THE LAZY DOG'S BACK 1234567890 TIMES.
THE QUICK BROWN FOX JUMPED OVER THE LAZY DOG'S BACK 1234567890 TIMES.
THE QUICK BROWN FOX JUMPED OVER THE LAZY DOG'S BACK 1234567890 TIMES.
THE QUICK BROWN FOX JUMPED OVER THE LAZY DOG'S BACK 1234567890 TIMES.
THE QUICK BROWN FOX JUMPED OVER THE LAZY DOG'S BACK 1234567890 TIMES.
THE QUICK BROWN FOX JUMPED OVER THE LAZY DOG'S BACK 1234567890 TIMES.
THE QUICK BROWN FOX JUMPED OVER THE LAZY DOG'S BACK 1234567890.TIMES.
THE QUICK BROWN FOX JUMPED OVER THE LAZY DOG'S BACK 1234567890 TIMES.
THE QUICK BROWN FOX JUMPED OVER THE LAZY DOG'S BACK 1234567890 TIMES.
THE QUICK BROWN FOX JUMPED OVER THE LAZY DOG'S BACK 1234567890 TIMES.
THE QUICK BROWN FOX JUMPED OVER THE LAZY DOG'S BACK 1234567890 TIMES.
THE QUICK BROWN FOX JUMPED OVER THE LAZY DOG'S BACK 1234567890 TIMES.
THE QUICK BROWN FOX JUMPED OVER THE LAZY DOG'S BACK 1234567890 TIMES.
THE QUICK BROWN FOX JUMPED OVER THE LAZY DOG'S BACK 1234567890 TIMES.
THE QUICK BROWN FOX JUMPED OVER THE LAZY DOG'S BACK 1234567890 TIMES.
THE QUICK BROWN FOX JUMPED OVER THE LAZY DOG'S BACK 1234567890 TIMES.
THE QUICK BROWN FOX JUMPED OVER THE LAZY DOG'S BACK 1234567890 TIMES.
THE QUICK BROWN FOX JUMPED OVER THE LAZY DOG'S BACK 1234567890 TIMES.
THE QUICK BROWN FOX JUMPED OVER THE LAZY DOG'S BACK 1234567890 TIMES.
THE QUICK BROWN FOX JUMPED OVER THE LAZY DOG'S BACK 1234567890 TIMES.
THE QUICK BROWN FOX JUMPED OVER THE LAZY DOG'S BACK 1234567890 TIMES.
THE QUICK BROWN FOX JUMPED OVER THE LAZY DOG'S BACK 1234567890 TIMES.
THE QUICK BROWN FOX JUMLED OVER THE LAZY DOG'S BACK 1234567890 TIMES.
THE QUICK BROWN FOX JUMPED OVER THE LAZY DOG'S BACK 1234567890 TIMES.
THE QUICK BROWN FOX JUMPED OVER THE LAZY DOG'S BACK 1234567890 TIMES.
THE QUICK BROWN FOX JUMPED OVER THE LAZY DOG'S BACK 1234567890 TIMES.
THE QUICK BROWN FOX JUMPED OVER THE LAZY DOG'S BACK 1234567890 TIMES.
THE QUICK BROWN FOX JUMPED OVER THE LAZY DOG'S BACK 1234567890 TIMES.
THE QUICK BROWN FOX JUMPED OVER THE LAZY DOG'S BACK 1234567890 TIMES.
THE QUICK BROWN FOX JUMPED OVER THE LAZY DOG'S BACK 1234567890 TIMES.
THE QUICK BROWN FOX JUMPED OVER THE LAZY DOG'S BACK 1234567890 TIMES.
THE QUICK BROWN FOX JUMPED OVER THE LAZY DOG'S BACK 1234567890 TIMES.
THE QUICK BROWN FOX JUMPED OVER THE LAZY DOG'S BACK 1234567890 TIMES.
THE QUICK BROWN FOX JUMPED OVER THE LAZY DOG'S BACK 1234567890 TIMES.
                                                                      T

THE K9))928,G IS ERANSMITTED .5QQ EENTY WAUMTYVQKK


THE FOLLOWING IS TRANSMITTED AT THIRTY WATTS
VTHE QBZ&KDBBOBN FOX JUMLED OVE
                BACU 2234567890 TIMES.
TRE1QUICK BROWN FOX JUMPED OVER THE LAZYOG'S BACK 1234567890 TIMES.(

    :( ?492, 19/ '7.03$ OVEZ
LLAZY DOG'                    IF
         S BACK 1234567890 TIMES.EA
T
THE8QUICK BROWN GEX JUMPLD OVER THE LAZY DOH'S LACGDW0
        .3.


THE FOLLOWING IS BEING TRANSMITTE
    FORTY WATTS
THE QUICK LROWN FOX JUMPED OVER THE LEZY DOG'S BAOK 1234567890 TIMS.
THE QUICK BROWN FOX JUMPED OVER THE LAZY DOG'S BACK 1234567890 TIMES.
TBZEQUIBE BRØWNDBOXSJBNEK 1234567890 TIMES.
THE QUICK BROWN FOX JUMPED OVER THF LAZY DOG'S BACK 1234567890 TIMERFM
THE QUICK BROWN NOX JUMPED OVER THE LAZY DOG'S BACK 123467890 TIMES.EA
                                                                     RZ
                                                                       T
                                                  H
        E
LQBZ&KDBROBNBROK JBBBX07078HZ&MES.
THE QUICK BROWN SOX JUMPED OVE
                                THE LAZY DOG'S BACK 1234567890.58.3.
THE QUICK BROWN FOX JUMPED OVER THE LA
                                      Y DOG'S BACK 124567890 TIMES.
```

b. Received from Syncom 3.

Figure VII-4—Teletype transmissions at 50 watts and lower.

TELETYPE TRANSMISSION TO PAA AIRCRAFT

On 22 November 1964 teletype messages were transmitted from the NASA Telemetry and Command trailer at Camp Roberts, California via the Syncom III satellite to Pan American flight 875 en route from San Francisco to Honolulu. This was the first transmission of information from a satellite to a commerical aircraft and marked the beginning of a new era in long-distance aircraft communication.

In these tests the Syncom III telemetry and command systems were used to transpond a 7.5-bit teletype code through the spacecraft using the 9.745-kc command execute tone as a subcarrier. Figure VII-6 is a block diagram of the equipment involved and Figure VII-7 is a general arrangement of the aircraft antenna.

```
TO DR ROBERT M WHITE
UNITED STATES DEPARTMENT OF COMMERCE
WEATHER BUREAU

THIS IS THE FIRST WEATHER MESSAGE EVER TO BE SENT VIA SYNCOM THREE.
LOS ANGELES WEATHER FORECAST
VARIABLE HIGH CLOUDS TONITE WITH INCREASING HIGH CLOUDS TOMORROW.
MOSTLY CLOUDY AND NOT QUITE SO WARM FRIDAY.
TEMPERATURES  HIGH 79  LOW 67.

TO DR ROBERT M WHITE
UNITED STATES DEPARTMENT OF COMMERCE
WEATHER BUREAU

THIS IS THE FIRST WEATHER MESSAGE EVER TO BE SENT VIA SYNCOM THREE.
LOS ANGELES WEATHER FORECAST
VARIABLE HIGH CLOUDS TONITE WITH INCREASING HIGH CLOUDS TOMORROW.
MOSTLY CLOUDY AND NOT QUITE SO WARM FRIDAY.
TEMPERATURES  HIGH 79  LOW 67.

TO DR ROBERT M WHITE
UNITED STATES DEPARTMENT OF COMMERCE
WEATHER BUREAU

THIS IS THE FIRST WEATHER MESSAGE EVER TO BE SENT VIA SYNCOM THREE.
LOS ANGELES WEATHER FORECAST
VARIABLE HIGH CLOUDS TONITE WITH INCREASING HIGH CLOUDS TOMORROW.
MOSTLY CLOUDY AND NOT QUITE SO WARM FRIDAY.
TEMPERATURES  HIGH 79  LOW 67.
```

a. Message transmitted to Syncom 3, 200 watt transmitter

```
TO DR ROBERT M WHITE
UNITED STATES DEPARTMENT OF COMMERCE
WEATHER BUREAU

THIS IS THE FIRST WEATHER MESSAGE EVER TO BE SENT VIA SYNCOM THREE.
LOS ANGELES WEATHER FORECAST
VARIABLE HIGH CLOUDS TONITE WITH INCREASING HIGH CLOUDS TOMORROW.
MOSTLY CLOUDY AND NOT QUITE SO WARM FRIDAY.
TEMPERATURES  HIGH 79  LOW 67.

TO DR ROBERT M WHITE
UNITED STATES DEPARTMENT OF COMMERCE
WEATHER BUREAU

THIS IS THE FIRST WEATHER MESSAGE EVER TO BE SENT VIA SYNCOM THREE.
LOS ANGELES WEATHER FORECAST
VARIABLE HIGH CLOUDS TONITE WITH INCREASING HIGH CLOUDS TOMORROW.
MOSTLY CLOUDY AND NOT QUITE SO WARM FRIDAY.
TEMPERATURES  HIGH 79  LOW 67.

TO DR ROBERT M WHITE
UNITED STATES DEPARTMENT OF COMMERCE
WEATHER BUREAU

THIS IS THE FIRST WEATHER MESSAGE EVER TO BE SENT VIA SYNCOM THREE.
LOS ANGELES WEATHER FORECAST
VARIABLE HIGH CLOUDS TONITE WITH INCREASING HIGH CLOUDS TOMORROW.
MOSTLY CLOUDY AND NOT QUITE SO WARM FRIDAY.
TEMPERATURES  HIGH 79  LOW 67.
```

b. Message received from Syncom 3.

Figure VII-5—Syncom messages.

The tests were begun on 19 November and ran through 22 November. On 19 November modulation and demodulation loop tests were conducted and modulation tests were made with the NASA transmitter operating into a dummy load. On 20 November, system loop tests were made using the Syncom III satellite with a portable three-element YAGI used in place of the nose-mounted aircraft antenna. Figure VII-8 shows some of the results obtained from this test. 25-wpm teletype messages were transponded through Syncom III and successfully received on a dipole (YAGI with reflector and director removed) antenna. Fifty-wpm teletype messages were also received using a two-element YAGI (director removed) with about 7db gain over isotropic. Tests at 100 wpm were attempted with the three element YAGI but the teletype printer would not copy at this speed. Failure of the miniature teletype machine was frequent throughout the day.

On Saturday, 21 November, the teletype machine was repaired and the receiver, demodulator, preamps, and teletype machine installed in the Pan American aircraft. Figure VII-9 shows this equipment. The modified Bendix Model RA-21 receiver is shown in the center with its preamplifier and bandpass filter. The unit to the right contains the miniature teletype printer and electronic control. The unit to the left contains signal strength and noise level monitoring circuits and strip chart recorder.

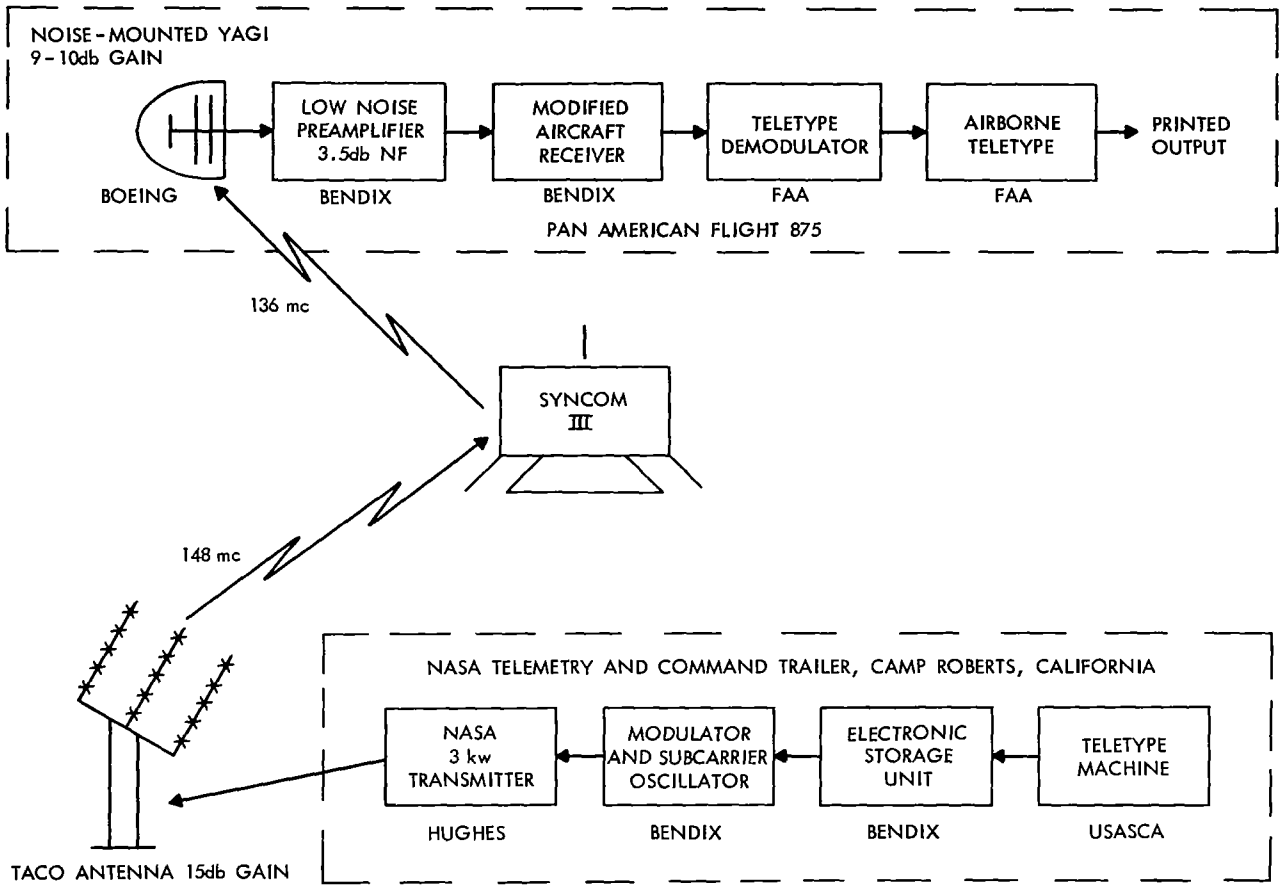

Figure VII-6—Satellite to aircraft communications test block diagram.

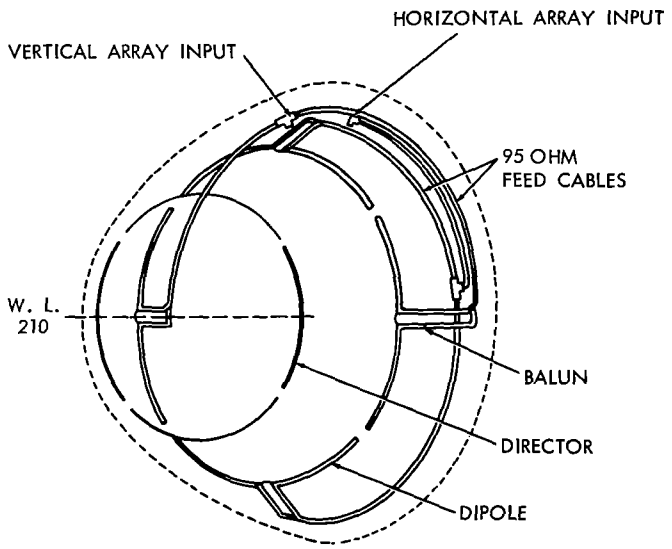

Figure VII-7—Nose radome YAGI array general arrangement.

25 WPM - Dipole Antenna
Bendix Receiver

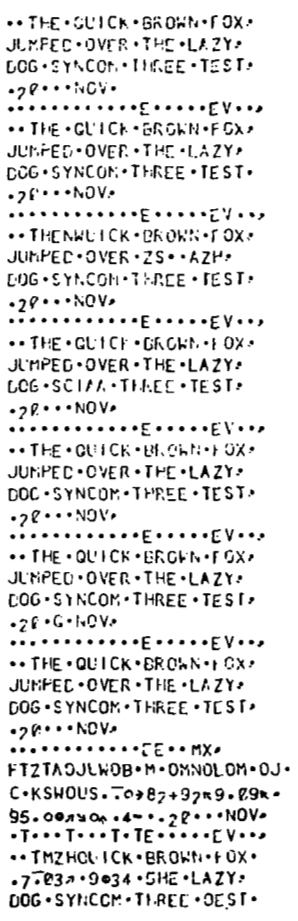

50 WPM - Two-Element Yagi
Bendix Receiver

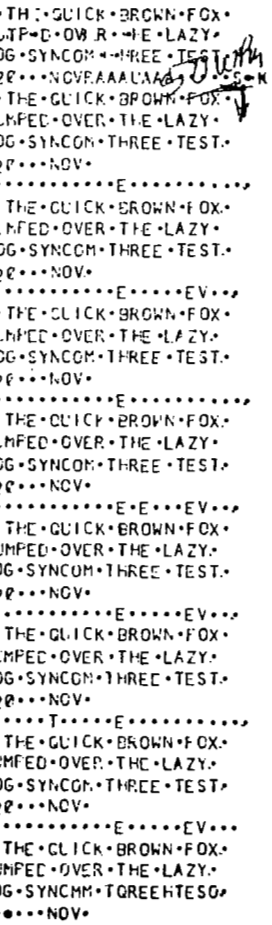

Figure VII-8—Results of VHF teletype transmission with Syncom III, 20 November 1964, Camp Roberts, California.

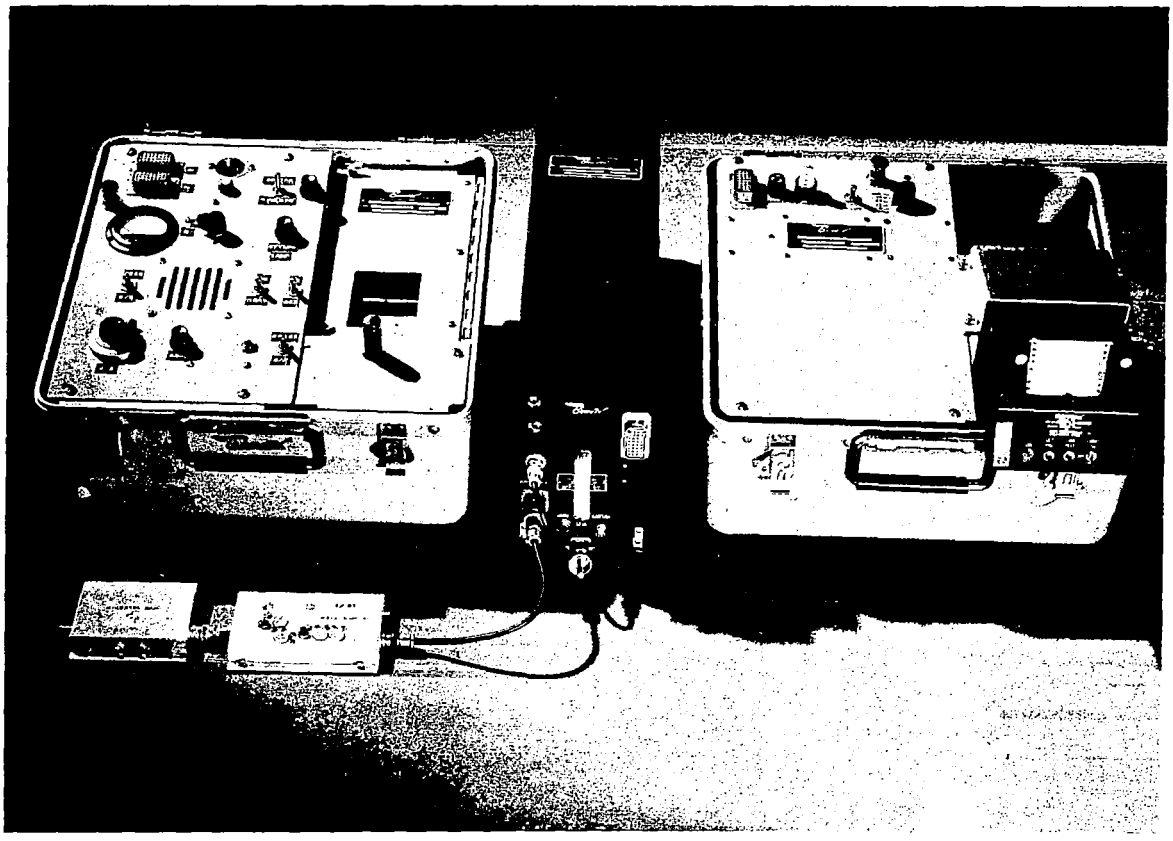

Figure VII-9—Aircraft equipments.

Equipment Configuration

The receiver used in these tests was a Bendix RA-21 solid-state receiver modified to provide phased-lock loop detection of both the carrier and the 9.745-kc subcarrier. The carrier demodulator provided signal-to-noise level indication and a diode detector in the IF was used to give a noise level indication. Figure VII-10 is a block diagram of the modified receiver. The subcarrier demodulator is a simple bi-phase, double-sideband, suppressed carrier demodulator providing 180° phase shift between mark and space. The electronic control unit, which is part of the FAA-supplied teletype printer, was capable of receiving standard 7-1/2-bit teletype at 6.25-, 12.50- 25- 50- and 100-wpm rates.

The transmitting equipment (Figure VII-11) consisted of a 100-wpm, Kleinschmidt Model 25 tape reader driving a Bendix-designed data buffer. This unit is capable of storing messages of up to 1500 bits, with readout at the previously mentioned rates.

The aircraft, a Boeing 707, was modified to include both horizontally and vertically polarized three-element YAGIs in the radome. These antennas (Figure VII-7) had a nominal gain of 10db. Preamplifiers were installed at the pressure bulkhead ahead of each antenna transmission line.

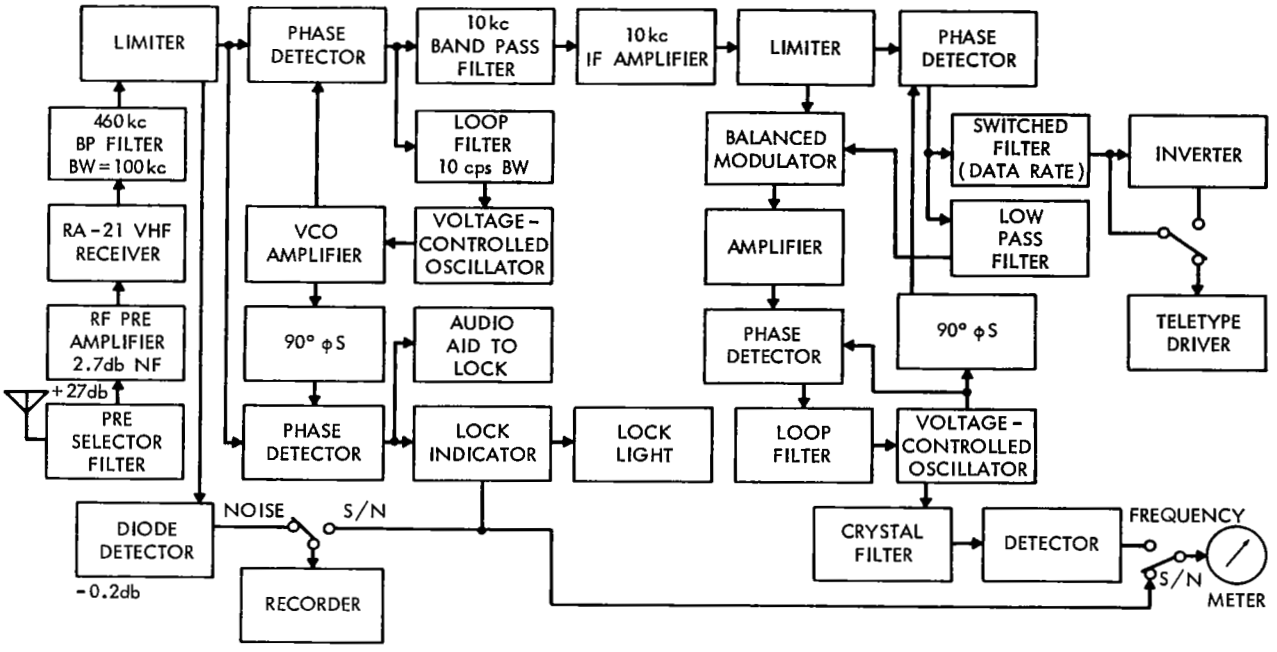

Figure VII-10—Bendix receiver block diagram.

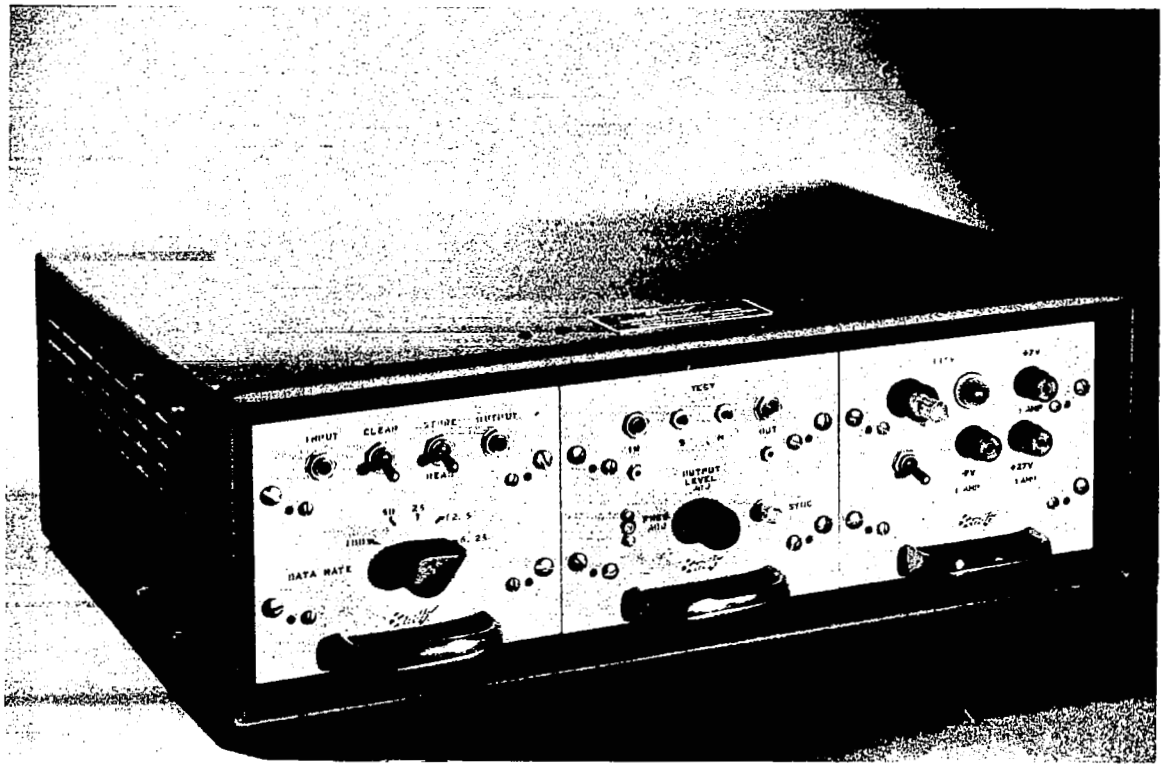

Figure VII-11—Buffer storage unit.

A third preamplifier was installed near the aircraft receiver for use with the top-mounted VHF blade. Transmission line losses of approximately 0.7db were measured between the nose-mounted antennas and the aircraft receiver and of approximately 1.0db between the blade and preamplifier.

The Bendix receiver was installed by substituting it for the number two RA-18 VHF receiver normally carried by Pan American. The two additional units were located immediately behind the cockpit.

Test Procedure

Takeoff was at 0708 Z on 21 November. The Syncom telemetry signal strength, measured at Camp Roberts on a three-element YAGI, indicated -132dbm horizontally polarized, within 1db of the calculated value. At 0730 Z the Camp Roberts transmitter was turned on and operated at 2-kw power level with 50 percent modulation. As expected, the Syncom telemetry was noted to be gated off.

Plans called for three test codes to be transmitted to the aircraft. In test code 1, a simple message would be sent repeatedly for five-minute intervals at 6.25, 12.5, and 25 wpm with initiation at the slowest speed on the quarter-hour. Test code 2 was identical, with a change in message speed to 12.5, 25, and 50 wpm. Test code 3 was again identical, with a change in message speeds to 25, 50, and 100 wpm. Initial tests were to be made on test code 1 with higher test codes transmitted only on request from the Pan American aircraft. These requests were to be made through ARINC HF radio and over land lines from the ARINC terminal to Camp Roberts.

At 0730 Z transmission of test code 1 was initiated. At 0750 Z signal strengths at Camp Roberts had increased by 1db; all signals appeared normal. Receiver signal strengths on both the three-element YAGI and the normal TACO antenna were recorded on a strip chart along with transmitter modulation and output of the 9.745-kc execute verify filter. This strip chart clearly shows successful transmission of teletype through the satellite and displays the executed time delay. Magnetic tapes were made of the receiver 2 output which was connected to the TACO antenna, along with a time code, transmitter modulation, and voice channel for annotation.

One hour after takeoff, as scheduled, it was possible to energize the aircraft receivers and start the test. At 0820 Z the aircraft successfully received a teletype message. Error-free copy at 12.50 wpm was received and recorded on the aircraft. Good copy continued at 6.25, 12.50, and 25 wpm. At 0839 Z Camp Roberts received a request for transmission of test code 2; at 0845 Z transmissions of test code 2 began. For the first five minutes, a special congratulatory message was transmitted in place of the normal format. Test code 2 was then transmitted for one hour. During this period, portions of messages were recorded on the aircraft at 12.50, 25, and 50 wpm. However, no complete messages were recorded. Figure VII-12 shows teletype messages received in the aircraft during the transmission of test code 1. Figure VII-13 shows garbled messages received during the transmission of test code 2. At 0930 Z adverse weather accompanied by heavy lightning was encountered by the aircraft. Subsequently, heavy corona and St. Elmo's fire were noted over a significant portion of the aircraft. The aircraft requested return to test code 1 and

Figure VII-12—Actual teletype printer readouts, test code 1.

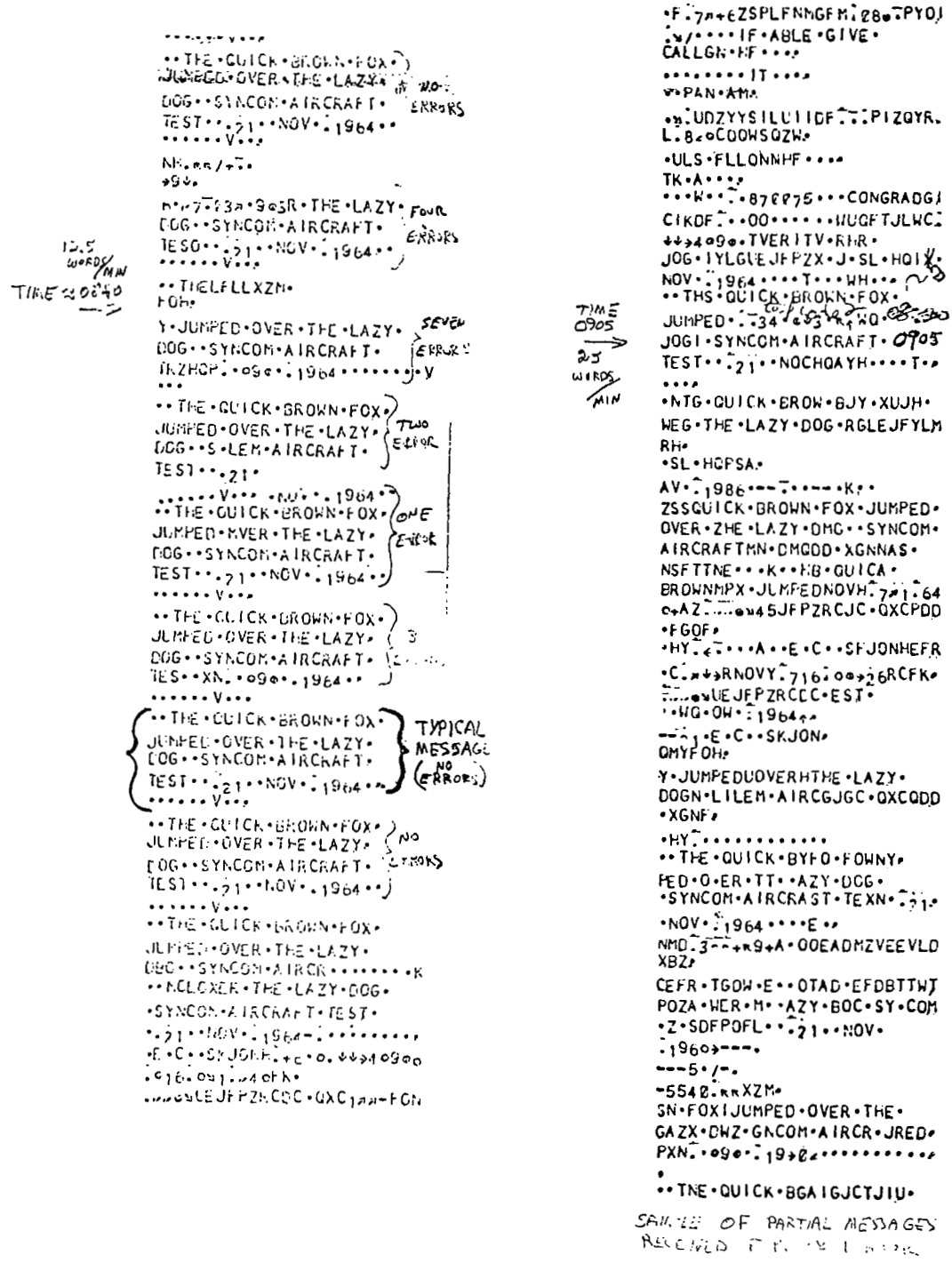

Figure VII-13—Actual teletype printer readouts, test code 2.

transmissions at 6.25 wpm were resumed at 0945 Z. For the remainder of the flight, considerable corona covered the insulated portions of the aircraft and further efforts to record teletype on any of the antennas proved fruitless. The remainder of the flight was used for analyzing the noise conditions produced by the unusual weather.

Analysis of Results

Adverse weather contributed to the poor copy received during most of the flight. In addition, signal strengths received at Camp Roberts from 0800 Z to 0900 Z showed the presence of other satellite signals within the bandpass of the receivers. The presence of these signals did not cause the Camp Roberts receivers to lose lock, nor was any loss of lock reported from the aircraft. The intruding satellite signals, however, were present during both the good and garbled portion teletype reception aboard the aircraft. Test conditions, thus, were not optimum for determining the capabilities of the satellite communications link.

During the flight, stripline recordings of signal-to-noise ratio were made on all three aircraft antennas. System noise level was also monitored thus providing a convenient measure of signal strength. The preamplifiers used had a noise figure slightly less than 3db. This established a limit on system sensitivity. Figure VII-14 shows the signal strength and noise levels received during portions of the flight along with calculated signal levels, based on the aircraft position, heading, and the gains of the three aircraft antennas. Initial recordings prior to the reception of good teletype showed variations in signal strength of 3db on the horizontal antenna and 5db on the vertical. This was probably due to sea reflections which would be expected to be stronger for the vertically polarized antenna because of its larger vertical beamwidth. Noise level variations were also observed with excursions between 580°K and 2000°K. When weather radar was turned off, the rapid noise variations were removed and it held constant between 600°K and 1000°K. During the period 0820 Z and 0900 Z, during which good copy was recorded, good signal levels, sufficient for 25 wpm teletype, were reported on both the horizontal and vertical antennas. Good teletype data were received, however, only on the horizontal antenna. It may be significant that this

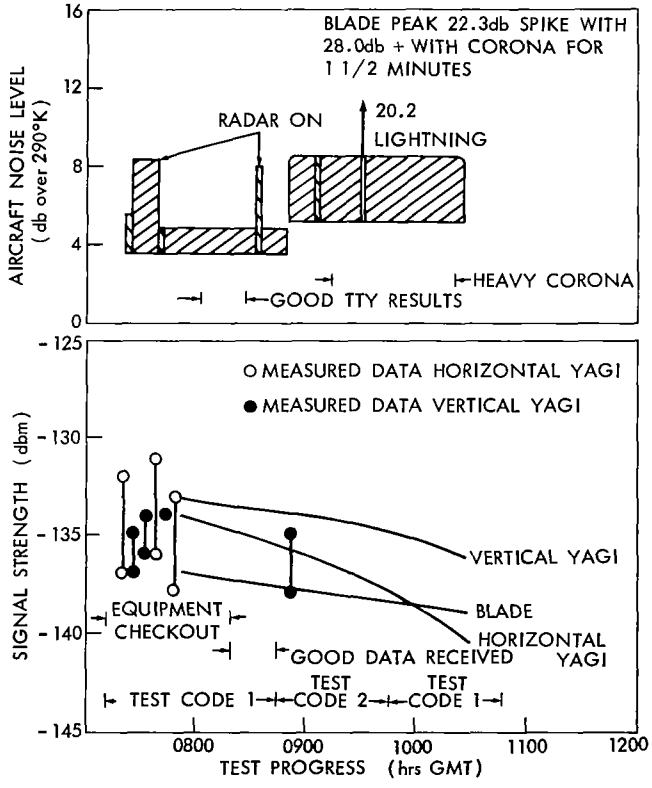

Figure VII-14—Signal strength and noise levels during Camp Roberts to PAA aircraft teletype transmission test.

antenna exhibited only a small, 1db random signal strength during the time the data were recorded. The failure to receive good copy on the vertical YAGI can probably be attributed to deep nulls due to sea reflection which did not appear on the strip chart recording.

Although signal strength was essentially constant until 0945 Z, poor copy was received for the last 45 minutes of the time interval. Later examination of the records showed that the weather radar had been turned on at 0910 Z, which can account for the poor copy received.

No copy at any time was received on the blade antenna despite the fact that calculated signal strengths on the blade were adequate for 25 wpm teletype. This was probably due to excessive noise picked up by this antenna.

For the last 45 minutes of the flight, noise measurements were made on all three antennas: on the horizontal antenna the minimum noise levels recorded were 1000°K with peaks, presumably caused by lightning, of 3000°K. This noise level is about 3db above that recorded earlier in the flight. On the vertical antenna, noise levels ranging from 580°K to 3500°K were recorded with peaks ranging to 14,000°K. Signal-to-noise ratios during this time were as to be expected. On the blade antenna, conditions were even more severe; the receiver dropped lock randomly, and the noise level varied from 600°K to 50,000°K. For a two-minute period during which heavy corona was noted, temperatures in excess of 200,000°K were recorded, dropping for short intervals to 1500°K. The maximum signal received on the blade antenna during the last hour of the flight was -143dbm. This is 5db below the maximum predicted value.

Conclusions

These tests proved the feasibility of satellite-to-aircraft communications. However, many questions remain unanswered: What caused the poor results obtained on the vertical blade? Will sea water reflection prove to be a significant problem in satellite-to-aircraft communication? Can RFI be reduced on external blade antennas? Only additional flight testing can answer these questions. All partners involved in this test, Hughes, Bendix, Pan American, ATA, and NASA, agreed that the tests should be continued. In a meeting at ATA on 1 December 1964 it was agreed to resume flight testing in mid-January with the goal of completing within a month a successful two-way communication test with Pan American aircraft from Camp Roberts, California.

(Manuscript received April 8, 1965)

Appendix A

Syncom III Nutation Before and After Third Stage Separation

Telemetry data from the spacecraft of the $\psi - \psi_2$ sun sensor variation (Figure A-1) and of the axial accelerometer (Figure A-2) were used to determine a rough estimate of:

1. Nutation angle and frequency of the combined spacecraft and burned out third stage before separation.
2. Nutation angle and damping time constant after separation.
3. Time at which nutation-producing torque occurred.
4. Angular impulse of nutation producing disturbance.

Results indicate a nutation angle θ_η = 12 to 12.5 degrees and nutation frequency (body coordinates) $\Omega \cong 147.5$ rpm immediately after burnout (~4.5 seconds), and an average value of Ω = 152.2 rpm between burnout and before third-stage separation at 63.82 seconds. The nutation angle

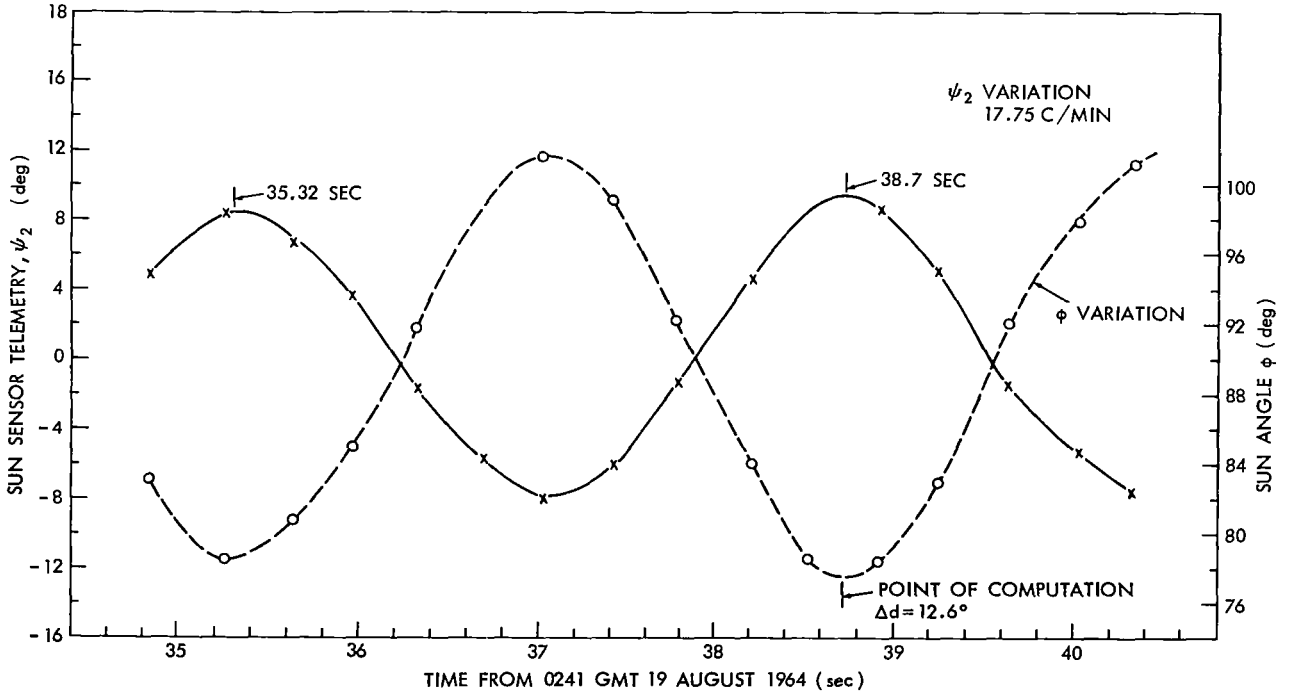

Figure A-1—Sun sensor telemetry and derived sun angle (data after third-stage burnout).

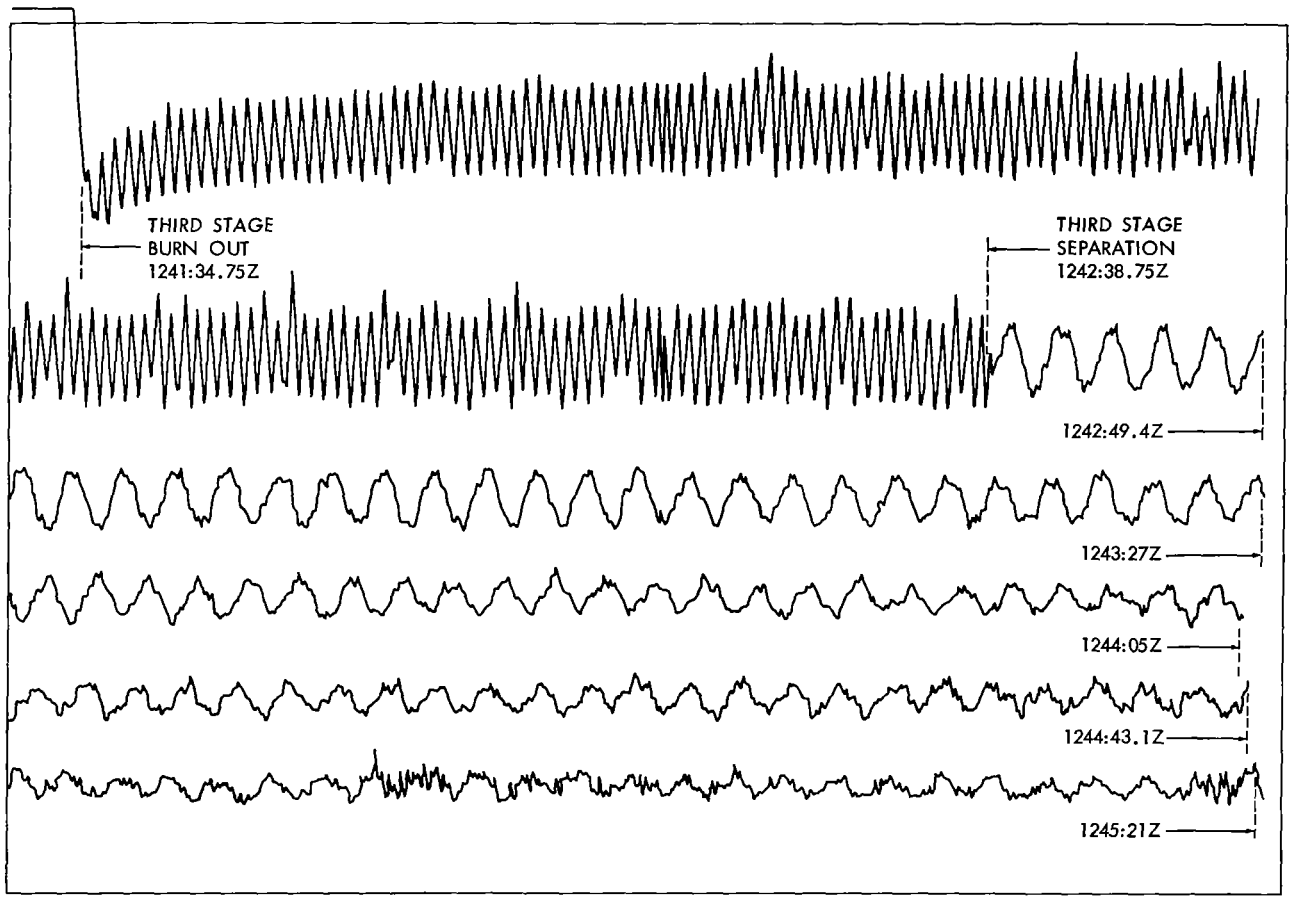

Figure A-2—Accelerometer trace showing nutation from third-stage burn-out through separation. (Ascension Island recording.)

immediately after separation was estimated as 1.9 degrees with a damping time constant of about τ = 51 seconds. Thus, the subsequently measured spacecraft attitude deviation of 14.5 degrees from nominal was mostly due to the large nutation angle before separation from the third stage. Since the incremental velocity magnitude imparted by the third-stage burn was close to nominal (within 25 fps), the torque, N, that induced the nutation probably occurred at or near burnout. The indicated spin speed ω_z during this portion of the flight varied between 166 to 165.8 rpm. Thus, the torque vector appears to be directed almost normal to the roll (spin) axis since very little spin speed change was noted. The angular impulse of the disturbance is estimated as $\Delta L = N(\Delta t) = 10.78$ ft-lb-sec.

Mott in Reference 2 shows values of θ_η = 11.0 degrees and Ω = 150 rpm before separation and θ_η = 1.2 degrees and Ω = -38.5 rpm after separation of the spacecraft from the third stage.

Angular Momentum Direction Before Separation

One may estimate the change in the direction and magnitude of the angular momentum vector, $\vec{L}$ before separation (after third stage burnout) from knowledge of:

1. Spin axis right ascension (RA), and declination (DEC) in the transfer orbit (after separation).
2. ψ_2 - angle history before and after separation, as in Figure 3 of Reference 2, which gives phase angle of coning relative to the sun vector at the epoch of separation.
3. Right ascension and declination of the third-stage incremental velocity vector, $\overline{\Delta V_3}$.

From Figure A-3, the phase angle between the line of sight to the sun and the direction of the incremental angular momentum vector ΔL (before and after separation) is about 164 ± 5 degrees. The magnitude of precession of $\vec{L}$ is the difference in the coning half-angles before and after separation (see Figure A-3):

$$\theta_{\eta i} - \theta_{\eta f} = 11.0° - 1.2° = 9.8° .$$

Since the epoch near separation defines the direction to the sun, the direction of $\vec{L}$ before separation may be calculated and compared with that of $\overline{\Delta V_3}$ determined from orbital data.

This was done by operating the REOR (Reorientation) program in the quadrant mode of the Syncom I 7090/7094 Computer System, Model 2 (May 1964). Table A-1 summarizes the pertinent results.

From Table A-1 the difference in (RA, DEC) between $\overline{\Delta V_3}$ and $\vec{L}$ is

$$\Delta RA = 4.75°$$

$$\Delta DEC = 10.46° .$$

Thus the angular momentum vector $\vec{L}$ has been rotated an amount ($\Delta L/L$) as determined from

$$\cos\left(\frac{\Delta L}{L}\right) = \cos\left[\Delta DEC\right] \cos\left[\Delta RA\right] = 0.980$$

$$\frac{\Delta L}{L} = 11.48° = 0.20 \text{ rad.}$$

Since the coning angle before separation is at least $\theta_{\eta i} = 11.0°$ (Mott), this suggests that the disturbance was almost impulsive. The constant amplitude behavior of the ψ_2-angle history between burnout and separation, Figures 2 and 3 of Reference 2, suggests further that the impulsive disturbance occurred at or near third-stage burnout. In addition, since $L \approx I_z \omega_z$ = (3.1)

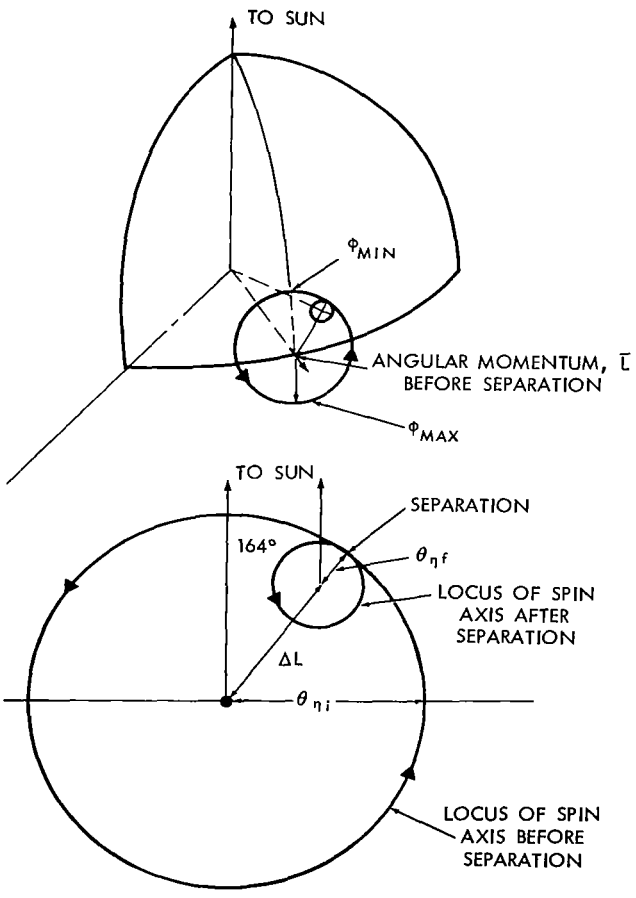

Figure A-3—Geometry relating sun, nutation angular momentum direction.

Table A-1

Right Ascension and Declination Data.

Direction of	Right Ascension (degrees)	Declination (degrees)	Sun Angle, ϕ (degrees)
Sun at 8/19/64 12 hrs, 42 min UT	148.77	12.67	-
Spin axis, after separation	229.33	3.51	80.03
Angular momentum, $\vec{L}$, before separation	237.94 ±0.44	-1.18 ±0.74	89.45
Third stage boost, $\overline{\Delta V_3}$	242.69	9.28	

(17.38) = 53.9 ft-lb-sec, Reference 1,

$$\Delta L \approx (0.20)L = (0.20)(53.9) = 10.78 \text{ ft-lb-sec.}$$

Some speculation exists that the cause of the large tipoff is due to a physical redistribution of the mass of the expended third stage (a permanent deformation) at burnout which gives rise to a principal axis rotation relative to the old roll (spin) axis. This does not appear reasonable from the available accelerometer data. The modulation envelope (represented by Figure A-2) of the accelerometer for the first 4 seconds after third-stage burnout (obtained from ascension telemetry tape) indicates a frequency of $\Omega_{meas.} \approx 147.5$ rpm. The calculated nutation frequency seen by the accelerometer is (from Reference 1 and spin speed data)

$$\Omega|_{calc.} = \left(1 - \frac{I_z}{I_x}\right)\omega_z = \left(1 - \frac{3.1}{25.7}\right)(166) .$$

This difference in Ω of only 1 percent (corresponding to a difference in inertia ratio,

$$\Delta\left(\frac{I_z}{I_x}\right)\Big/\left(\frac{I_z}{I_x}\right) \approx 8.7 \text{ percent}\Big) ,$$

suggests that the initial "coning" motion is almost entirely torque-excited nutation since the coning motion due to a principal axis rotation would occur at the spin frequency ω_z and would manifest itself as a permanent increase in the bias reading of the axial accelerometer prior to spacecraft separation.

The amount of case deformation or mass redistribution that may have occurred between third-stage burnout and spacecraft separation (63.82 second) can be roughly estimated by noting the

difference between the initial, Ω_i, and average, Ω_{av}, values of the nutation frequency in Figure A-2 and assigning this difference to the average change in roll-to-pitch inertia ratio, $\Delta\left(I_z/I_x\right)$:

$$\frac{\Delta\left(\frac{I_z}{I_x}\right)}{\left(\frac{I_z}{I_x}\right)_i} \approx \frac{\Omega_{av} - \Omega_i}{\omega_z \left(\frac{I_z}{I_x}\right)_i} = \frac{152.2 - 147.5}{(166)\ (0.111)} = 0.255 .$$

The above estimate of almost 26 percent decrease in inertia ratio assumes a constant spin speed ω_z = 166 rpm.

Possible Cause of Inertia Ratio Decrease, $\Delta(I_Z/I_X)$

Since the inertia distribution of the above configuration is that of a slender cylinder (cylinder axis = roll axis = z axis), most of the inertia ratio decrease is probably due to an increase in the pitch moment of inertia, I_x; i.e., the maximum radius of gyration change of a mass, Δm, occurs along the roll axis. Hence, if $|\Delta I_z| << |\Delta I_x|$, such that

$$\Delta I_z \approx \frac{I_z}{I_x}\left(\Delta I_x\right)$$

$$\Delta\left(\frac{I_z}{I_x}\right) \approx \frac{\Delta I_z}{I_x} - \frac{I_z}{I_x}\left(\frac{\Delta I_x}{I_x}\right) \approx -2\,\frac{I_z}{I_x}\left(\frac{\Delta I_x}{I_x}\right)$$

and

$$\frac{\Delta\left(\frac{I_z}{I_x}\right)}{\frac{I_z}{I_x}} \approx -2\,\frac{\Delta I_x}{I_x} = -0.255$$

$$\Delta I_x \approx \frac{0.255}{2}\,(25.7) = 3.28 \text{ slug-ft}^2$$

$$\approx (\Delta m)\, d_{max}^2 = (\Delta m)\, 25 \text{ slug-ft}^2 ,$$

where d_{max} is the maximum change in the radius of gyration of mass element, Δm. From the above relation, Δm is estimated as

$$\Delta m \approx \frac{\Delta I_x}{d_{max}^2} = \frac{3.28}{25} \simeq 0.131 \text{ slug} \simeq 4.23 \text{ lbs} .$$

Since the igniter assembly is located close to the cg at burnout and weighs 5 pounds initially, it appears to be a possible cause of the observed average change in inertia ratio if it broke loose

after third stage burnout and traveled toward the nozzle end of the motor case before separation.

References

1. "Delta Syncom A-27 Mission Orbit Error Analysis, Douglas SM-44001, Douglas Aircraft Company, March 1964.

2. Mott, D. L., "The Rotation of Syncom III During Launch," GSFC Document X-621-64-294, October 1964.

Appendix B

Syncom III 100 Day Power Report

The electrical power system performance of Syncom III remains satisfactory. After 100 days in orbit, the solar array power output has degraded less than the 5 percent originally predicted and is substantially less than the 20 percent experienced on Syncom II in a like period. Battery operation during launch, apogee motor firing and during eclipses was satisfactory and as predicted.

Since solar array power degradation to date is so slight, additional data will be necessary to further define the actual rate of degradation.

System Description

Unregulated dc power is supplied to the spacecraft bus from N-P silicon solar cells and Ni-Cd batteries. The solar array is installed on the outer cylindrical surface of the spacecraft. The array is composed of 768 solar cell modules consisting of 64 strings of 12 modules connected in series. Each string is connected to the bus through two blocking diodes in parallel. Two 22-cell Ni-Cd batteries, rated at 0.75 ampere-hour each, are installed to provide power for peak transient loads such as squib firing and eclipse operation when no power is available from the solar array. The battery charging current is limited to 0.065 ampere by use of a two-transistor "loss" type regulator.

System Operation

The electrical power system is shown in Figure B-1. Battery charging current is determined by the difference between the unregulated bus voltage and battery voltage. This difference is the voltage drop across the battery charging regulator, the characteristics of which are shown in Figure B-2. Since the "on-charge" voltage per battery must be in excess of 28.6 volts for any appreciable battery charging, no charging will occur if all spacecraft electronic equipment is in operation. To charge the batteries, it is necessary to turn off either or both the telemetry and communications systems.

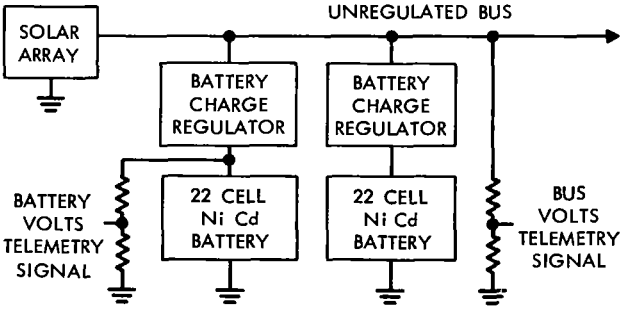

Figure B-1—Electrical power system block diagram.

The post regulators of the electronics equipment are designed to operate with a

minimum voltage input of -24.5 volts. Should the unregulated bus voltage fall below this point, sufficient electronic loads are to be turned off to maintain the bus voltage greater than -24.5 volts.

Solar Array Performance

The power output of the solar array is tested under closely controlled conditions at Table Mountain, California. However, these data must be extrapolated to space sunlight conditions to predict power output in space. The parameters which must be extrapolated are: the sunlight spectrum, sunlight intensity, sky radiation and solar cell temperatures. Therefore, the solar array I-V curve obtained at Table Mountain is corrected to space sunlight conditions in the following manner:

$$I_{space} = I_{T.M.} \cdot \eta_{spectrum} \cdot \eta_{intensity} \cdot \eta_{sky\ radiation} ,$$

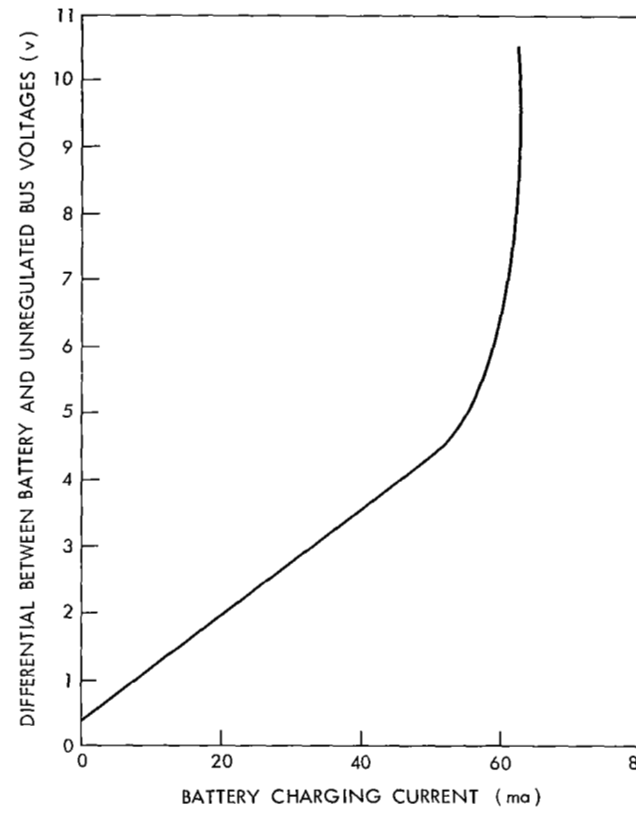

Figure B-2—Battery charge regulator characteristics.

where

I_{space} = current output in space

$I_{T.M.}$ = current output at Table Mountain

$$\eta_{spectrum} = \frac{\text{cell response at air mass zero}}{\text{cell response at air mass 1}} = 0.865$$

$$\eta_{intensity} = \frac{\text{solar constant near earth}}{\text{solar intensity at Table Mountain}}$$

$$\eta_{sky\ radiation} = \frac{\text{collimated solar intensity at Table Mountain}}{\text{uncollimated solar intensity at Table Mountain}} ,$$

and for the voltage

$$V_{space} = V_{T.M.} + 0.00254\,N\left(T_{T.M.} - T_{space}\right) ,$$

where

V_{space} = voltage output in space

$V_{T.M.}$ = voltage output at Table Mountain

N = number of solar cells in series (60)

$T_{T.M.}$ = solar cell temperatures at Table Mountain (°C)

T_{space} = solar cell temperatures in space (°C)

The 0.865 space attenuation factor for the solar cell response to space sunlight spectrum was determined from the results of various high altitude balloon flights and from the telemetered results of Syncom II and other spacecraft. The 0.00254 volts/°C change in cell voltage with change in cell temperature was determined by experimentation on similar cells. The near-earth solar constant is well established in literature and all other parameters were obtained by direct measurement. With these data, the predicted solar array power output prior to any radiation degradation was established and is shown in Figure B-3.

To account for the change in power output characteristics with increasing degradation due to radiation damage, a series of tests was conducted on identical solar cells. The cells were irradiated to various degrees of damage and their power output characteristics determined. These data (also shown in Figure B-3) then permitted predicting the spacecraft solar array characteristics after varying degrees of degradation.

Predicting the amount of degradation experienced by the solar array after a period of time necessitates making an estimate of the radiation dosage received by the spacecraft. This estimate was divided into two parts: (1) the dosage received during the two and one-half transfer orbits through the Van Allen belt, and (2) the dosage received at synchronous attitudes. The estimates were made entirely from the experience of Syncom II, i.e., its degradation in the Van Allen belt and at synchronous altitude. However, since Syncom II was equipped with P-N solar cells rather than N-P and also, since the Syncom II orbit was circularized at first apogee, suitable corrections to the data had to be made. In addition, the effects of the solar flare activity experienced shortly after the Syncom II launch had to be accounted for. Thus, the following estimates of the radiation environment were made:

dosage/one transfer orbit . . . . . 3.24×10^{11} e/cm^2
dosage/one synchronous orbit. . . . . 2.33×10^{11} e/cm^2.

Power degradation of a solar cell is given by the following empirical expression:

$$Q = 1 - \left[0.785 \left(\frac{\phi_t}{\phi_c}\right)^{1/2} + 1\right]^{-1/2},$$

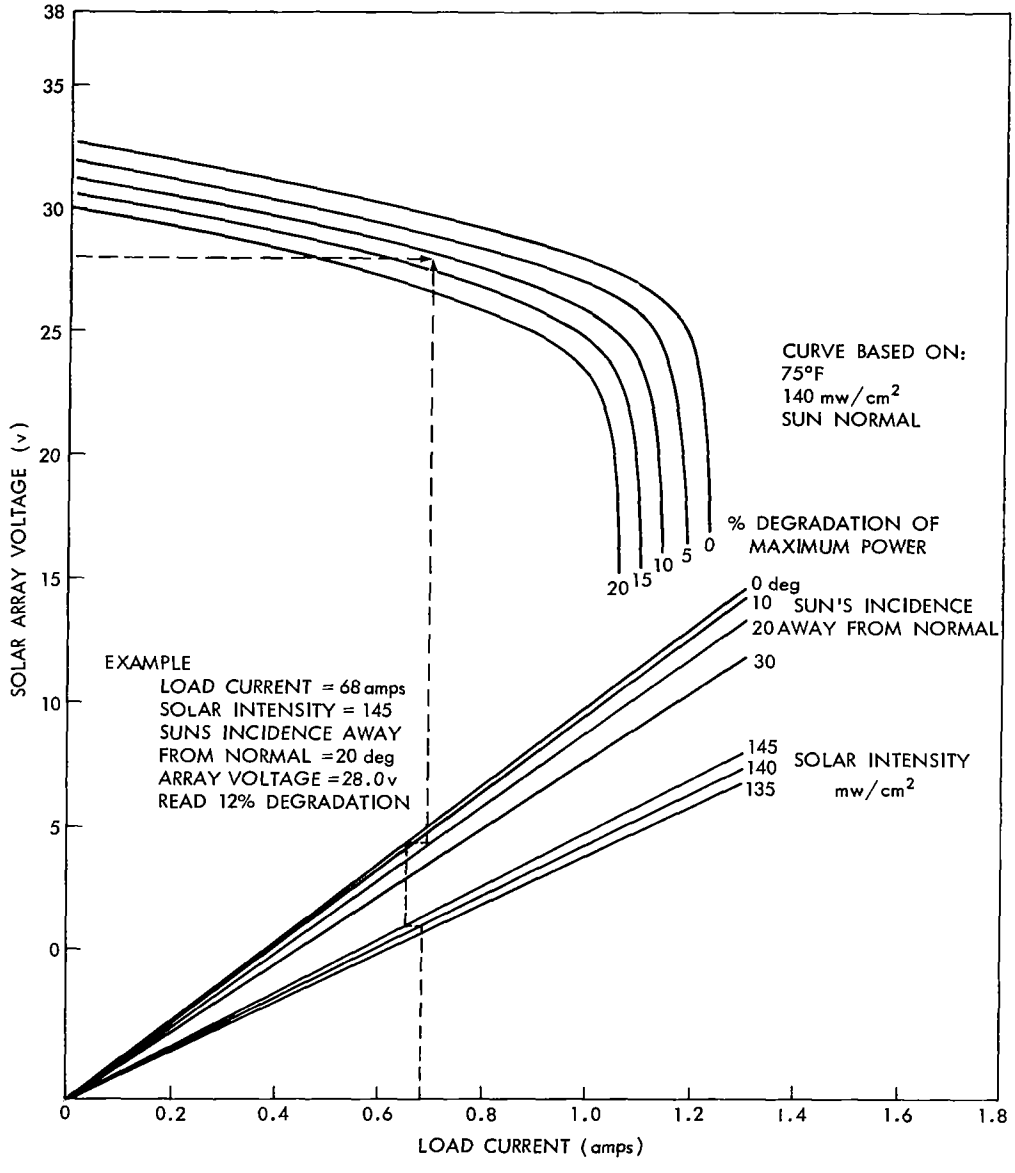

Figure B-3—Predicted power output of solar array in space environment.

where

Q = percent degradation

ϕ_t = radiation dosage up to time t

ϕ_c = radiation dosage to produce a 25 percent degradation in power.

ϕ_c for 10 ohm-cm base resistivity solar cells of the type used on Syncom III is approximately 1×10^{15} electrons/cm^2. Using this value and the space dosage estimates in the above expression yields the following power degradation values at the indicated periods:

After 100 days	5.8 percent
500 days	9.8 percent
1000 days	14.7 percent.

A curve showing the predicted power degradation as a function of time is shown on Figure B-4. Also shown is the power degradation of Syncom II and Syncom III experienced to date. Syncom II has the less radiation-resistant P-N cells and shows more than 25 percent damage after one year in space.

The data from Syncom III are quite scattered for the first 70 days in space; however, on the 68, 71, 79, and 86 days, closely controlled tests were conducted to determine the level of power available and more consistent results were obtained. The test results are shown in Figure B-5. These tests were conducted by turning on various known electrical loads (measured during acceptance testing) and recording the electrical bus and battery voltages. The results of these tests and the data obtained since launch indicated that the solar array power output characteristic curve, as predicted for the first day in space, is well substantiated. However, the rate of degradation due to radiation damage is not as great as originally predicted. At the end of 80 days, power degradation amounted to only 2-1/2 percent, whereas the predicted degradation for this period is 5 percent. The source of this discrepancy is probably in the radiation dosage estimate. Further experience with the spacecraft will be necessary to ascertain more accurately the actual rate of degradation.

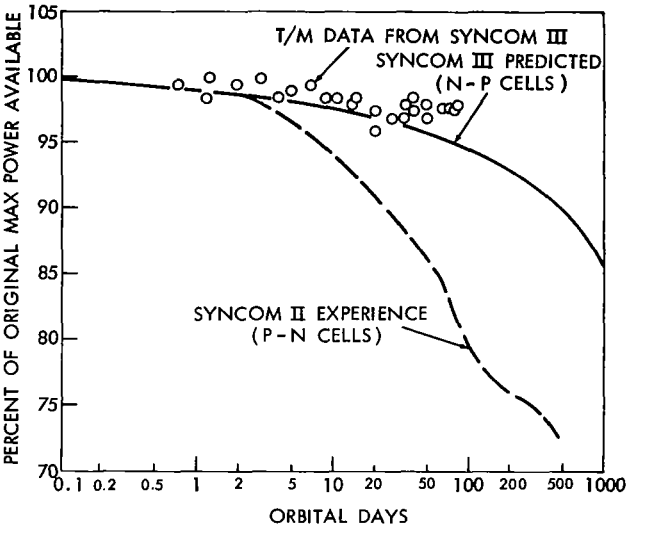

Figure B-4—Predicted power degradation.

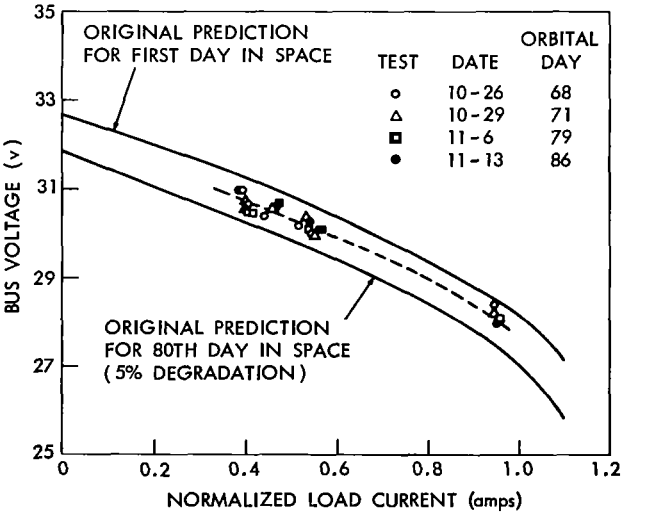

Figure B-5—Results of solar array electrical power output tests.

Battery System Performance

Under the maximum load condition (telemetry and transponder ON) the batteries become slightly discharged to a point where they are "floating" at the solar panel bus voltage. Except for this slight discharge, the batteries have not been used since the last eclipse period on October 15 except to power the attitude control

jets. Prior to the eclipse periods, the batteries were used during launch for firing the apogee motor squibs, the pulse the attitude control jets during reorientation, and velocity correction to the spacecraft.

During the 45 eclipses from 1 September to 15 October, the batteries powered the spacecraft load. The transponder was always turned off before each eclipse and after the first 10 eclipse periods, the telemetry system was also turned off. Battery discharge characteristics during several of the first 10 eclipse periods are shown in Figure B-6. These curves show that the batteries were fully charged at the start of the eclipse season and became fully discharged at the end of the tenth eclipse period. Calculations of the net energy received by the batteries during this period show that the transponder OFF period each day was of insufficient duration to replace all the energy used during the eclipse. The energy capacity available during the 10 eclipses is shown in Figure B-7.

After the tenth eclipse, the electrical load was reduced to 50 milliamperes by turning the telemetry OFF during eclipses. This permitted the batteries to be fully recharged each day for the remainder of the eclipse season.

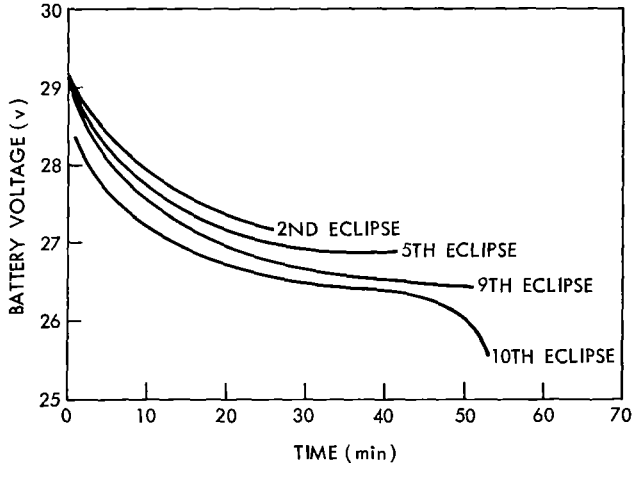

Figure B-6—Battery discharge characteristics during eclipses.

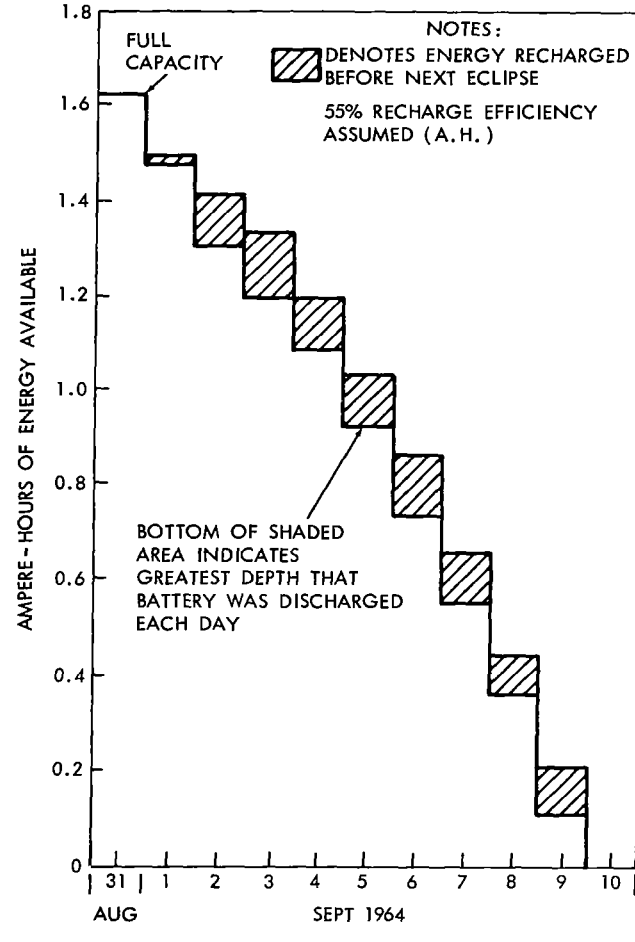

Figure B-7—Battery energy available during eclipses of September 1 through 10.

Appendix C

Syncom III Reliability Program

The basic concept of the spin-stabilized synchronous satellite is one of simplicity as far as the satellite design is concerned. The major design constraints were to design the satellite so that its weight and volume were compatible with the Thor-Delta launch vehicle. This meant that the maximum weight, including the apogee motor, was 150 pounds, and the diameter could not exceed 28 inches.

The contractual reliability requirements were:

1. The communications subsystem shall have a probability of 0.98 of surviving the launch environment and have a probability of 0.95 of operating for the first 30 days.
2. The control subsystem shall have a probability of 0.999 of surviving the launch environment and a probability of 0.99 of operating for the first 30 days.
3. The tracking, telemetry and command subsystem shall have a probability of 0.995 of surviving the launch environment and have a probability of 0.99 of operating for the first 30 days.

The three requirements are not independent as it turns out. There was no requirement for mean time to failure since this was an experimental program. However, the requirements were consistent with one year MTF for the design configuration chosen. Using failure rates based on a preliminary version of MIL Handbook 217, temperatures near 70°F and deratings to 10 percent throughout, except in a few cases of low population parts such as the traveling-wave tubes and power transistors, an estimate exceeding this requirement was made. Temperature conditions were ideal because of the spinning of the satellite.

As of this writing, there have been no failures or malfunctions on any portion of the system. Solar cell degradation has been less than predicted. It should be pointed out that the solar cells used on Syncom II were the P-N type with 0.006-inch microsheet cover slides. Syncom III solar cells have been changed to the more radiation-resistant N-P type cells with 0.012-inch fuzed silica quartz cover slides. This has resulted in more than an order of magnitude resistance to radiation damage.

Design Reviews

Design review of the system and each subsystem were conducted, as a minimum, once per month throughout the design and development phases. As a result of the reviews and reliability

analysis, several system components were considered to be critical in nature; therefore, more of them were fabricated and subjected to extended testing. These components were:

1. Separation switch
2. Transmitter antenna switching relay
3. Transponder antenna mechanism
4. Traveling wave tube
5. Pyrotechnic switch.

As a result of the test program, the transmitter relay initially procured for the program was discarded and an in-house design effort resulted in a highly satisfactory relay.

Test Program

The test program for the Syncom satellite was a very rigorous one. Each unit (command receiver, master oscillator, frequency multiplier, etc.) was subjected to vibration and temperature tests at qualification levels for prototype hardware and acceptance levels for flight hardware. The qualification level vibration was 1.5 times that expected and at twice the duration of flight acceptance testing. Qualification temperature tests were made at least 18°F above and below that expected in actual use. Acceptance levels were those actually expected during launch and orbit conditions. Subsequent to the successful completion of the unit environmental tests, the same units were assembled into the spacecraft, and each spacecraft was subjected to the qualification level environments (prototype) or the acceptance level environments (flight).

The basis of this redundant type testing (same units tested at unit and system level) was to assure that only system-based problems would occur at spacecraft level testing and that the program would not be delayed by discovering unit based failures at the system level. This type of test program did accomplish the goal of minimizing unit problems at the system level since it resulted in a thorough shakedown of the hardware at the unit level. Apparently this double testing of the hardware did not have any deleterious effect on Syncom II or Syncom III.

Parts Program

After the initial design was agreed upon by all concerned, it was felt that one way to assure success was to provide proper quality assurance implementation during fabrication and to further assure that only the most reliable parts were used for flight hardware.

The first portion of the parts program was to supply the designers with a list of preferred or space-qualified parts as a guide for parts selection. The preferred parts list consisted of those parts where the component engineers, through the various parts data exchange programs and other past usage information, felt that these parts would indeed operate satisfactorily in the Syncom environment. The qualified parts list consisted of those parts that had demonstrated their capability of operating in the Syncom environment. The second step was to reduce not only the quantity of

parts but also the number of different types and still meet the performance and reliability requirements of the system. The preferred parts were then qualified at the Syncom environment.

Once a part was selected and tests conducted to assure that it would operate in the Syncom environment, the next problem was to assure that the parts used in the flight spacecraft were representative of those that were tested early in the program. Procurement specifications were written that described the required parameters and tolerances and also the test conditions for each part. Each semiconductor was subjected to 240 hours of intermittent life (15 min. on, 5 min. off) at rated conditions. Passive components were subjected to similar tests. After receipt of the flight parts, they were subjected to 100 percent incoming inspection which included the verification of lead material (required for welded module circuits) and all of the physical and electrical parameters. Upon successful completion of the inspection, the parts were then routed to Bonded Stores, where they were made into kits for unit fabrication.

The parts program for present spacecraft contracts with Hughes has been changed as a result of the experience gained on Syncom. Those parts that are to be used on flight hardware are being procured as follows:

1. Prescreening tests which consist of temperature cycling, centrifuge, macroscopic and microscopic inspection prior to sealing, X-ray and serialization.
2. 240-hour intermittent life (15 min. on, 5 min. off) at rated power.
3. 1260 hours of power aging at half-rated power.

Readings on the parts are taken at 0.240, 250 and 1500 hours. Up to three times as many parts are purchased as required. The data on each device are plotted (by computer) and only those devices which remain stable and within specification are selected for flight use. Resident quality control engineers are assigned at each supplier to assure that the proper data is recorded, all tests are accomplished and that no "shortcuts" that would effect quality are made. Since all parts receive 100 percent inspection at the suppliers, only sample incoming inspection is performed. This inspection is primarily for reading correlation.

Syncom III Changes for Increased Reliability

The Syncom II spacecraft had one hydrogen peroxide and one high pressure nitrogen reaction control system. The two systems were used to complement each other in that the hydrogen peroxide system would be used for coarse velocity and attitude corrections while the nitrogen system would be used for the vernier corrections. Experience gained on Syncom II indicated that the hydrogen peroxide system is capable of making the necessary vernier maneuvers. On Syncom III the nitrogen system was therefore replaced with a hydrogen peroxide system. This change results in much more maneuver capability.

Another significant change incorporated in Syncom III was the use of the more radiation-resistant N-P solar cells with thicker cover slides. A new harness with redundant circuitry was installed, and the system was simplified by removing the automatic apogee motor firing circuitry. Firing of the motor was accomplished by command.

Conclusions

Syncom II and Syncom III have demonstrated the feasibility of using synchronous orbit satellites as a practical and economical means of attaining world-wide communications. The success of the Syncom satellites can be attributed to:

1. The basic simplicity of design of the spin-stabilized satellite. This resulted in a design that required no moving parts with the exception of the solenoid valves used in the reaction control system.
2. A rigorous test program that revealed problem areas early enough in the program to allow effective changes.
3. A parts program that provided screening that resulted in only high quality parts for flight spacecraft plus the fact that only "proven" parts were used in the design.
4. Effective use of design review.
5. A closed loop trouble/failure reporting system.

After 16 months of operation in orbit, there has been one failure in Syncom II. A 2N2185 PNP silicon alloy transistor in telemetry encoder 1 shorted. Syncom III has had no failures in the first 100 days. The only degradation has been in the solar array and this has followed the prelaunch predictions. This absence of failures in orbit when compared to the troubles that occurred on the ground (testing) over a comparable span of time, but with considerable less operating time, leads one to believe that the space environment at 22,000 miles is more suitable for long life than on the ground. This perhaps can best be explained by the absence of people handling the equipment plus a completely vibration- and atmosphere-free environment in space.

Appendix D

Syncom III Performance of Hydrogen Peroxide Reaction Control Systems,–First 100 Days

The performance of the two hydrogen peroxide reaction control systems was satisfactory during the first 100 days of operation in orbit. Syncom III is on station as a result of accurate orbital maneuvers provided by the control systems. Sufficient propellant remains to permit stationkeeping for at least another 33 months; however, orbital operation of the control system could be limited to two years because of reduced hydrogen peroxide concentration.

The primary difference in characteristics between the hydrogen peroxide control system in Syncom II and the two control systems in Syncom III is the comparatively high pressure rise in the Syncom III systems.

Although all peroxide systems supplied by the vendor were processed and checked to class I passivity, the flight-loaded system in Syncom II was *exceptionally* passive (about 0.5 psi per day perssure rise at 70°F) while the two systems in Syncom III were representative of a normal range of passivity (1 to 2 psi per day pressure rise at 70°F). Two additional factors contributing to a negligible peroxide pressure rise in Syncom II are the comparatively rapid use of peroxide and the lower spacecraft temperatures throughout orbital operation. The possibility that slight gas leakage also occurred cannot be overlooked.

The 2 to 3 psi per day pressure rise in the Syncom III peroxide systems after the first few maneuvers indicate the effects of the following:

1. Higher spacecraft operating temperatures.
2. Lower rates of propellant utilization per system.
3. Entry of more catalytic elements into the peroxide during servicing of the peroxide systems or during launch period shock and vibration or both.
4. Lower passivity of surfaces exposed to peroxide.

The performance of the peroxide systems in Syncom III is considered to be typical for the existing state of the art in system processing, the charging procedures employed, the rate of propellant utilization, and the operating temperature level in orbit.

With improvements in hardware processing, and propellant charging procedures and equipment, three years orbital operation for peroxide systems may be achieved. Such improvements have already begun on Comsat and ATS programs. Further improvements would accrue if the

average spacecraft temperature was reduced by redesign of the spacecraft thermal control systems.

Engine Performance

The calculation of ON-time (button-down) for any accurate orbital maneuver is dependent on accurate engine performance data. Pulsing performance data were lacking for the axial engines; however, lateral engine pulsing data were used for pulsing axial engine manuevers with outstanding results.

Steady-state vacuum specific impulse is shown in Table D-1 for all engines.

Continuous thrust hydrogen peroxide tank pressure is shown for all engines in Figure D-1.

Table D-1

Steady-State Vacuum Specific Impulse for Hydrogen Peroxide Engines.

System Number	Engine	Specific Impulse (seconds)
1	Axial	153.5
1	Lateral	150.5
2	Axial	152
2	Lateral	153

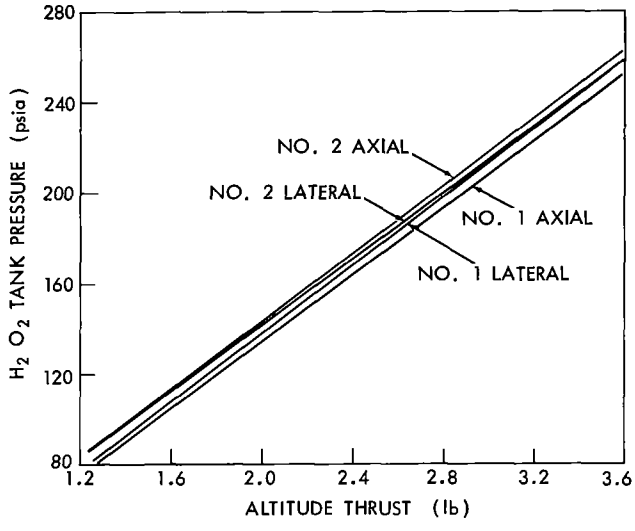

Figure D-1—Thrust versus hydrogen peroxide tank pressure for Syncom III control engines. Data from fourth cycle of runs of four 250-ms pulses.

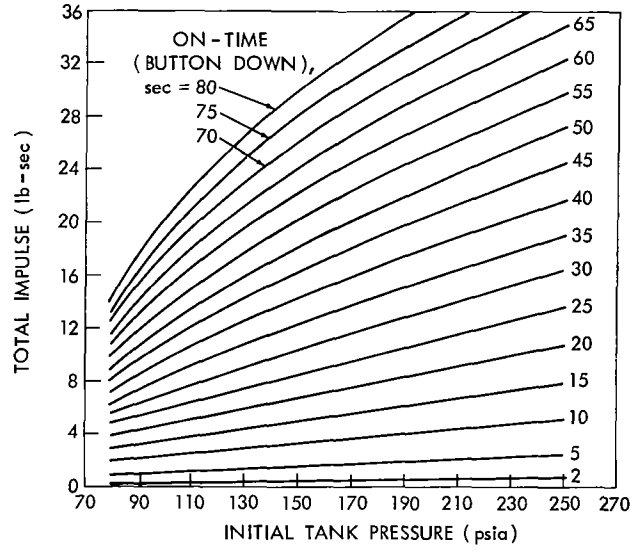

Figure D-2—Total impulse versus initial tank pressure and on-time (button down) for Syncom III control system 1 (lateral engine, pulsing mode for 165 rpm spin rate).

Pulsing performance for the lateral engines is shown in Figures D-2, D-3 and D-4. Figures D-2 and D-3 show total impulse versus initial tank pressure with ON-time as a parameter. Figure D-4 shows pulsing specific impulse versus ON-time with initial tank pressure as a parameter.

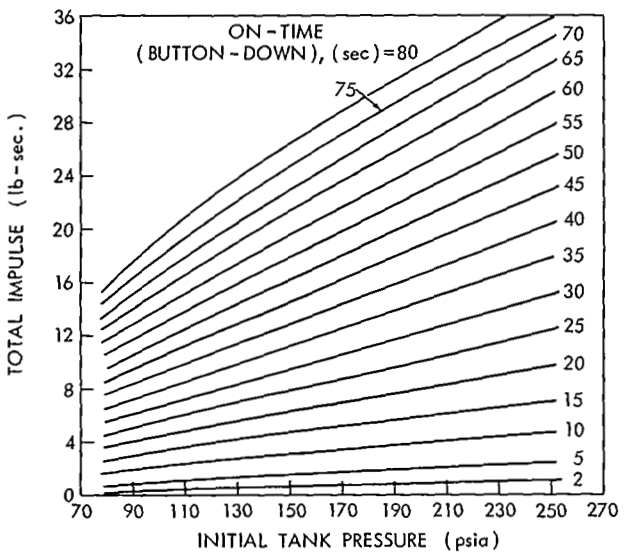

Figure D-3—Total impulse versus initial tank pressure and on-time (button down) for Syncom III control system 2 (lateral engine, pulsing mode for 165 rpm spin rate).

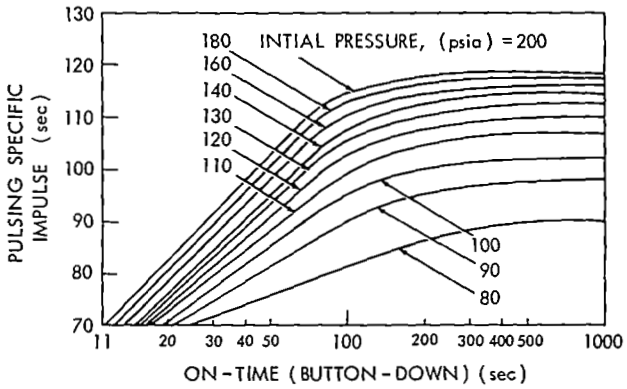

Figure D-4—Pulsing specific impulse versus on-time (button down).

These data proved to be highly accurate for most maneuvers, usually providing within 5 percent of the desired performance. However, space calibration of performance was necessary to correct for a 15 percent undershoot on the system 1 lateral engine and a 20 percent overshoot on the system 2 lateral engine observed during the first pulsing maneuver for each engine.

Pressure Rise in Syncom II and Syncom III

Pressure rise due to active oxygen loss was expected to be evident in the Syncom II hydrogen peroxide control system. However, throughout orbital operation, telemetry data from the system pressure transducer did not indicate conclusively either a pressure rise or a pressure loss at a constant peroxide level except during periods of temperature change. Total pressure drop in the system has been greater than can be accounted for by peroxide usage.

The two hydrogen peroxide systems in Syncom III behaved more characteristically than the one in Syncom II, indicating initial pressure rise rates between 2.5 and 3 psi per day (corrected to initial tank ullage volume and 70°F).

Pressure Rise Rate

A comparison of the pressure rise rates between Syncom II and Syncom III peroxide systems during surveillance while at the Kidde Company and after launch into orbit is made in Table D-2

(values corrected to a 4.9 pound propellant load and 70°F). The comparison shows the following:

1. The peroxide system in Syncom II was the most passive of the three systems.
2. Pressure rise rates of systems 1 and 2 in Syncom III were significantly higher than those of the Syncom II system during surveillance and in orbit.
3. Pressure rise rates of the flight-loaded systems 1 and 2 (Syncom III) were considerably higher in orbit than during surveillance.

Table D-2

Pressure Rise in Hydrogen Peroxide Systems During 24 hour Surveillance and After Launch (4.9 pounds H_2O_2 load).

H_2O_2 System	Pressure Rise 24 Hour Hold Test (psi per day)		Pressure Rise in Orbit (psi per day)	
	Average Temperature	Corrected to 70°F	Average Temperature	Corrected to 70°F
Syncom II	0.8 at 76°F	0.5	negligible (50° to 83°)	negligible
Syncom III (system 1)	1.1 at 73°F	1.0	3.5 at 75°F	2.8
Syncom III (system 2)	1.6 at 65°F	2.0	3.4 at 75°F	2.7

Further examination of the data in Table D-2 shows that there is not necessarily any correlation between surveillance pressure rise at the vendor's plant and pressure rise after launch into orbit.

The extremes of surveillance pressure rise rates applicable to all peroxide systems originally delivered and reworked were represented by the system in Syncom II (minimum) and system 2 in Syncom III (maximum). The surveillance pressure rise of system 1 in Syncom III was near the average for all systems.

In terms of apparently high passivity (low pressure rise rate), the Syncom II peroxide system provides a worthy standard for other systems.

Effects of Propellant Usage. For a given peroxide system, the pressure rise rate is directly proportional to the surface area exposed to the peroxide and inversely proportional to the tank ullage volume at constant temperature as shown in Figure D-5. The pressure rise rates versus the amounts of propellant consumed during the first 90 days in orbit are compared for systems 1 and 2 in Syncom III (as corrected to 70°F). As a matter of academic interest, a calculated variation in pressure rise rate versus propellant consumed is presented for Syncom II, assuming that the initial pressure rise rate equals the surveillance value.

Figures D-6 and D-7 show the effect that the rate of peroxide use has upon system pressure rise. As expected, the more rapidly peroxide is used, the faster pressure rise rate decreases.

Figure D-7 shows that the pressure rise rates in the Syncom II and Syncom III number 2 peroxide systems were reduced by at least a factor of two because over one-third of the total peroxide load in each system was used within three days after launch. If Syncom III systems 1 and 2 had been used equally during the first few days of orbital operation, perhaps peroxide pressure rise rates would have been low enough to cause little concern.

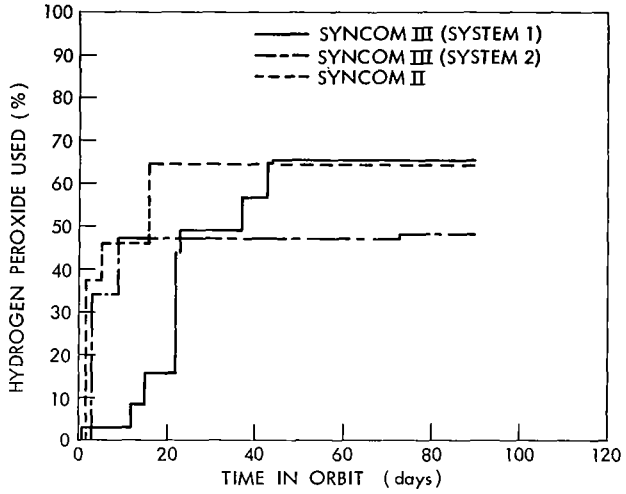

Figure D-6—Schedule of hydrogen peroxide usage, Syncom II and Syncom III for 90 days in orbit.

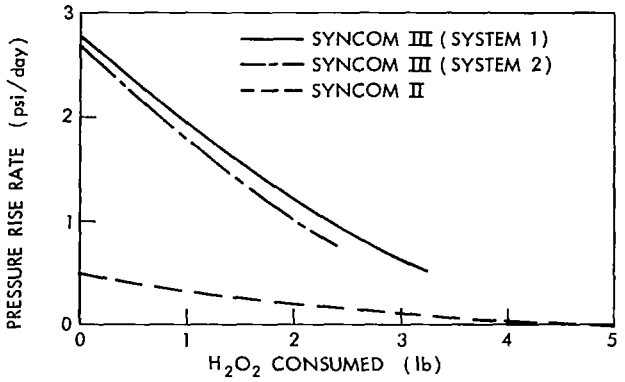

Figure D-5—Hydrogen peroxide pressure rise rate versus hydrogen peroxide consumed in 90 days.

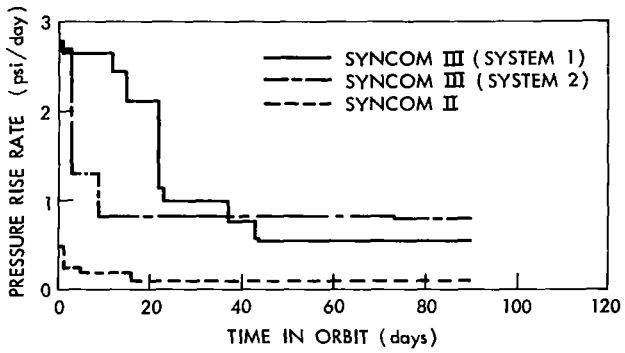

Figure D-7—Hydrogen peroxide pressure rise rate (corrected to 70°F) in Syncom II and Syncom III as a function of usage schedule, (Figure E-6).

Temperature Effects. Changes in peroxide active oxygen loss are highly sensitive to temperature changes. Every 10°F increase in temperature increases the active oxygen loss (pressure rise) by a factor of 1.6 (multiplication). Similarly, every 10°F decrease in temperature decreases the active oxygen loss by a factor of 1.6 (division). The variation in correction factor versus temperature (for a reference temperature of 70°F) is shown in Figure D-8. Figure D-8 indicates that if the hydrogen peroxide pressure rise rate is 1 psi per day at 70°F, increasing the peroxide temperature to 100°F (a 30°F increase) will cause a four-fold increase in a pressure rise rate to 4 psi per day. A 15°F decrease to 55°F will reduce the pressure rise by a factor of two to 0.5 psi per day.

The temperature effects are important when comparing peroxide system pressure rise rates in Syncom III with the negligible pressure rise in Syncom II. As shown in Figure D-9, Syncom

II ran cooler than Syncom III over most of the first 90 days in orbit. Especially significant is the low Syncom II temperature during the first five days in orbit (about 51°F). If Syncom III had been operating at that temperature level, the observed pressure rise rate in Syncom III hydrogen peroxide system 1 would not have exceeded 1.2 psi per day. The pressure rise in system 2 would have been lower because of the use of about 34 percent of its propellant.

Contamination Effects. Many materials such as dust, dirt particles, iron, nickel, lead, copper, silver, gold, platinum and others make excellent catalysts in the decomposition of hydrogen peroxide. Their presence, even in minute quantities, will increase the active oxygen loss or pressure rise rate of loaded hydrogen peroxide systems.

Ground Support Equipment. The ground support equipment used at Cape Kennedy consisted of a charge kit containing 90 percent hydrogen peroxide and a pressurized 99 percent nitrogen-helium gas mixture by volume. The charge kit is shown in Figure D-9 with discharge lines and filters attached.

While at Hughes Aircraft Company, the charge kit was LOX-cleaned, flushed with filtered 90 percent hydrogen peroxide, rinsed with filtered, triple-distilled water, and dried with filtered nitrogen. All filters used were of the 10-micron size (mil pore polyethylene). Particle counts from the hydrogen peroxide and nitrogen discharge lines were taken to determine the suitability of the charge kit using the tentative SAE, ASTM and AIA Class 0 standards.

At Cape Kennedy, the charge kit was flushed with suitable concentration and stability-tested 90 percent hydrogen peroxide. Then peroxide samples were taken from the kit for concentration

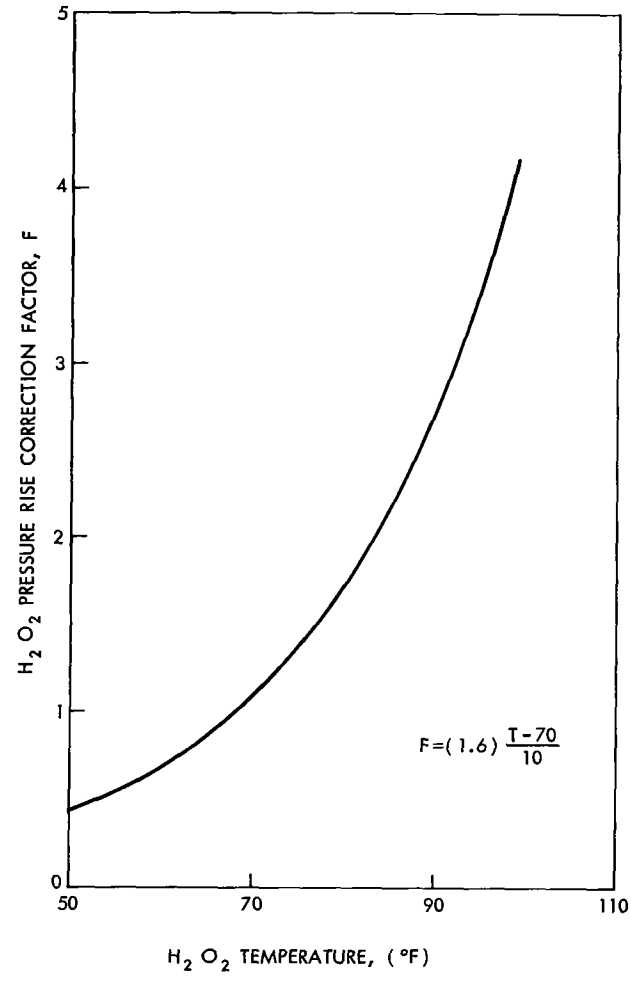

Figure D-8—Correction factor for hydrogen peroxide pressure rise rate (70°F) reference temperature).

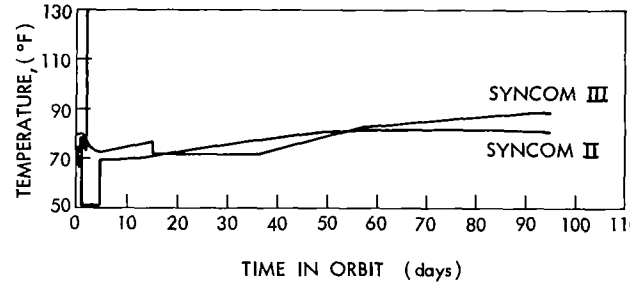

Figure D-9—Spacecraft temperature versus time in orbit for Syncom II and Syncom III.

and stability analysis. After the charge kit was used to service the Syncom III control system with peroxide and pressurizing gas, it was flushed with 5-micron filtered distilled water and dried with filtered low pressure nitrogen gas.

After return to Hughes, particle counts were taken from the peroxide and nitrogen discharge ports. Then hydrogen peroxide was loaded into the kit and stored for thirteen days. During the thirteen-day period, the peroxide was exposed to stainless steel lines as well as the polyethylene tanks, yet the pressure rise was low, averaging 0.7 psi per day corrected to Syncom propellant loading and ullage volume at 70°F.

Comparisons of particle counts and peroxide stabilities applicable before use at Cape Kennedy and after return to Hughes are shown in Tables D-3 and D-4. Particle counts and changes in peroxide stability and concentration were acceptable in all cases.

Table D-3

Charge Kit Particle Count.

Component	Particle Size Range (microns)	Before Use at Cape Kennedy	After Return to Hughes		SAE, ASTM, AIA Standards, Class 0*
		1 ft^3 N_2	1 ft^3 N_2	100 ml H_2O	1 ft^3 N_2 or 100 ml H_2O
H_2O_2 outlet	5-10	123	56	173	2700
	10-25	13	16	33	670
	25-50	3	2	19	93
	50-100	1	1	3	16
	> 100	1	0	1	1
	Fibers	0	0	0	
N_2 outlet	5-10	51	290		2700
	10-25	6	122		670
	25-50	0	53		93
	50-100	1	10		16
	> 100	1	2		1
	Fibers	0	0		

*Rarely attained in missile systems. See Millipore *Application Data Manual ADM-30,* 1964 Edition, p. 28.

Servicing Environment. The servicing environments at Hughes Aircraft Company and Cape Kennedy are non-ideal. At Hughes, servicing with the nitrogen-helium gas mixture is done in areas as clean and dust-free as possible. All connections of lines and adapters to the peroxide systems are performed under new polyethylene bags. At Cape Kennedy, servicing was done in the open on the gantry.

Table D-4

Hydrogen Peroxide Stability and Coneentration.

Source	Concentration (percent)	Stability (percent)
Cape Kennedy		
Carboy	90.3	99.6
Charge Kit H_2O_2 Tank		
No. 1	90.1	99.3
No. 2	90.1	99.0
Hughes Aircraft Company (After Launch)		
Carboy	89.0	95.9
Charge Kit H_2O_2 Tank (After 24 hours)		
No. 1	88.9	95.6
No. 2	88.8	95.6

It is highly desirable from a cleanliness standpoint to load the peroxide systems in a clean room before mating of the spacecraft to the third stage of the launch vehicle.

Prediction of Orbital Life

Both Hughes Aircraft Company and Walter Kidde and Company have made brief studies of the potential life in orbit of hydrogen peroxide systems similar to those in Syncom III. These studies indicate that the control systems in Syncom III should have peroxide at usable concentration greater than 70 percent for at least 20 months. Since hydrogen peroxide engines have operated satisfactorily using 70 percent peroxide at temperatures above 50°F, it is concluded that the Syncom III control systems will be operable for at least 20 months.

The results of Kidde studies for two-use schedules, assuming 2 percent per week active oxygen loss per week, with the peroxide at 60°F, are shown in Figures D-10 and D-11.

Case 1 assumes that 50 percent of the peroxide in both systems is used within the first two weeks of orbital operation, the balance being used at a uniform rate for 36 months. In this case, the concentration drops to the minimum allowable of 70 percent in 20 months.

Case 2 assumes that system 1 delivers peroxide following the peroxide usage and concentration of case 1 for 20 months. At this time, the concentration reaches the useful 70 percent limit of system 2 and is used. In 36 months, the concentration of peroxide in system 2 has been reduced to 78 percent.

The results of the Kidde study show that the peroxide use schedule at a given active oxygen loss has a significant bearing on the useful orbital life of peroxide systems. Therefore, it is

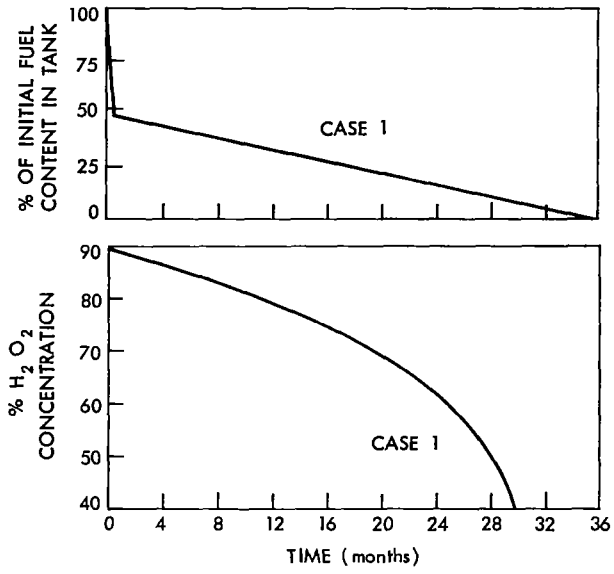

Figure D-10—Hydrogen peroxide concentration and tank pressure for assumed fuel use schedule versus time (case 1).

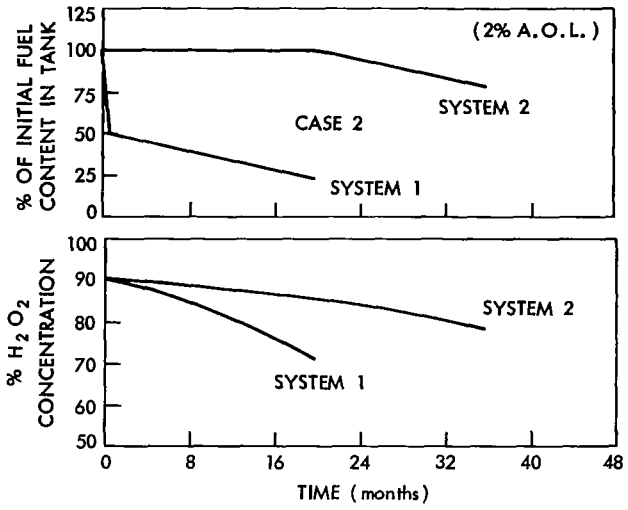

Figure D-11—Hydrogen peroxide concentration and tank pressure for assumed fuel use schedule versus time (case 2).

important to optimize the peroxide use schedule, as well as to minimize active oxygen loss. With such optimization, orbital life times of 3 years are probable with hydrogen peroxide systems.

More detailed studies are needed to provide additional useful information about how peroxide system orbital life may be maximized.

Increasing Orbital Life

Longer operating life in hydrogen peroxide systems is dependent primarily upon increasing their passivity during manufacture and acceptance, and upon minimizing contamination of the fluids entering the systems during checkout at Hughes Aircraft Company and servicing on the gantry before launch.

Certain important steps have already been taken to ensure improved, more uniform performance of future peroxide systems in HS-303 and ATS spacecraft as follows:

1. Additional cleaning processes and particle counts at the Kidde Company during manufacture and acceptance.
2. Longer surveillance periods to ensure suitable peroxide compatibility.
3. A maximum pressure rise rate of 1.5 psi per day at 70°F has been set for acceptance of system comparability with 90 percent hydrogen peroxide before delivery to Hughes Aircraft Company. The ultimate goal is to reduce this to 1 psi per day maximum.
4. Minimize the number of times which the systems are charged with nitrogen at Hughes.

5. All 10-micron filters in the charge kit have been replaced by ones with smaller pore sizes. Peroxide is filtered through two 1.5-micron polyethylene filters. Nitrogen is filtered through three 0.45-micron acetate paper filters.
6. Filters, lines and adapters connecting filters to the peroxide and nitrogen fill ports are used only once per servicing. They are replaced with certified clean items for any subsequent servicing.
7. Servicing of peroxide systems is to be done in the cleanest possible area, preferably in a class 1 clean room.

Recent events at Hughes Aircraft Company indicate that vibration testing of spacecraft with fully loaded peroxide systems results in loosening particulate matter not loosened in any other way. This occurrence suggests that vibratory cleaning should be part of the standard procedure in processing future peroxide systems.

Appendix E

Syncom III Thermal Control - 100 Day Report

Temperature predictions for the four sensors on Syncom III over the period of the complete year have been made. The thermal analyses performed have included the orbital variation effects (sun angle and earth-sun distance) and the internal power dissipation variations on the four on-board temperature sensors. As yet, only steady-state calculations have been performed for actual flight operations of Syncom III with the current analytical model. Several modifications to the analytical model have been made to correct or adjust the model to match flight telemetry.

The analytical model utilized for the post flight thermal analyses of Syncom III is a 75-node, lumped-mass thermal model made from the basic Comsat HS 303 analytical model modified to represent the Syncom spacecraft. It is expected that with slight parametric modifications made to the model, it will replace the more cumbersome 250-node previous Syncom model.

Steady-state temperature predictions for the Syncom III spacecraft for the complete year reflecting the spacecraft sun angle and earth-sun distance variations according to Figure E-1 have been made. Modifications have been made based on actual flight results in order to match the predicted temperature variations with the actual temperatures recorded by the four on-board temperature sensors. The predicted values for the four sensors are shown in Figure E-2 for the yearly variation at four different power modes within the spacecraft. It can be seen that the basic curves represent expected temperatures at the sensors for the spacecraft status of telemetry system 2 and transponder 2 operation with a tabulation for several other power operation modes. It must be noted that the predictions reflect steady-state temperature conditions and that the time constant of the spacecraft in changing from one telemetry system to the other has not as yet been established.

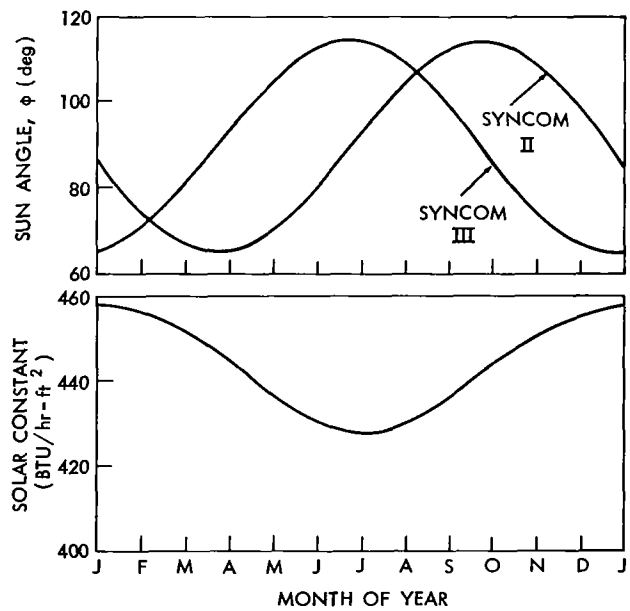

Figure E-1—Time of year and inclination variation for Syncom satellites.

A comparison of some of the temperatures with the available flight data shows varying degrees of correlation. The most direct

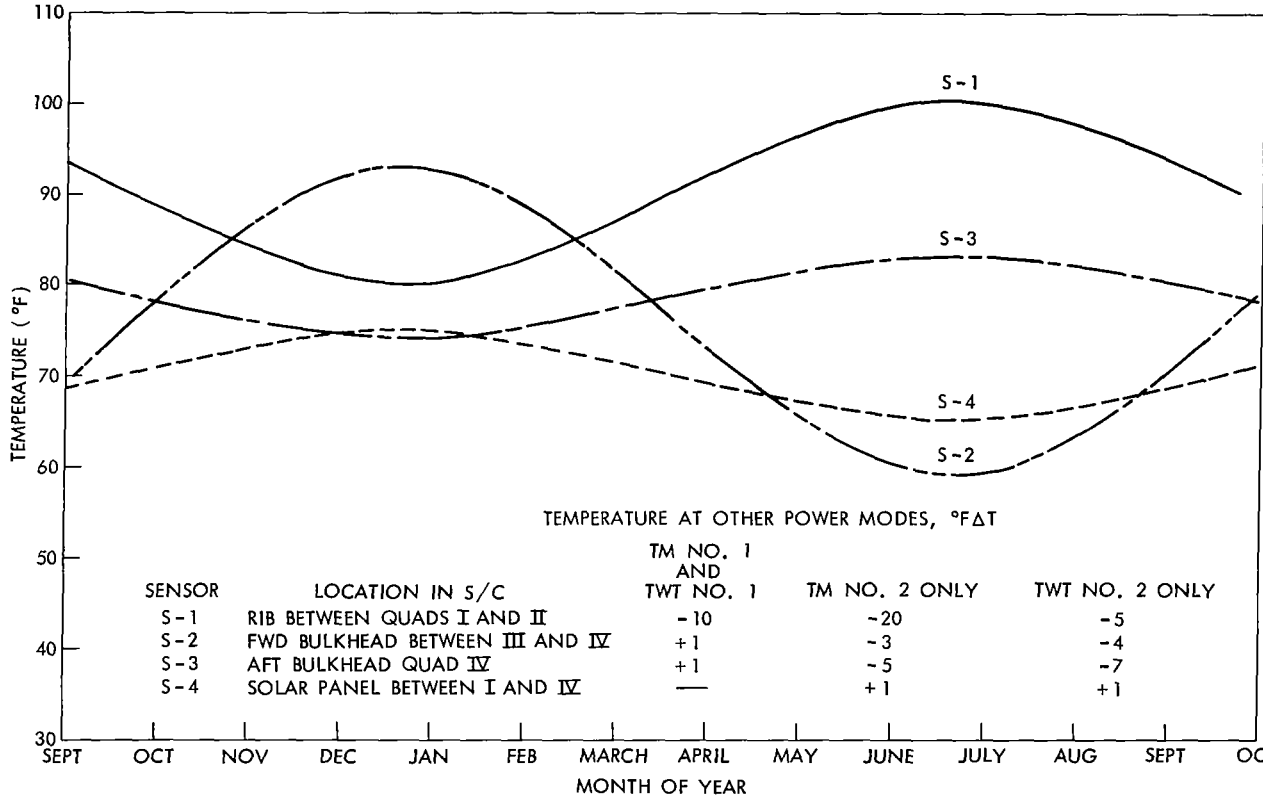

Figure E-2—Syncom III temperature predictions, 75 node analytical model, TM 2 and TWT 2 operation.

comparison available seems to be in the vicinity of 20 October where data are available for all four sensors (Table E-1).

It can be seen from Figure E-2 that the rib temperature sensor, S-1, is expected to reach its minimum temperature of 80°F at approximately the winter solstice when although the earth-sun distance is at a minimum, the sun angle, ϕ, is also at its minimum, i.e., ~66 degrees. At this same, time, the forward bulkhead and solar panel sensors are expected to be at their maximums, i.e., 93°F

Table E-1

Syncom III Temperatures, 20 October 1964.

Sensor	Mode	Recorded Temperature (°F)	Predicted Temperature (°F)
S-1	TM 1 and TWT 1	74	76
S-2	TM 2 and TWT 2	85	84
S-3	TM 1 and TWT 1	78	78
S-4	TM 2 and TWT 2	75	72

and 75°F respectively. At the summer solstice, the rib temperature is expected to rise to a maximum of 100°F for the mode of TWT 2 and TM 2 operation. At this time, the forward bulkhead is expected to drop to its minimum temperature of 59°F.

Changes to the basic analytical model that were required to match the flight telemetry are:

1. Increase radiant coupling between the forward bulkhead and the thermal barrier. This has of course raised the bulkhead temperature from earlier predicted levels.

2. Add solar illumination on the forward solar panel attach ring at the low sun angles; i.e., $0 \leq \phi \leq 90$. This had heretofore been ignored.

3. Increase radiant emission and solar absorption in the aft thrust tube area in the antenna mechanism cavity.

4. Increase overall vehicle axial thermal conductance; i.e., less thermal conduction in the structure and joints exists than previously assumed.

It is noted that only since the launch of Syncom III has there been any valid measurable temperature gradients within the structure of the spacecraft. Only the gradients due to localized electrical power dissipation have been heretofore measured while the axial gradient due to the unequal or nonsymmetrical solar illumination at the off-normal sun angles has been the largest unknown thermal parameter. It is expected that the telemetry information received from the spacecraft will continue to improve on the accountability of the thermal phenomena associated with the synchronous, spin-stabilized spacecraft.

Appendix F

Syncom III Problem Areas

Only two problems, one arising from a sun sensor miswiring and the other an apparent frequency shift in telemetry encoder 1, have been noted since the launch of the spacecraft.

Sun Sensor Miswiring

During the transfer orbit phase of the launch it was discovered that the ψ_2 angle reported by telemetry 1 did not agree with the ψ_2 angle reported by telemetry 2, nor did it agree with the attitude as measured by the polarization of the RF energy from the spacecraft communications antenna. It was also determined that the numerical values of the ψ_2 angle as reported by each telemetry system were equal but their signs were opposite (Figure F-1).

The only logical assumption that can be drawn is that the wiring from the ψ, ψ_2 sensors to encoder 1 in telemetry system 1 is reversed. As shown in Figure F-2, the ψ sensors connected to telemetry system 2 are also used in the quadrant mode of control system operation. The

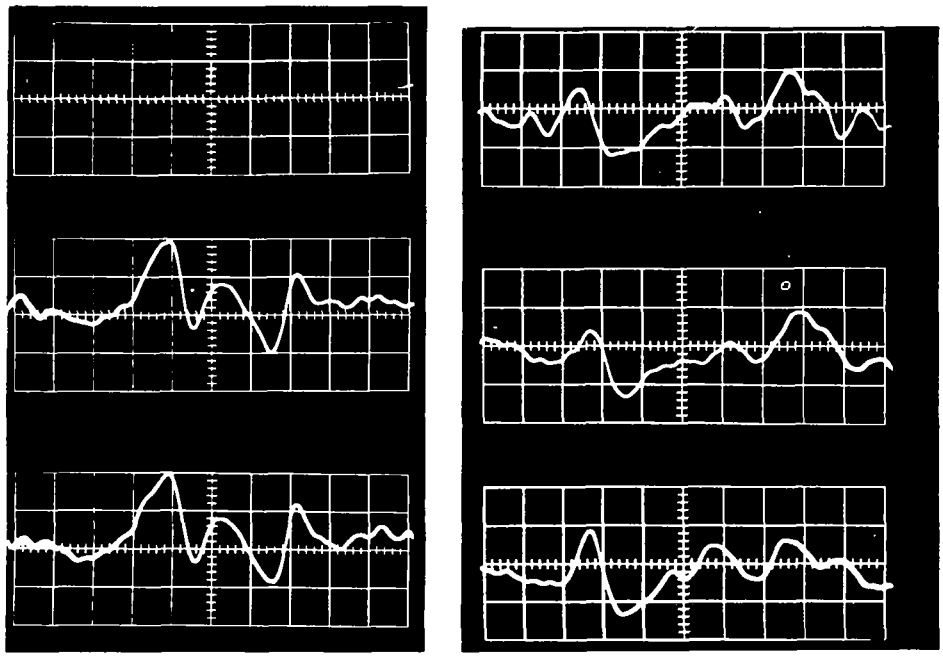

Figure F-1—Sun sensor telemetry returns from telemetry 1 and 2.

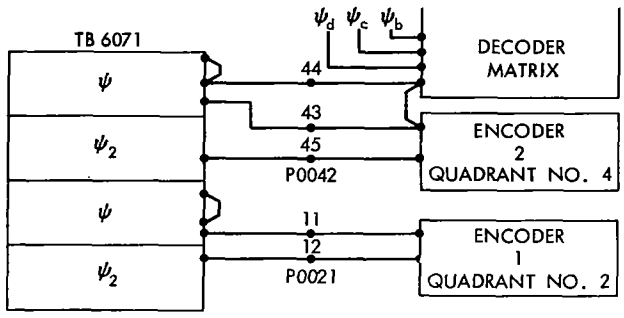

Figure F-2—Solar sensor to encoder wiring diagram.

operation of the quadrant mode was tested during each performance check of the spacecraft. The functioning of the ψ sensor connected to telemetry system 1 and the functioning of both ψ_2 sensors are tested by watching their output on an oscilloscope as a flash gun is flashed in front of the sensor. Obviously this test was not adequate because the overshoot was apparently mistaken for the pulse. Since it is very difficult to get a continuous light source of sufficient brilliance to activate the sun sensors, the best solution to prevent any future problem of this type from not being uncovered in testing is to spin the spacecraft in the sunlight and leisurely observe the telemetry return. This test was standard during the testing before the launch of Syncom I but was abandoned because the spacecraft was exposed to too much dirt and dust while outdoors.

The spacecraft records, the program for the automatic wiring harness checker, and the photographs of the installed wiring harness have been examined to determine where the wiring error was made. The results of this investigation are negative. The error could have been made in the sensors themselves, in the wiring harness or in the quadrant wiring but the specific problem area has not been identified.

The automatic wiring harness checker program has been examined and found corrected. The photographs of the wiring harness are very detailed but because they are in black and white, they do not show the color coding on the sun sensor wires. No photographs were made of quadrant 2 or the sun sensors while they were under construction.

Telemetry Encoder 1 Frequency Drift

On 21 August, the Telemetry and Command Station at Adelaide, Australia reported a decrease of 110 to 130 cps on all data channels during the period 0530 Z to 0730 Z. They were advised by the GSFC Operations Center to switch to telemetry 2.

The magnetic tape recording from the Adelaide station for this period of time was returned to Hughes for analysis. No data could be found on the magnetic tape for this period of time.

On 19 October, the Telemetry and Command Station at Camp Roberts, California reported that the telemetry system 1 VCO was unstable for approximately 11 minutes shortly after turn-on, but stabilized and remained steady for the remainder of the duty period of 8 hours at which time it was turned OFF.

These recordings from the Camp Roberts station were analyzed. The sequence of events is listed below:

19 October	
2336 Z	TM 1 turned ON.
2344 Z	Tape recorder turned OFF
2348 Z	TM panel lost lockon.
2349 Z	Tape recorder turned ON.
2349-2352 Z	Recording shows TM data drift (entire PAM train shifts down in frequency).
2352 Z	Tape recording shows TM data good.
2359 Z	Roberts reports TM data good.
20 October	
0630 Z	TM 1 turned OFF.

The recorded data taken between 2349 Z and 2352 Z show a frequency shift in the VCO data. Whether this is an actual or apparent shift or whether this shift is caused by spacecraft or ground equipment cannot be determined by the recorded data but, because the Australian telemetry and command station reported that the telemetry system required "about half an hour to stabilize," the problem most probably was caused by VCO drift in the spacecraft encoder.

Telemetry system 1 has been used on three occasions since this anomaly. On each occasion it has functioned properly.

"The aeronautical and space activities of the United States shall be conducted so as to contribute . . . to the expansion of human knowledge of phenomena in the atmosphere and space. The Administration shall provide for the widest practicable and appropriate dissemination of information concerning its activities and the results thereof."

—NATIONAL AERONAUTICS AND SPACE ACT OF 1958

NASA SCIENTIFIC AND TECHNICAL PUBLICATIONS

TECHNICAL REPORTS: Scientific and technical information considered important, complete, and a lasting contribution to existing knowledge.

TECHNICAL NOTES: Information less broad in scope but nevertheless of importance as a contribution to existing knowledge.

TECHNICAL MEMORANDUMS: Information receiving limited distribution because of preliminary data, security classification, or other reasons.

CONTRACTOR REPORTS: Scientific and technical information generated under a NASA contract or grant and considered an important contribution to existing knowledge.

TECHNICAL TRANSLATIONS: Information published in a foreign language considered to merit NASA distribution in English.

SPECIAL PUBLICATIONS: Information derived from or of value to NASA activities. Publications include conference proceedings, monographs, data compilations, handbooks, sourcebooks, and special bibliographies.

TECHNOLOGY UTILIZATION PUBLICATIONS: Information on technology used by NASA that may be of particular interest in commercial and other non-aerospace applications. Publications include Tech Briefs, Technology Utilization Reports and Notes, and Technology Surveys.

Details on the availability of these publications may be obtained from:

SCIENTIFIC AND TECHNICAL INFORMATION DIVISION

NATIONAL AERONAUTICS AND SPACE ADMINISTRATION

Washington, D.C. 20546